

Effects of symmetry breaking in finite quantum systems

J.L. Birman¹, R.G. Nazmitdinov^{2,3}, and V.I. Yukalov³

¹*Department of Physics, City College,
City University of New York, New York, NY 10031, USA*

²*Departament de Fisica,
Universitat de les Illes Balears, Palma de Mallorca 07122, Spain*

³*Bogolubov Laboratory of Theoretical Physics,
Joint Institute for Nuclear Research, Dubna 141980, Russia*

Abstract

The review considers the peculiarities of symmetry breaking and symmetry transformations and the related physical effects in finite quantum systems. Some types of symmetry in finite systems can be broken only asymptotically. However, with a sufficiently large number of particles, crossover transitions become sharp, so that symmetry breaking happens similarly to that in macroscopic systems. This concerns, in particular, global gauge symmetry breaking, related to Bose-Einstein condensation and superconductivity, or isotropy breaking, related to the generation of quantum vortices, and the stratification in multicomponent mixtures. A special type of symmetry transformation, characteristic only for finite systems, is the change of shape symmetry. These phenomena are illustrated by the examples of several typical mesoscopic systems, such as trapped atoms, quantum dots, atomic nuclei, and metallic grains. The specific features of the review are: (i) the emphasis on the peculiarities of the symmetry breaking in finite mesoscopic systems; (ii) the analysis of common properties of physically different finite quantum systems; (iii) the manifestations of symmetry breaking in the spectra of collective excitations in finite quantum systems. The analysis of these features allows for the better understanding of the intimate relation between the type of symmetry and other physical properties of quantum systems. This also makes it possible to predict new effects by employing the analogies between finite quantum systems of different physical nature.

keywords: Symmetry breaking, Finite quantum systems, Trapped atoms, Quantum dots, Atomic nuclei, Metallic grains

Contents

1. Preamble

2. Symmetry breaking

2.1. *Symmetry in macroscopic systems*

2.1.1. Symmetry of thermodynamic phases

2.1.2. Landau phase-transition theory

2.1.3. Symmetry and conservation laws

2.1.4. Thermodynamic limit and symmetry

2.1.5. Methods of symmetry breaking

2.2. *Symmetry in finite systems*

2.2.1. Asymptotic symmetry breaking

2.2.2. Effective thermodynamic limit

2.2.3. Fluctuations and thermodynamic stability

2.2.4. Equilibration in quantum systems

2.2.5. Convenience of symmetry breaking

2.3. *Geometric symmetry transformations*

2.3.1. Role of shape symmetry

2.3.2. Geometric shape transitions

2.3.3. Geometric orientation transitions

3. Trapped atoms

3.1. *BoseEinstein condensation*

3.1.1. Gauge symmetry breaking

3.1.2. Representative statistical ensemble

3.1.3. Equation for condensate function

3.1.4. Size and shape instability

3.1.5. Elementary collective excitations

3.2. *Atomic fluctuations and stability*

3.2.1. Uniform ideal gas

3.2.2. Trapped ideal gas

3.2.3. Harmonically trapped gas

3.2.4. Interacting nonuniform systems

3.2.5. Importance of symmetry breaking

3.3. *Nonequilibrium symmetry breaking*

3.3.1. Dynamic instability of motion

3.3.2. Stratification in multicomponent mixtures

3.3.3. Generation of quantum vortices

3.3.4. Topological coherent modes

3.3.5. Nonequilibrium crossover transitions

3.4. *Pairing of fermionic atoms*

3.4.1. Harmonically trapped fermions

3.4.2. Pair formation and superfluidity

3.4.3. Pairing and symmetry breaking

3.5. *On condensation of unconserved quasiparticles*

3.5.1. Conserved versus unconserved particles

3.5.2. No condensation of self-consistent phonons

3.5.3. No condensation of generic bogolons

3.5.4. No condensation of equilibrium magnons

3.5.5. Condensation of auxiliary quasiparticles

4. Quantum dots

4.1. *Basic features*

4.2. *Shell effects in a simple model*

4.2.1. Magnetic field and shapes

4.2.2. Magnetic properties

4.3. *Two-electron quantum dot: a new paradigm in mesoscopic physics*

4.3.1. Hidden symmetries in a two-electron quantum dot

4.3.2. Center-of-mass and relative-motion Hamiltonians

4.3.3. Classical dynamics and quantum spectra

4.4. *Dimensionality effects in ground-state transitions of two-electron quantum dots*

4.4.1. First singlet-triplet transition in a two-electron quantum dot

4.4.2. Topological transitions in a two-electron quantum dot

4.4.3. Effective charge

4.5. *Symmetry breaking: mean field and beyond*

4.5.1. Theoretical approaches

4.5.2. Hartree-Fock approximation

4.5.3. Roto-vibrational model

4.5.4. Geometric transformation in a two-electron quantum dot

4.5.5. Shell structure and classical limit

4.5.6. Ground state in random phase approximation

5. Atomic nuclei

5.1. *Signatures of symmetry breaking in nuclear structure*

5.2. *Nuclear structure models and symmetry breaking phenomena*

5.2.1. Geometric collective model

5.2.2. Algebraic approach: Interaction boson model

5.2.3. Microscopic models with effective interactions

5.2.4. Cranking approach

5.3. *Symmetry breaking in rotating nuclei*

5.3.1. Symmetries

5.3.2. Shape transitions in rotating nuclei

5.3.3. Collective excitations as indicator of symmetry breaking

6. Metallic grains

6.1. *General properties*

6.2. *Pairing effects and shell structure*

6.2.1. Theoretical approaches

6.2.2. Effects of magnetic field

6.2.3. Shell effects

7. **Summary**

Acknowledgments

Appendix. Two-dimensional harmonic oscillator in a perpendicular magnetic field

References

1 Preamble

Finite quantum systems are now intensively studied, since many of their specific properties promise a variety of applications in science and technology. Two basic features of these systems are encoded in the names *quantum* and *finite*. The first adjective implies that the correct description of such systems requires the use of quantum theory. And the second adjective distinguishes these objects from macroscopic systems. Generally, the finite systems, to be considered in the review, can be called *mesoscopic*. This means that their typical sizes are intermediate between microscopic sizes, related to separate quantum particles, and macroscopic sizes characterizing large statistical systems, such as condensed matter.

Being intermediate between microscopic and macroscopic sizes, mesoscopic systems exhibit the combination of properties of both their limiting cases. On the one hand, they inherit many physical properties of large statistical systems, while, from another side, they possess a number of properties, caused by their finiteness, which are absent in large systems. Examples of finite quantum systems are trapped atoms, quantum dots, atomic nuclei, and metallic grains. Though the physical nature of these systems is very different, they possess a variety of common properties caused by the fact that all of them are quantum and finite.

One should not confuse spontaneous symmetry breaking occurring under phase transitions in bulk matter and the more general notion of symmetry changes that can happen in finite systems. In the latter, it is not the finite-size corrections to extensive quantities, which are usually small, that are of interest, but the symmetry changes that result not in corrections, but in the effects principally distinguishing finite systems from bulk matter. For instance, though traps can house quite a number of atoms, but the spectrum of elementary excitations in traps is principally different from that in infinite condensed matter. The long-wave spectrum of trapped atoms is discrete and strongly dependent on the trap shape and its symmetry. These effects are described in Sec. 3.1. Moreover, despite that a trap can contain a number of atoms, the trap symmetry is crucially important for defining the stability of the system as a whole in the case of dipolar or attractive interactions, as is explained in Sec. 3.2. So, it would be wrong to identify trapped atoms with an infinite system in thermodynamic limit.

Throughout the review, we stress the similarity of physical effects in different finite systems. Thus, the long-wave spectrum of collective excitations for trapped atoms is practically the same as that for atomic nuclei and similar to the spectrum for quantum dots. The description of rotating Bose-Einstein condensates is analogous to that of rotating nuclei or quantum dots in magnetic fields. The pairing effects for trapped fermionic atoms are almost the same as these effects in atomic nuclei or metallic grains. Geometric shape transitions happen for atomic nuclei as well as for trapped atoms. We repeatedly emphasize the common physical features and analogous mathematical treatment of different finite systems.

The general feature of the finite systems, considered in the review, is their mesoscopic size, being intermediate between microscopic and macroscopic scales. Such systems possess the combination of the properties of both their limiting cases. From one side, they can inherit symmetry properties, related to large systems. But from another side, they can exhibit symmetry changes typical of only finite systems, e.g., shape and orientation

transitions accompanied by symmetry variations.

Thus, trapped atoms may carry features typical of many-particle systems and demonstrate Bose-Einstein condensation or superconducting fermion pairing. The typical size of a trapped atomic cloud can contain from just a few up to millions of atoms. The size of a quantum dot can be comparable to that of a trapped atomic cloud, though the number of particles, as is considered in the review, is varied between two to the order of ten. The recent progress in semiconductor technology has made it feasible to fabricate and probe such confined systems at different values of magnetic field and at low temperatures, close to those typical of trapped atoms. Quantum dots in an external magnetic field, atomic nuclei, and rotating trapped atoms share a lot of common physics as well as mathematics, despite rather different numbers of constituent particles.

It is remarkable that different finite systems, housing quite different numbers of particles, nevertheless, can exhibit similar physical features. For examples, shell effects exist in quantum dots with a small number of electrons, as well as in atomic nuclei with many nucleons, and even in metallic grains with a rather large number of particles. Shell effects are caused by the degeneracy of quantum spectra, which, for quantum dots, can be controlled by external magnetic fields. Contrary to this, the similar phenomenon can only be observed in rotating nuclei but not controlled. Therefore, the comparison of analogous effects in different systems may help to shed light on the physics of atomic nuclei, quantum dots, and metallic grains in external magnetic fields.

Magic numbers, associated with the degeneracy of quantum spectrum, define the shape symmetry and shape changes from spherical to deformed shapes, as is discussed for quantum dots in Sec. 4.2.1 and 4.5.5, and for rotating nuclei in Sec. 5.1. Such a symmetry breaking phenomenon, occurring in very different systems, is due to the finite number of the constituent particles.

The main aim of this review is to consider the specific symmetry properties of mesoscopic quantum systems, emphasizing their similarities. In Sec. 2, we briefly recall the symmetry properties of macroscopic systems and discuss their difference from those of finite systems. The characteristic features, due to the system finiteness, are described on the general level, which stresses their common origin. In the following sections, these typical properties are illustrated for several particular finite systems: for trapped atoms in Sec. 3, for quantum dots in Sec. 4, for atomic nuclei in Sec. 5, and for metallic grains in Sec. 6. Section 7 concludes, summarizing the main points.

In many places, we mention exact mathematical results and theorems. In doing this, we do not overload the review by the corresponding proofs and we do not enumerate all conditions required for the validity of the theorems. We remember the saying of Arnold [1] comparing mathematics and physics: "mathematics have always played absolutely subordinate role, like that of orthography or even calligraphy in poetry". At the same time, we know that understanding mathematical facts in a number of situations is crucial. Therefore, mentioning mathematical results, we always provide the references, where all details can be found.

Throughout the paper, when this does not yield confusion, the system of units is used where the Planck constant $\hbar = 1$ and the Boltzmann constant $k_B = 1$.

2 Symmetry Breaking

The mathematically rigorous meaning of symmetry is usually associated with infinite systems. Therefore, we start this section with the basic notions of symmetry as applied to such macroscopic systems and then pass to finite systems, explaining what they inherit from the former and what appears to be principally different.

2.1 Symmetry in macroscopic systems

2.1.1 Symmetry of thermodynamic phases

A physical system, composed of the same elements, say, atoms or molecules, can exhibit, under special conditions, several thermodynamic phases differing by their properties, among which one of the most important is the system symmetry. Thus, water can be gas, liquid, or solid in different regions of the pressure-temperature plane. Likewise, a solid can show phases differing in their crystalline structure. Magnetic materials can be in paramagnetic or magnetized states. Ferroelectrics can be in ferroelectric phase, having dipole moment, or in paraelectric phase, without such a dipole moment. Liquid helium-4 can be superfluid or normal. Each thermodynamic phase, as a rule, can be characterized by its symmetry. The symmetry property implies invariance under some transformations. The group of the related transformations forms a symmetry group. There are many good books on group theory, such as the classical monographs [2, 3]. Various applications of group theory to physical systems can be found in several books, e.g., [4–6].

One distinguishes the symmetry of the system Hamiltonian, or Lagrangian, from the symmetry of the order parameter. The system can be described by the same Hamiltonian, or the same Lagrangian, invariant under a general group of transformations, while its thermodynamic phases are characterized by the order parameters associated with some subgroups of the general group.

The order parameters are the quantities specifying thermodynamic phases and qualitatively distinguishing between the latter. For instance, magnetization \mathbf{M} is the order parameter distinguishing ferromagnet, with nonzero \mathbf{M} , from paramagnet, with $\mathbf{M} \equiv 0$. Similarly, dipole moment \mathbf{P} distinguishes ferroelectric, with nonzero \mathbf{P} , from paraelectric, with $\mathbf{P} \equiv 0$. A particle density $\rho(\mathbf{r})$ distinguishes between a crystal, with the density $\rho(\mathbf{r} + \mathbf{a}) = \rho(\mathbf{r})$, which is periodic with respect to lattice vectors \mathbf{a} , and a liquid, with the uniform density $\rho(\mathbf{r}) = \rho = \text{const.}$ Different crystalline structures are distinguished by the periodicity of the particle density over different lattice vectors. Generally, an order parameter can be a scalar, vector, or a tensor. Order parameters for particular substances have been appearing in different mean-field theories, such as the Weiss [7] mean-field theory of ferromagnetism. The order parameter, as a general concept, was defined by Landau in a series of papers starting with [8]. All these papers are reprinted in [9].

The qualitative change of the order parameter, in particular, of its symmetry, is associated with phase transitions. The common classification of phase transitions, accepted nowadays, distinguishes two main types of them. *First-order* phase transitions are characterized by a discontinuous jump of the order parameter at the transition point, for instance, as density in the crystal-liquid transition. *Second-order* phase transitions, also called critical phenomena, correspond to a continuous change of the order parameter at the critical point between an ordered phase, where it is non-zero, and a disordered phase,

where it is zero. The typical case is the ferromagnet-paramagnet phase transition, with a continuous change of magnetization. There is also the third kind of transitions, called *crossover*, when the order parameter varies continuously, but does not become exactly zero in the region corresponding to an almost disordered phase. This can be illustrated by the behavior of magnetization of a ferromagnet in the presence of an external magnetic field. Then the magnetization in the paramagnetic region is nonzero. Phase transitions in macroscopic systems are described in textbooks on statistical mechanics, e.g., [10–12]. There are several books entirely devoted to phase transitions, e.g., [13–16].

In finite systems, the majority of transitions are crossovers. However, when the number of particles in the finite system is sufficiently large, the crossover is so sharp that it becomes practically non-distinguishable from either first or second order phase transition.

When the system Hamiltonian enjoys a symmetry characterized by some general symmetry group, but the system is stable for a phase with the order parameter whose symmetry corresponds to a subgroup of the general group, this is termed *spontaneous symmetry breaking*. The majority of phase transitions are accompanied by such spontaneous breaking of symmetry. Also, the symmetry breaking at phase transitions is related to the change of state entanglement [17–19] and of entanglement production [20, 21].

2.1.2 Landau phase-transition theory

A very simple and general way of describing spontaneous symmetry breaking is provided by the Landau theory of phase transitions [8, 9]. Landau theory is based on the assumption that the system free energy F is an analytic function of the order parameter, and hence, can be expanded in powers of the latter. This, taking for illustration a scalar order parameter η , yields

$$F(\eta) = F(0) + a_2\eta^2 + a_3\eta^3 + a_4\eta^4, \quad (2.1)$$

where a_2 and a_3 can be of different sign, while $a_4 > 0$. The structure of the free energy is prescribed by the symmetry properties of the system. Minimizing the free energy with respect to the order parameter defines the stable physical state.

When there is inversion symmetry, so that $F(-\eta) = F(\eta)$, then $a_3 = 0$. In this case, for $a_2 > 0$, a disordered thermodynamic phase is stable, corresponding to zero order parameter $\eta = 0$. But for $a_2 < 0$, an ordered phase is stable with $\eta \neq 0$. The order-disorder phase transition is continuous, that is, of second order. When there is no inversion symmetry, and $a_3 \neq 0$, then the order-disorder phase transition occurs discontinuously, being a first-order phase transition.

The classification of phase transitions, based on the behaviour of the order parameter, onto first-order discontinuous and second-order continuous transitions, following from the Landau scheme, is now widely accepted, replacing the cumbersome Ehrenfest [22] classification, based on the behaviour of derivatives of thermodynamic potentials with respect to thermodynamic variables.

The Landau approach can be used for finite as well as for zero temperatures. The order parameter can also be a vector or a tensor. The theory can be applied for single-component and for multicomponent systems. Among the merits of Landau theory is its ability to predict symmetry changes occurring at phase transitions. An efficient symmetry group analysis has been developed for this purpose [23–26].

The form of the free energy (2.1) assumes that a uniform equilibrium system is treated, since the order parameter does not depend on spatial variables and time. The generalization to the nonuniform and, generally, nonequilibrium, case is done by the Ginzburg-Landau [9, 27, 28] approach, where the order parameter $\eta = \eta(\mathbf{r}, t)$ is considered as a function varying in space and time. The Ginzburg-Landau functional

$$G[\eta] = \int [F(\eta) + D(\nabla\eta)^2] d\mathbf{r} \quad (2.2)$$

generalizes the Landau free energy (2.1). The order parameter function $\eta(\mathbf{r}, t)$ is defined through the variational derivative of $G[\eta]$ over this function.

The Landau approach, as any mean-field approximation, becomes ineffective in the vicinity of a critical point. Thus, the theory predicts universal critical indices of the mean-field type, independently of the system details and dimensionality. The reason for the failure of Landau theory to correctly describe the peculiarities of the critical behaviour is caused by its inadequate treatment of fluctuations of the order parameter around its mean value. In Landau theory, these fluctuations are assumed to be Gaussian in all cases. The deviations of these fluctuations from the Gaussian character are usually stronger for lower dimensionalities and for order parameters with fewer components [26].

Even though Landau theory is designed to be applied to continuous phase transitions, ironically, it cannot even provide a sufficient condition whether the transition is continuous. It has been observed in some cases that Landau theory predicts a continuous phase transition, while in reality the transition is discontinuous due to fluctuations.

Fluctuations need to be taken into account beyond the Gaussian approximation in order to obtain the correct critical behaviour. This is done by applying renormalization group approach to Ginzburg-Landau-Wilson functional [15, 29–33]. This theory makes it possible to calculate accurate values of critical indices. In the frame of this approach, in order for a phase transition to be continuous, there should exist a stable renormalization-group fixed point, and the transition region should be within the attraction domain of that fixed point.

2.1.3 Symmetry and conservation laws

The existence of symmetries in a system is always related to some conservation laws. For example, let us consider the conservation of momentum. For quantum systems, this implies that the operator of momentum $\hat{\mathbf{P}}$ commutes with the system Hamiltonian:

$$[\hat{\mathbf{P}}, H] = 0, \quad \hat{\mathbf{P}} \equiv \int \psi^\dagger(\mathbf{r})(-i\nabla)\psi(\mathbf{r}) d\mathbf{r}. \quad (2.3)$$

Here and in what follows, the field operator $\psi(\mathbf{r}, t)$ is assumed to be in the Heisenberg representation, but the explicit dependence on time, for brevity, is not shown, when this does not lead to confusion. Under condition (2.3), the Hamiltonian is invariant with respect to the translation transformations characterized by the operators

$$\hat{T}(\mathbf{r}) = \exp(i\hat{\mathbf{P}} \cdot \mathbf{r}), \quad \hat{T}^+(\mathbf{r}) = \exp(-i\hat{\mathbf{P}} \cdot \mathbf{r}), \quad (2.4)$$

forming a unitary group, so that

$$\hat{T}^+(\mathbf{r})H\hat{T}(\mathbf{r}) = H. \quad (2.5)$$

This is called *translation symmetry* or *translation invariance*, which is just another side of the momentum conservation (2.3).

For an equilibrium system, under translation symmetry, one has

$$\begin{aligned} \left\langle \prod_{i=1}^m \psi^\dagger(\mathbf{r}_i + \mathbf{r}) \prod_{j=1}^n \psi(\mathbf{r}_j + \mathbf{r}) \right\rangle &= \\ &= \left\langle \prod_{i=1}^m \psi^\dagger(\mathbf{r}_i) \prod_{j=1}^n \psi(\mathbf{r}_j) \right\rangle , \end{aligned} \quad (2.6)$$

with \mathbf{r} being an arbitrary spatial vector. In particular, the density does not depend on the spatial variable:

$$\rho(\mathbf{r}) \equiv \langle \psi^\dagger(\mathbf{r}) \psi(\mathbf{r}) \rangle = \langle \psi^\dagger(0) \psi(0) \rangle , \quad (2.7)$$

which means that the system is always uniform. That is, the order parameter is trivial, corresponding to a disordered phase. Under these conditions, there can be no periodic crystalline matter.

Another example is the spin conservation, when the spin operator $\hat{\mathbf{S}}$ commutes with the system Hamiltonian,

$$[\hat{\mathbf{S}}, H] = 0 , \quad (2.8)$$

as it happens for the Heisenberg model. Under condition (2.8), there is *spin-rotation symmetry*. Then, for any equilibrium system, the average spin is exactly zero,

$$\langle \hat{\mathbf{S}} \rangle = 0 , \quad (2.9)$$

hence, magnetic moment is always zero. This means that magnetism is absent.

One more example is the conservation of the number of particles, when the number operator \hat{N} commutes with the system Hamiltonian:

$$[\hat{N}, H] = 0 , \quad \hat{N} \equiv \int \psi^\dagger(\mathbf{r}) \psi(\mathbf{r}) d\mathbf{r} . \quad (2.10)$$

Then the Hamiltonian is invariant under the global gauge transformations

$$\hat{U}_\varphi = e^{i\varphi \hat{N}} , \quad \hat{U}_\varphi^\dagger = e^{-i\varphi \hat{N}} , \quad (2.11)$$

where φ is a real number, so that

$$\hat{U}_\varphi^\dagger H \hat{U}_\varphi = H . \quad (2.12)$$

Transformations (2.11) form the gauge group that is the unitary group $U(1)$. Under this *global gauge symmetry*, one gets

$$\left\langle \prod_{i=1}^m \psi^\dagger(\mathbf{r}_i) \prod_{j=1}^n \psi(\mathbf{r}_j) \right\rangle = 0 \quad (m \neq n) . \quad (2.13)$$

Consequently, under this condition, there can be no anomalous averages, hence, no Bose-Einstein condensation and no superconductivity.

The above relations between conservation laws, symmetry properties, and order parameters are exact; their derivation can be found in literature [16, 34].

2.1.4 Thermodynamic limit and symmetry

As we know, phase transitions are usually accompanied by spontaneous symmetry breaking. However, the relations of the previous subsection are valid for any finite system, with the number of particles N in a given volume V . Strictly speaking, no symmetry breaking of the type considered above can occur in a finite system. This can happen only in thermodynamic limit that corresponds to the limiting procedure

$$N \rightarrow \infty, \quad V \rightarrow \infty, \quad \frac{N}{V} \rightarrow \text{const}. \quad (2.14)$$

To give a mathematically accurate definition of spontaneous symmetry breaking, one has to consider thermodynamic limit (2.14). This is a principal point to be kept in mind.

The structure of the space of microstates and of statistical states can be principally different for finite and infinite systems. Suppose the space of microstates for a finite system is a Hilbert space \mathcal{H} that is invariant with respect to a symmetry group G . And let the observable quantities are given by the statistical averages $\langle \hat{A} \rangle$ of self-adjoint operators from the algebra of local observables defined on \mathcal{H} . In thermodynamic limit, the unique space \mathcal{H} can split into a direct sum of spaces,

$$\mathcal{H} \rightarrow \bigoplus_{\nu} \mathcal{H}_{\nu}, \quad (2.15)$$

where each space \mathcal{H}_{ν} is invariant only with respect to a subgroup G_{ν} of the total group G . Respectively, the observables become the convex linear combinations

$$\langle \hat{A} \rangle \rightarrow \sum_{\nu} \lambda_{\nu} \langle \hat{A} \rangle_{\nu} \quad (2.16)$$

over ergodic states [35, 36].

The underlying idea of symmetry breaking is to incorporate in the process of taking thermodynamic limit such constraints that would lead not to the state combinations (2.16), but to a desired particular pure state $\langle \hat{A} \rangle_{\nu}$.

2.1.5 Methods of symmetry breaking

When the system Hamiltonian is invariant under transformations related to some symmetry group, the correct description of an ordered phase requires that the system symmetry be somehow broken. There exist several methods realizing the procedure of spontaneous symmetry breaking.

The oldest such a method is the use of the mean-field approximation when the order parameter, with the necessary symmetry properties, is explicitly introduced into the system Hamiltonian. The Weiss mean-field theory of ferromagnets [7] and Landau mean-field theory of phase transitions [8, 9] are the well known examples of this kind.

Another way of symmetry breaking is by imposing external potentials with the symmetry lower than that of the Hamiltonian. Kirkwood [37] suggested this method for lifting the degeneracy connected with the momentum conservation that results in the constant density (2.7). According to Kirkwood, in order to describe crystals, one has to impose external forces fixing in space the crystal position and orientation. Then the ambiguity in

the definition of density is removed and the latter acquires the periodicity of a crystalline phase [37].

Bogolubov [34,38] developed a general mathematical methodology of symmetry breaking by means of infinitesimal external sources. In this method, one adds to the system Hamiltonian an additional term lowering the symmetry. Thus, instead of the initial Hamiltonian H , one forms [34,38]

$$H_\varepsilon \equiv H + \varepsilon \hat{\Gamma} , \quad (2.17)$$

where the operator source $\hat{\Gamma}$ has a lower symmetry than H and $\langle \hat{\Gamma} \rangle \propto N$. Observable quantities, corresponding to operators \hat{A} from the algebra of local observables are defined through the double limit

$$\langle \hat{A} \rangle \equiv \lim_{\varepsilon \rightarrow 0} \lim_{N \rightarrow \infty} \langle \hat{A} \rangle_\varepsilon , \quad (2.18)$$

where the statistical average $\langle \hat{A} \rangle_\varepsilon$ is calculated with Hamiltonian (2.17). The average in the left-hand side of Eq. (2.18) is called *quasiaverage*.

By this construction, it is clear that the role of the infinitesimal source is just to break the symmetry, being removed afterwards. It is crucially important that the limits here do not commute. The thermodynamic limit has to be necessarily accomplished before the limit $\varepsilon \rightarrow 0$. This is connected with the fact that spontaneous symmetry breaking can occur only in thermodynamic limit, but cannot happen in a finite system. The described way of symmetry breaking is termed the *method of Bogolubov quasiaverages*.

The double limit (2.18) can be replaced by a single limit in the *method of thermodynamic sources*, or *method of thermodynamic quasiaverages*, [39,40]. Then, instead of Hamiltonian (2.17), one introduces the Hamiltonian

$$H_N \equiv H + \frac{1}{N^\alpha} \hat{\Gamma} \quad (0 < \alpha < 1) , \quad (2.19)$$

with the same source term $\hat{\Gamma}$, but with $1/N^\alpha$ instead of ε . The observables are defined through the single thermodynamic limit

$$\langle \hat{A} \rangle \equiv \lim_{N \rightarrow \infty} \langle \hat{A} \rangle_N , \quad (2.20)$$

where the average $\langle \hat{A} \rangle_N$ is calculated with Hamiltonian (2.19). The power $\alpha \in (0,1)$ in Eq. (2.19) is such that the value $1/N^\alpha$ would tend to zero slightly slower than $1/N$. This guarantees that the Hamiltonian symmetry be broken. If the symmetry breaking source would go to zero faster, it would not be able to break the symmetry.

In the process of symmetry breaking, one passes from the initial state of microstates \mathcal{H} to a state \mathcal{H}_ν corresponding to a phase with broken symmetry. Therefore, the straightforward way of symmetry breaking would be by calculating the averages not over the total space \mathcal{H} , but directly over the restricted space \mathcal{H}_ν . So that the statistical states, characterized by a statistical operator $\hat{\rho}$, would be given by the averages

$$\langle \hat{A} \rangle_\nu = \text{Tr}_{\mathcal{H}_\nu} \hat{\rho} \hat{A} , \quad (2.21)$$

involving the trace over \mathcal{H}_ν . This way is called the *method of restricted trace* [41].

As is clear, any method of symmetry breaking requires to impose some additional constraints. The ways of imposing the latter can be different. Except the methods described above, it is possible to invoke other ways, such as asymptotically weakly breaking commutation relations for operators or complimenting the equations of motion for correlation functions and Green functions by additional symmetry conditions. Different methods of symmetry breaking are discussed in review articles [42, 43].

2.2 Symmetry in finite systems

2.2.1 Asymptotic symmetry breaking

As is explained above, the concept of symmetry breaking can be rigorously defined only for macroscopic systems in thermodynamic limit. Then in what sense could one mean symmetry breaking in finite systems? It is evident that for small systems consisting of just a few particles, it is impossible to correctly define the notion of symmetry related to macroscopic systems. However, our aim here is to study *mesoscopic* systems, whose number of particles N is large, though finite. For $N \gg 1$, it is possible to define *asymptotic symmetry*, in the sense that it is approximate, but becomes exact in the limit $N \rightarrow \infty$.

In this asymptotic sense, it is admissible to consider phase transitions in finite systems. In these systems, as we know, there are no such strictly defined phase transitions as melting, magnetization, Bose-Einstein condensation, or superconductivity. But there are the related crossover transitions, which become more and more sharp as the number of particles increases. The thermodynamic characteristics, such as susceptibilities, in the case of a crossover, do not diverge, as at the critical point of a second-order phase transition. But the peaks of these characteristics, at the critical point, grow larger with increasing N and can become divergent in the limit of $N \rightarrow \infty$. In that sense, one can define asymptotic phase transitions and the related asymptotic symmetry changes.

How large should be the number of particles N for imitating well thermodynamic phases and phase transitions? As many computer simulations show, the systems of about 100 (or even 10) particles already form a kind of thermodynamic phases with the related approximate symmetries and also demonstrate the symmetry changes associated with phase transitions [44].

2.2.2 Effective thermodynamic limit

To check what type of asymptotic symmetry is realized in the system, one needs to resort to thermodynamic limit. The definition of thermodynamic limit (2.14) requires that the number of particles N be given and the system volume V be fixed. The number of particles is understood as the average number $N = \langle \hat{N} \rangle$. Therefore limit (2.14) is well defined even if the number of particles in microscopic reactions is not conserved, provided that the average number N is given.

A complication in understanding thermodynamic limit can arise when the system volume is not fixed. This happens when the system of finite number of particles is confined in a potential that extends to infinity. For instance, N atoms, ions, or other particles are trapped in a confining potential, e.g., a harmonic potential. How then could one understand thermodynamic limit?

It is possible to give a general definition of thermodynamic limit as follows [45,46]. Let A_N be an *extensive* observable quantity for a system with N particles. Then an effective thermodynamic limit is defined as

$$N \rightarrow \infty, \quad A_N \rightarrow \infty, \quad \frac{A_N}{N} \rightarrow \text{const}. \quad (2.22)$$

Recall that a quantity is extensive if it is proportional to N for large $N \gg 1$. Limit (2.22) does not depend on what observable is taken, provided it is an extensive observable. When the system volume V is prescribed, then an extensive observable quantity is also proportional to V . In the latter case, the definition of thermodynamic limit (2.22) reduces to the standard form (2.14). The effective thermodynamic limit (2.22) shows how one should vary the parameters of a trapping potential under the condition $N \rightarrow \infty$.

2.2.3 Fluctuations and thermodynamic stability

For macroscopic systems, there are the well known conditions that are required for thermodynamic phases to be stable, see, e.g., [12,47]. Generally, such conditions are expressed as inequalities for susceptibilities that are defined to be positive and finite.

It is a common understanding that phase transitions occur when one phase becomes unstable, because of which the system changes to another phase. Respectively, phase transition lines are called stability boundaries [12,47–49].

In order that an observable quantity would be measurable, it is necessary that its fluctuations would be smaller than the observable itself, which is just the requirement for the validity of the law of large numbers [12]. A susceptibility characterizes the fluctuations of an observable quantity and is represented through the variance of the related operator of the observable. Therefore, for an extensive observable, the ratio of the related variance, hence, susceptibility, over the number of particles has to be finite, provided the system is in equilibrium.

This is in agreement with the general definition of stable states as such states at which a system, being perturbed, returns to its initial state [50]. However, at a critical point, the relaxation time becomes infinite, which means that the system can never relax to the unperturbed state [13].

Also, one should distinguish real physical systems from cartoon models. This, for instance, concerns the case of the XY model in two dimensions, whose magnetic susceptibility diverges below the Kosterlitz-Thouless phase transition [51,52].

In real life, purely two-dimensional systems do not exist. Any, even the thinnest membrane, always possesses a finite, though maybe small, thickness. And the three-dimensional XY model enjoys a finite magnetic susceptibility everywhere except the critical point. The crossover from a three-dimensional XY model to a two-dimensional one can be done by reducing one of the spatial dimensions to zero. This crossover has been studied in several papers. A detailed analysis of such a limit can be found in [53]. It is shown that, when reducing the role of one of the spatial dimensionalities, some of the observable quantities of a three-dimensional XY model, for instance, energy and specific heat, do tend to the expressions that would correspond to the two-dimensional XY model. But the susceptibility is always finite below the critical point, and becomes infinite only in the unphysical limit of purely two-dimensional case.

So, the susceptibilities of real equilibrium systems, outside of the critical points, are always finite, which is confirmed by all existing experiments.

Susceptibilities are proportional to the variances of some operators of observables. It is therefore possible to represent the general form of stability conditions as follows. Let \hat{A} be an operator from the algebra of local observables. The operator variance

$$\text{var}(\hat{A}) \equiv \langle \hat{A}^2 \rangle - \langle \hat{A} \rangle^2 \quad (2.23)$$

characterizes the fluctuations of the related observable. By definition, the variance is non-negative, that is, either positive or zero. For macroscopic systems, extensive observables can be measured when their fluctuations do not diverge, in thermodynamic limit, faster than N . Thus, a statistical system is *thermodynamically stable* when the fluctuations of its observables are *thermodynamically normal*, such that

$$0 \leq \frac{\text{var}(\hat{A})}{N} < \infty \quad (2.24)$$

for any N , including thermodynamic limit.

As examples of susceptibilities that are expressed through operator variances, we can mention specific heat, expressed through the variance of internal energy, and isothermal compressibility, expressed through the variance of the number operator. Susceptibilities can diverge only at the points of phase transitions, where the system becomes unstable, which results in the change of thermodynamic phases. Condition (2.24) is to be valid everywhere outside of the phase transition points.

The same condition (2.24) should hold for finite systems. The sole difference is that the latter may require the use of thermodynamic limit in the general form (2.22). More detailed discussion of the relation between the fluctuations of observables and stability conditions can be found in classical books [12, 47] and in recent literature [54–57].

2.2.4 Equilibration in quantum systems

When ascribing a type of symmetry to a thermodynamic phase, one tacitly assumes an *equilibrium* thermodynamic phase. However, the notion of equilibrium for finite systems is essentially more complicated than that for macroscopic systems. The pivotal problem is whether a finite quantum system could equilibrate at all.

Let us consider an observable quantity, corresponding to the average

$$\langle \hat{A}(t) \rangle \equiv \text{Tr} \hat{\rho}(t) \hat{A} \quad (2.25)$$

of an operator \hat{A} from the algebra of local observables. For an isolated system, the evolution of the statistical operator is given by the equation

$$\hat{\rho}(t) = \hat{U}(t) \hat{\rho}(0) \hat{U}^\dagger(t) , \quad (2.26)$$

with the evolution operator $\hat{U}(t) = \exp(-iHt)$. Taking in the observable quantity (2.25) the trace over the eigenfunctions of the system Hamiltonian yields

$$\langle \hat{A}(t) \rangle = \sum_{mn} \rho_{mn}(0) A_{nm}(t) , \quad (2.27)$$

where

$$A_{nm}(t) \equiv A_{nm} e^{i(E_n - E_m)t}, \quad (2.28)$$

with E_n being the corresponding eigenvalues of H . The existence of an equilibrium time-independent state presupposes the existence of the time average

$$\bar{A} \equiv \lim_{\tau \rightarrow \infty} \frac{1}{\tau} \int_0^\tau \langle \hat{A}(t) \rangle dt. \quad (2.29)$$

This, assuming that the Hamiltonian spectrum is nondegenerate, can be written as

$$\bar{A} = \sum_n \rho_{nn}(0) A_{nn}. \quad (2.30)$$

However, it is evident that Eq. (2.27) is a quasiperiodic function that cannot tend to a time-independent stationary state, such as Eq. (2.30). Any given value of observable (2.27) will be reproduced after a *recurrence time* [58, 59]. Then the pivotal question arises whether it is admissible in principle to ascribe to finite quantum systems some equilibrium thermodynamic states and related symmetries. Or, in other words, how could a finite quantum system equilibrate?

The simplest way of understanding how this could happen is by assuming that the treated system is connected with a thermostat [12]. Even if there is no well defined thermostat, we have to remember that there are no absolutely isolated systems, but each system is immersed into its surrounding, being always a subsystem of a larger system. That is, each given system is always influenced by its surrounding [59, 60]. This could be the influence of uncontrollable random perturbations during the preparation period or during the system lifetime. Moreover, the notion of an absolute isolation as such is self-contradictory, since in order to check that the system is really isolated during a period of time, it is necessary to realize a series of measurements proving this, hence, influencing the system by measurement procedures [61, 62]. During sufficiently long time, even very weak random perturbations can lead to drastic changes in the system properties [63–65]. Incorporating into the system appropriate randomness, with an additional supposition that the variances of operators, representing observable quantities, are sufficiently small, it is possible to achieve equilibration in quantum systems [66–69]. Bogolubov [70] also mentioned that for rigorously proving the existence of equilibration in quantum systems it may be necessary to invoke thermodynamic limit, similarly to the use of this limit for rigorously defining the system symmetry and symmetry breaking [70]. For confined systems, thermodynamic limit should be understood in the general sense (2.22).

Even if one assumes an idealized situation of an isolated system, the latter spends on average most of the time in a quasiequilibrium state that can be described by a Gibbs ensemble called the representative Gibbs ensemble [43, 71–74]. Generally, finite quantum systems can equilibrate to stationary states that live sufficiently long for accomplishing with them the desired measurements. More references on the equilibration of finite quantum systems can be found in the recent review articles [75–78].

2.2.5 Convenience of symmetry breaking

Sometimes one says that, since finite systems do not experience exact symmetry breaking, there is no necessity of such a breaking at all, but it is possible to deal with the system

of the same symmetry for any thermodynamic parameters, treating a phase transition just as a sharp crossover. As a justification of this statement, one says that in computer simulations, such as Monte Carlo, one does not break any symmetry but can observe a kind of phase transitions.

This is certainly correct for computer simulations that always deal with a finite number of particles. Then, instead of first or second order phase transitions, one always observes crossovers. But, as has been stressed above, for a large number of particles $N \gg 1$ such crossovers become extremely sharp, closely imitating phase transitions.

One more complication in computer simulations is the necessity of imposing additional constraints in order to get nontrivial order parameters, as far as for finite systems these parameters, as is explained above, are always the same due to conservation laws.

Moreover, computer simulations, accomplished for a finite system, are always complemented by finite-size scaling allowing for an extension of the finite-volume results to effectively infinite system. Only with such a scaling, accounting for finite-size corrections, one is able to extract correct system characteristics, especially in the vicinity of phase transitions.

When one is interested in developing an analytical theory for finite systems exhibiting phase transitions, then, trying to describe the latter without symmetry breaking, results in extremely complicated calculations that are often even not accomplishable. While, taking into account symmetry breaking greatly simplifies calculations. Owing to the fact that, for a large number of particles, crossovers become so sharp that are practically non-distinguishable from phase transitions, it is reasonable to invoke symmetry breaking for describing ordered phases.

Thus, though for finite systems one could employ computer simulations without symmetry breaking, but this is extremely unpractical for analytical description of systems with phase transitions. Dealing with mesoscopic systems, for which $N \gg 1$, it is a wise idea to explicitly employ symmetry breaking, understanding that, strictly speaking, it is asymptotic symmetry breaking, as is defined above.

2.3 Geometric symmetry transformations

2.3.1 Role of shape symmetry

There exists a type of symmetry transformation that is specific for finite systems. This is shape symmetry breaking, when a finite system, under varying external or internal parameters, exhibits the change of its shape. This change can be spontaneous, in the sense that the shape form is not imposed from outside, but the system acquires the chosen form because it is energetically profitable.

In those cases when the finiteness of the system becomes important, the system shape may also play an important role. This role becomes crucial in several situations.

First of all, a system, composed of the same kind of particles, can be either stable or unstable depending on its shape and size. For instance, this concerns trapped atoms with attractive interactions and atoms with dipolar forces, which will be considered in the following section. Atomic nuclei is another example, where the shape is defined by the internal properties.

When the system shape is not prescribed by external potentials, but can be self-

organized, then the effect of spontaneous shape symmetry breaking can happen, as for rotating atomic nuclei.

Another characteristic of a finite system, where its shape starts playing role, is the spectrum of collective excitations. Elementary collective excitations in a finite system display two principally different types of behavior. For short wavelengths of such excitations, such that the wavelength $\lambda \ll L$ is much shorter than the characteristic system size L , respectively, when the excitation wave vector k is such that $kL \gg 1$, then these excitations are of the same kind as they would be in an infinite system. The spectrum of these short-wavelength excitations is usually continuous with respect to the wave vector. The form of the spectrum changes under phase transitions accompanied by symmetry breaking [26].

But, as soon as the wavelength is comparable or larger than the system size, hence $\lambda > L$, then the excitation spectrum becomes discrete and strongly dependent on the system shape. Then the shape symmetry is as important as the symmetry of the thermodynamic phase.

Examples, illustrating the influence of the system shape on the properties of collective excitations, will be given below for several finite quantum systems, such as trapped atoms, quantum dots, and atomic nuclei. Another example is provided by the behavior of spin waves in finite magnetic samples, which has been studied by Mills et al. [79–83].

Finally, in finite quantum systems there appear quantized collective excitations of the type that does not exist in macroscopic systems. This is because particles are bounded inside a finite system. The energy spectrum of bounded particles is discrete. The eigenfunctions, corresponding to these discrete energy states, form collective topological modes. The latter are termed topological, since the related wave functions and, respectively, particle densities display different spatial shapes, with different numbers of zero. The topological modes are principally different from elementary collective excitations. The latter correspond to small oscillations around a given topological mode and are described by linearized equations. While the topological modes are described by nonlinear equations. Explicit illustrations of these points will be given in the following sections.

2.3.2 Geometric shape transitions

Probably, the first model of shape transitions was suggested by Jahn and Teller for molecules. The Jahn-Teller effect, sometimes also known as Jahn-Teller distortion, describes the geometrical distortion of non-linear molecules under certain situations. This electronic effect was described by Jahn and Teller using group theory. They showed that orbital non-linear spatially degenerate molecules cannot be stable [84]. This essentially states that any non-linear molecule with a spatially degenerate electronic ground state will undergo a geometrical distortion that removes that degeneracy, because the distortion lowers the overall energy of the complex. This effect has been found to occur for a number of substances in chemistry and solid-state physics [85]. Similar shape transitions happen for some nuclei [86], for which different phenomenological approaches and models have been suggested. Because of the occurrence of such geometric distortions in a wide variety of substances and because of the special role of shape transitions for finite quantum systems, we delineate below the main ideas of the effect.

It is important to stress that in their original paper [84] Jahn and Teller studied a

molecule, that is, exactly a finite system, but not an infinite crystal. The Jahn-Teller distortion of a finite system necessarily results in its shape change, usually accompanied by a change of shape symmetry. The application of the Jahn-Teller effect to describing the shape and symmetry changes in molecules has been expounded in many textbooks, for instance, in [87, 88].

And only later the Jahn-Teller effect started being considered for infinite crystals. In both these cases, the physics of the effect is the same, being related to the Jahn-Teller distortion, which, for bulk crystals, leads to the symmetry variation of the crystalline lattice, while for finite systems, to their shape change. The Jahn-Teller effect for finite systems, such as molecules and clusters, has been intensively studied and is described in voluminous literature.

There exists the well known term *finite Jahn-Teller systems*. Numerous articles are devoted to symmetry changes in such finite Jahn-Teller systems, as molecules and clusters, where the molecule or cluster distortion changes their shape symmetry, which is called *geometric transformation* [89–92].

The shape variations of molecules, caused by the distortion of their structure, are described in a number of textbooks [93–96].

The common physical origin of the Jahn-Teller effect in finite and infinite systems is expounded in detail in numerous literature, for instance, in the books [97, 98].

As can be inferred from the cited literature, two principal mechanisms govern the physics of finite Jahn-Teller systems: *tunneling of particles between different orbitals* and the *coupling of these particles with phonons* [85, 86, 89–92]. It is exactly these mechanisms that lead to the system distortion. The fact that such a distortion results in the changes in the symmetry shapes of molecules is rather evident and numerous examples can be found in the cited literature. As the simplest illustration, imagine that a finite system enjoys cubic structure. The distortion of the atomic locations in the cube can easily result in the structures possessing either orthorhombic, or tetragonal, or rhombohedral, or triclinic symmetry [93–96].

In order to show how the distortion arises, due to the basic mechanisms of *orbital tunneling* and *atom-phonon coupling*, let us consider a system of N particles, say atoms, that interact with each other through an interaction potential $\Phi(\mathbf{r})$ and are confined in a finite volume by means of a confining potential $U(\mathbf{r})$. The related microscopic Hamiltonian is

$$\begin{aligned} \hat{H} = & \int \psi^\dagger(\mathbf{r}) \left[-\frac{\nabla^2}{2m} + U(\mathbf{r}) \right] \psi(\mathbf{r}) d\mathbf{r} + \\ & + \frac{1}{2} \int \psi^\dagger(\mathbf{r}) \psi^\dagger(\mathbf{r}') \Phi(\mathbf{r} - \mathbf{r}') \psi(\mathbf{r}') \psi(\mathbf{r}) d\mathbf{r} d\mathbf{r}', \end{aligned} \quad (2.31)$$

where $\psi(\mathbf{r})$ are the field operators satisfying either Bose or Fermi commutation relations. The particle statistics is not important for what follows. Assume that, as it is common for chemical molecules or solid clusters, there are in the system preferable atomic locations denoted by a set $\{\mathbf{r}_j\}$, with $j = 1, 2, \dots, N$. Due to the confining nature of the potential $U(\mathbf{r})$, the eigenproblem

$$\left[-\frac{\nabla^2}{2m} + U(\mathbf{r}) \right] \psi_n(\mathbf{r} - \mathbf{r}_j) = E_{nj} \psi_n(\mathbf{r} - \mathbf{r}_j) \quad (2.32)$$

defines the localized atomic orbitals $\psi_n(\mathbf{r}-\mathbf{r}_j)$ with a discrete spectrum labeled by a multi-index n pertaining to a discrete manifold. The orbitals with different indices n possess different spatial symmetries. The field operators can be expanded over the localized orbitals as

$$\psi(\mathbf{r}) = \sum_{nj} c_{nj} \psi_n(\mathbf{r} - \mathbf{r}_j) , \quad (2.33)$$

with the operators c_{nj} satisfying the no-double-occupancy constraint

$$\sum_n c_{nj}^\dagger c_{nj} = 1 , \quad c_{mj} c_{nj} = 0 . \quad (2.34)$$

As is stressed above, one of the main features of finite Jahn-Teller systems is the existence of orbital tunneling. Assuming that temperature is sufficiently low allows one to take into account only a few orbitals, with the lowest energy levels of the discrete spectrum $\{E_{nj}\}$. For instance, we can take two lowest levels labeled by $n = 1, 2$. This makes it straightforward to invoke the operator transformations

$$\begin{aligned} c_{1j}^\dagger c_{1j} &= \frac{1}{2} + S_j^x , & c_{2j}^\dagger c_{2j} &= \frac{1}{2} - S_j^x , \\ c_{1j}^\dagger c_{2j} &= S_j^z - iS_j^y , & c_{2j}^\dagger c_{1j} &= S_j^z + iS_j^y , \end{aligned} \quad (2.35)$$

in which the operators S_j^α satisfy the spin commutation relations, independently from the statistics of the atomic operators c_{nj} . Since the operators S_j^α do not need to describe real spins, but obey the spin algebra, they are termed *pseudospin* operators. The inverse transformations read as

$$\begin{aligned} S_j^x &= \frac{1}{2} \left(c_{1j}^\dagger c_{1j} - c_{2j}^\dagger c_{2j} \right) , & S_j^y &= \frac{i}{2} \left(c_{1j}^\dagger c_{2j} - c_{2j}^\dagger c_{1j} \right) , \\ S_j^z &= \frac{1}{2} \left(c_{1j}^\dagger c_{2j} + c_{2j}^\dagger c_{1j} \right) . \end{aligned} \quad (2.36)$$

Such a pseudospin representation is often invoked for finite-level systems of different physical nature, e.g., for double-well optical lattices [99, 100].

Then expansion (2.33) is substituted into Hamiltonian (2.31). The arising matrix elements of the interaction potential are denoted by $A(\mathbf{r}_{ij})$, $B(\mathbf{r}_{ij})$, and $C(\mathbf{r}_{ij})$, where $\mathbf{r}_{ij} \equiv \mathbf{r}_i - \mathbf{r}_j$. One introduces the notation for the average potential energy per atom

$$E_0 \equiv \frac{1}{2N} \sum_{nj} \langle nj | U | nj \rangle , \quad (2.37)$$

where $|nj\rangle$ is the corresponding orbital ψ_{nj} , for average kinetic energy per particle

$$\frac{p_j^2}{2m} \equiv \frac{1}{2} \sum_n \left\langle nj \left| \left(-\frac{\nabla^2}{2m} \right) \right| nj \right\rangle , \quad (2.38)$$

and for the orbital tunneling frequency

$$\Omega_j \equiv E_{2j} - E_{1j} + \sum_i C(\mathbf{r}_{ij}) . \quad (2.39)$$

As a result, Hamiltonian (2.31) reduces to

$$\begin{aligned} \hat{H} = E_0 N + \sum_j \left(\frac{p_j^2}{2m} - \Omega_j S_j^x \right) + \\ + \sum_{i \neq j} \left[\frac{1}{2} A(\mathbf{r}_{ij}) + B(\mathbf{r}_{ij}) S_i^x S_j^x - I(\mathbf{r}_{ij}) S_i^z S_j^z \right]. \end{aligned} \quad (2.40)$$

The physical meaning of the pseudospin operators is as follows. The operator S_j^x describes tunneling between the atomic orbitals, S_j^y corresponds to the internal Josephson current between the orbitals, and S_j^z characterizes interorbital coupling.

As is stressed above, the second basic mechanism leading to the atomic distortion and, hence, to shape changes of finite systems, is the atom-phonon coupling [85, 86, 89–92]. Taking account of the phonon degrees of freedom is a known procedure, because of which we delineate below only its general scheme.

To introduce vibrational degrees of freedom, one defines atomic deviations \mathbf{u}_j from a fixed location \mathbf{a}_j by the relation

$$\mathbf{r}_j = \mathbf{a}_j + \mathbf{u}_j.$$

Assuming that the deviations are small, one expands the terms of Hamiltonian (2.40) in powers of the deviations up to the second order. Then one represents the operators \mathbf{p}_j and \mathbf{u}_j by means of a canonical transformation introducing the phonon operators b_{ks} , labelled by a quasimomentum k and a polarization index s . The phonon and pseudospin degrees of freedom are decoupled by means of a self-consistent approximation based on the Bogolubov variational principle, after which it becomes possible to diagonalize the phonon part of the Hamiltonian and to calculate the average distortion $\langle \mathbf{u}_j \rangle$ of a j -th atom. The explicit elaboration of all details for this procedure can be found in the books [48, 101, 102]. As a result of this procedure, one gets the average distortion vector $\langle \mathbf{u}_j \rangle$ with the components

$$\langle u_i^\alpha \rangle = \sum_j \gamma_{ij}^\alpha C_j + \sum_{jff} \delta_{ijf}^\alpha C_j C_f,$$

which connects the distortion with the average

$$C_j \equiv \langle S_j^z \rangle,$$

playing the role of an order parameter. The coefficients γ_{ij}^α and δ_{ijf}^α are expressed through the derivatives over r_i^α of the interaction $I(\mathbf{r}_{ij})$ from Hamiltonian (2.40) (see details in [48, 101, 102]).

The system Hamiltonian, being invariant under the inversion $S_j^z \rightarrow -S_j^z$, allows for the existence of a trivial solution with the zero order parameter $C_j \equiv 0$, which corresponds to a symmetric state having no distortion. However, the symmetric state, under certain conditions, is unstable against the appearance of a nonzero order parameter $C_j \neq 0$. In that case, there happens geometric distortion of the sample, characterized by the distortion vector with the observable components given by the average of $\langle \mathbf{u}_j^\alpha \rangle$. The arising nontrivial order parameter can lead to the geometric distortion and the change of system shape. This change occurs spontaneously owing to the fact that the distorted

shape is more energetically favorable than the symmetric shape. This situation, as is explained above, is typical for the Jahn-Teller effect in finite systems.

As an illustration, we can again imagine a finite system enjoying cubic shape structure. Then a distortion of atomic locations can easily lead to the structures possessing either orthorhombic, or tetragonal, or rhombohedral, or triclinic symmetry [93–96].

2.3.3 Geometric orientation transitions

The fact that finite systems demonstrate geometric transformations, even when the system is as small as being composed of two particles, can be illustrated by the following example of the orientational transformation in a dimer formed by two monomers represented by their dipole vectors \mathbf{D}_1 and \mathbf{D}_2 . Dimer structures are very common in biophysics and biochemistry [103]. The Hamiltonian of the dimer can be written in the form

$$H = J\mathbf{D}_1 \cdot \mathbf{D}_2 - U(D_1^z + D_2^z) , \quad (2.41)$$

where J characterizes the interaction strength and U describes an external field acting on the dimer. Each vector \mathbf{D}_i is described by the set

$$\mathbf{D}_i = \{D\gamma_i^x, D\gamma_i^y, D\gamma_i^z\} , \quad (2.42)$$

in which the orientation factors

$$\gamma_i^x = \sin \vartheta_i \cos \varphi_i , \quad \gamma_i^y = \sin \vartheta_i \sin \varphi_i , \quad \gamma_i^z = \cos \vartheta_i \quad (i = 1, 2) \quad (2.43)$$

are expressed through the spherical angles ϑ_i and φ_i .

The spatial orientation of the vectors \mathbf{D}_1 and \mathbf{D}_2 are defined by minimizing the dimer energy over the spatial angles under the normalization constraint

$$(\gamma_i^x)^2 + (\gamma_i^y)^2 + (\gamma_i^z)^2 = 1 . \quad (2.44)$$

Accomplishing the minimization, we find that there exists a critical value of the external field

$$U_c \equiv 2JD , \quad (2.45)$$

separating two different types of orientation.

At the values of the field below U_c , we have

$$\gamma_1^x + \gamma_2^x = \gamma_1^y + \gamma_2^y = 0 , \quad \gamma_1^z = \gamma_2^z = \frac{U}{U_c} \quad (U < U_c) , \quad (2.46)$$

which gives the angles

$$\vartheta_1 = \vartheta_2 = \arccos \frac{U}{U_c} , \quad \varphi_1 - \varphi_2 = \pi . \quad (2.47)$$

The related energy is

$$E = -JD^2 \left[1 + 2 \left(\frac{U}{U_c} \right)^2 \right] \quad (U < U_c) . \quad (2.48)$$

This shows that the vectors \mathbf{D}_i deviate from the axis z by the same angle, ϑ_i , while their components on the $x - y$ plane are counter-aligned. The direction of the transverse components is not defined, though this degeneracy is lifted by an external infinitesimal field. Under the fixed vectors \mathbf{D}_i , the dimer possesses the symmetry of rotation around the z -axis with respect to the angles that are integers of π .

When the external field values are larger than U_c , the energy minimization yields

$$\gamma_1^x = \gamma_2^x = \gamma_1^y = \gamma_2^y = 0, \quad \gamma_1^z = \gamma_2^z = 1, \quad \vartheta_1 = \vartheta_2 = 0 \quad (U > U_c), \quad (2.49)$$

with the energy

$$E = JD^2 \left(1 - 4 \frac{U}{U_c} \right). \quad (2.50)$$

Then both vectors \mathbf{D}_i are aligned along the axis z . Hence the dimer enjoys the rotation symmetry with respect to an arbitrary angle φ .

In that way, at the critical field U_c , there happens the orientation transition. When lowering the field U , the system transforms from the state of the high rotational symmetry around the axis z to the broken symmetry state, having the lower π -rotational symmetry.

This example demonstrates that finite systems exhibit the type of transformations that are absent for infinite systems. These are shape and orientation transitions accompanied by symmetry changes. A similar orientation transition, as will be shown below, occurs in a two-electron quantum dot.

3 Trapped Atoms

Trapped particles can form finite quantum systems of different sizes, from just a few particles to millions of them. The possibility of varying the number of particles as well as other properties of trapped systems makes the latter the objects of high importance for both theoretical studies as well as for a variety of applications. Particles can be charged or neutral. Respectively, there are two rather distinct systems: trapped ions and trapped atoms. Here, we concentrate on the physics of neutral trapped atoms. Physics of trapped ions is a different topic requiring a separate consideration [104]. We analyze theoretical aspects related to symmetry breaking in the systems of trapped atoms. But we do not touch experimental methods of trapping atoms, whose description can be found in literature [105, 106].

3.1 Bose-Einstein condensation

3.1.1 Gauge symmetry breaking

If trapped atoms are bosons, it is possible to cool them down reaching Bose-Einstein condensation predicted by Bose [107] and Einstein [108]. Though superfluidity in liquid ^4He , since London, has been assumed to be accompanied by Bose-Einstein condensation [109], the measurement of the condensate fraction has been a complicated experiment task [110]. This is connected with strong interactions between helium atoms and the resulting strong condensate depletion. In superfluid helium, the condensate fraction at zero temperature is only about 10%. This is why the direct observation of Bose-Einstein

condensation of trapped atoms has become such an important experimental achievement. This phase transition was demonstrated in 1995 almost simultaneously in three groups, condensing the atoms of ^{87}Rb [111], ^{23}Na [112], and ^7Li [113]. By the present time, Bose-Einstein condensation has been achieved for the following trapped atoms: ^1H , ^4He , ^7Li , ^{23}Na , ^{39}K , ^{40}Ca , ^{41}K , ^{52}Cr , ^{84}Sr , ^{85}Rb , ^{86}Sr , ^{87}Rb , ^{88}Sr , ^{133}Cs , ^{170}Yb , and ^{174}Yb . Bosonic atomic molecules can also be condensed, such as boson-formed molecules: $^{23}\text{Na}_2$, $^{85}\text{Rb}_2$, $^{87}\text{Rb}_2$, and $^{133}\text{Cs}_2$, fermion-formed molecules: $^6\text{Li}_2$ and $^{40}\text{K}_2$, and heteronuclear boson-boson molecules: $^{85}\text{Rb}^{87}\text{Rb}$ and $^{41}\text{K}^{87}\text{Rb}$.

This phenomenon has been intensively studied both experimentally and theoretically. Numerous references can be found in the books [114,115] and review articles [46,54,116–125].

With regard to symmetry breaking under Bose-Einstein condensation, one can meet in literature contradictory statements. This phase transition is associated with the global gauge symmetry breaking. The global gauge symmetry corresponds to the group $U(1)$. The order parameter, characterizing this phase transition, is the average of the field operator $\langle\psi\rangle$. In the normal phase, the system Hamiltonian is invariant under the gauge transformations (2.11), which results in Eq. (2.13). Hence, the order parameter is zero, which is a particular case of Eq. (2.13). The order parameter becomes nonzero in the Bose-condensed phase, which requires gauge symmetry breaking. However, in literature, it is possible to meet statements that Bose-Einstein condensation does not necessarily require the gauge symmetry breaking. In order to be precise, we shall recall below rigorous mathematical theorems proving that *global gauge symmetry breaking is the necessary and sufficient condition for Bose-Einstein condensation*. As has been explained above, such rigorous mathematical facts correspond to thermodynamic limit. For finite systems, one has to keep in mind asymptotic symmetry breaking, as is formulated in Sec. 2.

In a *finite* system, the field operator of spinless bosons can be expanded over a basis $\{\varphi_k(\mathbf{r})\}$, where k is a quantum multi-index. Then the field operator can be decomposed into two terms

$$\psi(\mathbf{r}) = \sum_k a_k \varphi_k(\mathbf{r}) = \psi_0(\mathbf{r}) + \psi_1(\mathbf{r}) , \quad (3.1)$$

the first term, representing a quasicondensate, characterized by the index k_0 , and the second term, corresponding to uncondensed particles,

$$\psi_0(\mathbf{r}) \equiv a_0 \varphi_0(\mathbf{r}) , \quad \psi_1(\mathbf{r}) \equiv \sum_{k \neq k_0} a_k \varphi_k(\mathbf{r}) . \quad (3.2)$$

Here $a_0 \equiv a_{k_0}$ and $\varphi_0 \equiv \varphi_{k_0}$. By definition, *quasicondensate* is what would be condensate in thermodynamic limit. The index k_0 here is not specified, keeping in mind that condensation can happen in either uniform or nonuniform systems. For uniform systems, k becomes the wave vector and $k_0 = 0$.

It is of principal importance to stress that the expansion basis in Eq. (3.1) is in no way arbitrary, but it has to be the *natural basis* that is composed of *natural orbitals*, which are the eigenfunctions of the first-order density matrix [126,127]. Only in this case, the quasicondensate will become real condensate in thermodynamic limit.

Also, it is necessary to emphasize that, for a *finite* system, the parts ψ_0 and ψ_1 are not separate operators but just two parts of one field operator ψ , their commutation relations

being

$$\begin{aligned} [\psi_0(\mathbf{r}), \psi_0^\dagger(\mathbf{r}')] &= \varphi_0(\mathbf{r})\varphi_0^*(\mathbf{r}') , \\ [\psi_1(\mathbf{r}), \psi_1^\dagger(\mathbf{r}')] &= \sum_{k \neq k_0} \varphi_k(\mathbf{r})\varphi_k^*(\mathbf{r}') . \end{aligned} \quad (3.3)$$

All operators of observables are defined on the Fock space $\mathcal{F}(\psi)$ generated by the field operator ψ [129].

The fact that spontaneous gauge symmetry breaking yields Bose-Einstein condensation is rather straightforward. Let us define the quasiaverages as in Eq. (2.18), breaking the symmetry of the system Hamiltonian by an infinitesimal source, as in Eq. (2.17). Spontaneous gauge symmetry breaking implies that

$$\lim_{\varepsilon \rightarrow 0} \lim_{N \rightarrow \infty} \frac{|\langle a_0 \rangle_\varepsilon|^2}{N} > 0 . \quad (3.4)$$

When the latter holds true, then, from the Cauchy-Schwarz inequality $|\langle a_0 \rangle_\varepsilon|^2 \leq \langle a_0^\dagger a_0 \rangle_\varepsilon$, it follows that

$$\lim_{\varepsilon \rightarrow 0} \lim_{N \rightarrow \infty} \frac{\langle a_0^\dagger a_0 \rangle_\varepsilon}{N} > 0 , \quad (3.5)$$

which means Bose-Einstein condensation.

Ginibre [130] proved the theorem showing that the thermodynamic potential of a system with gauge symmetry breaking acquires, in thermodynamic limit, the form, where the quasicondensate field operator ψ_0 is replaced by the condensate order parameter η defined as the minimizer of the thermodynamic potential [130]. Bogolubov showed that the same replacement, in thermodynamic limit, of ψ_0 by η is valid for all correlation functions given by the averages with broken gauge symmetry [34]. Therefore, spontaneous gauge symmetry breaking is a *sufficient condition* for condensation.

The necessary condition was, first, proved by Roepstorff [131]. Recently, the proof was polished by several authors [132,133]. According to the Roepstorff theorem, the inequality

$$\lim_{N \rightarrow \infty} \frac{\langle a_0^\dagger a_0 \rangle}{N} \leq \lim_{\varepsilon \rightarrow 0} \lim_{N \rightarrow \infty} \frac{|\langle a_0 \rangle_\varepsilon|^2}{N} \quad (3.6)$$

is valid, where the left-hand side is defined without gauge symmetry breaking. This means that Bose-Einstein condensation necessarily results in gauge symmetry breaking [131].

Concluding, it is a rigorous mathematical fact that: *Spontaneous breaking of global gauge symmetry is the necessary and sufficient condition for Bose-Einstein condensation.* For finite systems, it is to be understood in the sense of asymptotic symmetry breaking. A more detailed discussion can be found in the review article [128].

3.1.2 Representative statistical ensemble

A system with broken symmetry requires to be correctly described, for which purpose, one has to employ representative statistical ensembles. A statistical ensemble, by definition, is a pair $\{\mathcal{F}, \hat{\rho}\}$ of the space of microstates \mathcal{F} and a statistical operator $\hat{\rho}$ describing the system. The temporal evolution of the statistical operator is governed by the evolution operator, with the system Hamiltonian H being the evolution generator. This can be denoted as the dependence $\hat{\rho}(H, t)$. For equilibrium and quasi-equilibrium systems, the

form of the statistical operator is prescribed by the principle of minimal information, that is, by minimizing the information entropy under given additional constraints [74].

It is important that the statistical ensemble should uniquely define the considered statistical system, for which it is necessary to include in the definition all conditions and constraints characterizing the system [71, 134]. Such an ensemble, correctly defining the system, is called *representative* [72, 73]. In the case of a system with condensate, one has to accurately take into account the global gauge symmetry breaking and the method by which this is realized.

Treating a system with Bose-Einstein condensate, one usually accepts one of the following two ways:

(i) One possibility is to work with a *finite system*, having one field operator ψ generating the Fock space $\mathcal{F}(\psi)$. The system evolution is described by a grand Hamiltonian that is the evolution generator. In defining the grand Hamiltonian, one takes into account physical constraints associated with the system. One such a constraint is the definition of internal energy as the average of the energy Hamiltonian \hat{H} . Another constraint is the definition of the number of particles as the average of the number operator \hat{N} . And one more constraint is the necessity of breaking the symmetry of the Hamiltonian by an infinitesimal source, as in Eq. (2.17). Then the grand Hamiltonian reads as

$$H_\varepsilon = \hat{H} - \mu\hat{N} + \varepsilon\hat{\Gamma} , \quad (3.7)$$

which is defined on the Fock space $\mathcal{F}(\psi)$. Using this approach, based on the statistical ensemble $\{\mathcal{F}(\psi), \hat{\rho}(H_\varepsilon, t)\}$, it is necessary to make calculations for a finite system, employing the commutation relations (3.3). At the end, one passes to thermodynamic limit in order to break gauge symmetry, as in Eq. (2.18). This way, though being in principle admissible [135], is extremely cumbersome and can be followed only by invoking heavy numerical calculations, for example, by using Monte Carlo numerical simulations.

(ii) Another approach, developed by Bogolubov [136] suggests to break the global gauge symmetry explicitly by introducing the so-called *Bogolubov shift* of the field operator, replacing the operator $\psi(\mathbf{r})$ by the field operator

$$\hat{\psi}(\mathbf{r}) = \eta(\mathbf{r}) + \psi_1(\mathbf{r}) , \quad (3.8)$$

in which $\eta(\mathbf{r})$ is the condensate wave function and $\psi_1(\mathbf{r})$ is the field operator of uncondensed particles. For the latter, the standard Bose commutation relations are valid,

$$\left[\psi_1(\mathbf{r}), \psi_1^\dagger(\mathbf{r}') \right] = \delta(\mathbf{r} - \mathbf{r}') , \quad (3.9)$$

which makes their use very convenient [34, 38, 136].

The Bogolubov shift (3.8) is a canonical transformation that is correctly defined for any Bose-condensed system. This transformation does not require that ψ_1 be in any sense small. It is important to emphasize that, after this canonical transformation, the operators of observables are defined on the Fock space $\mathcal{F}(\psi_1)$ generated by the field operator ψ_1 . The spaces $\mathcal{F}(\psi)$ and $\mathcal{F}(\psi_1)$ are asymptotically (as N tends to infinity) orthogonal, thus, realizing unitary nonequivalent operator representations with the unitary nonequivalent representations for commutation relations [137, 138].

Realizing the Bogolubov shift, one gets two independent field variables, η and ψ_1 that are orthogonal to each other,

$$\int \eta^*(\mathbf{r})\psi_1(\mathbf{r}) d\mathbf{r} = 0 . \quad (3.10)$$

Respectively, in addition to the definition of the internal energy, there are two normalization conditions, for the number of condensed particles,

$$N_0 = \int |\eta(\mathbf{r})|^2 d\mathbf{r} , \quad (3.11)$$

and for the number of uncondensed particles,

$$N_1 = \langle \hat{N}_1 \rangle , \quad \hat{N}_1 \equiv \int \psi_1^\dagger(\mathbf{r})\psi_1(\mathbf{r}) d\mathbf{r} . \quad (3.12)$$

There is also the restriction classifying the uncondensed particles as normal particles satisfying the condition

$$\langle \psi_1(\mathbf{r}) \rangle = 0 . \quad (3.13)$$

The latter condition can be rewritten in the standard form of a statistical average

$$\langle \hat{\Lambda} \rangle = 0 , \quad \hat{\Lambda} \equiv \int [\lambda(\mathbf{r})\psi_1^\dagger(\mathbf{r}) + \lambda^*(\mathbf{r})\psi_1(\mathbf{r})] d\mathbf{r} , \quad (3.14)$$

where $\lambda(\mathbf{r})$ is a complex function playing the role of the Lagrange multiplier guaranteeing the validity of Eq. (3.14). In that way, the grand Hamiltonian acquires the form

$$H = \hat{H} - \mu_0 N_0 - \mu_1 N_1 - \hat{\Lambda} , \quad (3.15)$$

with the Lagrange multipliers μ_0 and μ_1 conserving the normalization conditions (3.11) and (3.12).

This form of the grand Hamiltonian makes it possible to define a representative ensemble providing a completely self-consistent description of any Bose-condensed system [57, 139–141]. In order to stress that the field variables η and ψ_1 are independent, it is possible to define the grand Hamiltonian on the composite Fock space $\mathcal{F}_0(\eta) \otimes \mathcal{F}(\psi_1)$ [138]. Generally, the Lagrange multipliers μ_0 and μ_1 are different, though they can coincide in some particular cases, as in the Bogolubov approximation [136], corresponding to low temperatures and asymptotically weak interactions. The existence of two Lagrange multipliers resolves the Hohenberg-Martin dilemma [142], making the theory conserving and the spectrum gapless, as is prescribed by the Hugenholtz-Pines relation [143].

Both these ways, described above, are equivalent as far as the values of observable quantities do not depend on the used operator representation [34–36, 137].

The method of breaking the global gauge symmetry by means of the Bogolubov shift (3.8) seems to be more convenient than the method of infinitesimal sources (3.7) because the commutation relations (3.9) are much simpler than those in Eq. (3.3). But, breaking the gauge symmetry with the Bogolubov shift requires to be accurate, taking into account those constraints that uniquely define this method. If these constraints are not taken into account, the description will become not self-consistent and plagued with internal defects,

such as the appearance of a gap in the spectrum, breaking of general thermodynamic relations, and the loss of the system stability.

The equations of motion are obtained from Hamiltonian (3.15) in the standard way, by means of variational derivatives. The equation for the *condensate function* reads as

$$i \frac{\partial}{\partial t} \eta(\mathbf{r}, t) = \left\langle \frac{\delta H}{\delta \eta^*(\mathbf{r}, t)} \right\rangle . \quad (3.16)$$

And the equation for the operators of uncondensed particles is given by the variational derivative

$$i \frac{\partial}{\partial t} \psi_1(\mathbf{r}, t) = \frac{\delta H}{\delta \psi_1^\dagger(\mathbf{r}, t)} . \quad (3.17)$$

Note that the variational equations are equivalent to the Heisenberg equations of motion [125, 144]. For an equilibrium system, the condensate-function equation (3.16) reduces to the minimization of the Hamiltonian with respect to this function, which constitutes a necessary stability condition.

3.1.3 Equation for condensate function

The global gauge symmetry is broken in the system if and only if there exists a nonzero solution of the condensate-function equation (3.16). This equation, therefore, is of principal importance.

To explicitly illustrate the form of the equation for the condensate function, let us accept for the energy Hamiltonian the standard expression

$$\begin{aligned} \hat{H} = & \int \hat{\psi}^\dagger(\mathbf{r}) \left(-\frac{\nabla^2}{2m} + U \right) \hat{\psi}(\mathbf{r}) d\mathbf{r} + \\ & + \frac{1}{2} \int \hat{\psi}^\dagger(\mathbf{r}) \hat{\psi}^\dagger(\mathbf{r}') \Phi(\mathbf{r} - \mathbf{r}') \hat{\psi}(\mathbf{r}') \hat{\psi}(\mathbf{r}) d\mathbf{r} d\mathbf{r}' , \end{aligned} \quad (3.18)$$

in which $\Phi(\mathbf{r})$ is a pair interaction potential and $U = U(\mathbf{r}, t)$ is an external potential. Then the condensate-function equation (3.16) yields

$$\begin{aligned} i \frac{\partial}{\partial t} \eta(\mathbf{r}, t) = & \left(-\frac{\nabla^2}{2m} + U - \mu_0 \right) \eta(\mathbf{r}, t) + \\ & + \int \Phi(\mathbf{r} - \mathbf{r}') \langle \hat{\psi}^\dagger(\mathbf{r}') \hat{\psi}(\mathbf{r}') \hat{\psi}(\mathbf{r}) \rangle d\mathbf{r}' . \end{aligned} \quad (3.19)$$

This is the exact equation for the condensate function. Substituting here the Bogolubov shift (3.8), we meet the following densities: the condensate density

$$\rho_0(\mathbf{r}) = |\eta(\mathbf{r})|^2 , \quad (3.20)$$

the density of uncondensed atoms

$$\rho_1(\mathbf{r}) = \langle \psi_1^\dagger(\mathbf{r}) \psi_1(\mathbf{r}) \rangle , \quad (3.21)$$

and the total density

$$\rho(\mathbf{r}) = \rho_0(\mathbf{r}) + \rho_1(\mathbf{r}) . \quad (3.22)$$

One also needs the notation for the density matrix

$$\rho_1(\mathbf{r}, \mathbf{r}') = \langle \psi_1^\dagger(\mathbf{r}') \psi_1(\mathbf{r}) \rangle , \quad (3.23)$$

for the pair anomalous average

$$\sigma_1(\mathbf{r}, \mathbf{r}') = \langle \psi_1(\mathbf{r}') \psi_1(\mathbf{r}) \rangle , \quad (3.24)$$

and for the triple anomalous average

$$\alpha(\mathbf{r}, \mathbf{r}') = \langle \psi_1^\dagger(\mathbf{r}') \psi_1(\mathbf{r}') \psi_1(\mathbf{r}) \rangle . \quad (3.25)$$

The averages (3.24) and (3.25) are called anomalous, since they appear only when gauge symmetry is broken, while under preserved gauge symmetry, they are exactly zero, in view of Eq. (2.13).

Introducing a self-energy operator

$$\hat{\Sigma}(\mathbf{r}) = \hat{\Sigma}_N(\mathbf{r}) + \hat{\Sigma}_A(\mathbf{r}) , \quad (3.26)$$

consisting of the sum of the normal operator, defined by the equation

$$\hat{\Sigma}_N(\mathbf{r})\eta(\mathbf{r}) \equiv \int \Phi(\mathbf{r} - \mathbf{r}') [\rho(\mathbf{r}')\eta(\mathbf{r}) + \rho_1(\mathbf{r}, \mathbf{r}')\eta(\mathbf{r}')] d\mathbf{r}' , \quad (3.27)$$

and of the anomalous operator, defined by the relation

$$\hat{\Sigma}_A(\mathbf{r})\eta(\mathbf{r}) \equiv \int \Phi(\mathbf{r} - \mathbf{r}') [\sigma_1(\mathbf{r}, \mathbf{r}')\eta^*(\mathbf{r}') + \alpha(\mathbf{r}, \mathbf{r}')] d\mathbf{r}' , \quad (3.28)$$

we can rewrite Eq. (3.19) as

$$i \frac{\partial}{\partial t} \eta(\mathbf{r}, t) = \left(-\frac{\nabla^2}{2m} + U - \mu_0 \right) \eta(\mathbf{r}, t) + \hat{\Sigma}(\mathbf{r})\eta(\mathbf{r}, t) . \quad (3.29)$$

The statistical ensemble $\{\mathcal{F}(\psi_1), \hat{\rho}(H, t)\}$ provides a correct description of thermodynamics for Bose-condensed systems at finite temperatures and arbitrary interactions [145–147].

In the particular case of dilute gas, for which the interaction radius is much shorter than the mean inter-atomic distance, the interactions are modelled by the local potential

$$\Phi(\mathbf{r}) = \Phi_0 \delta(\mathbf{r}) , \quad \Phi_0 \equiv 4\pi \frac{a_s}{m} , \quad (3.30)$$

where a_s is s-wave scattering length. At zero temperature and very weak interactions, when practically all atoms are condensed, so that $\hat{\Sigma}_N(\mathbf{r}) = \Phi_0 \rho_0(\mathbf{r})$ and $\hat{\Sigma}_A(\mathbf{r}) = 0$, equation (3.29) reduces to the Gross-Pitaevskii equation [148–151]

$$i \frac{\partial}{\partial t} \eta(\mathbf{r}, t) = \left[-\frac{\nabla^2}{2m} + U - \mu_0 + \Phi_0 |\eta(\mathbf{r}, t)|^2 \right] \eta(\mathbf{r}, t) . \quad (3.31)$$

Gross interpreted this equation as the equation for a system of atoms all of which are in the same state [148–150], that is, in a coherent state [152].

3.1.4 Size and shape instability

Bose-Einstein condensate and, respectively, the occurrence of broken gauge symmetry, can happen only in stable systems. The stability of finite systems essentially depends on their sizes and shapes. Usually, the *size-shape instability* appears when particle interactions are either attractive or anisotropic, containing an attractive part.

In the case of isotropic interactions, the stability of Bose-condensed systems is connected with the sign of the integral pair interaction

$$\Phi_0 = \int \Phi(\mathbf{r}) d\mathbf{r} = 4\pi \frac{a_s}{m},$$

where $\Phi(\mathbf{r})$ is a pair interaction potential. A uniform system of atoms with effective attractive interactions, for which Φ_0 is negative, is known to be unstable [153]. However, a finite system of trapped atoms can be stable, when their positive kinetic energy compensates the negative potential energy. This imposes the limitation on the maximal number of atoms N_{max} that could form a stable finite system. This number has been calculated numerically for harmonic traps, employing the Gross-Pitaevskii equation (3.31) by several authors, as reviewed in [116]. An analytical formula has also been derived [154] in the form

$$N_{max} = \sqrt{\frac{\pi}{2}} \frac{l_x l_y l_z}{|a_s|(l_x^2 + l_y^2 + l_z^2)}, \quad (3.32)$$

in which $a_s < 0$ is attractive scattering length, $l_\alpha \equiv 1/\sqrt{m\omega_\alpha}$ is a characteristic trap length, $\alpha = x, y, z$, and ω_α is a trap frequency. The maximal number of atoms essentially depends on the trap size and its anisotropy. The trap symmetry plays an important role. For the purpose of housing more atoms, with the given scattering length, the spherical shape seems to be more favorable, as compared to anisotropic traps, elongated in one or two directions.

Typical anisotropic interactions are the dipole interactions, such as exist for ^{52}Cr atoms [155] which possess comparatively large magnetic dipole moments $\mu_0 = 6\mu_B$. The dipolar interactions, for dipoles polarized along the z -axis, are

$$D(\mathbf{r}) = \frac{\mu_0^2}{r^3} (1 - 3\cos^2 \vartheta), \quad (3.33)$$

where $r \equiv |\mathbf{r}|$, with \mathbf{r} being a vector between the interacting atoms, and ϑ is the angle between \mathbf{r} and the dipole orientation z . The same form of the dipole interactions exists for atoms with electric dipoles, for which the magnetic moment μ_0 should be replaced by the electric dipole moment d_0 [156].

Strictly speaking, atomic interactions are composed of the sum of the contact interaction (3.30) and the dipolar interaction (3.33). The magnitudes of these interactions can be varied in experiment. Dipolar interactions can be varied by applying magnetic or electric fields, while contact interactions can be varied by means of the Feshbach resonance techniques [157–160].

For the case of pure dipolar interactions (3.33), a spatially homogeneous Bose-condensed gas is unstable, similarly to the homogeneous Bose gas with attractive isotropic interactions. For a cigar shaped trap, with the aspect ratio $\omega_z/\omega_\perp \ll 1$, the effective dipole interactions are attractive and the gas can be stable only for the number of atoms less than

the maximal number N_{max} . For a pancake shaped trap, with the aspect ratio $\omega_z/\omega_\perp \gg 1$, there also exists the maximal number of atoms N_{max} , when the system becomes unstable, but this maximal number is much larger than that for the cigar shaped traps. The value of the maximal number of atoms depends on the trap shape and on the average interaction

$$D_0 = \frac{1}{N} \int D(\mathbf{r} - \mathbf{r}') \rho_0(\mathbf{r}) \rho_0(\mathbf{r}') d\mathbf{r} d\mathbf{r}' .$$

The pancake-shaped systems with dipolar interactions are always more stable than the cigar-shaped ones.

3.1.5 Elementary collective excitations

Finiteness of quantum systems influences their spectra of collective excitations. At zero temperature and very weak interactions, collective excitations are usually described by considering small deviations from the condensate function and linearizing the Gross-Pitaevskii equation (3.31). At finite temperatures and interactions, the correct description of collective excitations requires to consider the whole system Hamiltonian, whose diagonal part defines the spectrum of excitations [141]. Employing the Hartree-Fock-Bogolubov approximation, taking, for simplicity, the local interaction potential (3.30), and using the notation

$$\begin{aligned} \hat{\omega}(\mathbf{r}) &\equiv -\frac{\nabla^2}{2m} + U(\mathbf{r}) - \mu_1 + 2\Phi_0\rho(\mathbf{r}) , \\ \Delta(\mathbf{r}) &\equiv \Phi_0[\rho_0(\mathbf{r}) + \sigma_1(\mathbf{r})] , \end{aligned} \quad (3.34)$$

where $\sigma_1(\mathbf{r})$ is the diagonal anomalous average, Eq. (3.24), results in the Bogolubov equations for collective excitations

$$\begin{aligned} \hat{\omega}(\mathbf{r})u_k(\mathbf{r}) + \Delta(\mathbf{r})v_k(\mathbf{r}) &= \varepsilon_k u_k(\mathbf{r}) , \\ \hat{\omega}(\mathbf{r})v_k(\mathbf{r}) + \Delta^*(\mathbf{r})u_k(\mathbf{r}) &= -\varepsilon_k v_k(\mathbf{r}) . \end{aligned} \quad (3.35)$$

Generally, these equations for trapped atoms can be solved only numerically. Analytical solutions are available only in some particular cases.

Collective excitations, whose wavelength is much shorter than the system size and, respectively, the excitation frequency ω is much larger than the characteristic trapping frequency ω_0 , behave as bulk excitations that are continuous and can be described in the local density approximation [114, 115, 117, 161]. In this approximation, Eqs. (3.35) yield the local Bogolubov spectrum

$$\varepsilon(\mathbf{k}, \mathbf{r}) = \sqrt{c^2(\mathbf{r})k^2 + \left(\frac{k^2}{2m}\right)^2} , \quad (3.36)$$

where the local sound velocity is defined by the equation

$$mc^2(\mathbf{r}) = [\rho_0(\mathbf{r}) + \sigma_1(\mathbf{r})] \Phi_0 . \quad (3.37)$$

This form of the Bogolubov spectrum is in good agreement with experiment for short-wave excitations [162].

Collective excitations can also be defined as the poles of Green functions. For systems with broken gauge symmetry, the poles of single-particle and two-particle Green functions coincide [163]. In uniform systems, the spectrum of collective excitations is gapless, which is required by the Hugenholtz-Pines relation [143] and the condition of condensate existence [46]. Such gapless excitations correspond to massless Goldstone modes [164] arising under spontaneous breaking of a global continuous symmetry [26]. Collective excitations with the Bogolubov spectrum are called *bogolons*.

In finite quantum systems, those excitations, whose wavelength is of the order or larger than the system size and, equivalently, for which $\omega \lesssim \omega_0$, become discrete and essentially dependent on the system shape symmetry. At zero temperature and asymptotically weak interactions, such low-frequency excitations can be found from hydrodynamic equations derived from the Gross-Pitaevskii equation, with invoking the Thomas-Fermi approximation. Thus, for a harmonic spherical trap the discretized spectrum is [165]

$$\omega_{nl} = \omega_0 \sqrt{2n^2 + 2nl + 3n + l} , \quad (3.38)$$

where n and l are radial and orbital quantum numbers, respectively. The excitations with $n = 0$ are called *surface* excitations. A particular case is the *dipolar mode* ($n = 0, l = 1$). The excitations with $n \neq 0$ are termed *compressional*. The case with $n = 1, l = 0$ corresponds to *breathing mode*.

For cigar-shape harmonic traps ($\omega_z \ll \omega_\perp$), the low-frequency spectrum is [166, 167]

$$\omega_n = \frac{\omega_z}{2} \sqrt{n(n+1)} . \quad (3.39)$$

Particular cases are the *dipole mode* ($n = 1$) and the *quadrupole mode* ($n = 2$).

For disk-shape harmonic traps ($\omega_z \gg \omega_\perp$), the spectrum of the lowest modes becomes [167]

$$\omega_{nm} = \omega_\perp \sqrt{\frac{4}{3} n^2 + \frac{4}{3} nm + 2n + m} , \quad (3.40)$$

where m is azimuthal quantum number.

In a cylindrically symmetric trap, there is an excitation for which $m = \pm l$ and the spectrum is

$$\omega_l = \omega_\perp \sqrt{l} . \quad (3.41)$$

In the case of $l = 2$, these excitations are similar to quadrupole modes $K = 1^+$ well known for atomic nuclei [168]. Analogous excitations also exist in anisotropic traps, where, for $l = 2$, they have the frequencies $\sqrt{\omega_x^2 + \omega_y^2}$, $\sqrt{\omega_y^2 + \omega_z^2}$, and $\sqrt{\omega_z^2 + \omega_x^2}$ [169]. In literature on trapped atoms, they are called scissor modes, keeping in mind the modes in nuclei that describe out-of-phase oscillations of neutron and proton densities, which resembles the opening and closing of a pair of scissors [170].

The occurrence of collective excitations with discretized spectrum is a specific feature of finite quantum systems. In such systems, short-wave excitations demonstrate the properties of bulk excitations, with continuous spectra. While the long-wave excitations display discrete spectra, whose form essentially depends on the system shape.

3.2 Atomic fluctuations and stability

3.2.1 Uniform ideal gas

Equilibrium Bose-condensed systems can actually exist only when they are thermodynamically stable. This implies the validity of the stability conditions discussed in Sec. 2.2. The meaning of these conditions is straightforward, telling us that the fluctuations of observable quantities must be thermodynamically normal. In the other case, anomalous thermodynamic fluctuations destroy the equilibrium state of the system.

As a simple example, it is possible to mention the case of the ideal Bose gas in a d -dimensional box of volume V . The condensation temperature for this gas is

$$T_c = \frac{2\pi}{m} \left[\frac{\rho}{\zeta(d/2)} \right]^{2/d}, \quad (3.42)$$

where ρ is average particle density. Due to the properties of the Riemann zeta function $\zeta(\cdot)$, a finite transition temperature exists only for $d > 2$. This is the manifestation of the general feature of the absence of phase transitions in low-dimensional systems with continuous symmetry [171].

However, the finiteness of the transition temperature does not yet mean that below it the system can really exist, being stable. It is necessary to check the stability conditions for large numbers of particles [46, 57]. The fluctuations of energy satisfy the stability condition (2.24). But we need also to study particle fluctuations. The operator for the total number of particles in a Bose-condensed system,

$$\hat{N} = \hat{N}_0 + \hat{N}_1 \quad (3.43)$$

is the sum of the terms corresponding to condensed, \hat{N}_0 , and uncondensed, \hat{N}_1 , particles.

Here it is necessary to remember that, as is explained above, there are two ways of dealing with Bose-condensed systems.

If one separates the field operator into the sum $\psi = \psi_0 + \psi_1$ of two operators defined in the Fock space $\mathcal{F}(\psi)$, generated by the field operator ψ , then one has to calculate the variance of the operator \hat{N}_0 representing the number of condensed particles as well as the variance of the number operator of uncondensed particles [172].

However, when one employs the Bogolubov shift of the field operator by making the canonical transformation $\psi = \eta + \psi_1$, where η is the condensate wave function, one has to work in the Fock space $\mathcal{F}(\psi_1)$ generated by ψ_1 . In this representation, the number of condensed atoms is a nonoperator quantity $N_0 = \int |\eta|^2 d\mathbf{r}$ that defines the normalization condition for the condensate wave function. The variance of a nonoperator quantity, as is evident, is identically zero.

Of course, both these ways give the same value for the compressibility that is the observable quantity quantifying particle fluctuations. The observable quantities do not depend on the used operator representation [35, 36].

If the system gauge symmetry is broken by means of the Bogolubov shift (3.8), then $\text{var}(N_0)$ is identically zero. In that case,

$$\text{var}(\hat{N}) = \text{var}(\hat{N}_1). \quad (3.44)$$

In three-dimensional space, one has

$$\text{var}(\hat{N}_1) = \left(\frac{mT}{\pi} \right)^2 V^{4/3}. \quad (3.45)$$

The reduced variance $\text{var}(\hat{N}_1)/N$ is proportional to the isothermal compressibility, that has to be finite in thermodynamic limit. But from the above equation it follows that the compressibility diverges as $N^{1/3}$, for large N . This divergence contradicts the stability condition (2.24) and means that the ideal uniform Bose-condensed gas is unstable.

The fact that divergent compressibility of the ideal Bose gas implies its instability is easy to understand. If the compressibility of a system is infinite, then the sound velocity is zero and the system structure factor is infinite. Certainly, no one physical system displays such abnormal behavior. As is well known, the general stability condition of any equilibrium system requires that $\partial P / \partial V < 0$. This necessary condition is broken for the ideal Bose gas, for which this derivative becomes zero, as a result of which the compressibility diverges, implying instability [172]. The instability of the degenerate Bose gas is widely accepted and is explained in modern textbooks [173].

Moreover, to understand that a system with infinite compressibility is unstable, there is even no need to address textbooks, but it is sufficient to have just common sense. Really, infinite compressibility, being proportional to $\partial V / \partial P$, means that any arbitrarily weak noise in pressure would immediately result in the system explosion.

3.2.2 Trapped ideal gas

In order to check whether the ideal Bose gas could be stabilized being confined inside a trap, let us consider the most often used trap shape described by the power-law potential

$$U(\mathbf{r}) = \sum_{\alpha=1}^d \frac{\omega_{\alpha}}{2} \left| \frac{r_{\alpha}}{l_{\alpha}} \right|^{n_{\alpha}}, \quad (3.46)$$

where $\omega_{\alpha} \equiv 1/ml_{\alpha}^2$ are the characteristic trap frequencies.

An important quantity, defining the confining power of the trapping potential is the *confining dimension* [45]

$$s \equiv \frac{d}{2} + \sum_{\alpha=1}^d \frac{1}{n_{\alpha}}. \quad (3.47)$$

For ideal gases confined in the power-law trapping potentials, it is convenient to use the generalized quasi-classical approximation [45] yielding the results that are in agreement with the quantum consideration [174,175]. In this approximation, the condensation temperature is

$$T_c = \left[\frac{N}{Bg_s(1)} \right]^{1/s}, \quad (3.48)$$

where the generalized Bose function

$$g_s(z) \equiv \frac{1}{\Gamma(s)} \int_{u_0}^{\infty} \frac{zu^{s-1}}{e^u - z} du \quad (3.49)$$

is introduced and the notations

$$B \equiv \frac{2^s}{\pi^{d/2}} \prod_{\alpha=1}^d \frac{\Gamma(1 + 1/n_\alpha)}{\omega_\alpha^{1/2+1/n_\alpha}},$$

$$u_0 \equiv \frac{\omega_0}{2T}, \quad \omega_0 \equiv \left(\prod_{\alpha=1}^d \omega_\alpha \right)^{1/d} \quad (3.50)$$

are used. In the limit of $u_0 \rightarrow 0$, one returns to the standard semiclassical approximation [117, 176].

Considering the effective thermodynamic limit (2.22), we can take the internal energy E_N , which, for the Bose-condensed system, is

$$E_N = B s g_{1+s}(1) T^{1+s}. \quad (3.51)$$

Then the thermodynamic limit (2.22) becomes

$$N \rightarrow \infty, \quad B \rightarrow \infty, \quad \frac{B}{N} \rightarrow \text{const}. \quad (3.52)$$

For the usual case of unipower trapping potentials, with $n_\alpha = n$, limit (3.52) reduces to

$$N \rightarrow \infty, \quad \omega_0 \rightarrow 0, \quad N \omega_0^s \rightarrow \text{const}. \quad (3.53)$$

The variance of the particle number, below T_c , reads as

$$\text{var}(\hat{N}) = \frac{g_{s-1}(1)}{g_s(1)} \left(\frac{T}{T_c} \right)^s N. \quad (3.54)$$

Taking into account the effective limit (3.52), we find, at large N , the following behavior

$$\begin{aligned} \frac{\text{var}(\hat{N})}{N} &\propto N \quad (s = 1), \\ \frac{\text{var}(\hat{N})}{N} &\propto N^{(2/s)-1} \quad (1 < s < 2), \\ \frac{\text{var}(\hat{N})}{N} &\propto \ln N \quad (s = 2), \\ \frac{\text{var}(\hat{N})}{N} &\propto \text{const} \quad (s > 2). \end{aligned} \quad (3.55)$$

This tells us that the ideal Bose-condensed gas can be stabilized only in the traps with the confining dimension $s > 2$.

3.2.3 Harmonically trapped gas

The most common shape of traps is harmonic, when $n_\alpha = 2$. The condensation temperatures formally exist for all dimensions, being

$$\begin{aligned} T_c &= \frac{N\omega_0}{\ln(2N)} \quad (d = 1) , \\ T_c &= \omega_0 \left[\frac{N}{\zeta(d)} \right]^{1/d} \quad (d \geq 2) . \end{aligned} \quad (3.56)$$

This is contrary to the uniform case, where a finite T_c exists only for $d = 3$.

However, again, we have to remember that the formal existence of a transition temperature does not yet guarantee that the system could be stable [45]. It is necessary to check the stability conditions

Particle fluctuations are described by the variances

$$\begin{aligned} \text{var}(\hat{N}) &= 2 \left(\frac{T}{\omega_0} \right)^2 \quad (d = 1) , \\ \text{var}(\hat{N}) &= \left(\frac{T}{\omega_0} \right)^2 \ln \left(\frac{2T}{\omega_0} \right) \quad (d = 2) , \\ \text{var}(\hat{N}) &= \frac{\pi^2 N}{6\zeta(3)} \left(\frac{T}{T_c} \right)^3 \quad (d = 3) , \end{aligned} \quad (3.57)$$

which, for large N , yield

$$\begin{aligned} \frac{\text{var}(\hat{N})}{N} &\propto N \quad (d = 1) , \\ \frac{\text{var}(\hat{N})}{N} &\propto \ln N \quad (d = 2) , \\ \frac{\text{var}(\hat{N})}{N} &\propto \text{const} \quad (d = 3) . \end{aligned} \quad (3.58)$$

Therefore, only the three-dimensional harmonic trap stabilizes the ideal Bose-condensed gas.

Of course, it could be possible to say that the stability condition (2.24) is formally satisfied for a finite number of particles N . Thence, it would be admissible to assume that the ideal gas can form a kind of, maybe metastable, quasicondensate in one- and two-dimensional harmonic traps. However, to be classified as quasicondensate, it should allow for ascribing the notion of asymptotic symmetry breaking, which requires the validity of the stability condition (2.24) at asymptotically large N .

Taking into account interactions does not stabilize harmonically trapped Bose-condensed gas in low dimensions. According to the theorems, proved in Refs. [177, 178], there can be no Bose-Einstein condensate in harmonically trapped interacting Bose gas for dimensionalities $d = 1$ and $d = 2$.

3.2.4 Interacting nonuniform systems

To consider particle fluctuations for interacting systems, it is convenient to use the following expression for the variance:

$$\text{var}(\hat{N}) = N + \int \rho(\mathbf{r})\rho(\mathbf{r}')[g(\mathbf{r}, \mathbf{r}') - 1] d\mathbf{r}d\mathbf{r}' , \quad (3.59)$$

in which $g(\mathbf{r}, \mathbf{r}')$ is the pair correlation function. This expression (3.59) is valid for any system of N particles. Using the Hartree-Fock-Bogolubov and local-density approximations gives [179]

$$\text{var}(\hat{N}) = \frac{T}{m} \int \frac{\rho(\mathbf{r})}{c^2(\mathbf{r})} d\mathbf{r} . \quad (3.60)$$

Equation (3.60) holds true for three-dimensional nonuniform Bose-condensed systems in the presence of arbitrary external potentials. The integral here is proportional to N , provided that the sound velocity is nonzero. Therefore, the stability condition (2.24) is satisfied.

3.2.5 Importance of symmetry breaking

In this subsection, we emphasize that forgetting about the occurrence of gauge symmetry breaking in Bose-condensed systems is not as innocent, as one could think.

First of all, the appearance of Bose-Einstein condensate as such necessarily requires the global gauge symmetry breaking, as is explained above. Strictly speaking, if there is no gauge symmetry breaking, there can be no condensate.

If, forgetting the necessity of the symmetry breaking, one invokes a conserving-symmetry approach, then there arise unphysical divergences making calculations meaningless. For example, in the Hartree-Fock approximation, that preserves the gauge symmetry, the variance for the number of particles becomes thermodynamically anomalous, $\text{var}\hat{N} \propto N^2$. Then the stability condition (2.24) is not valid, which implies that the system is unstable. However, the appearance of this instability has no physical meaning, being caused just by the error of forgetting to break the gauge symmetry. This fictitious instability is immediately removed as soon as the gauge symmetry for the condensed phase is broken [153]. Similar unphysical divergences in the Hartree-Fock approximation occur for some other observable quantities, but become removed under gauge symmetry breaking [142]. This means that the approximations, preserving gauge symmetry, are principally inappropriate for describing systems with Bose-Einstein condensate. In particular, the standard Hartree-Fock approximation, preserving gauge symmetry, is inapplicable for such systems.

It is worth recalling that thermodynamically anomalous particle fluctuations imply the divergence of isothermic compressibility that is proportional to $\text{var}(\hat{N})/N$ [45, 55–57]. This quantity $\text{var}(\hat{N})/N$ is also proportional to the structure factor that is known to be finite for real systems with Bose condensate [162].

The occurrence of the global gauge symmetry breaking is necessary and sufficient not merely for the condensate existence, but also for the appearance of the anomalous averages, as in (3.24). Both, the condensate itself and the anomalous averages, either exist together or are together zero, in line with Eq. (2.13). Direct calculations [145–147] show

that the anomalous average is always either larger than the density of uncondensed atoms or larger than the density of condensed atoms, so practically can never be neglected, as has been suggested in the Shohnho model [180]. Moreover, omitting the anomalous averages makes the system unstable and results in the appearance of unphysical divergences, as it happens for the discussed above situation when gauge symmetry breaking is forgotten. The correct description of Bose-condensed systems necessarily requires to accurately take into account the anomalous averages and the related anomalous Green functions [181–183].

3.3 Nonequilibrium symmetry breaking

3.3.1 Dynamic instability of motion

The macroscopic occupation of a single quantum state by Bose-condensed atoms has clear similarities with conventional laser systems. Therefore it has been natural to try to realize directed beams of Bose-condensed atoms, which would imitate optical laser beams. Such devices that could be used for forming coherent atomic beams are called *atom lasers*. Two conditions are the most important for the latter, the atomic beam coherence [184, 185] and well defined directionality [186]. The coherent atomic beam, propagating with a given velocity, should be similar to a coherent photon ray with a given momentum [187]. The standard way of creating atomic beams is to form, first, a trapped ensemble of Bose-condensed atoms and then to direct these atoms out of the trap by an output coupler. There are many types of the output couplers and extensive literature on atom lasers, which can be found in the review articles [117, 188].

It is not our aim here to discuss the details of how a moving beam of coherent atoms could be created. But our goal is to recall that the beam coherence and, hence, the properties of the Bose-Einstein condensate in the beam, including its superfluidity, depend on the velocity of atomic motion. Increasing the velocity of moving atoms above a critical velocity, one can destroy the superfluid condensate, as is well known from the Landau criterion [9]. When the Bose condensate is destroyed, the system passes to the normal state. The destruction of the moving Bose condensate is, actually, a kind of a quantum phase transition. For a finite system, the Landau criterion can be generalized by taking account of the system spatial nonuniformity.

Suppose that the flow of Bose-condensed atoms moves with a constant velocity \mathbf{v} , being described by the Gross-Pitaevskii equation. The latter is invariant with respect to the Galilean transformation

$$\eta_v(\mathbf{r}, t) = \eta(\mathbf{r} - \mathbf{v}t, t) \exp \left(i m \mathbf{v} \cdot \mathbf{r} - i \frac{mv^2}{2} t \right), \quad (3.61)$$

where $v \equiv |\mathbf{v}|$. Considering small deviations from a stationary solution $\eta(\mathbf{r} - \mathbf{v}t)$ in the form

$$\eta(\mathbf{r} - \mathbf{v}t, t) = \eta(\mathbf{r} - \mathbf{v}t) + u_v(\mathbf{r})e^{-i\omega t} + v_v^*(\mathbf{r})e^{i\omega t}, \quad (3.62)$$

we substitute this form into the Gross-Pitaevskii equation. Then, by the standard procedure of the linearization of the Gross-Pitaevskii equation with respect to the small deviations, we come to a variant of the Bogolubov equations for the moving gas. In the local-density approximation, this gives the spectrum of collective excitations for the

moving system

$$\varepsilon_v(\mathbf{k}, \mathbf{r}) = \mathbf{v} \cdot \mathbf{k} + \sqrt{c^2(\mathbf{r})k^2 + \left(\frac{k^2}{2m}\right)^2}. \quad (3.63)$$

When all flow is Bose-condensed, the local sound velocity is given by the relation

$$mc^2(\mathbf{r}) = \rho_0(\mathbf{r})\Phi_0, \quad (3.64)$$

which is a particular form of Eq. (3.37).

The flow is everywhere stable if the excitation spectrum is everywhere positive. This requires the validity of the stability condition

$$v < v_c \equiv \min_{\mathbf{k}, \mathbf{r}} \frac{\varepsilon(\mathbf{k}, \mathbf{r})}{k} = \min_{\mathbf{r}} c(\mathbf{r}). \quad (3.65)$$

This condition is a slight generalization of the Landau criterion of superfluidity [9] to a nonuniform system treated in the local-density approximation. When atoms move with a low velocity, smaller than v_c , the system is in Bose-condensed state. However, as soon as the velocity exceeds the critical value v_c , there arise exponentially diverging solutions leading to the system instability. As a result, the unstable system has to pass to the normal state, without condensate and with no superfluidity.

3.3.2 Stratification in multicomponent mixtures

In a system, consisting of several components of atomic condensates, there can occur a phase transition accompanied by spontaneous breaking of translational symmetry. Then a uniform mixture of atomic species separates into different spatial parts, with each part filled by only one kind of atoms. This phase transition is called *stratification* [189, 190]. Conditions, when such a stratification arises, depend on atomic parameters and their interactions.

Let us have a mixture of several bosonic species, enumerated by an index $i = 1, 2, \dots$. Respectively, atomic masses of the species are denoted as m_i and the interaction potentials between the i -th and j -th components are $\Phi_{ij}(\mathbf{r})$. Keeping in mind the local-density approximation, we need the average interaction parameters

$$\Phi_{ij} \equiv \int \Phi_{ij}(\mathbf{r}) d\mathbf{r}. \quad (3.66)$$

The diagonal terms Φ_{ii} are assumed to be positive in order that each of the components of Bose atoms would be stable [153]. Two components can be uniformly mixed at zero temperature, provided that the stability condition

$$\Phi_{ij} < \sqrt{\Phi_{ii}\Phi_{jj}} \quad (3.67)$$

holds. The condition can be obtained from the minimization of the system energy [115]. If this condition does not hold, the system stratifies into separated spatial regions of single-component subsystems, so that the translational symmetry becomes broken.

The same condition (3.67) can be derived by analyzing the stability of the spectrum of collective excitations [189, 190]. For the mixture of two Bose-condensed components, the spectrum splits into two branches, given by the equation

$$\begin{aligned} \varepsilon_{\pm}^2(\mathbf{r}, \mathbf{k}) = & \frac{1}{2} \{ \varepsilon_1^2(\mathbf{k}, \mathbf{r}) + \varepsilon_2^2(\mathbf{k}, \mathbf{r}) \pm \\ & \pm \sqrt{[\varepsilon_1^2(\mathbf{k}, \mathbf{r}) - \varepsilon_2^2(\mathbf{k}, \mathbf{r})]^2 + 4\varepsilon_{12}^4(\mathbf{k}, \mathbf{r})} \} , \end{aligned} \quad (3.68)$$

where the notations

$$\begin{aligned} \varepsilon_{ij}^2(\mathbf{k}, \mathbf{r}) = & c_{ij}^2(\mathbf{r})k^2 + \delta_{ij} \left(\frac{k^2}{2m_i} \right)^2 , \\ c_{ij}^2(\mathbf{r}) = & \sqrt{\frac{\rho_i(\mathbf{r})\rho_j(\mathbf{r})}{m_i m_j}} \Phi_{ij} , \end{aligned} \quad (3.69)$$

and $\varepsilon_i \equiv \varepsilon_{ii}$ are used. The upper part of the spectrum, $\varepsilon_+(\mathbf{k}, \mathbf{r})$, describes the density wave propagating through the mixture, while the lower part, $\varepsilon_-(\mathbf{k}, \mathbf{r})$, corresponds to the oscillations of the components with respect to each other. The mixture stratifies when the lower spectrum goes to zero.

When there are two components moving with the velocities \mathbf{v}_i , then the spectrum of collective excitations is defined by the equation

$$\prod_{i=1}^2 [(\omega - \mathbf{v}_i \cdot \mathbf{k})^2 - \varepsilon_i^2(\mathbf{k}, \mathbf{r})] = \varepsilon_{12}^4(\mathbf{k}, \mathbf{r}) . \quad (3.70)$$

Then, even if the mixture has been stable in the immovable state, it becomes stratified as soon as the relative velocity of the second component through the first one reaches the critical value [191]

$$\begin{aligned} v_c = & \min_{\mathbf{r}} \frac{\sqrt{c_1^2(\mathbf{r})c_2^2(\mathbf{r}) - c_{12}^4(\mathbf{r})}}{c_1(\mathbf{r})} = \\ = & \min_{\mathbf{r}} \sqrt{\frac{\rho_2(\mathbf{r})}{m_2\Phi_{11}}} (\Phi_{11}\Phi_{22} - \Phi_{12}^2) , \end{aligned} \quad (3.71)$$

where $c_i \equiv c_{ii}$.

In uniform macroscopic systems, the stratification occurs simultaneously in the whole volume. But in finite systems, that are nonuniform, the stratification may start in a part of the system and then proliferate to other parts by a kind of shock waves producing turbulence [192]. This means that in finite systems, the stratification is easier achieved than in large uniform systems.

3.3.3 Generation of quantum vortices

Breaking of translational symmetry also happens when there appear quantum vortices. The straightforward way of creating vortices is by means of rotation. Suppose that the system is rotated with a constant angular frequency $\vec{\omega}$. The single-particle Hamiltonian,

in the Schrödinger representation, in the frame rotating with the same angular frequency, has the form [193]

$$\hat{H}_{rot}(\mathbf{r}) = \frac{\hat{\mathbf{p}}^2}{2m} - \vec{\omega} \cdot \hat{\mathbf{L}} + U(\mathbf{r}) , \quad (3.72)$$

with the momentum operator $\hat{\mathbf{p}} \equiv -i\nabla$ and angular momentum $\hat{\mathbf{L}} \equiv \mathbf{r} \times \hat{\mathbf{p}}$. Here $U(\mathbf{r})$ is a trapping potential. This Hamiltonian can also be represented as

$$\hat{H}_{rot}(\mathbf{r}) = \frac{(\hat{\mathbf{p}} - m\mathbf{v})^2}{2m} - \frac{mv^2}{2} + U(\mathbf{r}) , \quad (3.73)$$

with the linear velocity $\mathbf{v} \equiv \vec{\omega} \times \mathbf{r}$. This expression shows that the motion of a neutral particle in a rotating system is analogous to the motion of a charged particle in an external magnetic field, with a vector potential \mathbf{A} and magnetic field \mathbf{B} given by the relations

$$\frac{e}{c} \mathbf{A} \equiv m\mathbf{v} = m(\vec{\omega} \times \mathbf{r}) , \quad \mathbf{B} \equiv \vec{\nabla} \times \mathbf{A} = \frac{2m}{e} \vec{\omega} .$$

It is common to choose the direction of the angular frequency along the z -axis, so that $\vec{\omega} = \omega \mathbf{e}_z$. If the trapping potential is harmonic,

$$U(\mathbf{r}) = \frac{m}{2} \omega_{\perp}^2 (x^2 + y^2) + \frac{m}{2} \omega_z^2 z^2 , \quad (3.74)$$

then Hamiltonian Eq. (3.73) reads as

$$\begin{aligned} \hat{H}_{rot}(\mathbf{r}) &= \frac{(\hat{\mathbf{p}} - m\mathbf{v})^2}{2m} + \\ &+ \frac{m}{2} (\omega_{\perp}^2 - \omega^2) (x^2 + y^2) + \frac{m}{2} \omega_z^2 z^2 . \end{aligned} \quad (3.75)$$

The problem is equivalent to that describing the motion of a charged particle in a constant magnetic field in the presence of a harmonic potential [87, 194]. The eigenvalues of Hamiltonian (3.75) are

$$E_{nlk} = (2n + |l| + 1)\omega_{\perp} + \left(k + \frac{1}{2}\right)\omega_z - l\omega , \quad (3.76)$$

where $n = 0, 1, 2, \dots$ is the radial quantum number, $l = 0, \pm 1, \pm 2, \dots$ is the azimuthal quantum number, sometimes also called winding number or circulation quantum, and $k = 0, 1, 2, \dots$ is the axial quantum number. The spectrum reduces to the set of Landau levels if either $\omega = \omega_{\perp}$, $l \geq 0$ or $\omega = -\omega_{\perp}$, $l \leq 0$.

The many-particle system in the rotating frame is characterized by the energy Hamiltonian in the Heisenberg representation

$$\begin{aligned} \hat{H} &= \int \hat{\psi}^{\dagger}(\mathbf{r}) \hat{H}_{rot}(\mathbf{r}) \hat{\psi}(\mathbf{r}) d\mathbf{r} + \\ &+ \frac{1}{2} \int \hat{\psi}^{\dagger}(\mathbf{r}) \hat{\psi}(\mathbf{r}') \Phi(\mathbf{r} - \mathbf{r}') \hat{\psi}(\mathbf{r}') \hat{\psi}(\mathbf{r}) d\mathbf{r} d\mathbf{r}' . \end{aligned} \quad (3.77)$$

Substituting here the Bogolubov shift of the field operator, from the equation of motion, one obtains the equation for the condensate wave function, as is explained in Sec. 3.

This equation, for the case of weak interactions and temperatures, reduces to the Gross-Pitaevskii equation.

The first vortex, with the winding number $l = 1$, appears when the angular frequency reaches a critical value ω_c . An explicit expression of this value depends on the physical situation and the approximation involved. When the Bose system is trapped in a cylindrically symmetric harmonic potential, fully condensed, being described by the Gross-Pitaevskii equation, and allows for the Thomas-Fermi approximation, then the critical rotation frequency is

$$\omega_c = \frac{5}{2mR^2} \ln \left(0.7 \frac{R}{\xi} \right) , \quad (3.78)$$

where $\xi = 1/\sqrt{2m\rho_0\Phi_0}$ is the healing length, R , Thomas-Fermi radius, and $\rho_0 = \rho(0)$ is the condensate density at the trap center in the absence of rotation [115].

The vortices with the higher winding numbers $l > 1$ require larger critical frequencies. But such vortices have larger energies and are unstable with respect to the decay into the vortices with lower winding numbers [115, 117]. Increasing the rotation frequency generates, first, a small number of vortices and subsequently an array of many vortices forming a triangular lattice [195], with all the vortices having a single quantum of circulation $l = 1$. This vortex lattice is analogous to the triangular Abrikosov lattice of magnetic vortices in superconductors [196].

In experiment, vortices can be created in several ways. The straightforward method is by stirring the cloud of trapped atoms with a laser spoon. It is also possible to apply radio-frequency field for transferring atoms between hyperfine states, from a non-rotating state to a rotating state. There is a method of creating vortices that does not rely on mechanical stirring, but employs adiabatic transfer between hyperfine states, with the formation of spatially dependent geometric Berry phase [197].

More details on the physics of vortices in Bose-condensed systems can be found in review articles [198–201]. The mathematics of describing vortices in trapped atoms are similar to that of characterizing quantum dots in magnetic fields and rotating nuclei.

3.3.4 Topological coherent modes

Quantum vortices can be generated in macroscopic systems, such as ^4He , as well as in trapped gases. But in finite quantum systems there can be generated a larger variety of nonlinear excitations breaking translational and rotational symmetry, of which the vortices are just a particular type. These are the *topological coherent modes* [202] that are the stationary solutions of the condensate-function equation (3.29). For example, in the case of the fully Bose-condensed gas, when the Gross-Pitaevskii equation (3.31) is applicable, the stationary solutions are given by the eigenproblem

$$\left[-\frac{\nabla^2}{2m} + U(\mathbf{r}) \right] \eta_n(\mathbf{r}) + \Phi_0 |\eta_n(\mathbf{r})|^2 \eta_n(\mathbf{r}) = E_n \eta_n(\mathbf{r}) , \quad (3.79)$$

where n is a quantum multi-index enumerating the modes and $\mu_0 = \min_n E_n$.

The stationary nonlinear Schrödinger equation is the notion that is widely accepted. It enjoys the form $H_{NLS}\eta_n = E_n\eta_n$, with the H_{NLS} being the nonlinear Schrödinger Hamiltonian. This is the standard form of an eigenproblem equation. By the common definition, the eigenvalue of a Hamiltonian is termed energy.

Note the principal difference between these coherent modes, defined by the nonlinear Schrödinger equation (3.79), and the elementary collective excitations, described by the linear Bogolubov equations (3.35). The modes are called coherent, since they correspond to the condensate function that characterizes the coherent part of the Bose system. And they are termed topological, since different solutions of Eq. (3.79) have different spatial topology, with different numbers of zeros. Each coherent mode corresponds to a stationary nonground-state condensate.

In a finite system, where atoms are confined by a trapping potential, the spectrum of the eigenvalues of Eq. (3.79) is discrete. This makes the principal difference of the situation in finite systems from that of uniform macroscopic systems, where the spectrum is continuous. When the spectrum is discrete, it is possible to transfer atoms between different energy levels, thus, transferring atoms between different topological modes. Such a transfer can be effectively realized by means of the corresponding resonance fields [202–204]. The situation is similar to the case of resonance atoms, whose electrons can be transferred between their energy levels by resonance electromagnetic fields. The latter resonance transitions are well studied in the optical and infrared regions [205] and even are considered for the gamma region [206]. Another similarity is with spin systems that allow for realizing transitions between different discrete Zeeman levels [207]. The main feature of the considered case of Bose-condensed atoms is that the energy levels E_n , given by Eq. (3.79), correspond to many-particle states, but not to single-electron or single-spin states. Consequently, the related eigenproblem is nonlinear, including atomic interactions. The role of a resonant object is played by the whole trapped Bose system, but not by a single particle.

Trapped atoms can be transferred between their energy levels E_n , say between the levels E_1 and E_2 , by two main techniques. One method [202] is by modulating the trapping potential with a temporal variation

$$V(\mathbf{r}, t) = V_1(\mathbf{r}) \cos(\omega t) + V_2(\mathbf{r}) \sin(\omega t) , \quad (3.80)$$

tuning the modulation frequency ω close to the resonance with the desired transition frequency $\omega_{12} \equiv E_2 - E_1$, so that the resonance condition

$$\omega = \omega_{12} \quad (3.81)$$

be approximately satisfied. The modulating field is added to the trapping potential $U(\mathbf{r})$.

The other method [208, 209] is by modulating atomic interactions, which can be realized by Feshbach resonance techniques, so that the atomic interaction becomes alternating,

$$\Phi(t) = \Phi_0 + \Phi_1 \cos(\omega t) + \Phi_2 \sin(\omega t) , \quad (3.82)$$

with the frequency ω tuned to the resonance condition (3.81).

The solution to the time-dependent equation (3.31) can be presented as the expansion over the coherent modes,

$$\eta(\mathbf{r}, t) = \sum_n c_n(t) \eta_n(\mathbf{r}) e^{-i\omega_n t} , \quad (3.83)$$

with $\omega_n = E_n - E_0$. Fractional mode populations are given by the expressions

$$p_n(t) \equiv |c_n(t)|^2 . \quad (3.84)$$

The solution of the corresponding time-dependent nonlinear Schrödinger equation for the condensate function can be done by invoking averaging methods [202, 203] or numerically [204, 210, 211].

If the driving frequency of the alternating pumping field is tuned close to the resonance condition (3.81), then, for generating the coherent modes, it is sufficient to have a rather weak amplitude of the pumping field [202, 203]. Increasing the amplitude of this field makes it possible to generate coherent modes under the wider class of resonance conditions [204]. Thus, the modes are generated under the conditions of *harmonic generation*

$$n\omega = \omega_{12} \quad (n = 1, 2, \dots) . \quad (3.85)$$

If there are two modulating fields, with the frequencies ω_1 and ω_2 , coherent modes can be generated under the condition of *parametric conversion*

$$\omega_1 \pm \omega_2 = \omega_{12} \quad (3.86)$$

or the condition of *combined resonance*

$$n_1\omega_1 + n_2\omega_2 = \omega_{12} \quad (n_i = \pm 1, \pm 2, \dots) . \quad (3.87)$$

When there are several modulating fields, with the frequencies ω_i , coherent modes can be generated under the condition of *generalized resonance*

$$\sum_i n_i \omega_i = \omega_{12} \quad (n_i = \pm 1, \pm 2, \dots) . \quad (3.88)$$

The topological coherent modes, representing nonground-state condensates, possess a variety of interesting properties, such as interference patterns and interference current, mode locking, dynamical phase transitions and critical phenomena, chaotic motion, atomic squeezing, entanglement production, and Ramsey fringes [202–204, 212]. Examples of the coherent modes are the well known quantum vortices and the dipole mode that was generated in experiment [213].

3.3.5 Nonequilibrium crossover transitions

Among all topological coherent modes, the basic vortex with the unit circulation number $l = 1$ plays a special role. This is caused by the fact that the transition frequencies $\omega_n \equiv E_n - E_0$, characterizing the transitions from the ground state to an excited state with the energy E_n , depend on the parameter αg , where $\alpha \equiv \omega_z/\omega_\perp$ is the trap aspect ratio and $g \equiv 4\pi N a_s/l_\perp$ is the dimensionless interaction parameter. The transition frequencies for all modes, except the basic vortex mode, grow with this parameter as $(\alpha g)^{2/5}$. But the transition frequency of the vortex, vice versa, diminishes with this parameter [117, 203]. For instance, the critical frequency (3.78) depends on this parameter as

$$\omega_c = \frac{0.9}{(\alpha g)^{2/5}} \ln(0.8\alpha g) . \quad (3.89)$$

Therefore, at large parameter αg , the energy of the basic vortex mode is the lowest among all coherent modes. Therefore, all other modes, except the basic vortex mode,

are energetically unstable and, being created, decay into the basic vortices with unit circulation.

This unique feature of the basic vortex suggests that, by modulating either the trapping potential with the additional alternating field (3.80) or the atomic interaction, as in Eq. (3.82), it is admissible to generate multiple vortices and anti-vortices. For sufficiently large modulation amplitude and/or sufficiently long modulation time, a great number of vortices can be created. Contrary to the case of rotation, where only vortices are generated, in the considered case of modulation, the vortices are created in pairs with anti-vortices. And, instead of forming a triangular vortex lattice, as in the case of rotation, in the process of the alternating modulation, vortices and anti-vortices form a random vortex tangle.

Such a random vortex tangle is a typical feature of *quantum turbulence*. The latter has been widely studied for the case of turbulent superfluids ^3He and ^4He , and quantum gases, as is reviewed in literature [214–221]. Quantum turbulence of trapped atoms has been observed in experiments [222–224].

The state of the system, produced by means of the suggested modulation, depends on both, the modulation amplitude and modulation time. This is because both these characteristics are responsible for the amount of energy injected into the system. Let the total Hamiltonian consist of two terms, $H = H_0 + \hat{V}(t)$, where the first term does not depend on time, while the second term, $\hat{V}(t)$ accomplishes the modulation during the time t_{mod} . Then the amount of energy per atom, injected into the system by the modulating term, can be defined as

$$E_{inj} \equiv \frac{1}{N} \int_0^{t_{mod}} \left| \left\langle \frac{\partial \hat{V}(t)}{\partial t} \right\rangle \right| dt. \quad (3.90)$$

The injected energy plays the role of an effective temperature. If the effective amplitude of the modulating field is V_{mod} and the modulation frequency is ω , then the injected energy (3.90) can be estimated as $E_{inj} = \omega t_{mod} V_{mod}$.

The overall picture, under increasing the injected energy (3.90), is as follows. Let, the system be prepared in the Bose-condensed superfluid state without vortices. This state can be called *regular superfluid*. Switching on pumping, first, produces a small number of vortices, which forms what can be called the state of *vortex superfluid*. Increasing the injected energy (3.90) generates a random tangle of multiple vortices forming the state of *turbulent superfluid*.

Since the influence of the injected energy is analogous to that of temperature, increasing E_{inj} depletes the amount of condensed atoms, transferring them to the normal, uncondensed, fraction. When the normal fraction of atoms becomes substantial, the system stratifies into the pieces of Bose-condensed droplets separated by the regions of normal fluid. Inside each of the droplets, there exists coherence, but different droplets are not coherent with each other. The locations of the coherent droplets are random. Their shapes also are random, with the surfaces that can be fractal [225]. Such a state is equivalent to a heterophase system consisting of a random mixture of different phases [43, 226]. Hence, it can be called *heterophase fluid*. This heterophase state, consisting of coherent, Bose-condensed, and incoherent, normal, spatially separated regions, could also be called nonequilibrium Bose glass or granular condensate. The formation of this heterophase mixture could be called granulation.

Increasing further the injected energy depletes the condensate more and more, finally

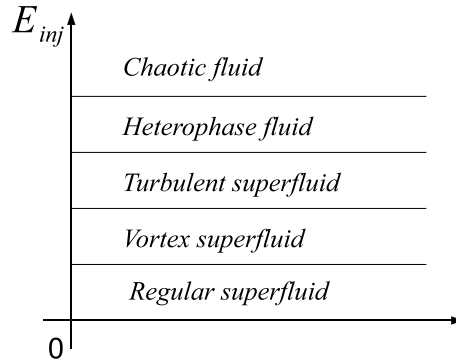


Figure 1: Qualitative scheme of the sequence of states for a trapped Bose system subject to the pumping of an alternating modulating field, with the increasing injected energy E_{inj} .

destroying all coherence in the system, making the whole fluid normal. But, since there is a strong external pumping field, the fluid is strongly nonequilibrium, demonstrating chaotic oscillations, because of which the state can be named *chaotic fluid*. This state reminds classical turbulence [227], such as occurs in plasma [228, 229].

The general sequence of the nonequilibrium states, arising under the pumping of the system of trapped Bose atoms, is shown in Fig. 1. Transitions from one state to another are not genuine phase transitions, but rather are crossovers. The sequence of the described states, under the rising amount of the injected energy, was observed in experiment [223, 224]. All the states, starting from the regular superfluid to the granulated heterophase fluid were demonstrated and studied. Only the last stage of chaotic fluid was not achieved.

3.4 Pairing of fermionic atoms

3.4.1 Harmonically trapped fermions

Several species of neutral Fermi atoms have been trapped and cooled down to low temperatures corresponding to quantum degenerate regime. These are, the alkali atoms potassium (^{40}K) and lithium (^6Li) and also ^3He and ^{173}Yb . The physics of ultracold degenerate trapped fermions has been discussed in the reviews [230–232]. Here, we emphasize only some basic facts concerning these gases, concentrating on their symmetry properties.

Trapped fermions provide a unique opportunity of studying different states of the same atomic system by varying atomic interactions, which can be done by means of Feshbach resonance techniques [233]. By these techniques, the scattering length can be varied by an external magnetic field in a very wide range between negative and positive values. The scattering length, as a function of the magnetic field B , is given by the expression

$$a_s(B) = a_s \left(1 + \frac{\Delta_B}{B - B_0} \right), \quad (3.91)$$

in which B_0 is the resonance magnetic field, Δ_B is the resonance width, and a_s is the off-resonant scattering length.

The principal difference between bosons and fermions is that Bose gases with large scattering lengths experience strongly enhanced inelastic collisions, which prevents the

experiments to reach the strongly interacting regime [234]. While Fermi gases, due to Pauli suppression effect, can be remarkably stable against inelastic decay, allowing for the formation of stable molecular quantum gases [231].

One usually considers harmonically trapped Fermi gases with spin 1/2. Their Fermi energy is

$$E_F = \omega_0(3N)^{1/3} , \quad (3.92)$$

where $\omega_0 \equiv (\omega_x \omega_y \omega_z)^{1/3}$ and N is the total number of fermions in the trap. The Fermi wave number k_F is defined through the relation

$$\frac{k_F^2}{2m} = E_F , \quad (3.93)$$

which gives

$$k_F = \frac{\sqrt{2}}{l_0} (3N)^{1/6} . \quad (3.94)$$

The atomic density at the center of the trap is

$$\rho(0) = \frac{k_F^3}{3\pi^2} . \quad (3.95)$$

Similar relations are valid for fermions in atomic nuclei, that is, neutrons and protons.

3.4.2 Pair formation and superfluidity

Dilute gases, whose interaction radius is much shorter than the mean interatomic distance, are described by the contact interaction potential (3.30). The interaction regimes are characterized by the dimensionless parameter $1/(k_F a_s)$. In the limit $1/(k_F a_s) \ll -1$, fermions form Cooper pairs with the standard Bardeen-Cooper-Schrieffer (BCS) ground state [235]. The Cooper pairs are formed by two atoms, with opposite momenta and spins, on the surface of the Fermi sphere. The pairing energy, i.e. the gap, is small compared with the Fermi energy, and the Cooper pair size greatly exceeds the typical inter-atomic spacing. The ground state is equivalent to the BCS superconducting state, but, since the atoms are neutral, the state is termed superfluid.

In the limit $1/(k_F a_s) \gg 1$, the fermions form bosonic molecules, with the ground state being Bose-Einstein condensate (BEC). The molecular binding energy is large compared with all other energies, and the molecular size is small compared with typical interatomic spacing. The physics of these small molecules is understood as that of composite bosonic atoms forming superfluid state.

The crossover region $-1 < 1/(k_F a_s) < 1$ corresponds to the strongly interacting regime, where the pairs are no longer pure Cooper pairs or pure bosonic molecules. Their binding energy is comparable to the Fermi energy, and their size is about the inter-atomic spacing. The ground state is also superfluid, but such that both bosonic and fermionic degrees of freedom are important, which is called *resonance superfluidity* [236, 237].

Weakly bound molecules, made of fermionic atoms near a Feshbach resonance, are called *dimers*. The elastic atom-molecule collisions [238, 239] are described by the effective scattering length a_{am} , and molecule-molecule collisions [240], by the scattering length a_{mm} , which are expressed through the atom-atom scattering length a_s by the relations [239, 240]

$$a_{am} = 1.18a_s , \quad a_{mm} = 0.60a_s . \quad (3.96)$$

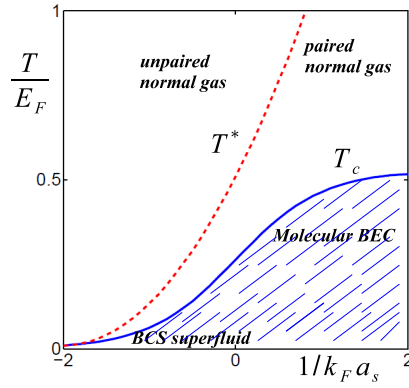


Figure 2: (Color online) Schematic phase diagram of the BCS-BEC crossover. The critical temperature T_c (solid line) shows the phase transition between the normal phase, with unbroken gauge symmetry, and superfluid phase, with broken gauge symmetry. The pairing temperature T^* (dashed line) marks the onset of pairing inside the normal phase. The superfluid region with broken gauge symmetry is shadowed.

The ground state at $T = 0$, throughout the whole range of interactions, is formed by pairs, either Cooper pairs or bosonic molecules, and it is superfluid for all $k_F a_s$. But the critical temperature of superfluid transition T_c , generally, does not coincide with the temperature of molecule formation T^* . In the framework of BCS theory, there is no difference between T_c and T^* , which means that the formation of Cooper pairs and superfluid transition occur simultaneously. But on the BEC side, molecules are formed at much higher temperatures than Bose-Einstein condensation occurs. Thus, $T_c \leq T^*$.

In the BCS limit, the characteristic temperatures are given [231] by the known expressions

$$\begin{aligned} T_c &= 0.277 E_F \exp \left(- \frac{\pi}{2 k_F |a_s|} \right) , \\ T^* &= T_c \quad \left(\frac{1}{k_F a_s} \ll -1 \right) . \end{aligned} \quad (3.97)$$

And in the BEC limit, the temperatures are defined [241] by the equations

$$\begin{aligned} 12 \left(\frac{T^*}{E_F} \right)^3 &= \exp \left\{ \frac{2 E_F}{T^* (k_F a_s)^2} \right\} , \\ T_c &= 0.518 E_F \quad \left(\frac{1}{k_F a_s} \gg 1 \right) . \end{aligned} \quad (3.98)$$

The transition between the BCS and BEC limits is a gradual crossover.

3.4.3 Pairing and symmetry breaking

In the region of temperatures $T_c < T < T^*$, pairs are formed, however, gauge symmetry is not yet broken. The gauge symmetry becomes broken only at temperatures below T_c . The difference from the case of Bose-Einstein condensation of bosonic atoms, is that the

breaking of gauge symmetry for fermions is accompanied by the appearance of only *even* anomalous averages, such as

$$\langle \psi_\sigma(\mathbf{r})\psi_{-\sigma}(\mathbf{r}') \rangle \neq 0 , \quad (3.99)$$

where $\psi_\sigma(\mathbf{r})$ is a Fermi field operator for a spin component σ [242]. But odd anomalous averages are zero, e.g.,

$$\langle \psi_\sigma(\mathbf{r}) \rangle = 0 , \quad (3.100)$$

which is related to the conservation of spin.

The schematic phase diagram illustrating the BCS-BEC crossover and the regions of broken and unbroken gauge symmetry is presented in Fig. 2. This diagram concerns atoms with the standard Hamiltonian including only contact interactions, characterized by *s*-wave scattering length. No dipole or spinor interactions are included. Recently, there have also appeared publications studying effective spin-orbit interactions of trapped atoms [243, 244]. Such additional interactions, of course, can change the whole picture.

3.5 On condensation of unconserved quasiparticles

3.5.1 Conserved versus unconserved particles

In all sections above, atomic systems are considered, where the total average number of atoms N has been fixed. In that sense the atoms, as such, are stable and conserved. There are also particles or quasiparticles whose total number is not fixed but can be varied by creating quasiparticles with applying external fields. While without external supporting fields, in an equilibrium system, the quasiparticles decay, so that their total number is not conserved. Examples of such quasiparticle excitations are excitons and polaritons.

Unconserved quasiparticles, whose number is not fixed, cannot form Bose-Einstein condensates in equilibrium systems. The chemical potential of unconserved quasiparticles is zero. When diminishing temperature, their density decreases, so that Bose condensation does not occur.

However, in nonequilibrium systems, subject to the action of external time-dependent fields, the density of unconserved quasiparticles can be supported at sufficiently high level, and condensation can be feasible. For example, there happens nonequilibrium condensation of excitons [245–248], polaritons [249–251], and photons [252].

Another type of unconserved quasiparticles is represented by elementary collective excitations, such as phonons (density fluctuations), bogolons (density fluctuations in a Bose-condensed system), and magnons (spin fluctuations). An important question is whether such collective excitations could form Bose-Einstein condensates by themselves, and, if so, under what conditions? As is explained above, Bose condensation is necessarily accompanied by the global gauge symmetry breaking. So, the question is whether this breaking can occur in a subsystem of collective excitations?

3.5.2 No condensation of self-consistent phonons

Phonons are introduced by defining, first, deviations \mathbf{u}_j from a given spatial point \mathbf{a}_j , and then representing these deviations through phonon operators b_{ks} . If the location \mathbf{a}_j is fixed, then formally phonons can start condensing at the point of a phase transition. But, if the vector \mathbf{a}_j is defined as the average location, then there is no phonon condensation,

but there is the variation of this location \mathbf{a}_j . The latter self-consistent procedure can be generalized to nonequilibrium situations, when atomic positions depend on time, so that one could write

$$\mathbf{r}_j(t) = \mathbf{a}_j(t) + \mathbf{u}_j(t) , \quad (3.101)$$

with the self-consistency condition

$$\mathbf{a}_j(t) = \langle \mathbf{r}_j(t) \rangle \quad (3.102)$$

definition the vector \mathbf{a}_j as the average location. Owing to this self-consistent way of introducing deviations, one has

$$\langle \mathbf{u}_j(t) \rangle = 0 . \quad (3.103)$$

Consequently, the corresponding phonon operators are such that

$$\langle b_{ks}(t) \rangle = 0 , \quad (3.104)$$

which implies the absence of Bose condensation of phonons.

In this way, if one introduces the deviation \mathbf{u}_j , counted from a given fixed location \mathbf{a}_j , then at the phase transition point there can arise phonon Bose condensation implying the necessity of changing the definition of the location vectors \mathbf{a}_j , which is equivalent to the change of the spatial system structure. However, if one imposes the self-consistency condition (3.102), then the phonons, defined in such a self-consistent way, cannot condense, whether in equilibrium or in nonequilibrium systems. This also concerns phase transition points, where there occurs a sharp variation of the mean locations \mathbf{a}_j .

3.5.3 No condensation of generic bogolons

Bogolons are quasiparticles characterizing elementary collective excitations in a Bose-condensed system. They are introduced by means of the Bogolubov shift that, for an arbitrary nonequilibrium system, reads as

$$\hat{\psi}(\mathbf{r}, t) = \eta(\mathbf{r}, t) + \psi_1(\mathbf{r}, t) , \quad (3.105)$$

where the condensate wave function is the system order parameter

$$\eta(\mathbf{r}, t) = \langle \hat{\psi}(\mathbf{r}, t) \rangle . \quad (3.106)$$

Recall that the Bogolubov shift (3.105) is not an approximation, but an exact canonical transformation that does not require that ψ_1 be in any sense small.

Because of this definition, one has the exact equality

$$\langle \psi_1(\mathbf{r}, t) \rangle = 0 . \quad (3.107)$$

The bogolon operators $b_k(t)$ are introduced through the Bogolubov canonical transformation

$$\psi_1(\mathbf{r}, t) = \sum_k \left[u_k(\mathbf{r}) b_k(t) + v_k^*(\mathbf{r}) b_k^\dagger(t) \right] , \quad (3.108)$$

in which k is a multi-index. In view of Eqs. (3.107) and (3.108), one has

$$\langle b_k(t) \rangle = 0 , \quad (3.109)$$

which tells us that the gauge symmetry for bogolons cannot be broken.

The self-consistent definition of bogolons shows that they cannot form Bose condensate in any system, whether equilibrium or not, similar to the absence of condensation of self-consistently defined phonons. This should be of no surprise, since bogolons, similarly to phonons, characterize density fluctuations, albeit in a Bose-condensed system. In that system, conserved atoms condense, yielding the order parameter (3.106), while unconserved bogolons cannot condense, possessing only the trivial parameter (3.109).

3.5.4 No condensation of equilibrium magnons

Between Bose systems and spin systems, there exists a direct analogy [253, 254]. Therefore, one should expect that the elementary collective excitations of spin systems, that is, magnons, should not be able to condense, at least in equilibrium systems, as has been stressed by Mills [255]. Despite this, many authors state that there can occur condensation of magnons in equilibrium. Below we show that this is impossible, provided magnons are correctly defined.

Let us consider a system of spins \mathbf{S}_j , enumerated by the index $j = 1, 2, \dots, N$. And let the system of coordinates be chosen so that the mean spin be directed along the z -axis. Magnon operators b_j are introduced by means of the Holstein-Primakoff [256] representation

$$S_j^+ = \sqrt{2S - b_j^\dagger b_j} b_j, \quad S_j^- = b_j^\dagger \sqrt{2S - b_j^\dagger b_j}, \quad S_j^z = S - b_j^\dagger b_j, \quad (3.110)$$

where S is the spin value. As is emphasized by Holstein and Primakoff, this representation is valid under the condition that the magnetization is directed along the z -axis,

$$\langle \mathbf{S}_j \rangle = \langle S_j^z \rangle \mathbf{e}_z, \quad (3.111)$$

and that it is close to the saturation value, so that

$$\frac{|S - \langle S_j^z \rangle|}{2S} \ll 1. \quad (3.112)$$

Condition (3.111) tells us that there is no transverse magnetization,

$$\langle S_j^\pm \rangle = 0, \quad (3.113)$$

while inequality (3.112) shows that the magnon density must be small,

$$\frac{\langle b_j^\dagger b_j \rangle}{2S} \ll 1. \quad (3.114)$$

This is a necessary condition for interpreting the roots of operators in Eq. (3.110) as expansions in Taylor series in powers of $b_j^\dagger b_j$. Note that the functions of operators are standardly defined as expansions over these operators. In the present case, the expansion over $b_j^\dagger b_j$, implies the smallness of the eigenvalues of $b_j^\dagger b_j / 2S$, which is a sufficient condition for the validity of condition (3.114).

In the lowest order, one has

$$S_j^+ \cong \sqrt{2S} b_j, \quad S_j^- \cong \sqrt{2S} b_j^\dagger.$$

In that way, by definition (3.113), we have

$$\langle b_j \rangle = 0, \quad (3.115)$$

implying that magnons cannot condense in an equilibrium system.

Conversely, from the absence of magnon Bose condensation, that is from the equation $\langle b_j \rangle = 0$, it immediately follows that $\langle S_j^+ \rangle = 0$, hence $\langle \mathbf{S}_j \rangle = \langle S_j^z \rangle \mathbf{e}_z$, corresponding to the mean spin direction along the z -axis.

It is, certainly, not necessary to choose the mean spin being directed along the z -axis, but it is just convenient. It is, of course, possible to consider the case of the mean spin directed arbitrarily and to write down the Holstein-Primakoff transformation for this case, as has been done by Rückriegel et al. [257]. In the general case of a mean spin $\langle \mathbf{S}_j \rangle$ directed arbitrarily, the spin components $\{S_j^1, S_j^2, S_j^3\}$ are the projections of the spin operator \mathbf{S}_j on the axes defined by the unit mutually orthogonal vectors \mathbf{e}^1 , \mathbf{e}^2 , and \mathbf{e}^3 , with the latter vector being

$$\mathbf{e}_j^3 = \frac{\langle \mathbf{S}_j \rangle}{|\langle \mathbf{S}_j \rangle|}.$$

The spin operator is represented as the sum

$$\mathbf{S}_j = \frac{1}{2} (S_j^+ \mathbf{e}_j^- + S_j^- \mathbf{e}_j^+) + S_j^3 \mathbf{e}_j^3,$$

in which

$$S_j^\pm \equiv S_j^1 \pm i S_j^2, \quad \mathbf{e}_j^\pm \equiv \mathbf{e}_j^1 \pm i \mathbf{e}_j^2.$$

Then the components S_j^\pm are given by the same transformations as above and S_j^3 , as the component S_j^z .

According to this construction, one has

$$\langle \mathbf{S}_j \rangle = \langle S_j^3 \rangle \mathbf{e}_j^3,$$

from where, as before, it follows that

$$\langle \mathbf{S}_j^\pm \rangle = 0, \quad \langle b_j \rangle = 0,$$

implying the absence of magnon condensation. This conclusion is clear, since physics does not depend on the choice of coordinates.

When one meets a formal magnon condensation in equilibrium, this just means that there appears a transverse spin component and there occurs magnetization rotation. Then, in order that the Holstein-Primakoff representation would be valid, one needs to redirect the z -axis along the new magnetization direction. The situation is completely analogous to the case of formal phonon condensation that simply signifies the occurrence of a phase transition and the necessity to redefine the system ground state.

Some authors assume that magnon condensation could be possible in nonequilibrium systems, where condensation could be achieved by parametric pumping of a magnetic material, such as yttrium-iron-garnet, by an external pumping field, whose frequency would play the role of an effective nonzero chemical potential determining the magnon density [258–261]. In the frame of this assumption, spin systems, prepared in a strongly nonequilibrium state, being coupled to a resonator, forming feedback field, as a result

of which exhibiting fast coherent relaxation accompanied by spin superradiance [262–266], could also be related to nonequilibrium magnon condensation, since their relaxation is connected with the formation of large transverse coherently rotating magnetization. However, for strongly nonequilibrium systems, the introduction of magnons does not look to be clear.

3.5.5 Condensation of auxiliary quasiparticles

Accomplishing operator transformations, one may introduce auxiliary quasiparticles that do not necessarily correspond to physical objects, but rather serve as convenient mathematical tools. Nevertheless, one may consider the formal occurrence of Bose-Einstein condensation of such auxiliary quasiparticles.

A very often employed transformation, convenient in describing dimerized magnets is the bond-operator representation [267]. One considers a system of spin dimers, consisting of two spins one-half in spatial locations \mathbf{r}_j , with $j = 1, 2, \dots, N$. A spin dimer is represented through auxiliary quasiparticle operators s_j and $t_{j\alpha}$, where $\alpha = x, y, z$. The former operator characterizes singlet states, so it can be assumed to be related to quasiparticles *singletons*. And the operators $t_{j\alpha}$ correspond to triplet states, hence the related quasiparticles can be termed *triplons*. Each dimer consists of two spins connected by bonds, one of the spins being represented as

$$S_{1j}^\alpha = \frac{1}{2} \left(s_j^\dagger t_{j\alpha} + t_{j\alpha}^\dagger s_j - i \sum_{\beta\gamma} \varepsilon_{\alpha\beta\gamma} t_{j\beta}^\dagger t_{j\gamma} \right) \quad (3.116)$$

and the second spin operator, as

$$S_{2j}^\alpha = -\frac{1}{2} \left(s_j^\dagger t_{j\alpha} + t_{j\alpha}^\dagger s_j + i \sum_{\beta\gamma} \varepsilon_{\alpha\beta\gamma} t_{j\beta}^\dagger t_{j\gamma} \right). \quad (3.117)$$

Here $\varepsilon_{\alpha\beta\gamma}$ is the completely antisymmetric unit tensor.

The introduced quasiparticles have two very important features. First, their statistics are not prescribed, so that they can be treated either as bosons or as fermions. Treating them as bosons is an arbitrary assumption. Second, by their definition, they must satisfy the *no-double-occupancy constraint*

$$s_j^\dagger s_j + \sum_{\alpha} t_{j\alpha}^\dagger t_{j\alpha} = N. \quad (3.118)$$

This means that these quasiparticles are conserved:

$$\sum_j \langle s_j^\dagger s_j \rangle + \sum_{\alpha} \langle t_{j\alpha}^\dagger t_{j\alpha} \rangle = N.$$

Since they are conserved, and assuming that they are bosons, they are formally allowed to exhibit Bose-Einstein condensation.

One should not confuse triplons with magnons. The former are auxiliary quasiparticles that can arbitrarily be defined as bosons; they are conserved, hence, allowing for

equilibrium condensation. On the contrary, magnons are well defined bosons that are not conserved, thus, not allowing for equilibrium condensation [255].

Another type of widely used auxiliary quasiparticles are introduced through the transformation

$$S_j^\alpha = \frac{1}{2} \sum_{\beta\gamma} a_{j\beta}^\dagger \sigma_{\beta\gamma}^\alpha a_{j\gamma} , \quad (3.119)$$

where $\sigma_{\beta\gamma}^\alpha$ is the element of the Pauli matrix. The unipolarity condition is imposed:

$$\sum_{\alpha} a_{j\alpha}^\dagger a_{j\alpha} = 2S . \quad (3.120)$$

Again, the quasiparticles, represented by the operators $a_{j\gamma}$, can be of any statistics, being either bosons or fermions. Bogolubov [268] considered the case of fermions, while Schwinger [269] treated these quasiparticles as bosons, because of which they acquired the name of Schwinger bosons.

In view of condition (3.120), the quasiparticles are conserved:

$$\sum_{j\alpha} \langle a_{j\alpha}^\dagger a_{j\alpha} \rangle = 2SN .$$

Being treated as bosons and being conserved, they can condense in equilibrium. But again, the Schwinger bosons have nothing to do with magnons.

The general conclusion of this section, is that conserved particles can form equilibrium as well as nonequilibrium Bose-Einstein condensates. But unconserved quasiparticles cannot condense in equilibrium, though, in some cases, they can condense in nonequilibrium states. The latter, for instance, concerns Bose-Einstein condensation of excitons and polaritons.

4 Quantum Dots

The development of semiconductor technology has made it possible the confinement of a finite number of electrons in a localized three-dimensional (3D) space of a few hundreds Angstroms [270, 271]. This mesoscopic system, which is made up of artificially trapped electrons between a few layers of various semiconductors and called quantum dot (QD), opens new avenues in the study of the interplay between quantum and classical behaviour at low-dimensional scale. The quantum dot is formed by removing the electrons outside the dot region with external gates (lateral dot), or by etching out the material outside the dot region (vertical dot) [272–274]. The dot is connected to its environment by electrostatic barriers, the so called source and drain contacts, and gates to which one can apply a voltage V_g . In order to observe quantum effects, QDs are cooled down to well below 1 K.

In vertical QDs there is a strong screening of Coulomb interactions in contrast to lateral ones [273]. This results in strong quantum effects of the confinement potential on the dynamics of confined electrons. The main effects discussed in the present review are directly relevant to vertical dots.

The smaller the quantum dot, the larger the prevalence of quantum effects upon the static and dynamic properties of the system. Almost all parameters of QDs,— size,

strength of a confining potential, number of electrons, coupling between dots, dielectric environment, the shape of tunnelling barriers, as well as external parameters, such as temperature and magnetic, electrical and/or electro-magnetic fields, – can be varied in a controlled way. It is precisely to stress this controllability that the names *artificial atoms* and *quantum dots* have been coined. Therefore, QDs can be considered as a tiny laboratory allowing direct investigation of fundamental properties of charge and spin correlations at the atomic scale [201, 272, 273, 275–278]. Another strong motivation for studying the properties of QDs is due to a rapid development of the field of quantum computing, since the entangled states of electrons confined in a quantum dot may give a natural realization of a quantum bit or "qubit" [279–281]. It is expected that QDs could lead to novel device applications in fields such as quantum cryptography, quantum computing, optics and optoelectronics, information storage, biology (fluorescent labelling of cellular targets).

For small QDs, where the number of electrons is well defined ($N \leq 30$), the mean free path of the electrons at Fermi energy ($\lambda_F \sim 100$ nm) appears to be larger or comparable with the diameter of the dot ($d \sim 10 - 100$ nm) [282]. It seems therefore natural to assume that the properties of the electron states in QDs close to the Fermi level should be determined by the effective mean-field potential of the "artificial atom", produced by non-trivial interplay of the external confinement governed by gate voltage and electron-electron interaction. However, the atom-quantum dot analogy should not be carried too far: unlike electrons in an isolated atom, carriers in semiconductor QDs interact strongly with lattice vibrations and could be strongly influenced by defect, surface, or interface states. In contrast to real atoms, for which the confining Coulomb potential is well known, the forces that keep the carriers in self-organized traps are difficult to estimate from first principles. The exact shape and composition of the traps often are not well known and depend on the growth procedure; in addition, complications are introduced by the complex band structure of the strained material and, in some cases, by the effect of piezoelectric forces. A good assessment of the effective confining potential inside the dot can be obtained from a combined study of the ground-state and excitation energies. Ground-state energies are investigated by capacitance spectroscopy or by single electron tunnelling spectroscopy [273, 274]. Far-infrared spectroscopy is used to study the excitations of N -electron states in the dots (see below). A rich information about the intrinsic structure of QDs and correlations effects is expected under the influence of the applied magnetic field.

The electron states of few-electron quantum dots subjected to a strong magnetic field have been studied extensively in various experiments. The electrodynamic response (far-infrared spectroscopy) of QDs is expected to be dominated by the many-body effects produced by confined and interacting electrons. Sikorski and Merkt [283] found experimentally, however, the surprising result that the resonance frequencies in the magneto-optical spectrum are independent of the number of electrons in the QD. In these systems, which have been experimentally realized, the extension in the $x - y$ - plane is much larger than in the z -direction. Based on the assumption that the extension in the z -direction can be effectively considered zero, a good description of the far-infrared resonance frequencies has been obtained [283] within a two-dimensional ($2D$) harmonic oscillator model in the presence of a magnetic field [194, 284]. This result was interpreted as a consequence of Kohn's theorem [285] which is applied for a parabolic potential [286, 287]. The proof is

based on the identities

$$\begin{aligned}\sum_{j=1}^N \mathbf{x}_j^2 &= N\mathbf{X}^2 + \sum_{i<j} (\mathbf{x}_i - \mathbf{x}_j)^2/N, \\ \sum_{j=1}^N \mathbf{p}_j^2 &= \mathbf{P}^2/N + \sum_{i<j} (\mathbf{p}_i - \mathbf{p}_j)^2/N,\end{aligned}$$

where the center-of-mass coordinate and momentum are $\mathbf{X} = \sum_j \mathbf{x}_j/N$ and $\mathbf{P} = \sum_j \mathbf{p}_j$, respectively. This implies that, for the parabolic confinement, the total Hamiltonian H_N can be separated into the center-of-mass motion term, the spin term, and the relative motion term that contains the electron-electron interactions. The wave length of the external laser field far exceeds the average dot diameter and, therefore, can be well approximated by a dipole electric term only. Since the radiation of an external electric dipole field couples only to the center-of-mass motion and does not affect the relative motion, the dipole resonance frequencies should be exactly the same as those of the non-interacting system with the parabolic confinement and, therefore, be independent from the electron-electron interaction. The more complicated resonance structure, observed by [288, 289], raised, however, the question on the validity of Kohn's theorem for QDs. In order to describe the experimental data, it has been assumed that there is a deviation of the confining potential from the parabolic form, and different phenomenological corrections have been introduced [290, 291]. Considering external gates and surrounding of a two-electron QD as the image charge, it was shown [292] that the effective potential has, indeed, anharmonic corrections to the parabolic potential. However, their contribution becomes less important with the increase of the magnetic field strength.

Recent single-electron capacitance spectroscopy experiments in vertical QDs [293–295] provide another strong evidence in favour of the parabolic potential as an effective confinement potential in small QDs. In these experiments, shell structure phenomena have been clearly observed. In particular, the energy needed to place the extra electron (addition energy) into a vertical QD at zero magnetic field has characteristic maxima which correspond to the sequence of magic numbers (due to a complete filling of shells) of a 2D harmonic oscillator. The energy gap between filled shells is approximately $\hbar\omega_0$, where $\hbar\omega_0$ is the lateral confinement energy of the 2D harmonic oscillator. In fact, these atomic-like features, when the confining energy is comparable to or larger than the interaction energy, have been predicted independently in several publications [296–299]. Indeed, for a small dot size and a small number of electrons, the confinement energy becomes prevalent over the Coulomb energy. This has been confirmed for the 3D parabolic potential for two interacting electrons [300] and in the Hartree-Fock approach for $N \leq 12$ electrons [301]. In small QDs with the incomplete shell, produced by the parabolic potential, the Hund's rule prior the first experiment in 1996 [293] was predicted [301–303].

These experimental and theoretical studies lead to the conclusion that, indeed, for a few-electron small QDs the parabolic potential is a good approximation for the effective confinement. Note that for a typical voltage ~ 1 V applied to the gates, the confining potential in small QDs is of the order of 1 eV deep, which is large compared to a few meV of the confining frequency. Hence, the electron wave function is localized close to the minimum of the well which can always be approximated by a parabolic potential. This approximation becomes especially attractive for comparing symmetry breaking effects in QDs in a perpendicular magnetic field with rotating BEC and rotating nuclei. In this

review we will pay a special attention to the manifestations of symmetry breaking due to the *three-dimensional* nature of small QDs, in contrast to reviews [201, 277, 278] which are devoted to *2D* approaches to QDs.

The simplest description of finite quantum systems of interacting fermions is based on the idea that their interactions create an effective potential in which particles are assumed to move independently. For finite Fermi systems, like nuclei and metallic clusters, the bunching of single-particle levels known as shells [168, 304–306] is one consequence of this description, since the mean free path is comparable with the size of the system. A remarkable stability is found in nuclei and metallic clusters at magic numbers that correspond to closed shells in an effective potential. According to accepted wisdom, strong shell effects are the manifestations of a high degree of symmetry of the effective potential of a quantum many-body system [168].

The rearrangement of the intrinsic structure of small QDs under the perpendicular magnetic field can be traced within a simple shell model [298]. For instance, the model describes the effect of symmetry breaking of the mean field due to the magnetic field and the number of electrons. For pedagogical purposes, in order to illustrate some basic features of structural properties of small QDs, we discuss this model in Sec. 4.2. In fact, this discussion will help us to understand some common properties of rotating nuclei and rotating trapped atoms. In Sec. 4.3, we trace the dynamical effects of the confinement strength, the magnetic strength, the Coulomb repulsion, and their mutual interplay in the model for a two-electron QD. We show that at a particular strength of the magnetic field the nonlinear dynamics of two-electron QD becomes separable. Sec. 4.4 is devoted to the comparison of theoretical and experimental results for the ground state energies of two-electron quantum dots in a perpendicular magnetic field. In Sec. 4.5, we discuss the symmetry breaking phenomena in N -electron quantum dots in a mean field and a random phase approximations.

4.1 Basic features

For the analysis of experimental data, several approximations are commonly used. The underlying lattice of the semiconductor material is taken into account by using the effective mass for the conduction electrons, and a static dielectric constant reducing the Coulomb repulsion. As it was mentioned above, an effective trapping potential in small QDs with a few electrons is quite well approximated by a parabolic confinement. The ground state energy of the dot is calculated assuming that the dot is isolated. This approximation is well justified, when the tunnelling between the QD and an external source and drain is relatively weak. Using these approximations, one can study the influence of magnetic field on the electron spectrum of the dot. Hereafter, the magnetic field is assumed to be perpendicular to the plane $x - y$ of the electron motion.

Thus, the Hamiltonian of an isolated quantum dot with N electrons in a perpendicular magnetic field reads as

$$H = H_0 + H_{int} = \sum_j^N h_j + \sum_{i>j=1}^N \frac{k}{|\mathbf{r}_i - \mathbf{r}_j|}, \quad (4.1)$$

$$h_j = \left[\frac{1}{2m^*} \left(\mathbf{p}_j - \frac{e}{c} \mathbf{A}_j \right)^2 + U(\mathbf{r}_j) + \mu^* \sigma_z(j) B \right],$$

where $k = e^2/4\pi\epsilon_0\epsilon_r$. Here, e , m^* , ϵ_0 and ϵ_r are the unit charge, effective electron mass, vacuum and relative dielectric constants of a semiconductor, respectively. The confining potential is approximated by a three-dimensional harmonic oscillator potential (HO)

$$U(\mathbf{r}) = m^*[\omega_x^2 x^2 + \omega_y^2 y^2 + \omega_z^2 z^2]/2, \quad (4.2)$$

where $\hbar\omega_i$ ($i = x, y, z$) are the energy scales of confinement in the x, y, z -directions, respectively, and σ_z is a Pauli matrix.

In a quantum dot, the natural unit of length is $a^* = \hbar^2/[m^*(e^2/\epsilon)]$, with $(4\pi\epsilon_0 = 1)$. In what follows (if not mentioned otherwise), we use in numerical examples the effective mass $m^* = 0.067m_e$ and the dielectric constant $\epsilon_r \approx 12$, which are typical for GaAs. In this case, the length unit $a^* \approx 180a_0$, where the Bohr radius $a_0 = \hbar^2/(m_e e^2) = 5.29 \times 10^{-2}$ nm. The energy unit in this case is $E^* = e^2/(\epsilon_r a^*) = e^2/a_0 \times (a_0/\epsilon_r a^*) \approx 12$ meV, where the atomic unit of energy $E_0 = e^2/a_0 = 27.2$ eV.

The effective spin magnetic moment is $\mu^* = g_L \mu_B$ with $\mu_B = |e|\hbar/2m_e c \approx 5.79 \times 10^{-2}$ meV/T (T is Tesla). The effective mass determines the orbital magnetic moment μ_B^{eff} for electrons through the expression of the Larmor frequency $\hbar\omega_L = \mu_B B m_e/m^* = \mu_B^{\text{eff}} B$ and leads to $\mu_B^{\text{eff}} \approx 15\mu_B$. Evidently, the orbital magnetic moment is much stronger than the effective spin magnetic moment (with the effective Lande factor $|g_L| = 0.44$). If the magnetic length $\ell_B = \sqrt{\hbar c/(eB)}$ equals the unit length a^* , one extracts the magnetic unit strength $B^* = (a_0/a^*)^2 B_0$, where $B_0 = e^3 m_e^2 c/\hbar^3 = E_0/(2\mu_B) \approx 2.35 \times 10^5$ T corresponds to free electrons. For GaAs one obtains $B^* \approx 7.2$ T. In other words, for magnetic fields that are available in the laboratory, one can study various phenomena related to orbital magnetism that can occur only in neutron stars.

4.2 Shell effects in a simple model

4.2.1 Magnetic field and shapes

The effect of an external homogeneous magnetic field on a three-dimensional (3D) harmonic oscillator potential can be taken into account exactly, irrespectively to the direction of the field [298, 307]. For a perpendicular magnetic field, we choose the vector potential with a gauge $\mathbf{A} = \frac{1}{2}\mathbf{B} \times \mathbf{r} = \frac{1}{2}B(-y, x, 0)$. In this case, the electronic spectrum, generated by the Hamiltonian (4.1) without interaction, is determined by the sum $H_0 = \sum_i^N h_i$ of the single-particle harmonic oscillator Hamiltonians $h = h_0 + h_z$ where

$$h_0 = \frac{p_x^2 + p_y^2}{2m^*} + \frac{m^*}{2} \sum_{i=1}^2 \omega_i^2 x_i^2 - \omega_L l_z. \quad (4.3)$$

Here, for a perpendicular magnetic field, we have

$$\omega_1^2 = \omega_x^2 + \omega_L^2, \omega_2^2 = \omega_y^2 + \omega_L^2, \quad (4.4)$$

and $\omega_L = |e|B/(2m^*c)$. Since the orbital momentum l_z

$$l_z = xp_y - yp_x \quad (4.5)$$

couples lateral variables, the dynamics in z direction is determined by one-dimensional harmonic oscillator $h_z = p_z^2/2m^* + m^*\omega_z^2 z^2/2$.

Before proceeding further, a few remarks are in order. First, the external field is the dominant part of the mean field, hence the effective confining potential should reflect the main features of this field. Yet it must also contain the effect of the interplay between the external fields which are governed by the charges in the adjacent layers and gates and the magnetic field. Due to these considerations, we assume that the confining potential should also take into account the changes that affect the properties of the single-electron states owing to a variation of the homogeneous magnetic field, as well as the slab thickness. We suppose that the system adjusts itself to the influence of the magnetic field, under the given particle number. Minimizing $E_{\text{tot}} = \langle H_0 \rangle$ connects the magnetic field strength with the related shape of the confining effective potential, which is defined by the oscillator frequencies. In other words, for a given magnetic field, we need to find the minimum of E_{tot} with respect to the variation of the oscillator frequencies. In this way, we accommodate the effect of the interplay between external fields, the external confinement and the magnetic field. Here, the Pauli principle is essential as it limits the accessible quantum configuration space for electrons. The variation cannot be unrestricted as the confining potential contains a fixed number of electrons. Assuming that the electron density area does not change, we introduce a fixed volume constraint which translates into the subsidiary condition $\omega_x \omega_y \omega_z = \omega_0^3$ with ω_0 fixed. Denoting the Lagrange multiplier by λ , we solve the variational problem

$$\delta(\langle g|H_0|g\rangle - \lambda\omega_x\omega_y\omega_z) = 0, \quad (4.6)$$

where $|g\rangle$ denotes the ground state. From Eq. (4.6), after the differentiation with respect to the frequencies and using the Feynman's theorem [308]

$$\frac{d}{d\omega_k} \langle g|H_0|g\rangle = \langle g|\frac{dH_0}{d\omega_k}|g\rangle, \quad (4.7)$$

we get the useful condition

$$\omega_x^2 \langle g|x^2|g\rangle = \omega_y^2 \langle g|y^2|g\rangle = \omega_z^2 \langle g|z^2|g\rangle, \quad (4.8)$$

which must be obeyed at the minimum of E_{tot} . We restrict ourselves to the consideration of a thin slab with large lengths in two dimensions. This is achieved by varying only ω_x and ω_y in the minimization procedure while keeping ω_z fixed at a value, which is several time (e.g., five times) larger than the other two frequencies. In this case, only the condition $\omega_x^2 \langle g|x^2|g\rangle = \omega_y^2 \langle g|y^2|g\rangle$ is to be fulfilled. Choosing different (fixed) values of ω_z allows one to study the dependence of the results on the slab thickness.

Since the electron interaction is crucial only for partially filled electronic shells [273, 277], we deal in this section mainly with closed shells. This case corresponds to the quantum limit $\hbar\omega_0 > k/l_0$, where k/l_0 is the typical Coulomb energy and $l_0 = (\hbar/m^*\omega_0)^{1/2}$ is the effective oscillator length. In fact, for small dots, where large gaps between closed shells occur [296, 297, 299, 309], the electron interaction plays the role of a weak perturbation, which, in the first approximation, can be neglected. But even in the regime $\hbar\omega_0 < k/l_0$, an essentially larger additional energy is needed for the addition of an electron to a closed shell [310]. We do not take into account the effect of finite temperature; this is appropriate for experiments which are performed at temperatures $k_B T \ll \hbar\omega_0$, with $\hbar\omega_0 \sim 2-5$ meV being the mean level spacing. Indeed, for experiments [293, 294] a typical

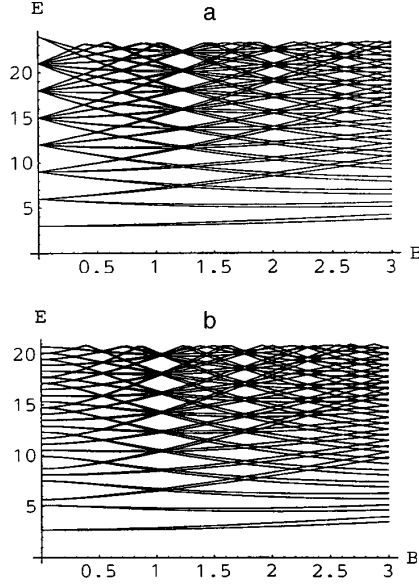


Figure 3: Single-particle spectra as a function of the magnetic field strength. Spectra are displayed for: (a) a plain isotropic ($\omega_x = \omega_y$) two-dimensional oscillator; (b) a deformed two-dimensional oscillator. From [311].

temperature is estimated to be below ~ 100 mK (~ 0.008 meV). In the following, we use meV for the energy units and T for magnetic field strength.

Evidently, for the dot with a fixed $\omega_z \gg \omega_{x,y}$, with the number of electrons $N \sim 20$, electrons occupy the states with $n_z = 0$. As a result, shell effects are determined by the ratio of the eigenmodes Ω_{\pm} in the lateral plane (see Appendix A). The shell structure occurs whenever the ratio of the two eigenmodes Ω_{\pm} of the Hamiltonian H_0 is a rational number with a small numerator and denominator. Closed shells are particularly pronounced if the ratio is equal to one (for $B = 0$) or two (for $B \approx 1.23$), or three (for $B \approx 2.01$), and are lesser pronounced if the ratio is $3/2$ (for $B = 0.72$) or $5/2$ (for $B = 1.65$) for a circular case $\omega_x = \omega_y$ (see Fig.3a). For illustration, we use for the spin splitting the value $2\mu_B$ instead of the correct μ^* in the Figures; the discussions and conclusions are based on the correct value. The values given here for B depend on m^* and $\omega_{x,y}$. As a consequence, a material with an even smaller effective mass m^* would show these effects for a correspondingly smaller magnetic field. For $B = 0$ the magic numbers (including spin) turn out to be the usual sequence of the $2D$ isotropic oscillator numbers, that is, $2, 6, 12, 20, \dots$. For $B \approx 1.23$, a new shell structure arises *as if* the confining potential would be a deformed harmonic oscillator without magnetic field. The magic numbers are $2, 4, 8, 12, 18, 24, \dots$, which are just the numbers obtained for the $2D$ oscillator, where $\omega_{>} = 2\omega_{<}$. Here $\omega_{>}$ and $\omega_{<}$ denote the larger and smaller values of the frequencies. Similarly, for $B \approx 2.01$ the magic numbers $2, 4, 6, 10, 14, 18, 24, \dots$ appear, which correspond to $\omega_{>} = 3\omega_{<}$. If one starts with a deformed mean field $\omega_x = (1 - \beta)\omega_y$ with $\beta > 0$, the degeneracies (shell structure), lifted at $B = 0$, re-occur at higher values

for B . In Fig. 3b, we display such an example referring to $\beta = 0.2$. Shell structures are restored by a magnetic field in an isolated QD that does not give rise to magic numbers at zero field strength due to deformation. Thus, the choice of $\beta = 0.5$ would shift the pattern, found for $B \approx 1.23$ in Fig. 3a, to the value $B = 0$. Closed shells are obtained for the values of B and β , which yield $\Omega_+/\Omega_- = l = 1, 2, 3, \dots$

The ground state energy of a QD, as a function of magnetic field, can be probed very elegantly by single-electron capacitance spectroscopy [312] or by single-electron tunnelling spectroscopy [313, 314]. At low temperature ~ 100 mK, a large electrostatic charging energy prevents the flow of current and, therefore, the dot has a fixed number of electrons. Applying a gate voltage to the contacts brings the electro-chemical potential of the contacts in resonance with the energy $\mu(N)$ that is necessary for adding the N -th electron, tunnelling through the barrier, into the dot with $N - 1$ electrons. Indeed, it is the shell structure caused by the effective mean field, which produces the maxima that are observed experimentally in the addition energy

$$\Delta\mu = \mu(N) - \mu(N - 1) \quad (4.9)$$

for $N = 2, 6, 12$ electrons [293], where $\mu(N) = E(N) - E(N - 1)$ is an electrochemical potential and $E(N)$ is the total ground state energy of an N -electron dot.

In order to shed light on this phenomenon let us calculate $\Delta\mu$ in a constant-interaction (CI) model that provides an approximate description of the electronic states of QDs [273]. In the CI model the total ground state energy of an N -electron dot is

$$E(N) = [e(N - N_0) - C_g V_g]^2 / 2C + \sum_i^N \varepsilon_i, \quad (4.10)$$

where $N = N_0$ for the gate voltage $V_g = 0$. The term $C_g V_g$ represents the charge (a continuous variable) induced on the dot by a gate voltage V_g , through the gate capacitance C_g . It is assumed that the Coulomb interactions of an electron on the dot with all other electrons, in and outside the dot, are parametrized by a constant total capacitance C . The total capacitance between the dot and the source, drain, and gate is $C = C_s + C_d + C_g$. The quantum contribution is determined by the sum over all occupied single-particle energies ε_i , which depend on the magnetic field. In the CI model it is assumed that the single-particle spectrum is calculated for non-interacting electrons. Electrons can flow from the source (left) to the drain (right) through a transport (bias) window eV_{sd} , when $\mu_{\text{left}} > \mu_{\text{dot}}(N) > \mu_{\text{right}}$ (with $-|e|V_{sd} = \mu_{\text{left}} - \mu_{\text{right}}$). With the aid of Eq.(4.10) one obtains the addition energy

$$\Delta\mu = \varepsilon_N - \varepsilon_{N-1} + e^2/C, \quad (4.11)$$

where ε_N is the highest filled single-particle state for an N -electron dot and e^2/C is the classical electrostatic energy. In the CI model the addition energies of single electrons are periodic in e^2/C , since the difference $\varepsilon_N - \varepsilon_{N-1}$ is usually neglected. In reality, however, it is the fluctuations (shell effects) of the difference that matter, at least for small QDs.

A similar effect is known in nuclear physics and for metallic clusters. For specific numbers of fermions, these systems are particularly stable. For example, the synthesis of superheavy nuclei is guided by a predicted shell structure for these systems (see, e.g.,

[315,316]). From the theoretical point of view, the shell effects, due to the single-particle motion, create fluctuations in the total potential energy that is dominated by the bulk energy, which is the classical liquid drop energy [304, 305, 317]. The analogy goes even further: in an isolated small QD, the external magnetic field acts like the rotation of a nucleus, thus creating a new shell structure; in this way superdeformation (axis ratio 2:1) has been established for rotating nuclei owing to the shell gaps in the single-particle spectrum [317].

Various shapes of the QD can be obtained by the energy minimization [307]. In this context, it is worth noting that, under particular values of the magnetic field, where a pronounced shell structure occurs, the energy minimum would be obtained for axially-symmetric (or circular) dots, if the particle number were chosen to be equal to one of the magic numbers. Deviations from these magic numbers usually give rise to deformed shapes at the energy minimum. To what extent these 'spontaneous' deformations actually occur is the subject of more detailed experimental investigations. The far-infrared spectroscopy in a small isolated QD could be a useful tool to provide pertinent data.

The question arises as to what extent the discussed findings depend on the particular choice of the mean field. The Coulomb interaction lowers the electron levels for the increasing magnetic quantum number $|m|$ in the parabolic potential [300, 318] and in a hard-wall potential of finite height [319]. One may add to the Hamiltonian H_0 (4.1) the term $-\gamma\hbar\omega_L L^2$, where L is the dimensionless z -component of the orbital momentum operator, to produce a similar result [320]. Indeed, for $\gamma > 0$, the additional term mimics the Coulomb interaction effect in the Coulomb blockade regime of deformed QDs [321], as well as the surface effect. In particular, the bunching of single-particle levels with high orbital momenta comes from the presence of the surface in the Woods-Saxon potential which could be suitable for modelling the surface effects in QDs. As a consequence, this term has the effect of interpolating between the oscillator and the square-well single-particle spectra. This behaviour is well known in nuclear systems [317] and recently has been used for explaining the dominance of prolate deformed shapes in contrast to oblate shapes for small finite quantum systems such as nuclei [322].

For $\omega_x = \omega_y \neq \omega_z$ and $\gamma \neq 0$, the combined Hamiltonian $H' = H_0 - \gamma\hbar\omega_L L^2$ is nonintegrable [320, 323], and the level crossings encountered in Figs.3 are replaced by the avoided level crossings. The shell structure, which prevails for $\gamma = 0$ throughout the spectrum at $B \approx 1.23$ or $B \approx 2.01$, is therefore disturbed to an increasing extent with increasing shell number. But even for $\gamma \leq 0.1$, for sufficiently low electron numbers, virtually any binding potential will produce the patterns found for the harmonic oscillator.

4.2.2 Magnetic properties

Orbital magnetism of an ensemble of QDs was discussed for noninteracting electrons [324–328], but little attention was paid to the shell structure of an individual dot. When the magnetic field is changed continuously for a QD with a fixed electron number, the ground state will undergo a rearrangement at the values of B , where level crossings occur (see discussion above). In fact, it leads to strong variation in the magnetization [275, 329] and should be observable also in the magnetic susceptibility $\chi = -\partial E_{\text{tot}}^2 / \partial B^2$ [302], since it is proportional to the second derivative of the total energy with respect to the field strength.

Note that if one replaces $B \Rightarrow \omega_L$, the susceptibility will be rescaled by a constant factor. However this replacement establishes the obvious link between the susceptibility and the nuclear dynamical moment of inertia $\mathcal{J}^{(2)} = -d^2 E/d\Omega^2$, where Ω is a rotational frequency of rotating nuclei. We will return to this point in Sec. 5.

We now focus on the special cases which give rise to the pronounced shell structure, that is, when the ratio $\Omega_+/\Omega_- = l = 1, 2, 3, \dots$. To avoid cumbersome expressions, we analyze in detail the circular shape ($\omega_x = \omega_y = \omega_0$, $\langle z^2 \rangle = 0$) for which the eigenmodes, Eq.(A.5), become $\Omega_{\pm} = (\Omega \pm \omega_L)$, with $\Omega = \sqrt{\omega_0^2 + \omega_L^2}$. In this case, the total energy for the closed QD (see Appendix A) is

$$E_{\text{tot}} = \Omega_+ \Sigma_+ + \Omega_- \Sigma_- - \mu^* B \langle S_z \rangle + E_z, \quad (4.12)$$

with $\Sigma_{\pm} = \sum_j^N (n_{\pm} + 1/2)_j$ and the shell number $N_{\text{sh}} = n_+ + n_-$ ($n_z = 0$). For the magnetization $M = -dE_{\text{tot}}/dB$, taking into account that, after the differentiation of the total energy (4.12), $\Omega_+ = l\Omega_-$ ($\hbar = 1$), we have

$$M = \mu_B^{\text{eff}} \left(1 - \frac{\omega_L}{\Omega}\right) (\Sigma_- - l \Sigma_+) - \mu^* \langle S_z \rangle \quad (4.13)$$

Let us consider a QD with $g_L = 0$, which results in zero spin contribution, since $\mu^* = 0$. From the orbital motion we obtain for the susceptibility

$$\chi = -d^2 E_{\text{tot}}/dB^2 = -\frac{\mu_B^{\text{eff}2}}{\Omega} \left(\frac{\omega_0}{\Omega}\right)^2 (\Sigma_+ + \Sigma_-) \quad (4.14)$$

It follows from Eq. (4.14) that, for a completely filled shell, the magnetization due to the orbital motion leads to diamagnetic behavior. For zero magnetic field ($l = 1$) the system is paramagnetic and the magnetization vanishes ($\Sigma_- = \Sigma_+$). The value $l = 2$ is reached for $B \approx 1.23$. When calculating Σ_- and Σ_+ , we have to distinguish between the cases, where the shell number N_{sh} of the last filled shell is even or odd. With all shells filled from the bottom we find:

(i) For the last filled shell even number:

$$\Sigma_+ = (N_{\text{sh}} + 2)[(N_{\text{sh}} + 2)^2 + 2]/12, \quad (4.15)$$

$$\Sigma_- = (N_{\text{sh}} + 1)(N_{\text{sh}} + 2)(N_{\text{sh}} + 3)/6, \quad (4.16)$$

which implies

$$M = -\mu_B^{\text{eff}} (1 - \omega_L/\Omega) (N_{\text{sh}} + 2)/2; \quad (4.17)$$

(ii) For the last filled shell odd number:

$$\Sigma_+ = \Sigma_-/2 = (N_{\text{sh}} + 1)(N_{\text{sh}} + 2)(N_{\text{sh}} + 3)/12, \quad (4.18)$$

which, in turn, implies $M = 0$.

Therefore, if $\Omega_+/\Omega_- = 2$, the orbital magnetization vanishes for the magic numbers 4, 12, 24, \dots , while it leads to diamagnetism for the magic numbers 2, 8, 18, \dots . A similar picture is obtained for $\Omega_+/\Omega_- = 3$, which happens at $B \approx 2.01$: for each third filled shell number (magic numbers 6, 18, \dots) the magnetization is zero. Since the presented results

are due to shell effects, they do not depend on the assumption $\omega_x/\omega_y = 1$, which was made to facilitate the discussion. The crucial point is the relation $\Omega_+/\Omega_- = l = 1, 2, 3, \dots$, which can be obtained for a variety of combinations of the magnetic field strength and the ratio ω_x/ω_y . Whenever the appropriate combination of the field strength and deformation is chosen to yield, say, $l = 2$, the above discussion is valid.

4.3 Two-electron quantum dot: a new paradigm in mesoscopic physics

Two-electron QDs have drawn a great deal of experimental and theoretical attention in recent years. Progress in semiconductor technology has made it possible to fabricate and probe such confined system at different values of magnetic field [273, 274, 295]. In particular, one observes transitions between the states that can be characterized by different quantum numbers m and a total spin S of the Fock-Darwin states [312]. These transitions have been earlier predicted in the $2D$ approximation: in numerical calculations [330] and in a perturbative approach in the limit of high magnetic fields [331]. The experiments stimulated numerous theoretical studies of two-electron QDs [276, 278]. Indeed, a competition between a confining potential, approximated quite well by the HO, and the repulsive electron-electron interaction produces a rich variety of phenomena. Being a simplest non-trivial system, a two-electron QD poses, however, a significant challenge to theorists.

It is well known that there is a restricted class of exactly solvable problems in quantum mechanics. Such examples serve as paradigms for illustrating fundamental principles or/and new methods in the respective fields. This is especially important for finite systems. In fact, a two-electron QD becomes a testing-ground for different quantum-mechanical approaches and experimental techniques that could provide highly accurate data for this system [271, 273, 274]. Therefore, two-electron systems play an important role in understanding electron correlation effects, since their eigenstates can be obtained very accurately, or in some cases, exactly.

For example, Pfannkuche *et al.* [332] compared the results of the Hartree, Hartree-Fock, and of the exact treatment of a $2D$ two-electron QD and found that the exchange effects are very important. The most popular model to study the electronic exchange-correlation energy in the density functional theory is the Hookean two-electron atom. The basic Hookean atom is formed by two electrons interacting by the Coulomb potential but bound to a nucleus by a harmonic potential that mimics a nuclear-electron attraction. For certain values of the confinement strength ($\omega_x = \omega_y$), there exist exact solutions for the $2D$ Hookean atom ground state [333, 334]. Turbinger [335] was able to show that some analytical solutions for this problem occur due to a hidden sl_2 algebraic structure. This model can be equally viewed as a model of a $2D$ quantum dot. At zero magnetic field, the $2D$ problem is integrable in two cases: $\omega_x : \omega_y = 1, 2$. For the circular symmetry, the problem of relative motion becomes separable in polar coordinates. Although a closed-form solution for the eigenfunctions was obtained with the aid of power series methods [336], the exact energies were calculated numerically. The separability in the case of $\omega_x : \omega_y = 2$ [337] provided a basis for algebraic solutions for certain values of ω_x [338]. For the Hookean atom placed in a perpendicular magnetic field, Taut found analytical solutions for a $2D$ case at particular values of the magnetic field for the circular case [339]. The circular dot at arbitrary values of the magnetic field was studied in various approaches

in order to find a closed-form solution [340–343]. Analytical solutions, developed for a 3D model of a QD [300, 344], provide the explicit completion of five integrable cases [345]. Discovery of the closed-form solutions stimulated additional efforts for understanding the validity of the density functional theory at large magnetic fields. In the case of 3D Hookean atom in an external magnetic field, the comparison with the exact solutions demonstrated clearly the major qualitative failures of several widely used approximate density functional theory exchange-correlation energy functionals [346].

The major aspect of Sec. 4.3 is to demonstrate that the hidden symmetries could be observed in a two-electron QD with a 3D effective parabolic confinement under a tunable perpendicular magnetic field. Note that these symmetries have been overlooked in a plain quantum-mechanical models. It is, therefore, necessary to focus our analysis on the nonlinear classical dynamics of such finite systems. At certain conditions, the motion becomes integrable, which indicates the existence of symmetries in the quantum spectrum.

4.3.1 Hidden symmetries in a two-electron quantum dot

A three-dimensional harmonic oscillator, with the frequencies in rational ratios (RHO), and a Coulomb system are the benchmarks for the hidden symmetries, which account for the accidental degeneracies of their quantum spectra, e.g., [87]. For the isotropic case, the hidden symmetries define the $so(n)$ symmetry algebra for the oscillator, and the $so(n+1)$ algebra for Coulomb systems, where n is a dimension. In both, the classical and quantum cases, the transformation $r = R^2$, where r and R denote the radial coordinates of Coulomb and oscillator systems, respectively, converts the $(n+1)$ -dimensional radial Coulomb problem to a $2n$ -dimensional radial oscillator. In three cases, $n = 1, 2, 4$, one can establish a complete correspondence between the Coulomb and oscillator systems with the aid of Bohlin (or Levi-Cevita) [347, 348], Kustaanheimo-Stiefel [349], and Hurwitz [350] transformations, respectively. For the n -dimensional case, it was found [351] that there exists a simple relationship between the energy and eigenstates of the hydrogen atom and those of the HO by means of $su(1, 1)$ algebra.

The degeneracies of the HO model, which occur when the frequency ratio is a rational number, have been the subject of several investigations in the 2D case [352, 353] and in the 3D case [354–359] in various fields. For example, these degeneracies result in the appearance of spherical and superdeformed magic gaps and magic numbers in nuclear systems [168, 317]. As is well known, the invariance group of the HO is $SU(3)$ [360], while that of the hydrogen atom is $O(4)$ [361].

If the HO and the Coulomb potential are combined, most of the symmetries are expected to be broken. Nevertheless, in particular cases, the Coulomb (Kepler) system and the RHO may have common symmetries, as it was already noticed a long time ago [352]. Jauch and Hill [352] could not find, however, a physical application for this phenomenon. These symmetries were rediscovered in the analysis of laser-cooled ions in a Paul trap [362] and of the hydrogen atom in the generalized van der Waals potential [363].

4.3.2 Center-of-mass and relative-motion Hamiltonians

Let us consider the Hamiltonian (4.1) of a two-electron QD in a magnetic field with the confining frequencies $\omega_x = \omega_y = \omega_0 \neq \omega_z$. In the present analysis, we neglect the spin

interaction (the Zeeman term), since the corresponding energy is small compared to the confinement and the Coulomb energies and is not important for our discussion.

By introducing the relative and center-of-mass (CM) coordinates

$$\mathbf{r} = \mathbf{r}_1 - \mathbf{r}_2, \quad \mathbf{R} = \frac{1}{2}(\mathbf{r}_1 + \mathbf{r}_2),$$

the Hamiltonian (4.1) can be separated into the CM and relative motion terms due to the Kohn theorem [285]: $H = H_{\text{cm}} + H_{\text{rel}}$, where

$$H_{\text{cm}} = \frac{\mathbf{P}^2}{2M^*} + \frac{M^*}{2} \left[\omega_\rho^2 (X^2 + Y^2) + \omega_z^2 Z^2 \right] - \omega_L L_z \quad (4.19)$$

$$H_{\text{rel}} = \frac{\mathbf{p}^2}{2\mu} + \frac{\mu}{2} \left[\omega_\rho^2 (x^2 + y^2) + \omega_z^2 z^2 \right] - \omega_L l_z + \frac{k}{r}. \quad (4.20)$$

Here $M^* = 2m^*$ and $\mu = m^*/2$ are the total and reduced masses, ω_L is the Larmor frequency and L_z and l_z are the z -projections of the angular momenta for the CM and relative motions, respectively. The effective confinement frequency for the ρ -coordinate, $\omega_\rho = (\omega_L^2 + \omega_0^2)^{1/2}$, depends, through ω_L , on the magnetic field. In this way, the magnetic field can be used to control the effective lateral confinement frequency of the QD for a fixed value of the vertical confinement, i.e., for a fixed ratio ω_z/ω_ρ .

The total two-electron wave function $\Psi(\mathbf{r}_1, \mathbf{r}_2) = \psi(\mathbf{r}_1, \mathbf{r}_2)\chi(\sigma_1, \sigma_2)$ is a product of the orbital $\psi(\mathbf{r}_1, \mathbf{r}_2)$ and spin $\chi(\sigma_1, \sigma_2)$ wave functions. Due to the Kohn theorem, the orbital wave function is factorized as a product of the CM and the relative motion wave functions $\psi(\mathbf{r}_1, \mathbf{r}_2) = \psi_{\text{CM}}(\mathbf{R})\psi_{\text{rel}}(\mathbf{r})$. The parity of $\psi_{\text{rel}}(\mathbf{r})$ is a good quantum number, as well as the magnetic quantum number m , since ℓ_z is the integral of motion. The CM eigenfunction is a product of the Fock-Darwin state (A.9) (the eigenstate of a single electron in an isotropic 2D harmonic oscillator potential in a perpendicular magnetic field) [194] in the (X, Y) -plane and the oscillator function in the Z -direction (both sets for a particle of mass M^*).

The CM eigenenergies are the sum of Fock-Darwin levels and oscillator levels in the z -direction,

$$E_{\text{cm}} = \hbar\omega_\rho (2N + |M| + 1) + \hbar\omega_z (N_z + 1/2) - \omega_L M. \quad (4.21)$$

Here $N = 0, 1, \dots$ is the radial quantum number, $M = 0, \pm 2, \pm 3, \dots$ is the azimuthal number, and $N_z = 0, 1, 2, \dots$ is the quantum number for the CM excitations in the z -direction.

In the following, we concentrate on the dynamics associated with H_{rel} . For our analysis, it is convenient to use the cylindrical *scaled* coordinates,

$$\tilde{\rho} = \rho/l_0, \tilde{p}_\rho = p_\rho l_0/\hbar,$$

$$\tilde{z} = z/l_0, \tilde{p}_z = p_z l_0/\hbar,$$

where $l_0 = (\hbar/\mu\omega_0)^{1/2}$ is the characteristic length of the confinement potential with the reduced mass μ . The strength parameter k of the Coulomb repulsion goes over to $\lambda = k/(\hbar\omega_0 l_0)$. Although our consideration is general, for a numerical demonstration, we choose the values: $\lambda = 1.5$ (GaAs); $\hbar\omega_0 \approx 2.8$ meV and $\omega_z/\omega_0 = 2.5$. Hereafter, for the sake of simplicity, we drop the tilde, i.e. for the scaled variables we use the same symbols as before scaling.

In these variables, the Hamiltonian for the relative motion takes the form (in units of $\hbar\omega_0$)

$$h \equiv \frac{H_{\text{rel}}}{\hbar\omega_0} = \frac{1}{2} \left(p_\rho^2 + \frac{m^2}{\rho^2} + p_z^2 + \tilde{\omega}_\rho^2 \rho^2 + \tilde{\omega}_z^2 z^2 \right) + \frac{\lambda}{r} - \tilde{\omega}_L m, \quad (4.22)$$

where $r = (\rho^2 + z^2)^{1/2}$, $\tilde{\omega} \equiv \omega/\omega_0$, $m = l_z/\hbar$.

Since the Coulomb interaction ($k \Rightarrow \lambda \neq 0$) couples the motions in ρ and z -directions, the eigenfunctions of the Hamiltonian for relative motion (4.22) are expanded in the basis of the Fock-Darwin states $\Phi_{n,m}(\rho, \varphi)$ and oscillator functions in the z -direction, $\phi_{n_z}(z)$ (for a particle of mass μ), i.e.

$$\psi_{\text{rel}}(\mathbf{r}) = \sum_{n,n_z} c_{n,n_z}^{(m)} \Phi_{n,m}(\rho, \varphi) \phi_{n_z}(z). \quad (4.23)$$

For non-interacting electrons the ground state is described by the wave function $\psi_{\text{rel}} = \Phi_{0,0} \phi_0$. For interacting electrons, however, the ground state (in the form (4.23)) evolves from $m = 0$ to higher values of m as the magnetic field strength increases. Since the quantum number m and the total spin are related by the expression

$$S = \frac{1}{2}[1 - (-1)^m], \quad (4.24)$$

this evolution leads to the singlet-triplet (S-T) transitions (see below Sec.4.4.1). Note that if the Zeeman term is included, the splitting (with $g^* < 0$) lowers the energy of the $M_S = 1$ component of the triplet states, while leaving the singlet states unchanged. As a consequence, the ground state is characterized by $M_S = S$.

4.3.3 Classical dynamics and quantum spectra

Due to the axial symmetry of the system the φ -motion is separated from the motion in the ρ, z -plane. Considering classical dynamics, we associate the Hamiltonian with the energy of our system. Evidently, the energy is the integral of motion, since we analyze the autonomous system. Besides the energy ($\epsilon \equiv h$), the z -component of the angular momentum l_z is an integral of motion. Therefore, the magnetic quantum number m is always a good quantum number. Since the Hamiltonian (4.22) is invariant under the reflection with respect to the origin, the parity π is also a good quantum number.

The classical trajectories can be obtained by solving (numerically) the Hamilton equations for a fixed energy [345]. Although the motion in φ is separated from the motion in the ρ, z -plane, the problem is in general non-integrable, since the Coulomb term couples the ρ and z -coordinates.

The examination of the Poincaré sections by varying the parameter ω_z/ω_ρ (see, e.g., Fig. 4) in the interval $(1/10, 10)$, with a small step, indicates that there are five integrable cases. The trivial cases are $\omega_z/\omega_\rho \rightarrow 0$ and $\omega_z/\omega_\rho \rightarrow \infty$, which correspond to 1D vertical and 2D circular QDs, respectively. The non-trivial cases are $\omega_z/\omega_\rho = 1/2, 1, 2$. These results hold for any strength of the Coulomb interaction and agree with the results for the Paul trap [362]. Below, we discuss the non-trivial cases only. The typical trajectories in cylindrical coordinates are shown in Figs. 5a,c.

The results, obtained with the aid of the Poincaré sections, are invariant under the coordinate transformation. On the other hand, the integrability is a necessary condition

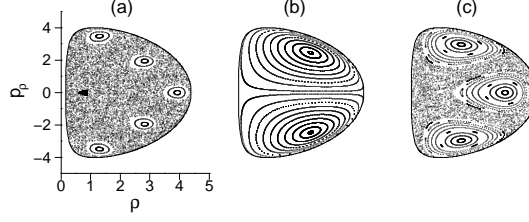


Figure 4: Poincaré sections $z = 0, p_z > 0$ for the relative motion ($\lambda = 1.5, \epsilon = 10, m = 0$), with: (a) $\omega_z/\omega_\rho = 5/2$, (b) $\omega_z/\omega_\rho = 2$ and (c) $\omega_z/\omega_\rho = 3/2$. The section (b) indicates that for the ratio $\omega_z/\omega_\rho = 2$ the system is integrable. From [345].

for the existence of a coordinate system, in which the motion can be separated. In turn, the analogous quantum mechanical system would be characterized by a complete set of quantum numbers.

- The case $\omega_\rho = \omega_z$

At the value $\omega'_L = (\omega_z^2 - \omega_0^2)^{1/2}$, the magnetic field gives rise to the spherical symmetry ($\omega_z/\omega_\rho = 1$) in an axially symmetric QD (with $\omega_z > \omega_0$) [364]. In this case, Hamiltonian (4.22) is separable in (scaled) spherical coordinates

$$h = \frac{p_r^2}{2} + \frac{(1/\hbar)^2}{2r^2} + \frac{\tilde{\omega}_z^2 r^2}{2} + \frac{\lambda}{r} - \tilde{\omega}'_L m \quad (4.25)$$

and the dynamics is integrable. The additional integral of motion is the square of the total angular momentum \mathbf{l}^2 .

Due to the separability of Hamiltonian (4.25) in spherical coordinates, the corresponding eigenfunctions can be written in the form

$$\psi(\mathbf{r}) = \frac{\phi_{lm}(r)}{r} Y_{lm}(\vartheta, \varphi) . \quad (4.26)$$

The functions $\phi_{lm}(r)$ are the solutions of the radial equation

$$\left[-\frac{d^2}{dr^2} + \frac{l(l+1)}{r^2} + \tilde{\omega}_z^2 r^2 + \frac{2\lambda}{r} - 2(\tilde{\omega}'_L m + \epsilon) \right] \phi_{lm}(r) = 0 , \quad (4.27)$$

where l and m are the orbital and magnetic quantum numbers, respectively. Eq. (4.27) can be solved numerically. Hence, good quantum numbers for this case are (n_r, l, m) , where the radial quantum number $n_r = 0, 1, 2, \dots$ enumerates the radial functions $\phi_{n_r, l, m}(r)$ within each (l, m) -manifold. For the spherical case, $\pi = (-1)^l$. Thus, the magnetic field, reducing the $O(4)$ symmetry, creates the dynamical symmetry $O(4) \supset O(3)$ (see also Alhassid *et al.* [363]).

In this case, it is straightforward to use a semiclassical quantization of Hamiltonian (4.25) to calculate the spectrum. The procedure reduces to the WKB quantization of r -motion, due to the separability of the problem in spherical coordinates. The momentum p_r , determined from Eq. (4.25), enters the action integral

$$I_r = \frac{\hbar}{2\pi} \oint p_r dr = \frac{\hbar}{\pi} \int_{r_{\min}}^{r_{\max}} |p_r| dr , \quad (4.28)$$

with the turning points r_{\min} , r_{\max} as the positive roots of equation $p_r(r) = 0$. The WKB quantization conditions

$$\begin{aligned} I_r(\epsilon) &= \hbar(n_r + \tfrac{1}{2}), \quad n_r = 0, 1, \dots, \\ |1| &= \hbar(l + \tfrac{1}{2}), \quad l = 0, 1, \dots, \\ m &= 0, \pm 1, \dots, \pm l \end{aligned} \tag{4.29}$$

determine the energy levels. For non-interacting electrons ($\lambda = 0$), the analytical calculation of the action integral leads to the (quantum mechanically exact) eigen-energies (A.13). For $\lambda \neq 0$, one can calculate the action integral (4.28) numerically with a few iterations to determine the eigenvalues. The results for the spherically symmetric case, obtained by the WKB approach and for the cases discussed below, can be found in [364].

The restoration of the rotational symmetry of the electronic states by the magnetic field for noninteracting electrons was discussed in Sec. 4.2.1. This phenomenon was also recognized in the results for *interacting* electrons in self-assembled QDs [299]. It was interpreted as an approximate symmetry that had survived from the noninteracting case due to the dominance of the confinement energy over a relatively small Coulomb interaction energy. However, as it is clear from the form of Eq. (4.25), the symmetry is not approximate but *exact* even for strongly interacting electrons, because the radial electron-electron repulsion does not break the rotational symmetry.

- The case $\omega_z = 2\omega_\rho$ and $\omega_z = \omega_\rho/2$.

The spherical coordinates are a particular limit of the spheroidal (elliptic) coordinates well suitable for the analysis of the Coulomb systems, e.g., [365]. Therefore, to search for separability in other integrable cases, it is convenient to use the spheroidal coordinates (ξ, η, φ) , where $\xi = (r_1 + r_2)/d$ and $\eta = (r_1 - r_2)/d$. In the *prolate* spheroidal coordinates $r_1 = [\rho^2 + (z + d)^2]^{1/2}$, $r_2 = r$. The parameter $d \in (0, \infty)$ is the distance between two foci of the coordinate system (with the origin at one of them). In the limit $d \rightarrow 0$, the motion is separated when $\omega_z/\omega_\rho = 1$ (see Fig.5b). In this limit $\xi \rightarrow \infty$, so that $r = d\xi/2$ is finite, $\eta = \cos\vartheta$, and we obtain the spherical coordinate system.

Let us turn to the case $\omega_z/\omega_\rho = 2$ which occurs at the value of the magnetic field $\omega_L'' = (\omega_z^2/4 - \omega_0^2)^{1/2}$. In the prolate spheroidal coordinates the motion is separated in the limit $d \rightarrow \infty$ (Fig. 5d). In fact, at $d \rightarrow \infty$: $\xi \rightarrow 1$, $\eta \rightarrow 1$, so that $\xi_1 = d(\xi - 1)$, $\xi_2 = d(1 - \eta)$ are finite, we obtain the parabolic coordinate system (ξ_1, ξ_2, φ) , where $\xi_{1,2} = r \pm z$. In these coordinates Hamiltonian (4.22) has the form

$$\begin{aligned} h &= \frac{1}{\xi_1 + \xi_2} \left[2(\xi_1 p_{\xi_1}^2 + \xi_2 p_{\xi_2}^2) + \frac{m^2}{2} \left(\frac{1}{\xi_1} + \frac{1}{\xi_2} \right) \right. \\ &\quad \left. + \frac{\tilde{\omega}_z^2}{8} (\xi_1^3 + \xi_2^3) + 2\lambda \right] - \tilde{\omega}_L'' m \end{aligned} \tag{4.30}$$

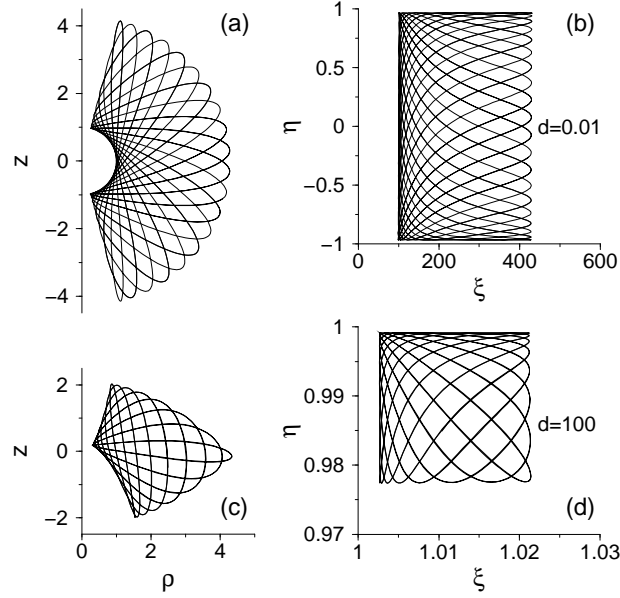


Figure 5: Typical trajectories ($\epsilon = 10$, $m = 1$) of the relative motion at $\lambda = 1.5$, for $\omega_z/\omega_\rho = 1$ (a,b) and $\omega_z/\omega_\rho = 2$ (c,d), are shown in cylindrical and prolate spheroidal coordinates, respectively. From [345].

and the equation $(\xi_1 + \xi_2)(h - \epsilon) = 0$ is separated into two decoupled equations for ξ_1 and ξ_2 variables,

$$2\xi_j p_{\xi_j}^2 + \frac{m^2}{2\xi_j} + \frac{\tilde{\omega}_z^2}{8}\xi_j^3 - (\epsilon + \tilde{\omega}_L'' m)\xi_j + \lambda = (-1)^j c, \quad j = 1, 2. \quad (4.31)$$

Simple manipulations define the separation constant

$$c = a_z - \tilde{\omega}_\rho^2 \rho^2 z, \quad (4.32)$$

which is the desired third integral of motion. Here a_z is the z -component of the Runge-Lenz vector

$$\mathbf{a} = \mathbf{p} \times \mathbf{l} + \lambda \frac{\mathbf{r}}{r}, \quad (4.33)$$

which is a constant of motion for the pure Coulomb system (i.e., when $\omega_\rho = \omega_z = 0$) [87]. The quantum mechanical counterpart of the integral of motion, Eq. (4.32), does not commute with the parity operator, and we should expect the degeneracy of quantum levels.

Due to the separability of the motion in the parabolic coordinate system, the eigenfunctions of the corresponding Schrödinger equation can be expressed in the form $\psi(\mathbf{r}) = f_1(\xi_1) f_2(\xi_2) e^{im\varphi}$, where the functions f_j are the solutions of the equations

$$\begin{aligned} \frac{d}{d\xi_j} \left(\xi_j \frac{df_j}{d\xi_j} \right) - \frac{1}{4} \left[\frac{m^2}{\xi_j} + \frac{\tilde{\omega}_z^2}{4}\xi_j^3 - 2(\epsilon + \tilde{\omega}_L'' m)\xi_j + \right. \\ \left. + 2\lambda - (-1)^j 2c \right] f_j = 0, \quad j = 1, 2. \end{aligned} \quad (4.34)$$

Eqs. (4.34) can be solved numerically. Let n_1 and n_2 be the nodal quantum numbers of the functions f_1 and f_2 , respectively. Note that Eqs. (4.34) are coupled by the constants of motion and, therefore, both functions depend on all three quantum numbers (n_1, n_2, m) . The states $|n_1, n_2, m\rangle$ have, in the coordinate representation, the explicit form

$$\psi_{n_1, n_2, m}(\mathbf{r}) = f_{n_1}^{(n_2, m)}(\xi_1) f_{n_2}^{(n_1, m)}(\xi_2) \frac{e^{im\varphi}}{\sqrt{2\pi}}. \quad (4.35)$$

The simple product of these functions has no definite parity. Since $\mathbf{r} \rightarrow -\mathbf{r} \Leftrightarrow \{\xi_1 \rightarrow \xi_2, \xi_2 \rightarrow \xi_1, \varphi \rightarrow \varphi + \pi\}$, the even/odd eigenfunctions are constructed as

$$\psi_{N, k, m}^{(\pm)}(\mathbf{r}) = \frac{e^{im\varphi}}{\sqrt{2}} [f_{n_1}^{(n_2, m)}(\xi_1) f_{n_2}^{(n_1, m)}(\xi_2) \pm (-1)^m f_{n_2}^{(n_1, m)}(\xi_1) f_{n_1}^{(n_2, m)}(\xi_2)], \quad (4.36)$$

where $N = n_1 + n_2$ and $k = |n_1 - n_2|$. These states are the eigenfunctions of h , l_z , c , and the parity operator. For $c > 0$, the eigenstates (4.36) appear in doublets of different parity and, therefore, of a different total spin. For $c = 0$ in Eqs. (4.34), $f_1 = f_2$ and, obviously, only the states with parity $\pi = (-1)^m$ exist. In this case, the dynamical symmetry is $O(4) \supset O(2) \otimes O(2)$.

For the magnetic field $\omega_L''' \equiv (4\omega_z^2 - \omega_0^2)^{1/2}$, we obtain the ratio $\omega_z/\omega_\rho = 1/2$. Hamiltonian (4.22), expressed in the *oblate* spheroidal coordinates ($r_1 = [z^2 + (\rho + d)^2]^{1/2}$, $r_2 = r$), is separable for $m = 0$ (at $d \rightarrow \infty$). For $m \neq 0$, the term m^2/ρ^2 and, consequently, Hamiltonian (4.22), is not separable in these coordinates. For $m = 0$, the cases $\omega_z/\omega_\rho = 1/2$ and 2 are equivalent, if we interchange the ρ and z coordinates and, hence, the additional integral of motion is $|a_\rho - \tilde{\omega}_z^2 z^2 \rho|$. For $m \neq 0$, the recipe [362] enables one to obtain the following integral of motion

$$C = [(a_\rho - \tilde{\omega}_z^2 z^2 \rho)^2 + a_\varphi^2 + 4m^2 \tilde{\omega}_z^2 r^2]^{1/2}, \quad (4.37)$$

where a_ρ and a_φ are the ρ and φ components of the Runge-Lenz vector, respectively. Due to the existence of three independent integrals of motion, h , m and c , which are in involution, the dynamics for $m \neq 0$, although non-separable, is integrable. The further analysis for $m = 0$ is similar to the previous one and we omit it here. The corresponding dynamical symmetry is $O(4) \supset O(3) \supset O(2)$.

4.4 Dimensionality effects in ground-state transitions of two-electron quantum dots

Experimental data, including transport measurements and spin oscillations in the ground state in a perpendicular magnetic field for two-electron QDs, can be explained by the interplay between electron correlations, lateral confinement, and a magnetic field. Using a $2D$ quantum dot model, one is able to reproduce a general trend for the first singlet-triplet transitions observed in two-electron QDs in a perpendicular magnetic field. However, the experimental positions of the singlet-triplet transition points are systematically higher [273, 295]. The ignorance of the third dimension is the most evident source of the disagreement, especially, in vertical QDs [300, 366, 367].

4.4.1 First singlet-triplet transition in a two-electron quantum dot

As is discussed above, the additional energy Eq. (4.9) is one of the major quantities which should be calculated and compared with the available experimental data. Here we are concerned with $\mu(1)$ and $\mu(2)$ only, which we calculate with the aid of the model considered in Sec. 4.3. The first is simply the harmonic oscillator energy for a single electron in the dot, $\mu(1) = E(1, B)$, where $E(N, B)$ denotes the total energy of the QD with N electrons under a magnetic field of strength B . The latter can be split into contributions from the relative and center-of-mass motion E_{CM} , where $E_{CM} = E(1, B)$. The addition energy (direct probe of electron correlation in the dot) takes the form $\Delta\mu \equiv \mu(2) - \mu(1) = \hbar\omega_0\epsilon - E(1, B)$, where ϵ is the relative energy determined by Hamiltonian (4.22) and $E(1, B) = \hbar\omega_p + \hbar\omega_z/2$.

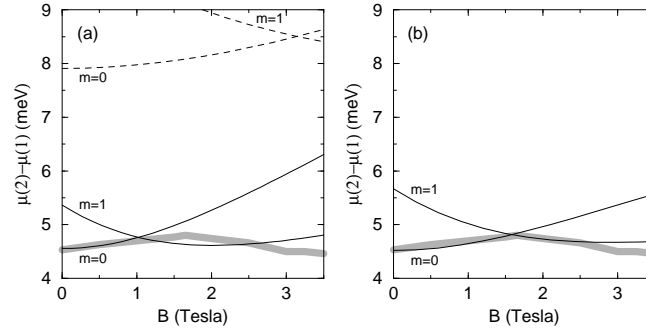


Figure 6: The addition energy $\Delta\mu$ (a shaded curve from experiment [312]). Part (a) shows the theoretical $\Delta\mu$ from a 2D quantum dot model, with $\hbar\omega_0 = 5.4$ meV (dashed) and $\hbar\omega_0 = 2.3$ meV (solid). Part (b) shows $\Delta\mu$ from a 3D model with $\hbar\omega_0 = 2.6$ meV and $\omega_z/\omega_0 = 2.4$ (solid). From [364].

In a number of papers (e.g., [312, 314, 368, 369]) $\mu(1, B)$ has been used to estimate the confining frequency $\hbar\omega_0$ in a 2D model of the QD. Indeed, with $\hbar\omega_0 = 5.4$ meV ($\hbar\omega_z = 0$), one obtains a very satisfactory fit to $\mu(1)$ [312]. However, with this $\hbar\omega_0$, neither $\Delta\mu$ (which is by almost a factor 2 too large) nor the value for B , where the first singlet-triplet transition occurs, are reproduced correctly, as is obvious from Fig. 6a. It has been argued that for the increasing magnetic field, $\mu(N, B)$ might not follow the behaviour modelled by a simple QD with a constant confining frequency, [314, 369]. It was suggested [364] to extract $\hbar\omega_0$ from the difference of the chemical potentials $\mu(2, 0) - \mu(1, 0)$ at zero magnetic field. Such a procedure, with $\hbar\omega_0 = 2.3$ meV ($\lambda = 1.66$), leads to the first singlet-triplet transition ($m = 0, S = 0 \Rightarrow m = 1, S = 1$) at $B = 1.02$ T (the Zeeman term is absent) (see Fig. 6a). This value differs from the experimental value of $B \approx 1.5$ T only by about 30%, contrary to the difference of more than a factor of 2 with $\hbar\omega_0 = 5.4$ meV (dashed line).

The discrepancy of 30% vanishes if one proceeds to a 3D description of the QD. In this case, $\hbar\omega_0 = 2.6$ meV ($\lambda = 1.56$) is needed to match $\mu(2, 0) - \mu(1, 0)$, only slightly different from the 2D case, but the first singlet-triplet transition occurs now at $B = 1.59$ T (see Fig. 6b). If one includes the contribution from the Zeeman energy $E_Z = \frac{1}{2}\mu^*B[1 - (-1)^m]$, with $\mu^* = g_L\mu_B$ ($g_L = -0.44$), then this value reduces to $B = 1.52$ T in a good agreement with the experiment. Of course, this agreement is achieved by tuning a second

parameter, available in the 3D case, namely $\omega_z/\omega_0 = 2.4$, i.e. the ratio of vertical to lateral confinement. On the other hand, a rough estimate assuming $\omega_z/\omega_0 \sim d_0/d_z$, with the experimental value $d_z = 175 \text{ \AA}$, reveals a lateral size of $d_0 \approx 420 \text{ \AA}$ which is of the correct order of magnitude, although the exact lateral extension in the experiment is not known [312]. The analysis shows that, in contrast to a 2D description, the 3D description provides a consistent way to describe the energy spectrum for small B , the value of the magnetic field for the first singlet-triplet transition, and the ratio of lateral to vertical extension of the dot. The details of the recent study of excited states in two-electron vertical QDs [295] confirm this point of view (see below).

It has been predicted that the ground state of an N -electron QD at a high magnetic field, becomes the spin polarized maximum density droplet (MDD) [370]. In the MDD case the single-particle orbitals in the lowest Landau level become singly occupied. A detailed discussion of different phases in N -electron 2D QDs in a magnetic field can be found in [277]. The spin-polarized droplet of electrons in the lowest Landau level has the lowest possible total angular momentum $L = N(N - 1)/2$, compatible with the Pauli principle. For a two-electron QD it is expected that the MDD occurs after a first singlet-triplet transition.

4.4.2 Topological transitions in a two-electron quantum dot

Theoretical calculations [300, 319, 330, 331, 342, 371, 372] assert that after the first singlet-triplet transition the increase of the magnetic field induces several ground state transitions to higher orbital-angular and spin-angular momentum states. This issue was addressed in the transport study of the correlated two-electron states up to 8 T and 10 T in a lateral [373] and vertical [294, 295] QDs, respectively. It is quite difficult to detect the structure of the ground states after the first singlet-triplet transition in a lateral QD due to a strong suppression of the tunnelling coupling between the QD and contacts. Altering the lateral confinement strengths exhibits the transitions, beyond the first singlet-triplet transition, reported in vertical QDs [295]. In fact, the variation of the confining frequency with *the same experimental setup* opens a remarkable opportunity for a consistent study of effects of the magnetic field on electron correlations.

Three vertical QDs, with different lateral confinements, have been studied in the experiment [295]. In all samples, clear shell structure effects for the electron numbers $N = 2, 6, \dots$ at $B = 0$ T have been observed, implying a high rotational symmetry. Although there is a sufficiently small deviation from this symmetry in a sample, classified by Nishi *et al.* [295] as C, a complete shell filling for two and six electrons was observed. Such a shell structure is generally associated with a 2D harmonic oscillator $x - y$ confinement [273]. However, a similar shell structure is produced by a 3D axially symmetric HO, if the confinement in the z -direction, with $\omega_z = 1.5\omega_0$, is only slightly larger than the lateral confinement ($\omega_x = \omega_y = \omega_0$). In this case, six electrons fill the lowest two shells of the Fock-Darwin energy levels with $n_z = 0$. It was also found that the lateral confinement frequency, for the axially symmetric QD, decreases with the increase of the electron number [374], since the screening in the lateral plane becomes stronger with large electron numbers. In turn, this effectively increases the ratio ω_z/ω_0 , making the dot effectively more "two-dimensional", since the vertical confinement is fixed by the sample thickness. Indeed, the N -dependence of the effective lateral frequency is observed in [295].

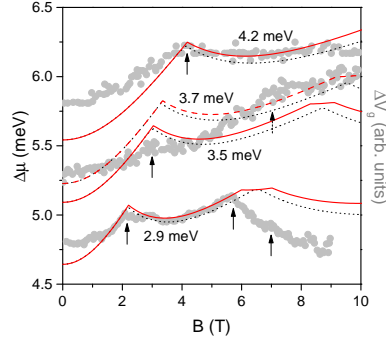


Figure 7: (Color online) The magnetic dependence of the addition energy $\Delta\mu$ in two-electron QDs with lateral confinement $\hbar\omega_0 = 4.2, 3.7, 3.5, 2.9$ meV (the first, second, and fourth values are experimental values for the samples A, B, and C, respectively [295]). The confinement in the third (z) direction $\hbar\omega_z = 8$ meV is fixed for all samples. The results for $|g^*| = 0.3(0.44)$ are connected by solid (dotted) line for $\hbar\omega_0 = 4.2, 3.5, 2.9$ meV and by dashed (dotted) line for $\hbar\omega_0 = 3.7$ meV. The solid gray lines display the experimental spacing ΔV_g as a function of B . The arrows identify the position of experimental ground state transitions [295]. From [375].

Fitting the B -field dependence of the first and second Coulomb oscillation peak positions to the lowest Fock-Darwin energy levels of the 2D HO with the potential $m^*\omega_0^2 r^2/2$, Nishi *et al.* [295] estimated ω_0 for all three samples A, B, and C. Although the general trend in the experimental data is well reproduced by the 2D calculations, the experimental positions of the singlet-triplet transition points are systematically higher. Different lateral confinements in the above experiment are achieved by the variation of the electron density, without changing the sample thickness.

Using the "experimental" values for the lateral confinement and the confinement frequency ω_z as a free parameter, it was found, by means of the exact diagonalization of Hamiltonian (4.1) for two interacting electrons, that the value $\hbar\omega_z = 8$ meV provides the best fit for the positions of kinks in the addition energy (4.9) with the Zeeman energy E_Z [375]. In Fig.7, the magnetic dependence of the experimental spacing between the first and the second Coulomb oscillation peaks $\Delta V_g = V_g(2) - V_g(1)$ for the samples A–C is shown. The spacing can be transformed to the addition energy $\Delta\mu$ [294, 295]. In the $\Delta V_g - B$ plot, the ground state transitions appear as upward kinks and shoulders. It was found from the Zeeman splitting at high magnetic fields that $|g^*| = 0.3$ [294] and the addition energy is calculated with this and the bulk values.

The experimental position of the first singlet-triplet transitions at $B = 4.2, 3, 2.3$ T in samples A, B, and C, respectively is reproduced quite well in the calculations (see Fig. 7). When the magnetic field is low, the difference between the calculations with different $|g^*|$ factors is negligible. Upon decreasing the lateral confinement $\hbar\omega_0$ from the sample A to the sample C (the increase of the ratio ω_z/ω_0), the Coulomb interaction becomes dominant in the interplay between electron correlations and the confinement [364]. In turn, the smaller the lateral confinement at fixed thickness (the stronger the electron correlations), the smaller the value of the magnetic field where the singlet-triplet transitions or, in

general, crossings between excited states and the ground state, may occur.

There is no signature of the second crossing in the ground state for the sample A at large B (up to 10 T). Here, the ratio $\omega_z/\omega_0 \approx 1.9$, and the effect of the third dimension is the most visible: the confinement has a dominant role in the electron dynamics, and a very high magnetic field is required to observe the next transition in the ground state due to electron correlations. Thus, the MDD phase survives until very high magnetic fields ($B \sim 10$ T).

A second kink is observed at $B = 7$ T in the sample B [295]. The calculations with the "experimental" lateral confinement $\hbar\omega_0 = 3.7$ meV produce the second kink at $B = 9.5$ T, which is located higher than the experimental value. The slight decrease of the lateral frequency until $\hbar\omega_0 = 3.5$ meV shifts the second kink to $B = 8.7$ T, improving the agreement with the experimental position of the first singlet-triplet transition as well. In addition, the use of $|g^*| = 0.3$ (instead of the bulk value) with the latter frequency creates a plateau, which bears resemblance to the experimental spacing ΔV_g . However, there is no full understanding of this kink. It seems, there is an additional mechanism responsible for the second kink in the sample B. In the sample C, the first experimental singlet-triplet transition occurs at $B = 2.3$ T, while the signatures of the second and the third ones are observed at $B \approx 5.8, 7.1$ T, respectively. The 2D calculations (with the "experimental" values $\hbar\omega_0 = 2.9$ meV, $|g^*| = 0.44$) predict the first, second, and third singlet-triplet crossings at lower magnetic fields: $B = 1.7, 4.8, 5.8$ T, respectively. The results can be improved to some degree with $|g^*| = 0.3$. To reproduce the data for $\Delta\mu$, Nishi *et al.* [295] increased the lateral confinement ($\hbar\omega_0 = 3.5$ meV, $|g^*| = 0.44$). As a result, the first, second, and third singlet-triplet transitions occur at $B = 2, 6.3, 7.5$ T, respectively. Evidently, 2D calculations overestimate the importance of the Coulomb interaction. The increase of the lateral confinement simply weakens the electron correlations in such calculations. In contrast, the 3D calculations reproduce quite well the positions of all crossings, with the "experimental" lateral confinement $\hbar\omega_0 = 2.9$ meV at $B = 2.3, 5.8, 7.1$ T (see discussion below).

One of the questions, addressed in the experiment [295], is related to a shoulder-like structure observed in a small range of values of the magnetic field (see Fig. 7). This structure is identified as the second singlet state $(2, 0)$ that persists till the next crossing with the triplet state $(3, 1)$. According to Nishi *et al.* [295], the ground state transition

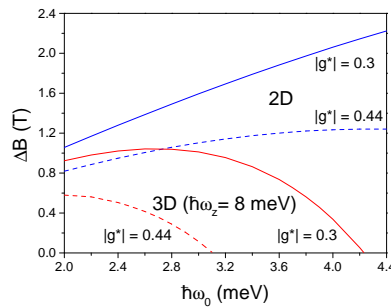


Figure 8: (Color online) The interval ΔB where the singlet state $(2, 0)$ survives as a function of the lateral confinement for 2D and 3D calculations. The confinement in the third (z) direction $\hbar\omega_z = 8$ meV is fixed for the 3D calculations. From [375].

from the triplet $(1, 1)$ state to the singlet $(2, 0)$ state is associated with the collapse of MDD state for $N = 2$. Therefore, a question arises: at what conditions it would be possible to avoid the collapse of the MDD phase (in general, to preserve the spin-polarized state); i.e., at what conditions the singlet $(2, 0)$ state will never show up in the ground state. In fact, the collapse of the MDD depends *crucially* on the value of the lateral confinement. It was found that in the 2D consideration, the $(2, 0)$ state always exists for experimentally available lateral confinement (see Fig. 8). Moreover, in this range of $\hbar\omega_0$, the 2D approach predicts the monotonic increase for the interval of the values of the magnetic field ΔB , at which the second singlet state survives with the increase of the lateral confinement. In contrast, in the 3D calculations, the size of the interval is a vanishing function of the lateral confinement for a fixed thickness ($\hbar\omega_z = 8$ meV). It is quite desirable, however, to measure this interval to draw a definite conclusion.

As discussed above, the decrease of the confinement, at a fixed thickness, increases the dominance of the electron correlations in the electron dynamics. For a low enough electron density, Wigner [376] predicted that electrons should localize, creating an ordered spatial structure that breaks the complete translational symmetry of the homogeneous electron gas. Therefore, the decrease of the confinement, related to the decrease of the electron density [295, 374], creates the favourable conditions for the onset of electron localization. According to a general wisdom, the Wigner crystallization in QDs, whose localized states are referred to as Wigner molecules [377, 378], should occur at significantly larger densities than in bulk. This is based on the argument that in QDs potential-energy contributions can easily exceed the kinetic terms and, therefore, electronic motion can be effectively quenched by manipulating the external confinement and/or an applied magnetic field.

The dynamics of electrons in QDs is determined by the ratio

$$R_W = \bar{\ell}_0/a^* \equiv \sqrt{2}\lambda = k/\bar{\ell}_0\hbar\omega_0, \quad (4.38)$$

where $\bar{\ell}_0 = \sqrt{\hbar/m^*\omega_0}$ is the oscillator length with the mass m^* and $\hbar\omega_0$ can be determined from the volume conservation condition (see Sec. 4.2.1). For a strong confinement, $R_W \rightarrow 0$, and the Coulomb energy can be neglected. In this case, the interaction acts merely as a small perturbation. In the opposite limit of a weak confining potential, $\omega_0 \rightarrow 0 \Rightarrow R_W \rightarrow \infty$, the interaction becomes arbitrarily strong and the system will undergo a phase transition to the Wigner crystal.

For the QDs considered in the experiments of Nishi *et al.* [295], in the 2D approach for a circular dot, $R_W \sim 3$. For a 2D two-electron QD, it is predicted that the Wigner molecule can be formed for $R_W \sim 200$ at zero magnetic field [379], or at very high magnetic field [380] for $\hbar\omega_0 \sim 3$ meV and small R_W , such as in the discussed experiments. In the 3D axially symmetric QDs the ratio between vertical and lateral confinements (anisotropy) may, however, affect the formation of the Wigner molecule. This problem can be studied by dint of the electron density

$$n(\mathbf{r}) = \int [|\Psi(\mathbf{r}, \mathbf{r}')|^2 + |\Psi(\mathbf{r}', \mathbf{r})|^2] d\mathbf{r}', \quad (4.39)$$

when one electron is at a position \mathbf{r} , while another is located at a position \mathbf{r}' . A criterion for the onset of the crystallization in two-electron QDs can be the appearance of a local electron density minimum in the center of the dot [378, 381]. For 2D QDs, this leads

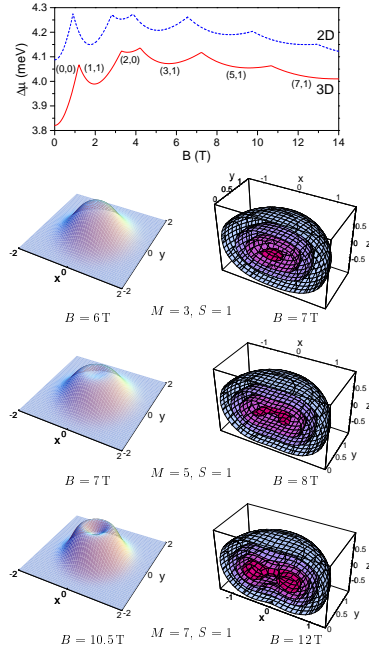


Figure 9: (Color online) Top: Magnetic dependence of the ground state in 2D and 3D ($\hbar\omega_z = 8$ meV) approaches for a lateral confinement $\hbar\omega_0 = 2$ meV. The 2D (left) and 3D (right) electron densities are displayed for different ground states (M,S) at corresponding magnetic fields. The largest 3D density grows, with the increase of the magnetic field, from the central small core over a ring to the torus. From [375].

to the radial modulation in the electron density, resulting in the formation of rings and roto-vibrational spectra [382,383].

The 3D analysis of the electron density (see Fig. 9) indicates that, at $B > 7.25$ T, the triplet state (5,1) may be associated with the formation of the Wigner molecule, in agreement with the above discussion. There is an evident difference between the 2D and 3D approaches: the 2D calculations predict the crystallization at the lower magnetic field ($\Delta B \sim 1$ T). The further increase of the magnetic field leads to the formation of a ring and a torus of the maximal density in 2D- and 3D-densities, respectively. Notice that if the geometrical differences are disregarded, 3D evolution of the ground state can be approximately reproduced in 2D approach with the effective charge concept [364,384].

4.4.3 Effective charge

It seems evident that in QDs, the Coulomb interaction couples lateral and vertical coordinates, and the problem, in general, is non-separable. By means of the exact diagonalization of 3D effective Hamiltonian, one can study the effect of the vertical confinement on the energy spectrum [374]. This can be done, however, only for QDs with a small number of electrons. Even in this case there are difficulties related to the evaluation of 3D interaction matrix elements.

The thickness of QDs is much smaller in comparison with the lateral extension. Therefore, the vertical confinement, with $\hbar\omega_z$, is much stronger than the lateral confinement, with $\hbar\omega_0$, and this fact is usually employed to justify a 2D approach to QDs. One can develop, however, the procedure that accounts for the thickness of QDs [384]. Note that there is a nonzero contribution from the vertical dynamics, since the energy level, available for each of noninteracting electrons in the z -direction, is $\varepsilon = \hbar\omega_z(n_z + 1/2)$. For the lowest state $n_z = 0 \Rightarrow \varepsilon_1 = \frac{1}{2} \hbar\omega_z$. Because of the condition $V_z(\pm z_m) \equiv m^*\omega_z^2 z_m^2/2 = \varepsilon_1$, one defines the turning points: $z_m = \sqrt{\hbar/(m^*\omega_z)}$. One may assume that the distance between turning points should not exceed the layer thickness, i.e., $2z_m \leq a$ (see Fig.10). Owing to this inequality, the lowest limit for the vertical confinement in the layer of thickness a is $\hbar\omega_z \geq 4\hbar^2/(m^*a^2)$. For typical GaAs samples, with the thickness a between 10 nm and 20 nm, this estimate gives the minimal value for $\hbar\omega_z$ between 45 meV and 11 meV, respectively. These estimates provide a genuine cause for the use of the adiabatic approach [385] in the case of QDs, since

$$T_z (= 2\pi/\omega_z) \ll T_0 (= 2\pi/\omega_0) . \quad (4.40)$$

To lowest order, the adiabatic approach consists of averaging the full 3D Hamiltonian (4.1) over the angle-variables $\theta_{z_i} = \omega_{z_i} t$ (fast variables) of the unperturbed motion ($k = 0$) of two electrons after rewriting the (z_i, p_{z_i}) variables in terms of the action-angle variables (J_{z_i}, θ_{z_i}) . As a result, the dynamics effectively decouples into an unperturbed motion in the vertical direction, governed by the potential $\sum_i V(J_{z_i}, \theta_{z_i})$, and the lateral motion governed by the effective potential $V_{\text{eff}}(\{x, y\}; \{J_z\})$ that contains the memory on z dynamics through the integrals of motion J_{z_i} [384]. The effective electron-electron interaction affects, therefore, only the dynamics in the lateral plane, where the confining potential is parabolic. Hence, the effective Hamiltonian for a two-electron QD is

$$H_{\text{eff}} = H_0 + E_z + V_{\text{int}}^{\text{eff}} , \quad (4.41)$$

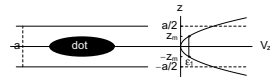


Figure 10: Left: the localization of QD in the layer of the thickness a . Right: the schematic representation of the position of zero-point motion in the parabolic confinement relative to the layer thickness. From [384].

where $E_z = \sum_i \varepsilon_i$ and ε_i is the electron energy of the unperturbed motion in the vertical direction. The term $H_0 = \sum_{i=1}^2 h_0(i)$ consists of the contributions related only to the lateral dynamics in the $x - y$ -plane of noninteracting electrons (see Eq.(4.3)).

The main idea of the procedure is based on the consideration of the Coulomb term determined by the effective value k_{eff} (effective charge) with the appropriate consideration of the vertical (z) dynamics, i.e.,

$$V_C = k/r_{12} \approx k_{\text{eff}}/\rho, \quad (4.42)$$

where $\rho = [(x_1 - x_2)^2 + (y_1 - y_2)^2]$. Thus, the procedure of evaluating the effective charge consists of two steps: (i) the averaging of the Coulomb term $V_C(\rho, z)$ over the angle variables in the z -direction, which gives the effective $2D$ potential

$$V_{\text{int}}^{\text{eff}}(\rho) = k f(\rho)/\rho; \quad (4.43)$$

(ii) the calculation of the mean value of the factor $f(\rho)$ upon the non-perturbed lateral wave functions, i.e.,

$$k_{\text{eff}} = k \langle f(\rho) \rangle \equiv \langle \rho V_{\text{int}}^{\text{eff}}(\rho) \rangle. \quad (4.44)$$

As a result, one has to solve only the Schrödinger equation for the $2D$ effective Hamiltonian where the full charge k is replaced by k_{eff} . The effective charge can be calculated as a quantum-mechanical mean value of the Coulomb term with the aid of the Fock-Darwin $|n_r, m\rangle$ and a one-dimensional harmonic oscillator $|n_z\rangle$ states:

$$k_{\text{eff}} = \langle \rho V_C(\rho, z) \rangle = k \langle (1 + z^2/\rho^2)^{-1/2} \rangle. \quad (4.45)$$

Since the lateral extension exceeds the thickness of the QDs by several times, one may suggest to consider the ratio $(z/\rho)^2$ as a small parameter of theory.

In the considered cases of the parabolic, square, and triangular well potentials [384], the value of the effective charge depends on the (good) quantum number m of the correlated state. In particular, for the parabolic confinement in the z -direction, the effective charge can be expressed in terms of the Meijer G -function [386]

$$k_{\text{eff}} = \frac{k}{\pi |m|!} G_{2,3}^{2,2} \left(\frac{\omega_\rho}{\omega_z} \left| \begin{array}{cc} 1/2 & 1/2 \\ 0 & m+1 \end{array} \right. \right). \quad (4.46)$$

The screening due to the sample thickness is especially strong for the quantum states with small values of the quantum number m . We recall that these states determine the structure of ground state transitions at small and intermediate values of the magnetic field. Therefore, the screening provides a consistent way to deal with the effect of thickness upon the position of the singlet-triplet transitions [373]. In particular, the screening should be taken into account for the analysis of the evolution of the energy difference between singlet and triplet states in a magnetic field. This energy is considered to be important for the analysis of entanglement and concurrence in QDs [387].

The comparison of the results with available experimental data demonstrates a remarkable agreement and provides a support to the validity of the approach (see Fig. 11). The results, based on the adiabatic approximation, are in a better agreement with the full $3D$ calculations, in contrast to those obtained with the aid of the plain quantum-mechanical averaging procedure. As discussed above, the adiabatic approach is based on

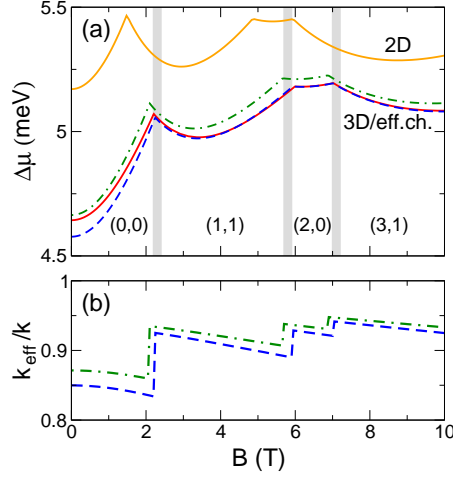


Figure 11: (Color online) (a) The addition energy $\Delta\mu$ as a function of the magnetic field in the parabolic model. The results of calculations with a lateral confinement only (the 2D approach, $\hbar\omega_0 = 2.9$ meV, $|g^*| = 0.3$) and full 3D approach [375] ($\hbar\omega_z = 8$ meV) are connected by the thick (orange) and thin (red) lines, respectively. The vertical gray lines indicate the position of the experimental crossings between different ground states in a sample C [295]. Ground states are labelled by (m, S) , where m and S are the quantum numbers of the operators l_z and the total spin, respectively. The results based upon the adiabatic approximation, and the plain quantum-mechanical averaging procedure, are connected by dashed (blue) and dot-dashed (green) lines, respectively. (b) The ratios k_{eff}/k as functions of the magnetic field, based on the adiabatic approach and the plain quantum-mechanical averaging, are connected by dashed (blue) and dot-dashed (green) lines, respectively. From [384].

the effective separation of fast (vertical) and slow (lateral) dynamics, with the subsequent averaging procedure. In contrast, the plain quantum-mechanical averaging represents a type of perturbation theory based on the first order contribution with respect to the ratio z/ρ only. The higher-order terms may improve the agreement at small magnetic field, since the vertical dynamics is not negligible and affects the lateral dynamics. The increase of the quantum number m , caused by the increase of the magnetic field strength, reduces the orbital motion of electrons in the vertical direction. The larger m , the stronger the centrifugal forces, which induce the electron localization inside a plane, and, therefore, the lesser importance of the vertical electron dynamics. In the limit of strong magnetic field (large m) the dot becomes rather a "two-dimensional" system. This explains the improvement of the accuracy of the plain quantum-mechanical averaging procedures at large m , i.e., for the ground states at high magnetic fields. It follows that the 2D bare Coulomb potential becomes reliable in the 2D approaches, for the analysis of the ground state evolution of QDs, only at large magnetic fields.

4.5 Symmetry breaking: mean field and beyond

4.5.1 Theoretical approaches

The studies of different phases in QDs [277, 278] shed light on a variety of aspects of strongly correlated *finite* systems, which can be controlled experimentally. This makes it possible to understand the common features of and the principal differences between finite-size systems and conventional condensed matter. One can analyze the relation between these systems, depending on the strength of electron-electron interactions and of external fields. In fact, the high controllability of QDs creates a remarkable opportunity to investigate in detail novel strongly correlated phenomena in various experimental setups.

Several approaches, based on the parabolic confining potential, including the exact diagonalization method, a diffusion Monte Carlo (DMC) and a path integral Monte Carlo (PIMC), density functional methods, have been applied with some degree of success to analyze the ground state energies of the N -electron QD; see for the recent reviews [201, 277, 278]. However, the exact diagonalization method is limited to relatively small particle number, e.g., [332, 369, 388–392]. The local-density approximation cannot properly describe the localized states, due to the lack of exact cancellation of the direct and exchange Coulomb interactions. The pros and cons of the density functional approach related to the description of symmetry breaking phenomena are discussed in [201]. PIMC treats an interaction accurately [393, 394]. However, it generates a thermal average of states with different L and S quantum numbers, preserving only S_z symmetry. The energy for low-lying excitations becomes very small in the low density limit (strong electron correlations), and, therefore, the constraint on the temperature becomes extremely stringent. DMC provides quite reliable results [395–398]. It contains some systematic “fixed-mode” error which are, however, smaller than the systematic and statistical errors of PIMC. A good introduction to the discussed methods, with applications to atomic gases and quantum dots, can be found in [399]. Among promising approaches, which could provide an accurate treatment of correlation and spin effects for the ground and excited states of QDs, we can mention the coupled cluster methods [400]. The comparison of the coupled cluster method results with the available analytical solutions [300, 333, 334, 336] shows that this method takes into account between 99% and 91% of the total energy from two to eight electrons [401].

4.5.2 Hartree-Fock approximation

In many cases, a convenient starting point to treat finite systems is a mean field description, like the Hartree-Fock (HF) approach [402–404]. In spite of its simplicity, the HF approach is extremely powerful. The nonlinearity of the HF equations allows for spontaneous breaking of fundamental symmetries of many-body Hamiltonians. In fact, this is a primary mechanism that enables one to incorporate various correlations into a single Slater determinant. Indeed, in a symmetry preserving approach, the wave function of the system must have the same symmetry as the many-body Hamiltonian. However, the most direct description of electron localization can be obtained by using the unrestricted HF approximation with broken rotational symmetry, when the wave function has a lower symmetry than the Hamiltonian. The problem of the transition from a rotationally symmetric solution to the so-called Wigner molecule [377] and crystal [405–408],

where electrons occupy fixed spatial sites, with the increase of the magnetic field, have been investigated in the geometrically unrestricted Hartree-Fock approach by Müller and Koonin [378]. The mean field solutions with broken rotational symmetry were interpreted as "intrinsic" states. Müller and Koonin [378] constructed the rotational states by projecting the Hartree-Fock Slater determinant onto eigenstates of a good angular momentum. These ideas, borrowed from nuclear physics [403], resolved doubts about the validity of the mean field approach. It is appropriate at this point to recall that the assumption of deformed shape in the case of open-shell nuclei is essential for the description of nuclear rotational spectra [168, 409–411]. In fact, axially deformed shapes for QDs, with up to 40 electrons, have been obtained in the Hartree-Fock calculations with isotropic harmonic confinement in all three spatial dimensions [412]. The quadrupole moment $q_{20} \sim \sum_{ij} \langle i | 2z^2 - x^2 - y^2 | j \rangle \rho_{ij}$, where ρ_{ij} is the Hartree-Fock density, vanishes for closed shells, being nonzero for open-shell QDs.

In the simpler case of a two-electron $2D$ quantum dot in zero magnetic field, Yannouleas and Landman [379] pointed out that the excited-state energies of this system closely follow the rotor sequence, when the repulsion-to-confinement ratio, given by the Wigner parameter R_W , is large enough (~ 200). This was shown to be a proof of the crystallization of two electrons in fixed positions in a rotating reference frame. Quite remarkably, the hypothesized *rotating Wigner molecule* fulfills at the same time the strict symmetry conditions of quantum mechanics –circularity in this case– and the obvious preference for opposite positions, when repulsion is large enough. This is the major difference from the above mentioned bulk case, where the translation Hamiltonian symmetry is broken by the crystallized state. For Wigner molecules, symmetries are preserved in the laboratory frame and one must consider an intrinsic (rotating) frame to notice the underlying deformation. A similar situation is found for particular states of two-electron atoms that have been much investigated in physical chemistry (we address the reader to the review paper [413]).

Although the exact ground-state wave function of the two-electron artificial atom can be obtained, at least numerically, it may seem paradoxical that one needs also the excited states in order to ascertain the existence of crystallization. In fact, this inability to disentangle in a clear way the system intrinsic structure from its full wave function can be taken as a weakness of the *ab initio*, symmetry preserving, approaches. In general, even in the cases where the exact ground- and excited-state wave functions and energies are known, an intrinsic deformation can only be inferred by comparing with the results for simpler models, in which either symmetries are relaxed or the intrinsic structure is imposed. A clear example of the former approach is given by the unrestricted HF method for the ground state [278, 378], followed by the random-phase approximation (RPA) for excitations [414]. On the contrary, the roto-vibrational model for two electrons [382, 383] could be included in the latter category.

One should be aware that when symmetries are relaxed, as in the Hartree-Fock approach, artifacts or non-physical properties may appear [415]. Therefore, a complete physical understanding requires both exact results and model solutions. In this way, the system intrinsic deformations are physically understood and, at the same time, artifacts can be safely discarded. As an example, the exact solutions, Hartree-Fock and RPA solutions were compared for two-electron $2D$ parabolic QD [382].

4.5.3 Roto-vibrational model

In order to trace the evolution of the spectra from weak to strong interaction and/or magnetic field, it is convenient to introduce two dimensionless parameters:

$$R_{mp} = \frac{k}{\ell_\Omega \hbar \Omega}, \quad W_{mp} = \frac{\omega_c}{\Omega}. \quad (4.47)$$

Here, $\Omega = \sqrt{\omega_0^2 + \omega_c^2/4}$, where $\omega_c = eB/m^*c$ is the cyclotron frequency, and the length $\ell_\Omega = \sqrt{\hbar/m^*\Omega}$ characterizes the effective lateral confinement. In the absence of a magnetic field, R_{mp} coincides with the Wigner parameter R_W (see Eq.(4.38), Sec. 4.4.2). Note also that W_{mp} has a maximal value $W_{mp} = 2$ that corresponds to a zero confinement $\omega_0 = 0$. With these dimensionless parameters, the Hamiltonian (4.1) transforms into

$$\mathcal{H} = \frac{H}{\hbar\Omega} = \sum_{i=1}^N \left[-\frac{1}{2} \nabla^2 + \frac{1}{2} r^2 + \frac{W_{mp}}{2} \ell_z \right]_i + R_{mp} \sum_{i>j=1}^N \frac{1}{r_{ij}} + \frac{g^* m^*}{2} W_{mp} S_z, \quad (4.48)$$

where $r \rightarrow r/\ell_\Omega$. Note that we use the effective electron-electron interaction, where the parameter R_{mp} is associated with the effective charge (a screening parameter), discussed in Sec. 4.4.3.

For the two-electron problem, introducing the standard center of mass (R, Θ) and relative (r, θ) coordinates, the Hamiltonian can be separated and, therefore, the wave function factorizes. The center of mass problem is that of a single particle in a harmonic potential and magnetic field, having an analytic solution in terms of the Fock-Darwin orbitals and energies (see Sec. 4.3.2). Focusing next on the relative problem, one introduces the wave function $e^{im\theta} u_{nm}(r)/\sqrt{r}$ having good ℓ_z angular momentum (m) and an additional quantum number n whose meaning will be clarified below. The equation for the unknown $u_{nm}(r)$ reads

$$u_{nm}'' + \left[\tilde{\varepsilon}_{nm}^{(rm)} - \left(\frac{1}{4} r^2 + \frac{R_{mp}}{r} + \frac{m^2 - 1/4}{r^2} \right) \right] u_{nm} = 0, \quad (4.49)$$

where we have defined $\tilde{\varepsilon}_{nm}^{(rm)} = \varepsilon_{nm}^{(rm)} - mW_{mp}/2$ in terms of the relative-motion energy $\varepsilon_{nm}^{(rm)}$ and the parameter W_{mp} .

The above Eq. (4.49) resembles a Schrödinger one-dimensional equation with an effective potential

$$V_{eff}(r) = \frac{1}{4} r^2 + \frac{R_{mp}}{r} + \frac{m^2 - 1/4}{r^2} \quad (4.50)$$

that includes the rotational motion term $\sim m^2/r^2$ characterized by the angular momentum quantum number m . We can expect a rigid-rotor behaviour if $V_{eff}(r)$ has a deep minimum at a particular value $r = r_0$. When this occurs, the situation resembles that of diatomic molecules like H_2 , where the potential well for nuclear motion is described by the Morse potential [416].

The minimization of $V_{eff}(r)$ yields the rotor radius from the equation

$$\frac{r_0}{2} - \frac{R_{mp}}{r_0^2} - \frac{2(m^2 - 1/4)}{r_0^3} = 0. \quad (4.51)$$

Neglecting the third contribution on the left-hand-side (the assumption that is valid for large enough r_0), one finds the asymptotic law $r_0 \approx (2R_{mp})^{1/3}$. Now, expanding up to second order of deviations around r_0 , we approximate

$$\begin{aligned} V_{eff}(r) &\approx V_{eff}(r_0) + \frac{1}{2} \left(\frac{3}{2} + 2 \frac{m^2 - 1/4}{r_0^4} \right) (r - r_0)^2 \\ &= \text{const.} + \frac{1}{2} k (r - r_0)^2. \end{aligned} \quad (4.52)$$

This result, after the substitution into Eq. (4.49), leads to the analytical prediction

$$\tilde{\varepsilon}_{nm}^{(rm)} = \frac{1}{4} r_0^2 + \frac{R_{mp}}{r_0} + \frac{m^2 - 1/4}{r_0^2} + \left(n + \frac{1}{2} \right) \sqrt{3 + 4 \frac{m^2 - 1/4}{r_0^4}}. \quad (4.53)$$

Equation (4.53) has a clear physical interpretation. It contains a rotor-like contribution, $\sim m^2/(2\mathfrak{I})$, with the moment of inertia given by $\mathfrak{I} = r_0^2/2$, and a vibrational contribution, characterized by the quantum number n . The vibrational frequency $\omega_{vib} = \sqrt{k/\mu}$ ($\mu = 1/2$) is given by the last square-root factor. Similarly to atomic molecules, there is a roto-vibrational coupling, since the vibration frequency depends on m , and also a centrifugal distortion, since r_0 also depends on m . For large enough values of R_{mp} , implying large r_0 and, therefore, small average densities, the centrifugal distortion disappears and one has $r_0 \approx (2R_{mp})^{1/3}$ for all m 's. In this limit, the rotational terms become negligible, as well as the roto-vibrational ones. Thus, Eq. (4.53) reduces to a simple m -independent asymptotic expression

$$\tilde{\varepsilon}_n^{(rm)} = \frac{3}{2^{4/3}} R_{mp}^{2/3} + \sqrt{3} \left(n + \frac{1}{2} \right). \quad (4.54)$$

Adding magnetic field transforms the roto-vibrational energy to

$$\begin{aligned} \varepsilon_{nm}^{(rm)} &= \tilde{\varepsilon}_{nm}^{(rm)} + mW_{mp}/2 \simeq \frac{(m + W_{mp}r_0^2/4)^2}{r_0^2} + \\ &+ \frac{R_{mp}}{r_0} + \left(n + \frac{1}{2} \right) \omega_{vib} - \left[\frac{r_0 W_{mp}}{4} \right]^2, \end{aligned} \quad (4.55)$$

in agreement with the expectations for two interacting electrons in a strong magnetic field [417].

The validity of the roto-vibrational model has been proved by the comparison with the exact results [382]. As a matter of fact, for $R_{mp} > 2$ the discrepancy for $\tilde{\varepsilon}_{00}$ is always below 2%, even with the asymptotic expression Eq. (4.54). The roto-vibrational model allows one to determine the crystallization onset from the criterion that the rotation and vibration motions decouple when intrinsic-frame electron localization sets in. On the contrary, when the coupling is strong, the system could be represented by either *a vibrating rotor* or *a rotating vibrator* and, therefore, the situation can not be clearly resolved. It is also worth stressing that the roto-vibrational model describes all possible excitations of the relative-motion problem. For this particular system, this amounts to a description of all excitations, since the center-of-mass and spin degrees of freedom can be analytically integrated out. Indeed, with $B = 0$ in the limit $r_0 \approx (2R_{mp})^{1/3}$, the model describes three basic excitations: (i) the Kohn mode ω_0 corresponding to the excitation

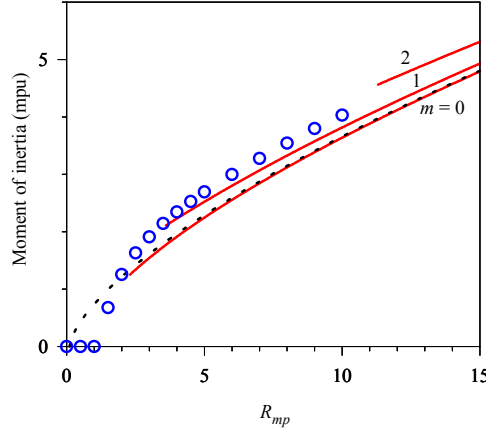


Figure 12: (Color online) Moment of inertia, computed in the RPA approximation (circles) at $W_{mp} = 0$, as a function of the dimensionless parameter R_{mp} . Solid lines show the evolution of the corresponding values in the analytical model of Sec.4.5.3 for different m -states. Each line starts at the crystallization onset for the corresponding angular momentum, according to the criterion $(\omega_{vib} - \sqrt{3})/\sqrt{3} > 0.01$. The dashed line represents the asymptotic value $\mathfrak{S} = r_0^2/2$ taking $r_0 \approx (2R_{mp})^{1/3}$, to which all solid lines converge at very high values of R_{mp} . From [414].

of the center-of-mass; (ii) the breathing mode with a frequency $\omega = \sqrt{3}$ corresponding to the vibration of the mean square radius; and (iii) the frequency $\omega = 0$ corresponding to the rotation of the circular system as a whole. These modes are excitations of classical electrons in a parabolic potential and are independent on N [418].

As will be discussed in Sec. 4.5.6, the RPA determines the moment of inertia associated with the collective rotation of a deformed HF structure. Fig. 12 presents the evolution, with R_{mp} , at $W_{mp} = 0$, of the RPA moment of inertia \mathfrak{S}_{RPA} (circles). For comparison, the values computed through the solution of Eq. (4.51) of the roto-vibrational model, $\mathfrak{S} = r_0^2/2$, are also shown (solid lines). Each \mathfrak{S} -line starts at the crystallization onset for the corresponding angular momentum. Note that \mathfrak{S}_{RPA} remains zero until the HF solution breaks the rotational symmetry at $R_{mp} \simeq 1$. After this, it reasonably agrees with the exact values, somehow averaging the exact results for different m . The molecule stretching, yielding larger r_0 (\mathfrak{S}), as m increases, is obviously outside RPA. All \mathfrak{S} values slowly converge to a common result with increasing R_{mp} , i.e., to an exact rigid-rotor behaviour.

4.5.4 Geometric transformation in a two-electron quantum dot

The roto-vibrational model demonstrates a transition from the circular to the deformed shape due to the effect of strong interaction and magnetic field in the 2D case. The question remains to answer about the contribution of the third dimension. In particular, how vibrational frequencies would evolve at a shape transition in the 3D case? These questions may shed light on the similarity and difference between shape transitions and, in general, quantum phase transitions (QPTs) in finite systems.

Quantum phase transitions in many-body systems, driven by quantum fluctuations at zero temperature, attract a considerable attention in recent years [419]. They are

recognized as abrupt changes of the ground state of a many-body system, with varying a non-thermal control parameter (magnetic field, pressure etc.) in the Hamiltonian of the system. Although the phases should be characterized by different types of quantum correlations on either side of a quantum critical point (actual transition point), in some cases they cannot be distinguished by any local order parameter. Particular examples are the integer and fractional quantum Hall liquids [420,421], which cannot be understood in terms of the traditional description of phases based on symmetry breaking and order parameters. Nowadays, there is a growing interest in using quantum entanglement measures for study such transitions [422] and, in general, quantum correlations in many-body systems [21,423]. Although finite systems can only show precursors of the QPT behaviour, they are also important for the development of the concept.

It was shown in Sec. 4.3.3 that at the value $\omega_L^{\text{sp}} = (\omega_z^2 - \omega_0^2)^{1/2}$ the magnetic field gives rise to the *spherical symmetry* ($\omega_z/\Omega = 1$) in the *axially-symmetric* two-electron QD (with $\omega_z > \omega_0$). A natural question arises how to detect such a transition looking on the *ground state density distribution* only. The related question is, if such a transition occurs, what are the concomitant structural changes?

To this end we employ the entanglement measure based on the linear entropy of reduced density matrices (cf [127])

$$\mathcal{E} = 1 - 2 \text{Tr}[\rho_r^{(orb)^2}] \text{Tr}[\rho_r^{(spin)^2}], \quad (4.56)$$

where $\rho_r^{(orb)}$ and $\rho_r^{(spin)}$ are the single-particle reduced density matrices in the orbital and spin spaces, respectively. This measure is quite popular for the analysis of the entanglement of two-fermion systems, in particular, for two electrons confined in the parabolic potential in the absence of the magnetic field [424–428]. Notice that the measure (4.56) vanishes when the global (pure) state describing the two electrons can be expressed as one single Slater determinant.

The trace $\text{Tr}[\rho_r^{(spin)^2}]$ of the two-electron spin states with a definite symmetry χ_{S,M_S} has two values: (i) 1/2 if $M_S = 0$ (anti-parallel spins of two electrons); (ii) 1 if $M_S = \pm 1$ (parallel spins). The condition $M_S = S$ (see Sec.4.3.2, Eq.(4.24)) yields $\text{Tr}[\rho_r^{(spin)^2}] = \frac{1}{2}(1 + |M_S|) = (3 - (-1)^m)/4$.

The trace of the orbital part

$$\text{Tr}[\rho_r^{(orb)^2}] = \int d\mathbf{r}_1 d\mathbf{r}_1' d\mathbf{r}_2 d\mathbf{r}_2' \psi(\mathbf{r}_1, \mathbf{r}_2) \psi^*(\mathbf{r}_1', \mathbf{r}_2) \psi^*(\mathbf{r}_1, \mathbf{r}_2') \psi(\mathbf{r}_1', \mathbf{r}_2') \quad (4.57)$$

is more involved. Indeed, in virtue of Eq. (4.23), it requires cumbersome calculations of eightfold sums of terms (integrals) obtained analytically [429]. The magnetic field dependence of the entanglement \mathcal{E} naturally occurs via inherent variability of the expansion coefficients.

We choose the value $R_W = 1.5$ (see Eq.(4.38), Sec.4.4.2) which corresponds for GaAs QDs to the confinement frequency $\hbar\omega_0 \approx 5.627$ meV. The linear entropy \mathcal{E} is calculated using the basis with $n_{\text{max}} = n_z^{\text{max}} = 4$, which gives $\sim 3.9 \times 10^5$ terms in Eq. (4.57).

At zero magnetic field ($\omega_L/\omega_0 = 0$) the entanglement of the lowest state with $m = 0$ decreases if the ratio ω_z/ω_0 decreases from ∞ (2D model) to 1 (spherically symmetric 3D model); see open symbols (diamonds) in Fig. 13(a). This effect could be explained

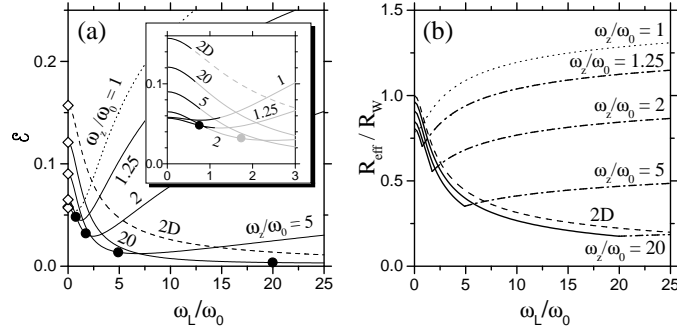


Figure 13: (a) The entanglement measure \mathcal{E} of the lowest state with $m = 0$ at $R_W = 1.5$ and various ratios ω_z/ω_0 as a function of the parameter ω_L/ω_0 . The initial (black) parts of the measure (shown in the inset) correspond to the intervals of ω_L/ω_0 , when the lowest state $m = 0$ is the ground state. Full circles denote the values of ω_L/ω_0 , when the effective 3D confinements become spherically symmetric. (b) The relative strengths of the Coulomb interaction $R_{\text{eff}}^{(2D)}/R_W$ (solid line) and $R_{\text{eff}}^{(1D)}/R_W$ (dash-dotted line) for the lowest state $m = 0$ at various ratios ω_z/ω_0 as functions of the parameter ω_L/ω_0 .

by introducing the effective charge k_{eff} , which determines the effective electron-electron interaction $V_C^{\text{eff}} = k_{\text{eff}}/\rho_{12}$ in the QD. (see Eq.(4.42), Sec.4.4.3). In a 3D dot the electrons can avoid each other more efficiently than in the 2D case. Consequently, the Coulomb interaction has a smaller effect, when $\omega_0 \approx \omega_z$ (the ratio $k_{\text{eff}}/k \approx 0.5$), than in the anisotropic case $\omega_0 \ll \omega_z$ ($k_{\text{eff}}/k = 1$). Therefore, a decreasing of the ratio ω_z/ω_0 yields the effect analogous to the reduction of the electron-electron interaction – a weaker mixing of the single-particle states and, consequently, the lowering of the entanglement.

By increasing the magnetic field from zero to $B_{\text{sph}} \sim \omega_L^{\text{sph}} = \sqrt{\omega_z^2 - \omega_0^2}$ (see full circles in Fig. 13(a)) the entanglement decreases. Similar to the case $B = 0$, one would expect the decrease of the effective electron-electron interaction with the evolution of the effective confinement from the disk shape ($\Omega < \omega_z$) to the spherical form ($\Omega = \omega_z$). Further increase of the magnetic field yields the increase of the entanglement. The effective confinement becomes again anisotropic (now with $\Omega > \omega_z$). Evidently, for $\omega_z/\omega_0 \rightarrow \infty$ (2D model) the minimum of \mathcal{E} is shifted to infinity, i.e. in this case the entanglement decreases monotonically with the increase of the field (dashed line in Fig. 13(a)).

The entanglement evolution can be explained by the influence of the magnetic field on the effective strength of the electron-electron interaction, which transforms the Wigner parameter R_W to the form $R_{mp} \equiv R_\Omega = l_\Omega/a^*$.

For the quasi-2D system ($\Omega \ll \omega_z$), the influence of magnetic field on the effective strength $R_\Omega \Rightarrow R_{\text{eff}}^{(2D)} = (k_{\text{eff}}^{(2D)}/l_\Omega)/\hbar\Omega$ is twofold. Here $k_{\text{eff}}^{(2D)}$ is determined by Eq.(4.44). The magnetic field affects the effective confinement $\hbar\Omega$ as well as the effective charge. With the increase of the effective confinement the effective charge $k_{\text{eff}}^{(2D)}/k \rightarrow 1$ and, therefore, the effective strength decreases as $R_{\text{eff}}^{(2D)} \sim 1/\sqrt{\Omega}$ (see Fig. 13(b)).

For $\Omega \gg \omega_z$ (very strong magnetic field) the electrons are pushed laterally towards the dot's center. The magnetic field, however, does not affect the vertical confinement. As a consequence the electrons practically move only in the z -direction, and the QD becomes a quasi-1D system. In this case the effective strength is $R_\Omega \Rightarrow R_{\text{eff}}^{(1D)} = (k_{\text{eff}}^{(1D)}/l_z)/\hbar\omega_z$.

Here the effective charge $k_{\text{eff}}^{(1D)} = \langle |z_{12}| V_C \rangle$, and $l_z \equiv z_m = \sqrt{\hbar/m^*\omega_z}$ is the oscillator length of the vertical confinement. For the lowest state with $m = 0$, it can be shown that $k_{\text{eff}}^{(1D)}/k = (1 + \sqrt{\omega_z/\Omega})^{-1}$. At a very strong magnetic field the ratio $k_{\text{eff}}^{(1D)}/k \rightarrow 1$, which yields the maximal value $R_{\text{eff}}^{(1D)} \sim 1/\sqrt{\omega_z}$.

When $\Omega = \omega_z$ the 3D system is far from both the 2D and the 1D limits. As a result, $R_{\text{eff}}^{(2D)}$ and $R_{\text{eff}}^{(1D)}$ do not match smoothly (see Fig. 13(b)). However, it is clear that the effective strength reaches the minimum around this point, i.e. when the transition from the lateral to the vertical localization of two electrons takes place.

In order to get a deeper insight into this transition we examine the probability density $|\psi(\mathbf{r}_{12})|^2$ for the ground state, when $m = 0$. Such a ground state can be realized for a near spherical QD with $\omega_z/\omega_0 = 1.25$. For this ratio and $R_W = 1.5$, the first S-T transition occurs at $\omega_L/\omega_0 \approx 1.11$ (see the inset in Fig. 13(a)). The onset of the spherical symmetry ($\Omega = \omega_z$) takes place at $\omega_L^{\text{sph}}/\omega_0 = 0.75$, i.e., in the ground state. For the magnetic field strengths $\omega_L < \omega_L^{\text{sph}}$, with $\Omega < \omega_z$, the density maximum forms a ring in the (x_{12}, y_{12}) -plane (a consequence of the axial symmetry). Fig. 14(a) shows the cut of this density with the (ρ_{12}, z_{12}) -plane at arbitrary azimuthal angle φ . For $\omega_L = \omega_L^{\text{sph}}$ the maximum of the probability density forms a spherical shell (visible if we rotate Fig. 14(b) around z_{12} -axis). For $\omega_L > \omega_L^{\text{sph}}$, with $\Omega > \omega_z$, two separate density maxima start to grow, located symmetrically in the z_{12} -axis (see Fig. 14(c)). In contrast to the corresponding behaviour of the entanglement, a fuzzy transition manifests itself in the probability density for the chosen dot parameters. In fact, the entanglement evolution guides us to trace a geometrical transition from the lateral to the vertical localization of the electrons.

The probability density evolution due to the magnetic field shown in Figs. 14(a-c) can be elucidated by means of the analysis of the effective potential

$$V_{\text{eff}} = \frac{1}{2} \mu (\Omega^2 \rho_{12}^2 + \omega_z^2 z_{12}^2) + k/r_{12} + \hbar^2 m^2 / (2\mu \rho_{12}^2). \quad (4.58)$$

Here, for the relative coordinate $\mathbf{r}_{12} = \mathbf{r}_1 - \mathbf{r}_2$, we introduce the following notations:

$$\rho_{12} = (x_{12}^2 + y_{12}^2)^{1/2}, \quad \varphi = \arctan(y_{12}/x_{12}), \quad r_{12} = (\rho_{12}^2 + z_{12}^2)^{1/2}. \quad (4.59)$$

The maxima of the probability density for the ground state are directly related to the minima of V_{eff} . For $\omega_L < \omega_L^{\text{sph}}$, the potential surface has the minimum at $\rho_{12} = \rho_0$, $z_{12} = 0$, where $\rho_0 = (k/\mu\Omega^2)^{1/3}$, if $m = 0$. By increasing the magnetic field to values $\omega_L > \omega_L^{\text{sph}}$, this minimum transforms to the saddle point in the (ρ_{12}, z_{12}) -plane, but two new minima divided by this saddle (potential barrier) appear. For $m = 0$, these minima are located at $z_{12} = \pm z_0$, where $z_0 = (k/\mu\omega_z^2)^{1/3}$.

For weakly anisotropic (near spherical) systems it is convenient to use the spherical coordinates $(r_{12}, \theta, \varphi)$, where the polar angle is $\theta \equiv \arctan(\rho_{12}/z_{12})$. In these coordinates the positions of the minima are $r_{12} = \rho_0$, $\theta = \pi/2$ for $\Omega < \omega_z$ and $r_{12} = z_0$, $\theta = 0, \pi$ for $\Omega > \omega_z$; see the cases $\omega_L/\omega_0 = 0$ and 1, respectively, in Fig. 14(d). Note, that due to the axial symmetry the azimuthal angle φ is arbitrary. The maximum at $\theta = \pi/2$ for $\Omega > \omega_z$ (the case $\omega_L/\omega_0 = 1$ in Fig. 14(d)) corresponds to the saddle point at $z_{12} = 0$.

Applying similar to the roto-vibrational model ideas (see Sec. 4.5.3), we consider small oscillations around a minimum of the effective potential. The effective potential can be written as the expansion up to the quadratic terms)

$$V_{\text{eff}} \approx V_0 + \frac{1}{2} \omega_1^2 q_1^2 + \frac{1}{2} \omega_2^2 q_2^2, \quad (4.60)$$

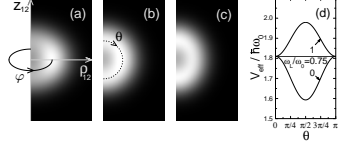


Figure 14: The ground state probability density (the relative motion part, $m = 0$) for the near-spherical ($\omega_z/\omega_0 = 1.25$) two-electron QD with $R_W = 1.5$ ($\hbar\omega_0 = 5.627$ meV) and $g^* = -0.44$ at different values of the magnetic field: (a) $\omega_L/\omega_0 = 0$, (b) $\omega_L/\omega_0 = 0.75$, (c) $\omega_L/\omega_0 = 1$. For the spherically symmetric case (b) the maximum of the probability density spreads uniformly over the spherical shell of a radius r_0 . The panel (d) displays the potential $V_{\text{eff}}(\rho_{12}, z_{12})$ on this sphere ($\rho_{12} = r_0 \sin \theta$, $z_{12} = r_0 \cos \theta$) for the cases (a-c).

where $q_1 = \Delta r$, $q_2 = r_0 \Delta \theta$ are the normal coordinates. Here $r_0 = \rho_0$, when $\Omega < \omega_z$, whereas $r_0 = z_0$, when $\Omega > \omega_z$. The corresponding normal frequencies (if $m = 0$) are: (i) $\omega_1 = \sqrt{3}\Omega$, $\omega_2 = (\omega_z^2 - \Omega^2)^{1/2}$ for $\Omega < \omega_z$; and (ii) $\omega_1 = \sqrt{3}\omega_z$, $\omega_2 = 2(\Omega^2 - \omega_z^2)^{1/2}$ for $\Omega > \omega_z$. For the spherically symmetric case ($\Omega = \omega_z$), one has $\omega_2 = 0$ and the minima of V_{eff} degenerate to the sphere of radius $r_0 = \rho_0 = z_0$. In other words, the potential V_{eff} becomes independent on the angle θ ; see the case $\omega_L/\omega_0 = 0.75$ in Fig. 14(d). As a consequence, the wave function becomes spherically symmetric (Fig. 14(b)). The quantum oscillations evolve in a way similar to those of quantum phase transitions studied for model systems [419].

Note that the considered geometric transformation in a two-electron quantum dot reminds, to some extent, the orientation transition of Sec. 2.3.3.

4.5.5 Shell structure and classical limit

Recently Maksym *et al.* [430] developed a model of a vertical QD and reproduced quite well experimental addition energies for $N = 2, 3, 4$. Although the three-dimensional nature of QDs is accounted for, the real calculations are based on the $2D$ parabolic potential. The authors constructed the effective two-dimensional electron-electron interaction (the screened Coulomb interaction) which does not depend on the magnetic field. They diagonalized the model Hamiltonian in the many-electron basis consisting of Slater determinants.

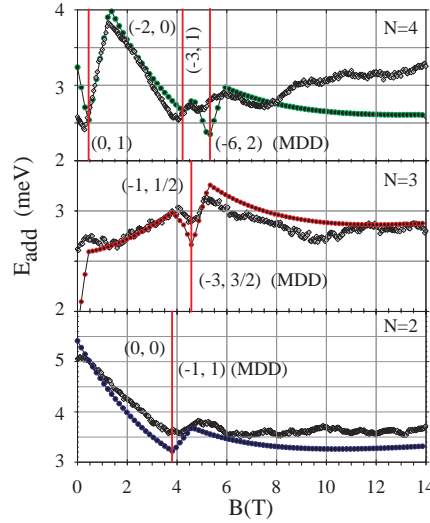


Figure 15: (Color online) Experimental and theoretical addition energies $E_{\text{add}}(N)$ for $N = 2, 3, 4$ as functions of the magnetic field B . Open diamonds correspond to experimental data [430]; full circle corresponds to the Hartree-Fock results. Ground states are labelled by (L_z, S_z) . The vertical line indicates the transition between different ground states. From [431].

Similar data were analyzed in a symmetry preserving Hartree-Fock approach [431]. The Hartree-Fock ground state is chosen as an eigenfunction of the z -component of the angular momentum L_z , the parity, and the spin. To compare with the results [430], the following parameters for InGaAs QDs have been used $\hbar\omega_0 = 4.5$ meV, $m^* = 0.0653$,

dielectric constant $\epsilon_r = 12.7$. These values provide for the strength of the bare Coulomb interaction the following estimate: $R_{mp}(\omega_c = 0) \equiv R_W \approx 1.56$. The effective value $R_W = 0.78$ is taken to reproduce the available experimental data.

For $N = 2$, it was found [431] that the singlet $(L_z, S_z) = (0, 0)$ state is replaced by fully polarized triplet $(-1, 1)$ state (MDD phase) at $B_{HF} = 3.8$ T (L_z and S_z are the quantum numbers of the z -component of the total orbital momentum and of the total spin, respectively). The experimental transition takes place at $B_{exp} = 4.2$ T, while the theoretical calculations of Maksym *et al.* [430] give $B_{theor} = 3.8$ T.

For $N = 3$, the HF calculations [431] predict that the state $(-1, 1/2)$ is the lowest state till $B_{HF} = 4.72$ T. Two electrons occupy the lowest available states with $m = 0$, but with different $S_z = \pm 1/2$ quantum numbers. The next available state is characterized by $m = -1$, and the largest possible value for this configuration has $S_z = 1/2$. At $B_{HF} = 4.72$ T, the onset of the MDD phase $(-3, 3/2)$ occurs.

At small magnetic field $B_{HF} < 0.46$ T, for $N = 4$ the ground state is $(0, 1)$ [431]. A partially polarized state is favourable due to the HF exchange term which supports the configuration with two aligned spins. At $B_{HF} = 0.46$ T ($B_{exp} = 0.33$ T, $B_{theor} = 0.3$ T), the magnetic field overcomes the exchange contribution and the HF calculations predict $(-2, 0)$ state. This state persists till $B_{HF} < 4.42$ T. At $B_{HF} = 4.42$ T ($B_{exp} = 4.06$ T, $B_{theor} = 4.0$ T), the magnetic field partially polarizes the system, and, with the aid of the exchange term, the HF calculations produce the ground state $(-3, 1)$. At $B_{HF} \geq 5.33$ T, the onset of the MDD phase $(-6, 2)$ takes place. At $B_{HF} = 14.31$ T, the MDD state is replaced by the ground state $(-10, 2)$.

The HF calculations [431] reproduced a double peak structure for $N = 3$ and $N = 4$ around 4–6 T. The spike, observed for $N = 3$ at $B_{HF} = 3.8$ T, is due to the transition to the MDD phase in the two-electron system. The following dip is caused by the transition from $(-1, 1/2)$ to $(-3, 3/2)$ for $N = 3$, while the transition from $(-2, 0)$ to $(-3, 1)$ for $N = 4$ changes only the slope of the former transition. The next spike, observed for $N = 3$ at $B_{HF} = 5.33$ T, is due to the transition $(-3, 1) \rightarrow (-6, 2)$ for $N = 4$. The large peak at $B_{HF} = 1.3$ T for $N = 4$ is due to the ground state transition $(-1, 1/2) \rightarrow (-4, 1/2)$ for $N = 5$ (not shown). The next transition for $N = 5$, that is, $(-4, 1/2) \rightarrow (-6, 3/2)$ at $B_{HF} = 4.80$ T, has a little effect. However, the transition to the MDD phase $(-6, 3/2) \rightarrow (-10, 5/2)$ for $N = 5$ is responsible for the small spike in the addition energy of $N = 4$ at $B_{HF} = 5.87$ T.

Although the agreement is good in general till $B_{exp} \leq 6$ T, there are some discrepancies at high magnetic field for $N = 4$ case (see Fig. 15). A similar problem appears in more sophisticated calculations of [430]. The analysis of finite-thickness effects in two-electron QDs reveals a magnetic-field dependence of the screening of the effective interaction [384]. The stronger the magnetic field, the lesser the expected screening effect in QDs. One of the possible reasons for this discrepancy is the change of the effective confining potential (the parabolic confinement frequency) at a high magnetic field. It follows from the calculations [431] that there is a visible suppression of the electron-electron interaction in the observed experimental data. Indeed, the experimental evidence [294] is that the QD has a high degree of a circular symmetry. We can conclude that, for this device, the electron dynamics is mainly due to the confining potential.

The origin of the magic values for the orbital momentum, which occur after the onset of the MDD phase for $N = 4$ ($L_z = 6, 10, 14, \dots$), can be understood from the symmetry

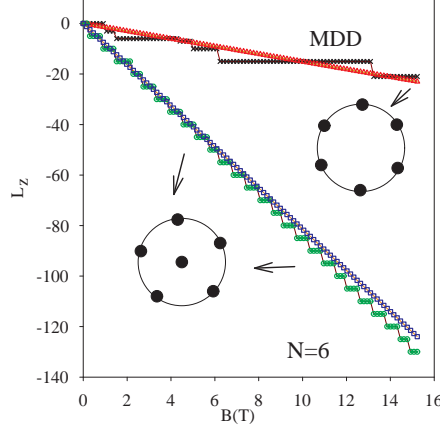


Figure 16: (Color online) The ground state orbital momentum for six electrons as a function of magnetic field. The symbols are: \times (black) corresponds to $R_W = 0.8$; open circle (green) corresponds to $R_W = 10$. In both cases the MDD phase has $L_z = 15$ (the longest plateau is for $R_W = 0.8$). For $R_W = 0.8(10)$, starting from the MDD phase, the ground state orbital momentum follows the sequence of magic numbers $L_z = 15, 21, \dots$ ($L_z = 15, 20, 25, \dots$). Open triangles correspond to the values of L_z from Eq. (4.63) for $R_W = 0.8(10)$. The equidistant points on the circles are associated with the equilibrium configurations at a given R_W . The equilibrium classical configurations are $N = 5 + 1$ ($R_W = 10$). From [431].

properties of the total wave function of a few-electron QD. The classical minimum-energy configuration of a few point charges in a parabolic potential is highly symmetric [432]. Such configurations takes place if N point charges create equidistant nodes on the ring, with the angle $\alpha = 2\pi/N$. It is reasonable to suppose that a quantum ground state is localized around the equilibrium classical state (see below). However, one has to take into account that the total wave function should be antisymmetric. Note that the rotation on the angle α is equivalent to a cyclic permutation of the particle coordinates on the ring. Since the spatial part of the total wave function Φ_r is the eigenstate of the L_z operator, one can require the fulfillment of the following symmetry condition [433]

$$R_z(\alpha)\Phi_r = \exp(i\frac{2\pi}{N}L_z)\Phi_r \equiv P_p\Phi_r = \varepsilon\Phi_r. \quad (4.61)$$

Here $\varepsilon = \pm$ is the parity of the permutation for the N point charges located on the ring. If the permutation is odd, then $\exp(i\frac{2\pi}{N}L_z)\Phi_r = -\Phi_r$, and the total orbital momentum takes the values $L_z = N(2k+1)/2$ ($k = 1, 2, \dots$). If the permutation is even, one has $\exp(i\frac{2\pi}{N}L_z)\Phi_r = \Phi_r$. As a result, the lowest quantum states carry the magic orbital momenta $L_z = Nk$ ($k = 1, 2, \dots$). The classical configuration ($R_W \gg 1$) for $N \geq 6$ contains a few rings [405–408]. In this case, the magic numbers can be determined by the number of electrons in the external or in the internal rings starting from the orbital momentum $L_z^{(MDD)}$ of the MDD phase. For nonzero magnetic field, this number must obey also the condition Eq. (4.63) (see below).

The total energy for Hamiltonian (4.1) can be written in the following form

$$E_N = \left\langle \sum_{i=1}^N \left[\frac{p_x^2 + p_y^2}{2m} + \frac{m}{2}(\omega_0^2 + \omega_L^2)r^2 + \omega_L \ell_z \right]_i \right\rangle + \langle V(r) + g^* \mu_B B S_z \rangle, \quad (4.62)$$

where $\omega_L = \omega_c/2$ and $\langle \dots \rangle$ means a mean field value. Note that the potential $V(r)$ depends only on the relative distance r between particles. For a nonzero magnetic field, there is a sequence of different energies for a fixed value of the total orbital momentum L_z . Using the Hellman-Feynman theorem, we have for the lowest equilibrium state, for a fixed value of the total orbital momentum L_z at a given magnetic field,

$$\left. \frac{\partial E_N}{\partial \omega_L} \right|_{L_z=L} = 0 \quad \Rightarrow \quad L_z = \left\langle \sum_{i=1}^N \ell_z \right\rangle = -m \omega_L \left\langle \sum_{i=1}^N r_i^2 \right\rangle = -\omega_L \mathfrak{S}. \quad (4.63)$$

With the moment of inertia $\mathfrak{S} \sim R_W^{2/3}$, one obtains an estimate for the optimal sequence of values of the ground state orbital momentum L_z at different values of the magnetic field (ω_L) and for different values of the Wigner parameter R_W (\mathfrak{S}) (see Fig. 16).

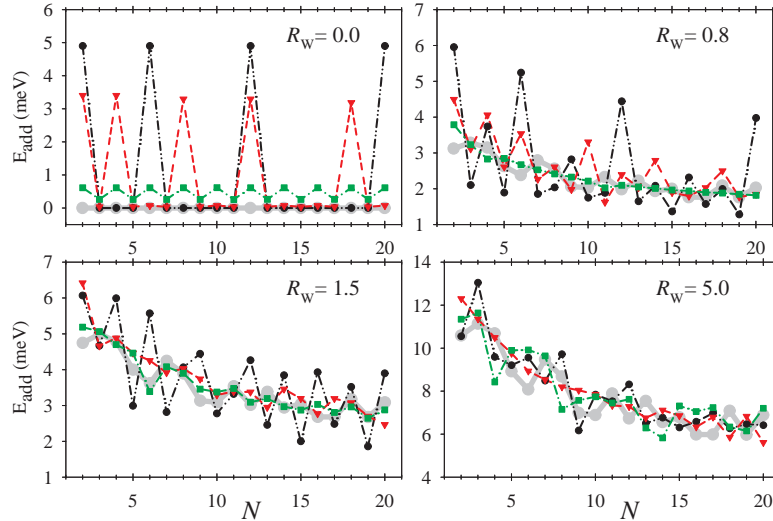


Figure 17: (Color online) Addition energy E_{add} as a function of the magnetic field B and the strength parameter R_W . The values of E_{add} , at different values of the magnetic field: dash-dotted-dash line connects the maxima of full circles for $B = 0$ T; dashed line connects the maxima of triangle-down for $B = 2$ T; dashed-dotted line connects the maxima of full squares for $B = 15$ T; a thick line displays the classical limit. From [431].

To trace the evolution of the shell structure, the addition energy for the QD up to $N = 20$ electrons at different values of the strength parameter R_W and the magnetic field B has been calculated [431](see Fig.17). With the increase of the interaction strength $R_W = 0.8$, the shell structure survives only without the magnetic field. The magnetic field compresses the energy gaps between energy levels forming the Hall liquid. At relatively large $R_W = 5$, one observes the onset of the classical limit (Thomson model) [432, 434]. We recall that the classical limit can also be reached at a high magnetic field but with

a relatively small R_W . In the classical limit at $B = 0$, the total energy (determined by Hamiltonian (4.48) without the kinetic term) for one-ring equilibrium configuration is

$$E_N = \frac{Na^2}{2} + \frac{R_W NS_N}{4a}, \quad S_N = \sum_{j=1}^{N-1} \frac{1}{\sin \frac{\pi j}{N}}, \quad (4.64)$$

where a is the equilibrium radius of the electrons equispaced on the ring. The equilibrium condition $dE_N/da = 0$ enables one to define a and to obtain finally

$$E_N^{cl} = (3/8)(2R_W S_N)^{2/3} N \hbar \omega_0. \quad (4.65)$$

While the quantum shell structure diminishes, one observes the onset of the *classical shell structure* (see Fig. 17) due to the optimal packing of electrons in various two-dimensional rings with $R_W \gg 1$. In the classical limit, one has, for example, the following sequences of rings: $N = 6 \Rightarrow (1, 5)$; $N = 10 \Rightarrow (2, 8)$; $N = 20 \Rightarrow (1, 7, 12)$ [432, 434]. A general expression for the classical energy with N electrons localized on a few rings can be found in [278].

4.5.6 Ground state in random phase approximation

As discussed above, for large enough values of the ratio R_W ($B = 0$) the HF field breaks the circular symmetry. The spontaneous symmetry breaking leads to a specific geometric distributions of electrons. In Fig. 18, the density for the $N = 6$ - and 12-electron QDs is displayed for $R_W = 1.89$. Both cases show a clear symmetry breaking; the $N = 6$ having the electrons localized on a ring while the 12-electron dot has a central electron dimer surrounded by a ring with 10 electrons.

The restoration of the broken symmetries can be attained via projection techniques [403, 404]. Examples demonstrating their use for the case of QDs have been recently presented by Yannouleas and Landman [278]. We shall focus our analysis on the RPA description of the ground state and its connection to the excited states.

We recall that it was proved by Thouless [435, 436] that, when the HF solution corresponds to a minimum on the energy surface, the RPA equations provide only real solutions. To solve the RPA eigenvalue problem for QDs, the quasi-boson approximation (QBA) developed in nuclear physics has been used [414]. Each particle-hole pair (mi) is considered as an elementary boson, i.e., $b_{mi}^\dagger = a_m^\dagger a_i$. A standard definition for the phonon (vibron) operator

$$O_\lambda^\dagger = \sum_{mi} \left(X_{mi}^{(\lambda)} a_m^\dagger a_i - Y_{mi}^{(\lambda)} a_i^\dagger a_m \right), \quad [O_{\lambda'}, O_\lambda^\dagger] = \delta_{\lambda', \lambda} \quad (4.66)$$

is used, whose action on the (yet unknown) ground state $|0\rangle$ yields the excited vibrational states $|\lambda\rangle = O_\lambda^\dagger |0\rangle$.

One can introduce the generalized momenta and coordinates related to the vibron modes [437]

$$\mathcal{P}_\lambda = -i\hbar \sqrt{\frac{M_\lambda \Omega_\lambda}{2\hbar}} (O_\lambda - O_\lambda^\dagger); \quad \mathcal{X}_\lambda = \sqrt{\frac{\hbar}{2M_\lambda \Omega_\lambda}} (O_\lambda + O_\lambda^\dagger), \quad (4.67)$$

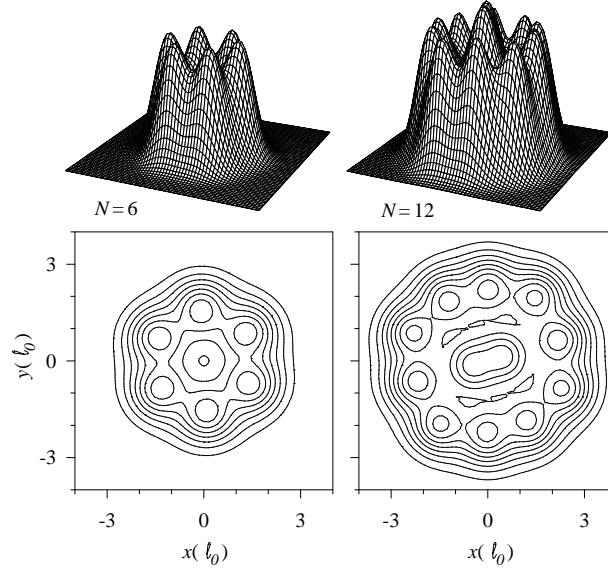


Figure 18: HF densities for the $N = 6$ - and 12 -electron QDs at $R_W = 1.89$. For clarity, the upper plots display a 3D view of the corresponding densities. Each line from the outermost contour line inwards corresponds, respectively, to a density of $0.05, 0.10, 0.15 \dots$, etc in units of ℓ_0^{-2} . From [414].

which fulfill the commutation relations for the conjugate momenta and coordinates. The number M_λ is a mass parameter which should be defined. The Hamiltonian, expressed in terms of the vibron operators, can be represented through the generalized momenta and coordinates

$$H_{RPA} = E_{HF} - \frac{1}{2} \text{Tr} A + \sum_{\lambda} \left(\frac{\mathcal{P}_{\lambda}^2}{2M_{\lambda}} + \frac{M_{\lambda}}{2} \Omega_{\lambda}^2 \mathcal{X}_{\lambda}^2 \right), \quad (4.68)$$

where the submatrix A is defined in [414]. The operators \mathcal{P}_{λ} , \mathcal{X}_{λ} , therefore, obey the equations of motion

$$[H_{RPA}, \mathcal{P}_{\lambda}] = i\hbar \Omega_{\lambda}^2 M_{\lambda} \mathcal{X}_{\lambda}; \quad [H_{RPA}, \mathcal{X}_{\lambda}] = -\frac{i\hbar}{M_{\lambda}} \mathcal{P}_{\lambda}. \quad (4.69)$$

To preserve the symmetry, broken in the mean field level and associated with a generator (a generalized momenta \mathcal{P}_0), one must require the fulfillment of the obvious condition:

$$[H_{RPA}, \mathcal{P}_0] = 0, \quad (4.70)$$

which determines a spurious (with zero energy) RPA solution (Nambu-Goldstone mode). The second equation (4.69) defines the mass parameter M_0 . In this case, Hamiltonian (4.68) transforms to the form

$$H_{RPA} = E_{RPA} + \sum_{\lambda > 0} \hbar \Omega_{\lambda} O_{\lambda}^{\dagger} O_{\lambda} + \frac{\mathcal{P}_0^2}{2M_0}, \quad (4.71)$$

where the third term describes a *collective mode* associated with the broken symmetry mean field solution in the *intrinsic frame*. The total energy in the RPA (E_{RPA}) can be split into the mean field contribution (E_{HF}) and a correction (Δ_{RPA}), as

$$E_{RPA} = E_{HF} - \Delta_{RPA}. \quad (4.72)$$

The RPA correction reads [403, 404]

$$\Delta_{\text{RPA}} = \sum_{\lambda>0} \hbar\Omega_{\lambda} \sum_{mi} |Y_{mi}^{\lambda}|^2 + \frac{\langle HF | \mathcal{P}_0^2 | HF \rangle}{2M_0} = \frac{1}{2} \left(\text{Tr} A - \sum_{\Omega_{\lambda}>0} \hbar\Omega_{\lambda} \right). \quad (4.73)$$

The above Eq. (4.73) includes the contribution from the vibrons at positive frequencies Ω_{λ} and, also, from the spurious mode. Note that Eq. (4.73) is the result of a partial cancellation between two large terms. In practice, this may cause Δ_{RPA} to converge rather slowly with a space dimension, especially for a large particle number. For example, in heavy nuclei, the number of the RPA eigenfrequencies is of order 10^4 and each of them should be determined with a high accuracy. This problem was reduced drastically by extending the RPA eigenvalues onto the complex plane [438]. Using this trick, one can express the RPA correlation Δ_{RPA} as the contour integral

$$\frac{1}{2} \left(\sum_{\Omega_{\lambda}>0} \hbar\Omega_{\lambda} - \text{Tr} A \right) = \frac{1}{4\pi i} \oint dz z \frac{\phi'(z)}{\phi(z)}. \quad (4.74)$$

Here $\phi(z) = F(z)/F_0(z)$. The analytical function $F(z)$ of the complex variable z is defined by the general RPA eigenvalue equation

$$F(z) = \det(H - z) = 0, \quad (4.75)$$

where H means the RPA matrix representation of the total Hamiltonian. The function $F_0(z) = \lim_{V \rightarrow 0} F(z)$ is defined by poles of the RPA problem (e.g., particle-hole excitations obtained from the HF solutions). The integration can be done numerically. The crucial practical advantage of the formula, Eq. (4.74), is that we are free to choose the rectangular contour sufficiently distant from the poles such that the spectral function

$$S(z) = \phi'(z)/\phi(z) \quad (4.76)$$

becomes a smooth integrand. Then, the necessary grid needs not be dense any more. In practical cases, considered for some nuclear models [438], the number of integration points were reduced by a factor 10^2 without loss of a precision which reduces the computational time drastically. The extension of this method for nonzero temperatures can be found in [439].

To treat the spurious mode related to rotation, it is convenient to introduce the canonical conjugate operators L_z and an *angle* operator Φ ; the latter being defined by the following relations [435–437]

$$[H, L_z] = 0, \quad [H, C] = \hbar L_z, \quad [L_z, C] = \hbar \mathfrak{I}_0, \quad (4.77)$$

where $C = i\mathfrak{I}_0\Phi$ is an anti-Hermitian operator and \mathfrak{I}_0 is the Thouless-Valatin moment of inertia [440]. The coefficients of the RPA operator

$$L_z = \sum_{mi} \left(\ell_{mi}^{(z)} b_{mi}^{\dagger} + \ell_{mi}^{(z)*} b_{mi} \right) \quad (4.78)$$

are directly given by the single-particle HF matrix elements. In contrast, for the operator

$$C = \sum_{mi} \left(c_{mi} b_{mi}^{\dagger} - c_{mi}^* b_{mi} \right), \quad (4.79)$$

one needs to solve the linear system of equations

$$\begin{pmatrix} A & B \\ B^* & A^* \end{pmatrix} \begin{pmatrix} c \\ c^* \end{pmatrix} = \hbar \begin{pmatrix} \ell^{(z)} \\ \ell^{(z)*} \end{pmatrix}, \quad (4.80)$$

where the sub-matrix B is defined in [414]. Once these two sets of coefficients are determined, the Thouless-Valatin moment of inertia \mathfrak{S}_0 may be calculated as

$$\mathfrak{S}_0 = \sum_{mi} \left(\ell_{mi}^{(z)*} c_{mi} + \ell_{mi}^{(z)} c_{mi}^* \right). \quad (4.81)$$

It was checked numerically [414] that the Thouless-Valatin moment of inertia coincides, with a good accuracy, with the value obtained from a constrained HF calculation for $\mathcal{R} = \mathcal{H} - \lambda L_z$ as

$$\mathcal{J}_0 = -\frac{d^2 \langle \mathcal{R} \rangle}{d\lambda^2} = \frac{d \langle L_z \rangle}{d\lambda}. \quad (4.82)$$

We stress that the equivalence between the two moments of inertia can be fulfilled *if and only if* a self-consistent HF minimum solution is found.

The operators L_z and C , together with the RPA phonons O_λ^\dagger , O_λ , form a complete set for any operator linear in the bosons b_{mi}^\dagger and b_{mi} . For an arbitrary one-particle-one-hole operator the expansion in terms of RPA excitations (for a single spurious mode) reads as

$$F = \sum_{\omega_\lambda > 0} \left([O_\lambda, F] O_\lambda^\dagger + [F, O_\lambda^\dagger] O_\lambda \right) + \frac{1}{\mathfrak{S}_0} ([F, C] L_z + [L_z, F] C). \quad (4.83)$$

Note that \mathfrak{S}_0 is nonzero only for the case in which the symmetry is broken by the HF solution. Otherwise, the second term in Eq. (4.83) vanishes identically (see also [403]).

In order to construct the RPA ground state for a circular-symmetric dot, two conditions are used [414]:

$$O_\lambda |0\rangle = 0, L_z |0\rangle = 0, \quad (4.84)$$

which insure the rotational invariance of the ground state. One looks for the solutions of the form

$$|0\rangle = N_0 e^{\mathcal{S}} |HF\rangle, \quad \mathcal{S} = \frac{1}{2} \sum_{minj} Z_{minj} b_{mi}^\dagger b_{nj}^\dagger, \quad (4.85)$$

with the \mathcal{S} operator involving the creation of two bosons [403]. Here N_0 is a normalization constant and the matrix Z_{minj} , in general, is complex and symmetric in the boson indices, i.e., $Z_{minj} = Z_{njmi}$. Using the general identity

$$F e^{\mathcal{S}} = e^{\mathcal{S}} \left(F + [F, \mathcal{S}] + \frac{1}{2} [[F, \mathcal{S}], \mathcal{S}] + \dots \right) \quad (4.86)$$

for the operators $F \equiv O_\lambda$ and $F \equiv L_z$, as well as the condition of rotational invariance, and the QBA, one finds

$$(F + [F, \mathcal{S}]) |HF\rangle = 0. \quad (4.87)$$

For the case of unbroken symmetry, the above requirement leads to the following equations for the Z_{minj} coefficients:

$$Y_{mi}^{(\lambda)*} = \sum_{nj} Z_{minj} X_{nj}^{(\lambda)*}. \quad (4.88)$$

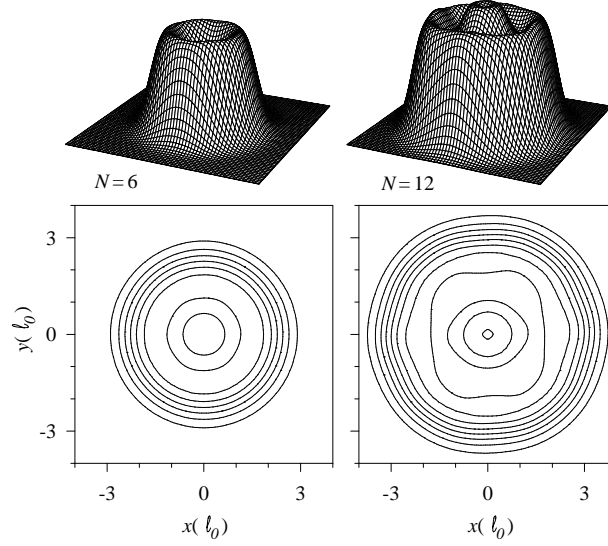


Figure 19: RPA symmetry restoration of the HF densities displayed in Fig. 18. From [414].

When the mean field breaks rotational symmetry, we have to complement the above system of equations for phonons, which are reduced to one equation, with the additional condition for the spurious mode

$$\ell_{mi}^{(z)} = - \sum_{nj} Z_{minj} \ell_{nj}^{(z)*}. \quad (4.89)$$

Finally, with the aid of these conditions and the expansion of the boson operators b_{mi}^\dagger in terms of phonons and spurious modes, Eq. (4.83), one obtains [414]:

$$\begin{aligned} \langle 0 | a_m^\dagger a_m | 0 \rangle &= \frac{1}{2} \sum_{i\lambda} |Y_{mi}^\lambda|^2 + \langle 0 | \Phi^2 | 0 \rangle \sum_i |\ell_{mi}^z|^2, \\ \langle 0 | a_i^\dagger a_i | 0 \rangle &= 1 - \frac{1}{2} \sum_{m\lambda} |Y_{mi}^\lambda|^2 + \langle 0 | \Phi^2 | 0 \rangle \sum_m |\ell_{mi}^z|^2. \end{aligned} \quad (4.90)$$

These equations generalize the result known in the literature [402] by introducing an additional term related to the canonical variables of the spurious mode $\{L_z, \Phi\}$. It should be noted that the factor 1/2 in Eqs. (4.90) is introduced following [441], where the occupation numbers were calculated using fermionic anticommutator rules, without referring to the QBA.

The above results were used to obtain the expectation value of any one-body operator, such as, e.g., the particle density

$$\hat{\rho}(\mathbf{r}) = \sum_{\alpha\beta} \rho_{\alpha\beta}(\mathbf{r}) a_\alpha^\dagger a_\beta, \quad \rho_{\alpha\beta}(\mathbf{r}) = \varphi_\alpha^*(\mathbf{r}) \varphi_\beta(\mathbf{r}),$$

where indexes α and β run over all the HF set of orbitals (with $\varphi_{\alpha(\beta)}$ being the HF wave functions).

An excellent restoration of the circular symmetry is obtained for the $N = 6$ dot (compare Figs. 18,19). For $N = 12$, the RPA density, though more circular than the HF

one, still has some residual deformation. This can be surely attributed to incompleteness of the RPA space considered in the numerical calculation. We emphasize that the circular symmetry can be restored within the RPA only if the contribution from the spurious mode is taken into account.

The mean field solutions, obtained within variational approaches, are related to the classical equilibrium points on the total energy surface of the full Hamiltonian [403]. Performing the RPA after the mean field treatment (mean field+RPA approach), one takes into account the quantized weak amplitude motion, not included into the static mean-field solution. The quantum fluctuations in finite systems lead not only to series of collective excitations, corresponding to rotations and vibrations, but also give rise to typical correlations in the ground state, which change its properties. Hence, the calculation of the RPA correlation energy is an important ingredient of a consistent description of the ground state properties of finite quantum systems within the mean field+RPA approach. Note that the correction Δ_{RPA} , with a minus sign, gives the standard correlation energy of the system. A decrease in the ground state energy ($\Delta_{\text{RPA}} > 0$) implies an improvement with respect to the mean field theory. However, since RPA is not based on the energy minimization, it is not bound to fulfill the variational principle and, therefore, E_{RPA} could be even lower than the exact energy. In other words, the correlation energy could be overestimated in RPA, as it has been suggested in literature [404]. We conclude that self-consistent mean field calculations, combined with the RPA analysis, could be useful to reveal structural changes in mesoscopic systems, allowing for the detection of quantum shape transitions. In the considered cases, the broken mean-field solution (the Wigner molecule) can be detected through the appearance of rotational states in a quantum spectrum of the dot.

5 Atomic Nuclei

5.1 Signatures of symmetry breaking in nuclear structure

The evolution of nuclear structure, with the change of proton (Z) and neutron (N) numbers, is one of the fundamental issues in nuclear physics [168,317,442]. The shell structure is one of the most important quantum features of nuclei. A remarkable stability, found in nuclei at magic numbers 2, 8, 20, 28, 50, 82, and 126, was a principal step in the development of the shell model, based on the inversion and rotational symmetries. The introduction of a spin-orbit splitting in the nuclear shell model was crucial to reproduce the nuclear magic numbers. The modern level of the nuclear shell model and the results which illustrate the global features of the approach are outlined in a review [443]. Recent progress in ion beam facilities provides the technical possibility of exploring nuclei with extreme proton-to-neutron ratios, far from the valley of stability. Experimental results on mass, nuclear radius, and spectroscopy, obtained in the last decade, indicate that location and magnitude of the shell gaps in the neighbourhood of the valley of stability may change, giving rise to new magic numbers; see, e.g., [444,445]. Evidently, the study of the nuclear shell gaps, far from the stable isotopes, provides a new impetus for the development of nuclear structure theory. In particular, it requires the development of new concepts and ideas on the properties of quasi-stationary open quantum systems. The possible extension of the shell model for the description of weakly bound nuclei can be

found in the review [446]. The recent status of experimental results, related to general trends in the evolution of shell closures with the increase of N/Z numbers, including nuclei far from stability lines, is discussed in the review [447]. Note, that the evolution of shell gaps of neutron rich nuclei is important for modelling the mass processing along the astrophysical rapid neutron capture pathway.

In finite systems such as quantum dots, metallic clusters and nuclei, the quantization of a system of fermions, moving in a common potential, leads to a bunching of levels in the single-particle spectrum, known as shells. When the levels of a bunch are filled, the system is stable; an additional particle fills a level in the next bunch at considerably higher energy and, therefore produces a less stable system. In stable nuclei, the shell effects are discerned by deviations of the binding energies from the smooth variation obtained from the liquid-drop model or as oscillations in the radial density distribution as a function of particle number and of deformation [317, 403]. Consequently, spherical symmetry leads to very strong shell effects manifested in the stability of the noble gases, nuclei and metallic clusters [168, 304]. When a spherical shell is only partially filled, breaking of spherical symmetry, resulting in an energy gain, can give rise to a deformed equilibrium shape.

Due to spin-orbit interaction between nucleons, neither spin nor orbital angular momentum are good quantum numbers. The experimental excitation spectra can be quite complex. However, the density of states near the ground state is low, and one can study discrete quantum levels by means of nuclear spectroscopy. These levels are characterized by good quantum numbers, such as the total angular momentum and parity I^π . For example, in even-even (N, Z are even) nuclei the ground state has positive parity and the total angular momentum $I^\pi = 0^+$. The study of the first low-lying states, with positive parity and angular momentum $I^\pi = 2^+$ and $I^\pi = 4^+$ with their ratio $R = E(4_1^+)/E(2_1^+)$ in various even-even nuclei, indicates the transition from spherical to deformed shapes, if one starts from a nucleus, that has all occupied shells in the framework of the nuclear shell model, towards that with a half filled next shell [317, 442]. Indeed, a remarkably simple phenomenology appears for these quantities (among other empirical observables on shape-phase transitions) discussed in terms of very simple models in a recent review [86]. For nuclei with either N or Z equal or close to the magic value, the ratio $R \approx 2.2 - 2.4$, which can be interpreted as a ratio between one and two-phonon states of a quadrupole harmonic vibrator with a spherical ground-state. For nuclei with both N and Z well away from magic numbers, $R \approx 3.33$, which corresponds to non-spherical deformed nuclei that rotate according to the eigenvalue expression for a quantum mechanical symmetric rotor $E \sim I(I+1)$. Although the excitation nuclear spectra are quite complex, experimentalists classified nuclear energy levels according to the intensity of electromagnetic transitions of low multipolarity ($E2, M1, E1, E3$), which establishes a link between the states of similar nature. In agreement with this procedure, the measured γ -transitions, according to their multipolarity and intensities, are arranged in rotational bands. In fact, a transparent signature of a broken spherical symmetry in a nucleus are the strongly enhanced electric quadrupole ($E2$) γ -transitions between $\Delta I = 2\hbar$ states of a rotational band. The reduced transition probabilities, $B(E2)$, are proportional to the square of the quadrupole moment, Q^2 . The larger the deformation, the stronger the $E2$ transitions between the rotational energy levels.

Nuclear rotation has features that are rather different from the rotation of molecules. The common practice in the analysis of the empirical data in terms of the rotational

frequency. The latter is defined by means of the classical canonical relation

$$\Omega = \frac{dE}{dJ} = \frac{E(I+1) - E(I-1)}{2}, \quad J = I - 1/2. \quad (5.1)$$

In these equations, one must associate the classical angular momentum J with the quantum value I for a given stretched quadrupole γ -transitions $\Delta I = 2$ [410]. Here, the term $1/2$ is a quantum correction that appears in the RPA; see discussion in [448, 449]. Two characteristics of the rotational band are used in nuclear structure, namely the kinematical $\mathfrak{S}^{(1)}$ and dynamical $\mathfrak{S}^{(2)}$ moments of inertia:

$$\mathfrak{S}^{(1)} = \frac{I}{\Omega}, \quad \mathfrak{S}^{(2)} = \frac{dI}{d\Omega} \approx \frac{4}{\Delta E_\gamma}. \quad (5.2)$$

Here, $\hbar\Omega = E_\gamma/2$, E_γ is the γ -transition energy between two neighbouring states that differ in two units of the angular momentum I , and ΔE_γ is the difference between two consecutive γ -transitions.

The moment of inertia $\mathfrak{S}^{(1)}$, extracted from the rotational band at low spin region, is essentially below that of a rigid rotor, but deviates from the value of a classical liquid drop of the same volume. It was one of the indications of pairing correlations in even-even nuclei noticed by Bohr *et al.* [450]. The empirically observed energy gap between the ground state and the first single-particle excitation in even-even nuclei was the other important fact indicating the importance of pairing correlations in low excited states of deformed nuclei [450, 451]. These facts led these authors to the conclusion on the similarity of the nuclear spectrum of even-even nucleus to that of the superconducting metal and on the existence of superfluidity in nuclei.

Rotational bands may terminate after a finite number of transitions [452]. It is accepted that the states with the lowest angular momentum, at a given excitation energies (called *yrast* states), are characterized by zero temperature. The sequence of these states is called the *yrast line*. A paradigm of structural changes in a nucleus under rotation is a *backbending*; the property that is exhibited by a sudden increase of a nuclear moment of inertia $\mathfrak{S}^{(1)}$ in the yrast rotational band at some critical angular momentum or rotational frequency [453] (see experimental results for ^{156}Dy and ^{162}Yb in Fig. 20). This phenomenon may be explained as a result of the rotational alignment of angular momenta of a nucleon pair occupying a high- j intruder orbital near the Fermi surface along the axis of collective rotation [456]. The alignment breaks the singlet Cooper pairing in the pair and decreases the superfluidity of a rotating nucleus. The effect of rotation is similar to the effect of magnetic field on a superconductor, as was noticed long ago [457].

While one observes a similar pattern for the backbending in the considered nuclei (see Fig. 20a,b), a different response of the nuclear field to rotation becomes more evident with the aid of the experimental dynamical moment of inertia $\mathfrak{S}^{(2)}$ as a function of the angular frequency (see Fig. 20 c, d). Indeed, the dynamical moment of inertia, due to the obvious relation

$$\mathfrak{S}^{(2)} = \mathfrak{S}^{(1)} + \Omega \frac{d\mathfrak{S}^{(1)}}{d\Omega}, \quad (5.3)$$

is very sensitive to structural changes of a nuclear field. At the transition point, $\mathfrak{S}^{(2)}$ wildly fluctuates with a huge amplitude in ^{156}Dy , whereas these fluctuation are quite

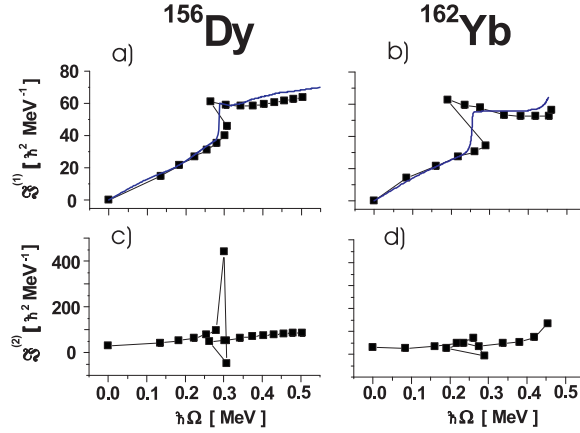


Figure 20: Rotational behaviour of the experimental, kinematical $\mathfrak{I}^{(1)}$ and dynamical $\mathfrak{I}^{(2)}$, moments of inertia. The experimental data denoted by black squares are taken from [454]. The experimental rotational frequency at the transition point is $\hbar\Omega_c \approx 0.27, 0.32$ MeV for ^{162}Yb and ^{156}Dy , respectively. The results of calculations for $\mathfrak{I}^{(1)}$ are connected by a solid line. From [455].

mild in ^{162}Yb . Continuing the analogy between the backbending and the behaviour of superconductors in a magnetic field, the dynamical moment of inertia is similar to a susceptibility of a sample. Its description poses a real challenge for the microscopic approaches.

The shell structure plays a prominent role in the formation of rotational nuclear states. It was suggested [458] that strongly deformed nuclei could occur because of the formation of a new shell structure. In 1986 Twin *et al.* [459] discovered a very regular pattern of closely spaced γ -transitions in the spectrum of ^{152}Dy between the spin levels ranging from $60\hbar$ to $24\hbar$. The moment of inertia $\mathfrak{I}^{(1)}$ of the associated rotational band was close to that of the axially symmetric rigid rotor with a 2 : 1 axis ratio. This nucleus was called superdeformed. Evidently, the high level density around the Fermi level corresponds to less stable system. Superdeformed rotating nuclei are among the most fascinating examples, where the deviation from the spherical shape are a consequence of strong shell closures giving rise to the largest level bunching, i.e., the largest degeneracy or the lowest level density around the Fermi level. The experimental results on superdeformed rotating nuclei are reviewed in [460, 461].

The discovery of superdeformed nuclei triggered the concept of pseudo- $SU(3)$ symmetry [462–464] to explain many features of superdeformed states described well by means of phenomenological nuclear potentials [465]. In the new scheme, the spin-orbit splitting appears to be very small and the properties of the single-particle spectrum are similar to those observed in 3D harmonic oscillator with rational ratios of frequencies [359, 466]. In this scheme, rotation stabilizes a very large quadrupole deformation and acts like a magnetic field in QDs, giving rise to new magic numbers (see Fig. 3 and the following discussion in terms of a simple shell model for QDs in Sec. 4.2.1).

Thanks to novel experimental detectors, a new frontier of discrete-line γ -spectroscopy at very high spins has been opened in the rare-earth nuclei; see, e.g., [467, 468] and references therein. These nuclei can accommodate the highest values of the angular mo-

mentum, providing one with various nuclear structure phenomena. The quest for the manifestations of non-axial deformation is one of the driving forces in the current high spin physics.

In recent years, rotational-like sequences of strongly enhanced $M1$ transitions between $\Delta I = 1\hbar$ states (as opposed to the strongly enhanced $E2$ transitions in the case, for example, of the superdeformed band) have been observed in spherical or near-spherical nuclei. The occurrence of regular, rotational-like band structures may be explained by an effective interaction between the excited high- j particles and holes [410]. The high- j particles and holes have energetically favourable alignments in the slightly deformed potential. A consecutive alignment of these two large vectors along the total angular momentum vector \mathbf{J} produces rotational-like band structure. Since this process resembles the closing of two blades of shears it was named a *shears mechanism*. The coupling of the proton-particle and neutron-hole orbitals, each with high spin j , results in a large transverse component of the magnetic moment vector, μ_{\perp} that rotates around the total angular momentum, I , and creates enhanced $M1$ transitions between the shears states. This type of excitation has been named *magnetic rotation* [410] to distinguish it from the well-known rotation of deformed nuclei. A summary of the experimental evidence for the shears mechanism and of a semi-empirical description of the observations was given in [469].

One of the most important features of the nuclear many-body system is that the nucleon density inside the nucleus is almost constant for the most stable nuclei, and so is the binding energy per nucleon. Therefore, it is a spatially and energetically saturated system with a relatively sharp boundary. In virtue of a constant density with a sharp boundary, a shape deformation can be chosen as a collective degree of freedom. In the geometrical approach [168], where the concept of shape deformation is one of the basic cornerstones, effects produced by quadrupole degrees of freedom are well understood for various effective potentials. The need for multipole deformations higher than the quadrupole has been recognized in numerous calculations in order to explain experimental data [409]. The hexadecapole deformation is essential for the understanding of equilibrium shapes and fission process in normal and super-deformed nuclei [409, 465]. In some nuclei, a transition to a pear-shaped (octupole) nuclear shape, that breaks reflection symmetry in the intrinsic reference frame, has also been found [470, 471]. Whether octupole degrees of freedom are of any importance and how they are manifested,—these questions stimulate a noticeable fraction of experimental efforts in high spin physics; see, e.g., [472, 473].

The presence of higher multipoles in the effective nuclear potential leads, however, to a non-integrable problem from the theoretical point of view. In fact, the single-particle motion turns out to be chaotic. Accordingly, in the transition from ordered to chaotic motion the quantum numbers lose their significance, and the system behaves like a viscous fluid in a container [474]. Therefore, the disappearance of the shell structure should be expected in the analogous quantum case [475, 476]. It was found, however, that shell structure can appear at strong octupole deformation [477–481]. In particular, it was shown that for the prolate systems there is a remarkable stability against chaos when the octupole deformation is switched on [479]. This result is in agreement with the fact that there are more prolate than oblate nuclei. The major conclusion of [480] is that, albeit nonintegrable, an octupole and hexadecapole admixtures to a quadrupole oscillator potential lead, for some values of the higher multipole strengths, to a shell structure

similar to a plain but more deformed quadrupole potential.

A transition from quadrupole deformed shapes (regular motion) to deformed shapes with higher multipoles (chaotic motion) can be traced by means of tools developed in the random matrix theory. An introduction into the basic concepts of random matrix theory and a survey of the extant experimental information, related to the manifestation of nuclear chaotic motion, can be found in the recent review [482]. A deep understanding of shell structure phenomena, in terms of classical trajectories, has been achieved by Balian and Bloch [483], based on the periodic orbit theory [476]. According to the semiclassical theory [476], the frequencies in the level density oscillations of single-particle spectra of finite quantum systems (nuclei, quantum dots, metallic clusters) are determined by the corresponding periods of classical closed orbits. The short periodic orbits give the major contribution to the gross shell structure [168, 484–486].

An important goal of nuclear structure physics is to understand these phenomena microscopically, when one deals with nucleon degrees of freedom and their interactions. However, the microscopic origin of a nuclear shell model still remains a major challenge. Collective model approaches, which express structure directly in terms of the many-body degrees of freedom, symmetries, and their associated quantum numbers, provide an invaluable help in the formulation of the basic elements of the microscopic approaches to many-body nuclear problem. In Sec. 5.2 we discuss the most popular theoretical approaches to symmetry breaking phenomena in nuclear structure. Sec. 5.3 reviews a few examples for the analysis of shape phase transitions in rotating nuclei within the cranking model+random phase approximation.

5.2 Nuclear structure models and symmetry breaking phenomena

Theoretical description of nuclear systems involves a number of simplifications to tackle a problem of interpreting nuclear structure from quark-gluon interactions. The analysis of experimental data related to ground and excited states of different nuclei, up to the excitation energies ~ 20 MeV above the yrast line with a maximal angular momentum $I \sim 60\hbar$, in all nuclear models, demonstrates that treating nuclei in terms of nucleons, moving in an effective potential, provides a reliable description. The non-relativistic treatment of nuclei seems to be rather well justified, if one compares the depth of the nuclear potential well $V \leq 60$ MeV with the nucleon mass $M \simeq 1000$ MeV. However, the relativistic nature of the nucleon motion can not be excluded from the consideration. Various versions of the relativistic models for nuclear structure calculations have been discussed in several reviews; see, e.g., [487–490]. Among many applications, we can mention the following studies related to the subject of the present review: (i) quantum phase transitions in the ground state in the region $Z = 60, 62, 64$, with $N \approx 90$ [491], and (ii) a thorough analysis of the time-odd mean fields (nuclear magnetism) in rotating nuclei [492].

5.2.1 Geometric Collective Model

The observation of rotational states in many nuclei led to models similar to those developed in molecular physics. The theoretical analysis of the rotational properties of many-particle systems requires the definition of the rotating reference frame (usually de-

noted as the “body-fixed frame” or, shortly, body frame). Note, however, that there is no unique choice for such a system and its definition should be based on the physical peculiarities of the problem.

Various choices of body frames were analyzed by Eckart [493,494] within the framework of the classical mechanics. Initially, Eckart proposed to use the body frame defined by the principal axes of the inertia tensor. He obtained the following expression for the rotational part of the kinetic energy

$$K_{rot} = \frac{\mathcal{J}_x L_x^2}{2(\mathcal{J}_y - \mathcal{J}_z)^2} + \frac{\mathcal{J}_y L_y^2}{2(\mathcal{J}_x - \mathcal{J}_z)^2} + \frac{\mathcal{J}_z L_z^2}{2(\mathcal{J}_x - \mathcal{J}_y)^2}, \quad (5.4)$$

where \mathcal{J}_k denotes the k -th principal moment of inertia. As is seen, this expression diverges when some moments of inertia coincide and it does not reproduce the kinetic energy of a rigid rotator. It means that the Coriolis couplings in the principal axes frame are not small for the small amplitude displacements of particles from their equilibrium positions. Thus, the principal axes frame is not suitable for the analysis of molecular vibrations.

Later, Eckart formulated the so-called “Eckart condition”, which demands that, in the body frame, the vector identity $\sum_{i=1}^N [\mathbf{r}_i \times \mathbf{r}_i^{(eq)}] = 0$ be fulfilled [494]. Here, the vector $\mathbf{r}_i^{(eq)}$ describes the equilibrium position of the i -th particle. Physically, this condition means that, under small vibrations, the components of the angular momentum in the body frame must be proportional to the amplitude of these vibrations. Explicit expressions for the basis vectors and the corresponding roto-vibrational decomposition of the Hamiltonian for the Eckart frame were recently derived in [495,496]. It was demonstrated that, under small vibrations, the Coriolis part of the kinetic energy, corresponding to the Eckart frame, is also small [496].

Eckart frame is widely used in molecular physics. Its application to the problems of nuclear physics is limited by the observation that a nucleus physically is more similar to a liquid drop than to a rigid body. It is interesting that, since the quantum liquid drop, with some equal moments of inertia, cannot rotate around the remaining axis, the divergences of the rotational energy (5.4) vanish for the liquid drop model. Therefore, the principal axes frame can be efficiently used to describe the rotational motion of physical systems modelled by a quantum liquid. For example, this can be the case when trapped atoms are considered. For QDs, in the “Wigner crystallization” regime, the use of the Eckart frame can be more adequate. Various aspects of molecular description of QDs in the Eckart frame can be found in the review [276].

Theoretical studies of nuclear shape transitions are typically based on the macroscopic geometric collective model introduced by Bohr [497]. In this model, the nucleus is considered as a droplet and the nuclear shape is parametrized in terms of the multipole expansion of the nuclear radius into spherical harmonics $R = R_0(1 + \sum_{\lambda\mu} \alpha_{\lambda\mu} Y_{\lambda\mu})$. Because of the assumption that the dominant nuclear deformation is the quadrupole one $\lambda = 2$, the Bohr Hamiltonian is parametrized in terms of two quadrupole deformation parameters β and γ : $\alpha_{20} = \beta \cos \gamma$, $\alpha_{21} = \alpha_{2-1} = 0$, $\alpha_{22} = \alpha_{2-2} = -\beta \sin \gamma$ [168,317]. These parameters describe the nuclear shape in the intrinsic (body-fixed) frame connected with the principal axes of the quadrupole tensor. The dependence on the Euler angles $(\theta_1, \theta_2, \theta_3)$, which describe the orientation of a nucleus in a laboratory frame, is eliminated. Due to the symmetries of the above equations, it is sufficient to consider the sector

$\beta \geq 0$, $0^\circ \leq \gamma \leq 60^\circ$ only. Prolate and oblate shapes correspond to $\gamma = 0^\circ$ and 60° , respectively. The other values of γ describe the triaxial shapes (see Fig. 21).

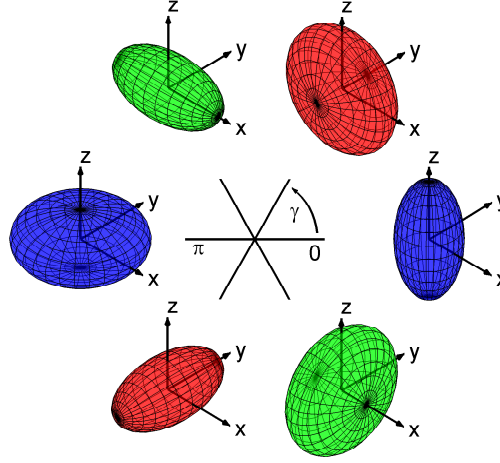


Figure 21: (Color online) Quadrupole shapes in the geometric model. The spherical symmetry is at the center, while axially symmetric prolate and oblate shapes are obtained along the various axes. A genuine triaxial quadrupole deformation occurs between different axes. Adapted from [481].

In this model the shape phase transitions can be related to the concept of critical-point symmetries that provide parameter-independent predictions for excitation spectra and electromagnetic transition rates for nuclei at the phase transition point; see details in [86].

5.2.2 Algebraic approach: Interaction Boson Model

In the so-called interacting boson approximation, proposed by Arima and Iachello [498–500], collective excitations of nuclei are described in terms of bosons, which are associated with pairs of valence fermions. To describe the quadrupole collectivity in nuclei, one needs to consider a five-dimensional space. Although this problem can be formulated in terms of boson variables [501], it is nonlinear in terms of quadrupole bosons. By considering the boson number as an additional degree of freedom, the Interaction Boson Model (IBM) [502] introduces a scalar boson as a dynamical variable. This leads to the subsequent realization [503] of s and d bosons as pairs of nucleons coupled to the angular momentum $\lambda = 0^+$ and $\lambda = 2^+$, respectively.

The finiteness of the boson number is based on the supposition that each d -boson is a boson image of a quadrupole nucleon pair occupying the levels of the valence shell in a given nucleus. Therefore, the d -boson number can not exceed the half of the number of the valence nucleons or holes. In the IBM, however, the total number of bosons N_b is taken as a parameter. Due to this fact, the IBM can be easily extended to thermodynamical limit $N_b \rightarrow \infty$ to study nuclear shape phase transitions at zero temperature [86]. The model naturally incorporates different symmetry limits associated with specific nuclear properties: different shapes coincide with particular dynamical symmetries of some algebraic structure [504]. For example, the rotational limit of this model is associated with

$SU(3)$ symmetry of axially symmetric rotor, while the vibrational limit is associated with $U(5)$ symmetry.

The geometric model and the IBM can be related by using the coherent state formalism [505, 506]. The evaluation of the expectation value of the algebraic Hamiltonian in the coherent state allows one to establish a correspondence between the symmetry limits of the IBM and collective shape variables of the Bohr Hamiltonian.

The IBM does not, however, take into account the interplay between single-particle and collective degrees of freedom in even-even nuclei. Evidently, the shell effects are beyond the framework of the model, though they may be crucial for the study of quantum phase transitions in rotating nuclei, where static and dynamical properties are coupled. Recent review on various aspects of the IBM and the role of dynamical symmetries, which yield benchmarks of nuclear shapes of the ground state, can be found in [86].

5.2.3 Microscopic models with effective interactions

The *ab initio* non-relativistic models attempt to reproduce the basic features of nuclear properties with the aid of an effective free nucleon-nucleon interaction, which describes the nucleon-nucleon scattering data [507]. This approach is, however, limited to very light nuclei. Similar to trapped atoms and QDs, the nuclear many-body problem for heavy nuclei is attacked in the mean field approach; see, e.g., review articles [409, 508, 509]. In the nuclear shell model (SM), one usually starts with a phenomenological single-particle model, defines a valence space (inert core, active shells), and, with the aid of the residual interaction, performs configuration-mixing calculations [510]. The concept of the isospin symmetry for proton and neutron plays an important role in the nuclear structure. However, the first obvious difference between these particles arises due to the electric charge of a proton. The analysis of the data for nuclei with $N = Z$ may shed light on the evolution of nuclear structure due to the isospin symmetry breaking under excitation. The use of the SM to study experimental data, related to the isospin symmetry breaking effects of different origins, in the region of nuclei between $A \sim 30$ and $A \sim 60$ with increasing energy and angular momentum, is reviewed in [511]. Recent development of the SM, in which a two-body effective interaction between valence nucleons is derived from the free nucleon-nucleon potential, is outlined in [443, 512]. The drastic increase of the configuration space for medium and heavy systems makes, however, the shell-model calculations extremely difficult if not almost impossible in a nearest future. In addition, one needs to invoke some model considerations to interpret the SM results.

Nowadays, the concept, closely related to the density functional theory in electronic systems, is popular in nuclear structure calculations [509]. In this approach, one proceeds from an energy functional, motivated from *ab initio* theory, but with the actual parameters adjusted by fits to nuclear structure data. Mean-field calculations with effective density-dependent nuclear interactions, such as Gogny or Skyrme forces, or a relativistic mean-field approach, still do not provide sufficiently accurate single-particle spectra for a reliable description of experimental characteristics of low-lying states [513]. The RPA analysis based on such mean-field solutions is focused only on the description of various giant resonances in non-rotating nuclei, when the accuracy of single-particle spectra near the Fermi level is not important; see, e.g., [514–517]. Furthermore, a practical application of the RPA for the non-separable effective forces in rotating nuclei requires a too large

configuration space and is in its infancy. The discussion of open problems of the nuclear density functional theory can be found, e.g., in [518–520]. The difficulties in using the density functional theory, discussed in Sec. 4.3 for QDs, as well as the above discussion, raise fundamental issues on the principles of foundation for this approach to many-body problem of *finite* systems. A few approaches to the non-relativistic density functional theory for nuclei, based on a microscopic nuclear Hamiltonian that describes two-nucleon and few-body scattering and bound observables, in analogy to calculations in quantum chemistry for Coulomb systems, are reviewed in [521].

5.2.4 Cranking approach

To elucidate the similarities and differences between nuclei and already discussed finite systems, trapped atoms and QDs, it is convenient to consider a similar physical situation. Rotation, being one of the simplest collective motions in many body systems, is a unique phenomenon which enables one to understand the general and specific features of the systems addressed in this review. Therefore, we will discuss, with a few exceptions, the properties of an even-even medium and heavy nuclei at high angular momenta, when the nucleon motion can be substantially modified by inertial forces. Indeed, in high spin experiments, various symmetry breaking effects are exemplified most clearly by rotation. On the other hand, this permits a semiclassical mean-field description of nuclear rotation within the *cranking model* (CM) introduced by Inglis [522, 523]. In the CM, for a given many-body Hamiltonian $\mathcal{H} = T + V$, one defines the Routhian operator \mathcal{R} as

$$\mathcal{R} \equiv \mathcal{H} - \vec{\Omega} \vec{J}. \quad (5.5)$$

In this model, nucleons move in an external field of single-body nature, with a constant angular frequency $|\Omega|$. One can readily recognize that the Routhian (5.5) is the Hamiltonian (3.72) used for the description of vortices created by rotation of Bose-condensed trapped atoms.

In order to justify the CM, Thouless and Valatin [440] considered the time-dependent Hartree-Fock solutions defined by the equation

$$i\partial\hat{\rho}/\partial t = [\mathcal{R}, \hat{\rho}] \quad (5.6)$$

in the intrinsic frame. The moment-of-inertia tensor \mathfrak{I} defines the principal axes of the frame of reference:

$$\langle \hat{J}_i \rangle = Tr \hat{J}_i \hat{\rho} = \mathfrak{I}_i^{(1)} \Omega_i \quad (i = 1, 2, 3), \quad (5.7)$$

where $\mathfrak{I}_1^{(1)}, \mathfrak{I}_2^{(1)}, \mathfrak{I}_3^{(1)}$ are the principal kinematical moments of inertia. They have shown that the change in the average angular momentum components in the body-fixed frame obeys the classical equation of motion

$$d\langle \vec{J} \rangle / dt = \langle \vec{J} \times \vec{\Omega} \rangle. \quad (5.8)$$

For the stationary rotation

$$d\langle \vec{J} \rangle / dt = 0, \quad (5.9)$$

one obtains the principal axis rotation. It is usually assumed that at $\Omega = 0$, the symmetry axis is the z -axis. In the case of an axial symmetry (for example, $\mathfrak{I}_1^{(1)} = \mathfrak{I}_2^{(1)}$), the CM

describes the uniform rotation about an axis perpendicular to the symmetry axis. Within the CM, one has to minimize the energy

$$R(\Omega) = \langle \Phi | \mathcal{R} | \Phi \rangle \quad (5.10)$$

to obtain the yrast state, where $|\Phi\rangle$ is a Slater determinant. The angular momentum is defined according to the semiclassical quantization

$$J(\Omega) = \langle \Phi | \hat{J}_x | \Phi \rangle . \quad (5.11)$$

The total energy, as a function of the angular momentum, is

$$E(J) = R(\Omega) + \Omega J(\Omega) . \quad (5.12)$$

Additional quantum correlations can be incorporated into the CM by means of the RPA, which describes small oscillations about the mean field of a rotating nucleus. As is demonstrated in Sec. 4.5.6, the RPA, being an efficient tool to study these quantum fluctuations (vibrational and rotational excitations), also provides a consistent way for treating broken symmetries. Moreover, it separates collective excitations, associated with each broken symmetry, as the spurious RPA modes, and fixes the corresponding inertial parameter. The alternative approach to treating broken symmetries is based on the projection technique presented in the textbooks [403, 404]. All pros and cons of this approach for the description of high spin states are discussed in the reviews [410, 411]. More technical details and recent progress in the application of variational calculations, based on the projection techniques, are reviewed in [524].

During many years, various refined prescriptions have been adopted to obtain an effective mean-field potential. It appears, however, that it closely resembles a Woods-Saxon shape, that is, a rounded square well that asymptotically goes to zero at a distance of a few femtometers [442]. This potential supplemented by a spin-orbit interaction, nicely reproduces the famous magic numbers. Inclusion of pairing correlations allows one to trace a transition from the paired phase to a rigid body rotation. A harmonic oscillator potential, supplemented by a spin-orbit interaction and l^2 to mimic the surface effect of the nuclear mean-field potential (a Nilsson potential), serves as another labor horse for the analysis of nuclear structure effects at high spins. These potentials allow one to construct also a self-consistent residual interaction, neglected on the mean-field level. The RPA, with a separable multipole-multipole interaction based on these phenomenological potentials, is an effective tool to study low-lying collective excitations at high spins [525, 526]. In fact, most issues addressed in this review can be understood in the framework of the CM, using either a three-dimensional harmonic oscillator or the Nilsson potential. In order to keep the presentation simple and transparent, we use both these models as an effective nuclear mean field.

Although the CM can be formulated in a self-consistent way (see, e.g., [508]), the simplest, but the most efficient version of the CM, consists in the combination of the Strutinsky's shell correction method [527] to account for nuclear shell structure and a rotating liquid drop model to describe bulk properties of nuclear matter [317]:

$$E(\alpha, I) = E_{LDM}(\alpha, I) + \delta E_{shell}(\alpha, I) . \quad (5.13)$$

Here the quantum shell correction energy,

$$\delta E_{shell} = \sum_{occ} \varepsilon_i - \tilde{E}_{shell} , \quad (5.14)$$

and \tilde{E}_{shell} is the smooth Strutinsky energy. The single-particle energies ε_i are produced by a phenomenological nuclear potential, like Nilsson or Woods-Saxon ones, with or without pairing interaction. E_{LDM} is the deformation energy of the rotating liquid drop with rigid-body moments of inertia, and $\{\alpha\}$ is a set of deformation parameters which can be found from the minimization of the energy functional $E(\alpha, I)$. This approach has been, over many years, a powerful tool for analyzing and interpreting experimental data of high spin states. The most exciting example is the prediction of the formation of the superdeformed high-spin states [528, 529], which have been discovered by Twin *et al.* [459].

In this review we discuss typical, or representative, results, since it is impossible to review all developments related to symmetry breaking phenomena in high spin physics. To keep the discussion simple and transparent, we will also use the results obtained in a fully self-consistent and analytically solvable model [530–533].

The early development of high spin nuclear physics and a mean-field description of nuclear rotation within the *cranking model*, can be found in the books [317, 403, 534]. The experimental data and theoretical interpretation for the properties of pear shaped rotating nuclei are discussed in [471]. The uniform rotation about an axis tilted with respect to the principal axes of the density distribution, magnetic rotation, and band termination is reviewed in [410]. The experimental properties of the $M1$ bands, observed in near-spherical nuclei, and the theoretical approaches, that have lead to the understanding of the magnetic rotation, are outlined in [535]. The progress in the development of the mean field description of high-spin states is discussed in [411]. The basic ideas of the cranking mean field+RPA (CRPA) approach are outlined in [525]. The overview of pair correlations at high spins is given in [536].

5.3 Symmetry breaking in rotating nuclei

5.3.1 Symmetries

For the main part of this review we assume that the Routhian (5.5) is invariant with respect to space inversion \hat{P} . In this case, the parity π is a good quantum number:

$$\hat{P}|\Phi\rangle = \pi|\Phi\rangle , \quad (5.15)$$

and the rotational bands are characterized by a fixed parity π . The spin-sequences in the rotational bands indicate broken/conserved symmetries. In particular, the sequence of rotational levels I^π , $(I+2)^\pi$...of a given parity is associated with a principal axis rotation (broken rotational symmetry), but with the preserved symmetry, called a *signature* $r = \pm 1$, for the system with even and $\pm i$, for the system with odd particle number [168]. Indeed, for even-even nuclei, the cranking Hamiltonian (5.5) adheres to the D_2 spatial symmetry with respect to the rotation by the angle π around the rotational axis x , i.e.,

$$[H - \Omega \hat{J}_x, \hat{R}_x] = 0, \quad \hat{R}_x = \exp(-i\pi \hat{J}_x) . \quad (5.16)$$

On the other hand, the internal CM wave function is subject to the condition

$$\hat{R}_x|\Phi\rangle = \exp(-i\pi J)|\Phi\rangle = \exp[-i\pi(I - 1/2)]|\Phi\rangle = i \exp(-i\pi I)|\Phi\rangle = ri|\Phi\rangle. \quad (5.17)$$

Another definition of signature $\alpha = 0, 1$ [410] is connected with the r via the relation $r = \exp(-i\pi\alpha)$. Consequently, all rotational states can be classified by the quantum number signature $r = \exp(-i\pi\alpha)$ leading to the selection rules for the total angular momentum $I = \alpha + 2n$, $n = 0, \pm 1, \pm 2 \dots$ and $\alpha = 0, 1$. In particular, in even-even nuclei, the yrast band, characterized by the positive signature quantum number $r = +1$ ($\alpha = 0$), consists of even spins only. The members of the rotational bands, with the conserved signature, are connected via strong, stretched $E2$ γ -transitions.

The observation of parity doublets is associated with the parity violation in the intrinsic frame [537]. For a uniform rotation around the principal axis x , the parity \hat{P} and signature \hat{R}_x are broken. However, the conservation of the simplex quantum number $\hat{S}_x = \hat{P}\hat{R}_x^{-1}$ [538–540] leads to the alternating parity $\pi = (-1)^I$ of the bands $I^+, (I+1)^-, (I+2)^+, \dots$ connected by enhanced $E1$ γ -transitions.

The classification of rotational states, with respect to discrete symmetries, such as parity, signature, and $\hat{T}\hat{R}_y(\pi)$ operations (\hat{T} is the time reverse operation) for the Hamiltonian $H - \Omega J_z$, is discussed thoroughly in [410]. These symmetries are the special cases of the complete scheme which classifies the mean field solutions in accordance to time-reversal symmetry \hat{T} , spatial $\hat{R}_i(\pi)$, and $\hat{T}\hat{R}_i(\pi)$ ($i = x, y, z$) symmetries [541, 542].

5.3.2 Shape transitions in rotating nuclei

Nuclei are finite systems and phase transitions should be washed out by quantum fluctuations. Nevertheless, long ago Thouless [435] proposed to distinguish two kinds of "phase transitions" even for nuclei. Such phase transitions may be connected with shape transitions, for example, from spherical to deformed or from axially deformed to nonaxially deformed shapes. This idea was put ahead in the analysis of shape transitions in hot rotating nuclei, based on the cranking+Nilsson model [543]. In this case the statistical treatment of the finite-temperature mean-field description had provided a justification for an application of the Landau theory for nuclei [544]. Within this approach, simple rules for different shape-phase transitions, induced by the variation of angular momentum and temperature, were found [544, 545].

With the increase of excitation energy, macroscopic effects, i.e., the liquid drop part, dominates in the evolution process, in particular, in the changes of the parameters of the effective mean field. Typical excitation energies of compound states, populated in heavy-ion reactions, are of the order of 20-30 MeV. Thus, the shell effects cannot influence the equilibrium deformation of such states. The γ - decay mode of the de-excitation process becomes prevalent when the excitation energy, measured from the yrast line, decreases to about 7-10 MeV. According to calculations [543], this region of excitations is characterized by large fluctuations of the shape. This facilitates quadrupole transitions from such states, that is, the de-excitation, which carries away the angular momentum and leaves nuclei above the yrast line. And only when the excitation energy is reduced to about 5 MeV above the yrast line, the evolution of the nuclear shape starts to follow the valleys in the shell component of the deformation potential energy. At this stage, the emergence of shell irregularities of the single-particle spectrum is essential for the description of all

physical phenomena. The effect of shell structure could be seen quite clearly even in the region of giant resonances ($\sim 10 - 20$ MeV; see for a recent review [546]). The shape of the photo-absorption cross section of the giant dipole resonance strongly depends on the type of symmetry of the rotating effective mean field, discussed for the first time in [547, 548]. The experimental results and the role of shell effects for giant dipole resonances in hot rotating nuclei can be found, for example, in [549–551].

Quantum phase transitions, that occur at zero temperature when varying some non-thermal control parameters, attract a considerable attention in recent years. The concept of a quantum phase transition refers to a sudden change in the structure of the ground state, as a result of varying a parameter. Since thermal fluctuations are absent, the sole cause, responsible for the sudden changes, are quantum fluctuations. The study of such transitions has been initiated in condensed matter physics in order to understand the properties of low-dimensional systems [419] and quantum behaviour in a variety of materials at critical points [26]. In nuclear structure, quantum phase transitions are reflected by rapid structural changes, with varying N or Z , or rotational frequency.

It appears that the evolution of the shell structure governs the variation of ground-state nuclear shapes along isotopic and isotonic chains. Shape transitions reflect the underlying modifications of interactions between valence nucleons. Evidently, rotation acts as an additional external field enforcing various interactions between single-particle orbitals. It is similar to the phenomenon of the magnetic field for QDs. The basic difference consists in the fact that the magnetic field creates an additional confinement in QDs, while in nuclear systems, the rotation works against the confinement created by attractive nucleon-nucleon interactions.

The phase transition is usually detected by means of an order parameter as a function of a control parameter. In many cases, an order parameter is calculated with the aid of model considerations. In particular, in rotating nuclei, one can suggest several order parameters, like deformation parameters of a nuclear effective potential, β and γ , that characterize the geometrical configuration [552, 553], as a function of the rotational frequency, playing the role of a control parameter. In order to elucidate this aspect the experimental data in ^{156}Dy and ^{162}Yb (see Fig. 20) have been analyzed [455, 554] with the aid of the cranking Hamiltonian

$$\mathcal{R} = H - \sum_{\tau=N,P} \lambda_{\tau} \hat{N}_{\tau} - \Omega \hat{J}_x + H_{\text{int}} . \quad (5.18)$$

The term $H = H_N + H_{\text{add}}$ contains the Nilsson Hamiltonian H_N and the additional term that restores the local Galilean invariance of the Nilsson potential in the rotating frame. The interaction includes separable monopole pairing, double stretched quadrupole-quadrupole (QQ) and monopole-monopole terms. The details on this model Hamiltonian can be found in [554].

At each rotational frequency, the total mean-field energy $R = \langle \mathcal{R} \rangle$ is minimized on the mesh $\beta = 0.0 - 0.6$, $\gamma = -\pi/3 - +\pi/3$. The results for the rotational dependence of equilibrium deformation parameters β and γ (see for definitions Sec. 5.2.1) exhibit a transition to the triaxiality $\gamma \neq 0$ at $I = 8\hbar \rightarrow I = 10\hbar$ in ^{162}Yb and $I = 14\hbar \rightarrow I = 16\hbar$ in ^{156}Dy (see Fig. 22). In ^{162}Yb , a stable, single minimum $E_{\Omega}(\beta, \gamma) = \langle \mathcal{R} \rangle$ slowly moves on the potential energy surface (β, γ) from the axially symmetric shape to the triaxial one, with the increase of the rotation frequency. Hereafter, $\langle \dots \rangle$ means the averaging over the

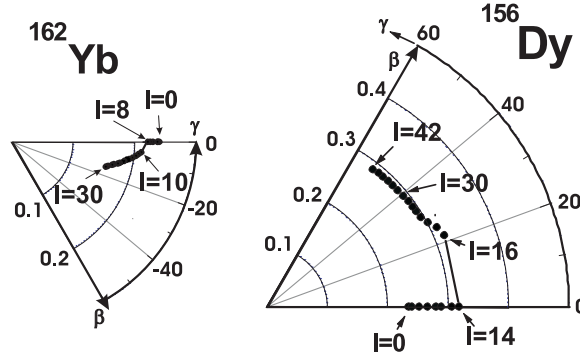


Figure 22: Equilibrium deformations on the $\beta - \gamma$ plane, under varying the angular momentum $I = \langle \hat{J}_x \rangle - 1/2$ (in units of \hbar). From [554].

mean-field states. In contrast, in ^{156}Dy at the vicinity of the transition point, there is a coexistence of the axially symmetric ($\gamma = 0$) and non-axial ($\gamma \neq 0$) configurations. Slightly above the transition point, the configuration suddenly changes from the axially symmetric into the triaxial one. The agreement between experimental and calculated values for the kinematical moment of inertia (Fig. 20) confirms the validity of the calculations. In principle, projection methods should be used in the transition region, since the angular momentum is not a good quantum number in the CM. A theory of large amplitude motion would provide a superior means to solve this problem [555, 556].

To elucidate the different character of the shape transition from axially symmetric to the triaxial shape, one can choose the deformation parameter γ as the order parameter that reflects the broken axial symmetry [455, 554]. Such a choice is well justified, since the deformation parameter β preserves its value before and after the shape transition in both nuclei: $\beta_t \approx 0.2$ for ^{162}Yb and $\beta_t \approx 0.31$ for ^{156}Dy . Thus, one considers the mean-field value of the cranking Hamiltonian, $E_\Omega(\gamma; \beta_t) \equiv \langle \mathcal{R} \rangle$, for different Ω (state variable) and γ (order parameter) at a fixed value of β_t .

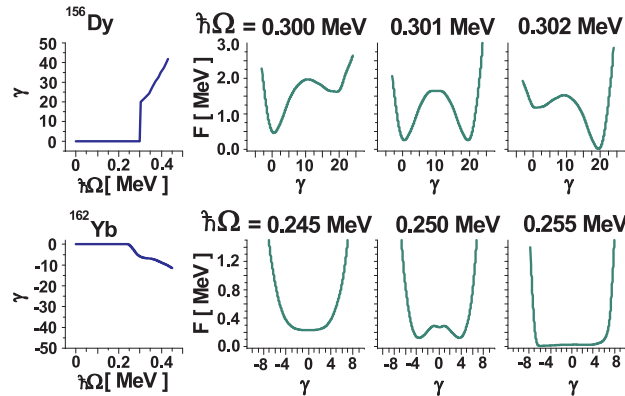


Figure 23: (Color online) Rotational dependence of the order parameter γ and the energy surface sections $F(\Omega, \gamma) = E(\gamma, \beta_t) - E_{min}$ for ^{156}Dy (top) and ^{162}Yb (bottom) before and after the transition point. The energy is counted relatively to the value $E_{min} = E_\Omega(\beta_t, \gamma)$ at $\hbar\Omega = 0.255$, 0.302 MeV for ^{162}Yb and ^{156}Dy , respectively. From [554].

For ^{156}Dy , one observes the emergence of the order parameter γ above the critical

value $\hbar\Omega_c = 0.301$ MeV of the control parameter Ω (see a top panel in Fig. 23). Below and above the transition point, there is a unique phase whose properties are continuously connected to one of the coexisting phases at the transition point. The order parameter changes discontinuously as the nucleus passes through the critical point from the axially symmetric shape to the triaxial one. The polynomial fit of the potential landscape section at $\hbar\Omega_c = 0.301$ MeV yields the following expression

$$F(\Omega; \gamma) = F_0(\Omega) + F_2(\Omega)\gamma^2 - F_3(\Omega)\gamma^3 + F_4(\Omega)\gamma^4. \quad (5.19)$$

One can transform this polynomial to the form

$$\bar{F} = \frac{F(\Omega; \gamma) - F_0(\Omega)}{\bar{F}_0} \approx \alpha \frac{\eta^2}{2} - \frac{\eta^3}{3} + \frac{\eta^4}{4}, \quad (5.20)$$

where

$$\bar{F}_0 = \frac{(3F_3)^4}{(4F_4)^3}, \quad \alpha = \frac{8F_2F_4}{9F_3^2}, \quad \eta = \frac{4F_4}{3F_3}\gamma. \quad (5.21)$$

Expression (5.20) represents the generic form of the anharmonic model of *the structural first order phase transitions* in condensed matter physics (see Sec. 2.1.2 and [557]). The condition $\partial\bar{F}/\partial\eta = 0$ determines the following solutions for the order parameter η

$$\eta = 0, \quad \eta = \frac{1 \pm \sqrt{1 - 4\alpha}}{2}. \quad (5.22)$$

If $\alpha > 1/4$, the functional \bar{F} has a single minimum at $\eta = 0$. Depending on the values of α , defined in the interval $0 < \alpha < 1/4$, the functional \bar{F} manifests the transition from one stable minimum at zero order parameter via one minimum+metastable state to the other stable minimum with the nonzero order parameter. In particular, at the universal value of $\alpha = 2/9$ the functional \bar{F} has two minimal values, with $\bar{F} = 0$ at $\eta = 0 \rightarrow \gamma \approx 0^0$ and $\eta = 2/3 \rightarrow \gamma \approx 27^0$ and a maximum at $\eta = 1/3 \rightarrow \gamma \approx 13.5^0$ (using the numerical values for the coefficients $F_{2,3,4}$ extracted from the fit of the potential landscape section, Eq. (5.19)). The correspondence between the actual value $\gamma \approx 20^0$ and the one obtained from the generic model is quite good. Thus, the backbending in ^{156}Dy possesses typical features of *the first order phase transition*.

In the case of ^{162}Yb , the energy $E(\Omega; \gamma)$ and the order parameter (Fig. 23) are smooth functions in the vicinity of the transition point Ω_c . This implies that the phases with $\gamma = 0$ and $\gamma \neq 0$ should coincide at the transition point. Therefore, for Ω near the transition point Ω_c , one may expand the functional $F(\Omega, \gamma) = E_\Omega(\gamma, \beta_t) - E_{min}$ (see Fig. 23) in the form [554]:

$$F(\Omega; \gamma) = F_1(\Omega)\gamma + F_2(\Omega)\gamma^2 + F_3(\Omega)\gamma^3 + F_4(\Omega)\gamma^4 + \dots \quad (5.23)$$

It can be shown that $F_1(\Omega) = 0$ and at the transition point Ω_c ($\gamma = 0$) $F_2(\Omega_c) = F_3(\Omega_c) = 0$. Assuming that $F_3 = 0$ for all Ω , one obtains for the order parameter

$$\gamma_1 = 0, \quad \gamma_{2,3}^2 = -\frac{F_2(\Omega)}{2F_4(\Omega)} = \begin{cases} \neq 0 & \text{for } \Omega \neq \Omega_c \\ = 0 & \text{for } \Omega = \Omega_c. \end{cases} \quad (5.24)$$

At the transition point $F_2(\Omega_c) = 0$, it is possible to propose the following definition of the function $F_2(\Omega)$:

$$F_2(\Omega) \approx \frac{dF_2(\Omega)}{d\Omega} (\Omega - \Omega_c) . \quad (5.25)$$

Thus, for the order parameter, one has $\gamma \sim (\Omega - \Omega_c)^\nu$, with the critical exponent $\nu = 1/2$, in agreement with the classical Landau theory, where the temperature is replaced by the rotational frequency. The observed phenomenon resembles very much the structural phase transition discussed within the anharmonic Landau-type model in solid state physics [557]. One may conclude that the backbending in ^{162}Yb is classified as *the phase transition of the second order*.

Extensive experimental data have been obtained on low-lying states of negative parity [470, 471]. For the Ra-Th ($Z \sim 88, N \sim 134$) and Ba-Sm ($Z \sim 56, N \sim 88$) nuclei, low 3^- states, parity doublets, and alternating parity bands with enhanced dipole ($E1$) γ -transitions have been found. Since the octupole interactions are the strongest when the pairs of orbitals from the intruder sub-shell (l, j) and the normal parity sub-shell ($l-3, j-3$) are near the Fermi surface, the octupole correlations are expected to become important for these nuclei [168, 409]. The features, observed in nuclei, are similar to those familiar from molecular physics. In molecules, a stable octupole deformation leads to the appearance of rotational bands with alternating parity levels connected by strong $E1$ intra-band transitions. Möller and Nilsson [558] used the assumption on the symmetry breaking of the intrinsic reflection symmetry of the single-particle potential and demonstrated the instability with respect to the axial octupole deformation in the Ra-Th region. The analysis was performed within the macroscopic + microscopic approach (see Sec. 5.2.4) for the Nilsson model at zero rotational frequency. Later, within this approach, numerous results, based on various single-particle phenomenological potentials, have been reported regarding the presence of a stable axial octupole deformation in the ground state of some nuclei in the actinide region [471]. The cranking macroscopic+microscopic approach was also used (see Sec. 5.2.4) to analyze the properties of rotating nuclei with a stable axial octupole deformation [538–540].

The potential energy surface, found in different calculations, is, however, quite shallow. Experimental nuclear spectra show also a pronounced parity splitting at low angular momenta. Rather dynamical octupole effects (vibrations) are dominant over static effects (octupole deformations) at low spins. The increase of the angular momentum decreases the pairing correlations which reduce the octupole interaction, since the pairing correlations couple the orbitals with the same parity. With rotation, the density of different parity states near the Fermi level becomes enhanced. Indeed, one observes a smooth decrease of the parity splitting with the increase of the rotational frequency in several nuclei. The cranking+Hartree-Fock-Bogolubov (HFB) approach with Gogny forces has been applied for the analysis of the data in Ba-Sm region [559]. In order to compare with experimental data, the approximate parity projection, before variation, has been developed. Within this approach, a good agreement was obtained between the calculated and experimental data for the energy splitting of positive and negative parity states, as well as for the projected $B(E1)$ -transition probabilities. Note that at high spins the differences between projected and unprojected HFB solutions become less pronounced.

The problem of non-axial octupole deformations has attracted much attention during recent years. The study of non-axial octupole deformations could shed light on the ten-

dency, for systems in the way towards fission, to avoid superdeformation [168]. Further, a tilted axis rotation [410] and non-axial octupole deformations could be complementary parts of a signature symmetry breaking phenomenon in rotating nuclei. Calculations, by means of the macroscopic+microscopic method with the Woods–Saxon potential, predict the importance of the banana-type Y_{31} deformation for highly deformed nuclei [560]. Manifestations of pronounced shell effects have been discovered, when non-axial octupole deformations are added to a harmonic oscillator model [481]. The cranking HFB calculations with Skyrme [561] and Gogny [562] forces predict a non-axial Y_{31} octupole deformation in light nuclei at high spins. The results based on the Skyrme interaction demonstrate the importance of a nonaxial Y_{32} octupole deformation in actinide nuclei at fast rotation [563]. The onset of a non-axial octupole deformation was found in ^{162}Yb [564]. Notice that rotation induces the contribution of non-axial quadrupole and octupole components of effective nuclear potentials.

Recently it was suggested [565] that strong octupole correlations in the mass region $A \approx 226$ might be interpreted as rotation-induced condensation of octupole phonons having their angular momentum aligned with the rotational axis of a triaxial nucleus. This idea was proposed for the first time by Briancon and Mikhailov [566]. However, another prediction is the possible existence of tetrahedral shapes and, in particular, in the actinide region [567, 568]. Such shapes are characterized by a triaxial octupole deformation Y_{32} , together with a near-zero quadrupole deformation Y_{20} . This implies vanishing in-band $E2$ γ -transitions. Evidently, the negative-parity bands, with missing in-band $E2$ γ -transitions, are the candidates for the rotation of a tetrahedral shape. The most favourable region for observing tetrahedral states is in the mass region of $A \sim 160$ [569]. Measurements of quadrupole moments of low-lying negative-parity bands in this region have not supported the tetrahedral hypothesis [570]. It was found, however, that the experimental systematics of the the dipole ($E1$) γ -transitions [473] are in good agreement with the increasing triaxial quadrupole deformation [563, 565]. A lot of experimental efforts is required to understand better the nature of octupole instability.

5.3.3 Collective excitations as indicator of symmetry breaking

The description of rotational states is one of the oldest, yet not fully solved, problem in nuclear structure physics. While various microscopic models, based on the cranking approach, describe reasonably well the kinematical moment of inertia

$$\mathfrak{S}^{(1)} = -(dE/d\Omega)/\Omega \quad (5.26)$$

for a finite angular frequency Ω , there is still a systematic deviation [571] of the dynamical moment of inertia

$$\mathfrak{S}^{(2)} = -(d^2E/d\Omega^2) . \quad (5.27)$$

Here, the classical canonical relation $dE/d\Omega = -J$ is used (see also Sec. 5.1); E is the total energy in the rotating frame, defined in the CM approach as $E = \langle \mathcal{R} \rangle$ or as $E = E_I - \Omega I$ from the experimental data at high spins. Since the moments of inertia are the benchmarks for the microscopic models of collective motion in nuclei, the understanding of the source of the discrepancy becomes a challenge for a many-body theory of finite Fermi systems.

The description of the moments of inertia could be improved, if quantum oscillations around the mean solution were incorporated, as it was suggested by Thouless and

Valatin [440]. The effects of pairing correlations on the moments of inertia were considered [536]. For the case of pairing and quadrupole vibrations, such calculations, in a restricted configuration space (only three shells have been included), were performed [572]. For medium and heavy nuclei, realistic calculations require a large configuration space and are less reliable in the backbending region, where there are large fluctuation of the angular momentum. If one neglects pairing correlations (high spin limit), it is possible to calculate the total energy, including the mean-field and the RPA correlation energies using a self-consistent rotating harmonic oscillator [532]. This model provides a relatively simple, but still realistic, frame to calculate the Thouless-Valatin moment of inertia and the desired contributions of shape oscillations without the usual restrictions of the configuration space.

Let us consider the mean-field part of the many-body Hamiltonian (Routhian) Eq. (5.5) as $\mathcal{R} = \sum_i^N h_i$, where $h = h_0 + h_z$ are defined in Sec. 4.2.1. The single-particle triaxial harmonic oscillator Hamiltonian is aligned along its principal axes (PA). For rotating nuclei we have to use $\omega_1^2 = \omega_x^2$, $\omega_2^2 = \omega_y^2$, $\omega_L \equiv \Omega$, and consider the rotation around x -axis. In this case, all x -variables are to be renamed as z -variables. We call this model as a PAC (a principal axis cranking). Using the transformation (A.1), with x replaced by z , one arrives to the well known results [573–575], where to simplify notation, the \hbar , entering the angular momentum and the frequencies, is suppressed:

$$R = \omega_x \Sigma_x + \omega_+ \Sigma_+ + \omega_- \Sigma_- \quad (5.28)$$

where the eigenmodes ω_{\pm}

$$\omega_{\pm}^2 = \frac{1}{2}(\omega_y^2 + \omega_z^2 + 2\Omega^2 \pm \Delta), \quad (5.29)$$

$$\Delta = [(\omega_y^2 - \omega_z^2)^2 + 8\Omega^2(\omega_y^2 + \omega_z^2)]^{1/2},$$

$$\Sigma_k = \langle \Sigma_j^N (n_k + 1/2)_j \rangle. \quad (5.30)$$

Here, $n_k = a_k^+ a_k$ ($k = x, +, -$), where a_k^+ , a_k are the oscillator quantum operators. The lowest levels are filled from the bottom, which gives the ground state energy in the rotating frame. The Pauli principle is taken into account, so that only two particles occupy a single level. The minimization of the total energy Eq. (5.28) with respect to all three frequencies, subject to the volume conservation condition $\omega_x \omega_y \omega_z = \omega_0^3$, yields the self-consistent condition Eq. (4.8) (adapted for the nuclear rotation) at a finite rotational frequency [530]. Since all shells are mixed, we go beyond the approximation used in [572] (for a cranking harmonic oscillator, see also [317]). In this section, to distinguish the CM model for nuclear rotation from the model of QD in the magnetic field, we can call the condition Eq. (4.8), adapted for nuclear rotation, as the nuclear self-consistent condition (NSCC).

It should be pointed out that, generally, the NSCC provides the absolute minima, in comparison with the local minima obtained from the condition of the *isotropic velocity distribution* [574, 575]

$$\omega_x \Sigma_x = \omega_+ \Sigma_+ = \omega_- \Sigma_- , \quad (5.31)$$

which describes only a rigid rotation. By means of the transformation (A.1) (adapted for the PAC), one can show that this condition is equivalent to the condition

$$\omega_x^2 \langle X^2 \rangle = (\omega_y^2 - \Omega^2) \langle Y^2 \rangle = (\omega_z^2 - \Omega^2) \langle Z^2 \rangle. \quad (5.32)$$

In semiclassical approximation, one can assume that $\langle X^2 \rangle = R_x^2$, $\langle Y^2 \rangle = R_y^2$, and $\langle Z^2 \rangle = R_z^2$, where R_i ($i = x, y, z$), are spatial extensions of the many body system. As a result, for $\omega_y = \omega_z = \omega_\perp$, one obtains from the condition (5.32)

$$\frac{R_z}{R_x} = \frac{\omega_x}{\sqrt{\omega_\perp^2 - \Omega^2}} \quad (5.33)$$

the aspect ratio, which has been used as a convenient diagnostic tool to infer the actual angular velocity of the rotating Bose condensates [200].

As it is stressed in Sec. 5.1, because of constant density, with a sharp boundary, in stable nuclei, the shape deformation can be chosen to represent a collective degree of freedom. Due to short-range attractive nuclear forces, one can conclude that the deformation of the density distribution and that of the potential are the same [168]. As a result, when the nuclear system undergoes collective excitations with a change in the density distribution, it must be accompanied by the same change in the potential $\delta\rho = \delta V$. Then nucleons, moving in this potential, will have to readjust their orbits. Such readjustments result in the change in the nucleon density distribution. Since a nucleus is a self-sustained system, a collective motion itself is connected to the nucleon degrees of freedom, and therefore the change in the density thus produced must be the same density change that is caused by the collective excitations. The self-consistency between the particle and collective degrees of freedom is indeed the basic ingredient responsible for inducing the effective interactions.

Based on the concept of nuclear saturation and the self-consistency between the shape of the mean-field potential (the triaxial harmonic oscillator) and that of a density distribution, Sakamoto and Kishimoto [576] have employed the Landau theory of Fermi liquid [12] and derived the effective multipole-multipole interaction due to shape and angular momentum oscillations; see also [577]. According to this result, the CRPA Hamiltonian has the following form

$$H_{RPA} = \mathcal{R} - \frac{\chi}{2} \sum_{\mu=-2}^{\mu=2} Q_\mu^+ Q_\mu = \tilde{H} - \Omega L_x. \quad (5.34)$$

Here, the quadrupole operators $Q_\mu = r^2 \tilde{Y}_{2\mu}$ are expressed in terms of the stretched coordinates $\tilde{q}_i = (\omega_i/\omega_0)q_i$, ($q_i = x, y, z$). The effective quadrupole interaction restores the rotational invariance of the non-rotating triaxial harmonic oscillator, so that in the frame of RPA,

$$[\tilde{H}, L_i] = 0, \quad (i = x, y, z). \quad (5.35)$$

The NSCC, Eq. (4.8), fixes the quadrupole strength

$$\chi = (4\pi/5)m\omega_0^2/\langle r^2 \rangle, \quad \langle r^2 \rangle = \langle \tilde{x}^2 + \tilde{y}^2 + \tilde{z}^2 \rangle. \quad (5.36)$$

If the NSCC is fulfilled, in addition to the volume conserving constraint, the self-consistent residual interaction does not affect the equilibrium deformation obtained from the minimization procedure, since $\langle \tilde{Q}_\mu \rangle = 0$ ($\mu = 0, 1, 2$).

Using the transformation (A.1) (adapted for the CHO), one solves the RPA equations of motion

$$[H_{RPA}, \mathcal{X}_\lambda] = -i\omega_\lambda \mathcal{P}_\lambda, \quad [H_{RPA}, \mathcal{P}_\lambda] = i\omega_\lambda \mathcal{X}_\lambda, \quad [\mathcal{X}_\lambda, \mathcal{P}_{\lambda'}] = i\delta_{\lambda,\lambda'}, \quad (5.37)$$

where ω_λ are the RPA eigenfrequencies in the rotating frame and the associated phonon operators are

$$O_\lambda = (\mathcal{X}_\lambda - i\mathcal{P}_\lambda)/\sqrt{2}. \quad (5.38)$$

Here, $\mathcal{X}_\lambda = \sum_s X_s^\lambda \hat{f}_s$, $\mathcal{P}_\lambda = i \sum_s X_s^\lambda \hat{g}_s$ are bilinear combinations of the quanta a_k^+ , a_k , such that $\langle [\hat{f}_s, \hat{g}_{s'}] \rangle = V_s \delta_{s,s'}$, where the quantities V_s are proportional to different combinations of $\sum_i (i = x, +, -)$. Since the mean field violates the rotational invariance, among the RPA eigenfrequencies, there exist two spurious solutions. One solution with zero frequency is associated with the rotation around the x - axes, since

$$[H_{RPA}, L_x] = 0. \quad (5.39)$$

The other "spurious" solution at $\omega = \Omega$ corresponds to the collective rotation [578], since

$$[H_{RPA}, L_\pm] = [H_{RPA}, L_y \pm iL_z] = \mp \Omega L_\pm. \quad (5.40)$$

The Hamiltonian Eq. (5.34) possesses the signature symmetry (see Sec. 5.3.1), i.e., such that it can be decomposed into positive and negative signature terms, $H_{RPA} = H(+) + H(-)$, that can be separately diagonalized [525, 578].

The positive signature Hamiltonian contains the zero-frequency mode, defined by

$$[H(+), \phi_x] = -\frac{L_x}{\mathfrak{S}_{TV}}, \quad [\phi_x, L_x] = i, \quad (5.41)$$

and allows one to determine the Thouless-Valatin moment of inertia [437]. Here, the angular momentum operator $L_x = \sum_s l_s^x \hat{f}_s$ and canonically conjugated angle $\phi_x = i \sum_s \phi_s^x \hat{g}_s$ are expressed via \hat{f}_s and \hat{g}_s , which obey the condition $\hat{R}_x \hat{d}_s \hat{R}_x^{-1} = \hat{d}_s$ ($\hat{d}_s = \hat{f}_s$ or \hat{g}_s). The negative signature Hamiltonian contains the rotational mode and the vibrational mode describing the wobbling motion (see below).

The Thouless-Valatin moment of inertia has been compared with the dynamical moment of inertia $\mathfrak{S}^{(2)} = -d^2 R/d\Omega^2$ calculated in the mean-field approximation in the exact model [532]. The basic outcome is that, if the mean-field equations are solved *self-consistently*, then the mean-field dynamical moment of inertia, calculated in the rotating frame, is *equivalent* to the Thouless-Valatin moment of inertia calculated in the CRPA approach. It is the strongest test for the validity of a microscopic model of nuclear rotation.

Regular rotational bands, identified in spectroscopic data, are the most evident manifestations of an anisotropy of a spatial nuclear density distribution. While an axial deformation of a nuclear potential is well established, there is a long standing debate on the existence of a triaxial deformation. A full understanding of this degree of freedom in nuclei may give impact for other mesoscopic systems as well. In particular, the importance of nonaxiality is discussed recently for metallic clusters [579] and atomic condensates (see [580] and references therein).

Let us consider rotation around the symmetry axis, i.e., around the z axis, similar to the rotation of the Bose-condensed trapped atoms (see Sec. 3.3.3). Without loss of generality, we consider only one type of particles (protons or neutrons) in this model. The eigenmodes have the simple form (see Appendix A, where $\omega_1^2 = \omega_x^2$, $\omega_2^2 = \omega_y^2$, $\omega_L \equiv \Omega$), and in this case the NSCC leads to the nontrivial solution which must satisfy the equation

$$(\omega_+ \omega_- - \Omega^2) = 0. \quad (5.42)$$

Setting $\omega_x = \omega_y = \omega_\perp^0$, one obtains the bifurcation point [531]

$$\Omega_{cr} = \omega_\perp^0 / \sqrt{2} . \quad (5.43)$$

For $\Omega > \Omega_{cr}$, the axial symmetry is broken and the system is driven into the domain of triaxial shape under the PAC rotation. This situation is reminiscent of a striking feature established experimentally in the rotating Bose condensate [581, 582] (see also discussion in Sec. 3.3.1). According to our analysis, the dynamical instability in a nuclear system and in the rotating Bose condensate is of similar nature, in spite of the different character of the interaction between nucleons (attractive) and between atoms (repulsive). The origin of this similarity is the trapping of each system by the harmonic oscillator potential. For the nuclear system it is the mean field and for the Bose condensate it is the effective external magnetic field.

To understand this result, let us consider an axially deformed system, defined by the Hamiltonian \tilde{H} in the laboratory frame that rotates about a symmetry axis z with a rotational frequency Ω . The angular momentum is a good quantum number and, consequently,

$$[\hat{J}_z, O_K^\dagger] = K O_K^\dagger . \quad (5.44)$$

Here, the phonon O_K^\dagger describes the vibrational state, with K being the value of the angular momentum carried by the phonons O_K^\dagger along the symmetry axis, that is, the z axis. Thus, one obtains

$$[\mathcal{R}, O_K^\dagger] = [\tilde{H} - \Omega \hat{J}_z, O_K^\dagger] = (\tilde{\omega}_K - K\Omega) O_K^\dagger \equiv \omega_K O_K^\dagger , \quad (5.45)$$

where $\tilde{\omega}_K$ is the phonon energy of the mode K in the laboratory frame at $\Omega = 0$. This equation implies that, for the rotational frequency

$$\Omega_{cr} = \tilde{\omega}_K / K , \quad (5.46)$$

one of the RPA frequencies ω_K vanishes in the rotating frame [531, 583]. At this point of bifurcation we could expect the symmetry breaking of the rotating mean field, due to the appearance of the Goldstone boson related to the multipole-multipole forces with the quantum number K . Indeed, solving the RPA equations (5.37) for the Hamiltonian (5.34) with $L_x \rightarrow L_z$, one obtains the RPA solution

$$\omega_{K=2+} = \sqrt{2}\omega_\perp^0 - 2\Omega \quad (5.47)$$

for the quadrupole phonons, with the largest projection $K = 2$ [533]. This mode is the quadrupole excitation having two more units of angular momentum than the vacuum state. When $\omega_{K=2+} = 0$, the transition from non-collective rotation (around the z axis) to triaxial collective rotation takes place, i.e., at $\Omega_{cr} = \omega_\perp^0 / \sqrt{2}$, which is just the bifurcation point of the mean field discussed above. This bifurcation point applies for any axially symmetric system (prolate and oblate). For the $K = 1^+$ mode the RPA solution is

$$\omega_{K=1+} = \sqrt{\omega_\perp^2 + \omega_z^2} - \Omega . \quad (5.48)$$

The condition $\omega_{K=1+} = 0$ yields the critical frequency at which the onset of the nonprincipal axis (tilted) rotation should occur for the prolate system, i.e., at

$$\Omega_{cr} = \sqrt{\omega_\perp^2 + \omega_z^2} . \quad (5.49)$$

However, the energy to create this mode of angular momentum $1\hbar$ is too high, the system rather prefers the PAC rotation around the axis perpendicular to the symmetry axis. As a consequence, this model does not allow tilted rotations for systems which are prolate at $\Omega = 0$, i.e., when $\Sigma_1 = \Sigma_2$. This frequency is related to vibrational excitations carrying one unit of angular momentum in an axially symmetric system, whether it is oblate or prolate.

Using the triaxial harmonic oscillator, Troudet and Arvieu have shown that for prolate systems the PAC leads to triaxial shapes [530]. With increasing rotational velocity, the change of the shape, for the critical frequency $\Omega_{cr}^{(1)}$, leads to an oblate shape, with the rotational axis coinciding with the symmetry axis. For a certain value $\Omega_{cr}^{(2)} > \Omega_{cr}^{(1)}$, the oblate rotation may transform to a tilted rotation [533].

For the oblate rotation around the symmetry axis x one can choose the axis x as a quantization axis. In this case the projection λ of the angular momentum L_x is a good quantum number as

$$[\hat{J}_x, O_\lambda^\dagger] = \lambda O_\lambda^\dagger. \quad (5.50)$$

We thus obtain an equation similar to Eq. (5.45) after replacing K by λ . At the rotational frequency $\Omega_{cr} = \tilde{\omega}/\lambda$ one of the RPA frequencies vanishes. The bifurcation point

$$\Omega_{cr}^{(2)} = 2\sqrt{\frac{\omega_x^2 + \omega_\perp^2}{3}} \cos \frac{\psi + \pi}{3}, \quad (5.51)$$

$$\cos \psi = \sqrt{27} \frac{\omega_x^2 \omega_\perp}{(\omega_x^2 + \omega_\perp^2)^{3/2}} \frac{r - 1}{r + 1}, \quad (5.52)$$

where $r = \Sigma_3/\Sigma_2$, signals on the transition from the oblate rotation around a symmetry axis to the tilted rotation [533]. It is worth stressing that tilted rotations do occur for $\Omega > \Omega_{cr}^{(2)}$, when all three values of Σ_i differ from each other, i.e., the shape departs from the axial symmetry. Note that there were numerous attempts to find a stable tilted solution with the triaxial harmonic oscillator either with a PAC or a three-dimensional rotation. However, the solution was overlooked for a long time; see the history in [410, 411].

The analysis of specific low-lying excited states near the yrast line could shed light on the existence of the nonaxiality. For nonaxial shapes, one expects the appearance of low-lying vibrational states, that may be associated with the classical wobbling motion. Such excitations (called wobbling excitations) were suggested, first, by Bohr and Mottelson [168] in rotating even-even nuclei, and analyzed within simplified microscopic models [584–586]. According to the microscopic approach [587, 588], the wobbling excitations are the vibrational states of the negative signature built on the positive signature yrast (vacuum) state. Their characteristic feature are collective $E2$ transitions with $\Delta I = \pm 1\hbar$ between these and yrast states. First experimental evidence of such states in odd Lu nuclei was reported only recently [589–594].

The CRPA provides a natural framework for the microscopic analysis of the wobbling excitations [595, 596]. It can be shown that, in the PAC regime for the triaxial nuclei, the wobbling mode is described by the equation

$$\omega_{\nu=w} = \Omega \sqrt{\frac{[\Im_x - \Im_2^{eff}][\Im_x - \Im_3^{eff}]}{\Im_2^{eff} \Im_3^{eff}}}, \quad (5.53)$$

with the microscopic effective moments of inertia [588]

$$\mathfrak{S}_{2,3}^{eff} = \mathfrak{S}_{y,z} + \Omega S \frac{\mathfrak{S}_x - \mathfrak{S}_{y,z} - \omega_\nu^2 S / \Omega}{\mathfrak{S}_{z,y} + \Omega S}, \quad (5.54)$$

depending on the RPA frequency. Here,

$$\mathfrak{S}_x = \frac{\langle \hat{J}_x \rangle}{\Omega}, \quad S = \sum_{\mu} \frac{J_{\mu}^y J_{\mu}^z}{(E_{\mu}^2 - \omega_{\nu}^2)}, \quad \mathfrak{S}_{y,z} = \sum_{\mu} \frac{E_{\mu} (J_{\mu}^{y,z})^2}{(E_{\mu}^2 - \omega_{\nu}^2)}, \quad (5.55)$$

and $E_{\mu} = \varepsilon_i + \varepsilon_j$ ($E_{i\bar{j}} = \varepsilon_i + \varepsilon_{\bar{j}}$) are two-quasiparticle energies, and $J_{\mu}^{y,z}$ are two-quasiparticle matrix elements (see details in [595]). The first attempts to describe wobbling excitations in the framework of the CRPA approach for odd nuclei are faced with difficulties related to the fulfillment of the self-consistency between the effective mean field and the RPA excitations [596]. The CRPA approach provides useful criteria for identifying wobbling excitations in even-even nuclei [586, 595].

6 Metallic Grains

6.1 General properties

Experimental advances in sample fabrication and measurement techniques have revealed novel aspects of superconductivity, related to size and shape effects of finite systems. Already fifty years ago, Anderson [597] noted that superconductivity should disappear in small metallic grains when the single-particle mean level spacing $d = 1/\rho$ (ρ is the spectral density per spin species) at the Fermi energy is comparable or becomes larger than the energy gap $\tilde{\Delta}$ of a macroscopic superconductor. This gap is caused by the formation of Cooper pairs describing correlated electron pairs in time-reversed states. Pairing correlations in superconductors tend, therefore, to minimize the total spin of the electron system. Ferromagnetic correlations, on the other hand, prefer to maximize the total spin and form a macroscopic magnetic moment. The ratio $\tilde{\Delta}/d$ provides an approximate number of electronic levels available for the formation of Coopers pairs. Evidently, if $\tilde{\Delta}/d \ll 1$, then there are no active levels accessible for pair correlations and, consequently, the ferromagnetic correlations determine the system properties. By changing the grain size and the number of electrons one can vary the single-particle mean level spacing in such systems and, therefore, control the desired properties. The basic questions are: does the system remain superconducting or transforms into normal metal under the transition from $d < \tilde{\Delta}$ to $d \geq \tilde{\Delta}$? What are the minimal requirements in terms of the size and shape of a metallic grain to retain superconducting properties? In other words, under what conditions the gauge symmetry, related to the appearance of superconductivity, can be considered as approximately broken? Understanding answers to these questions is important for technological applications.

The size dependence of the critical temperature and superconducting gap was studied for a rectangular grain [598] and for a nanoslab [599]. Thermodynamic properties of superconducting grains were investigated in [600, 601]. For rectangular grains, the situation has been interpreted within the standard BCS theory of superconductivity [235]. Ralph,

Black, and Tinkham (RBT) [602–604] have experimentally studied the excitation spectrum of individual ultra-small metallic grains (of radii $r < 5$ nm and mean level spacings $d > 0.01$ meV), using a single-electron-tunnelling spectroscopy, similar to the experiments with QDs (see Introduction to Sec. 4). Attaching such a grain via oxide tunnel barriers to two leads, they constructed a single-electron transistor having the grain as a central island, and showed that a well-resolved, discrete excitation spectrum could indeed be extracted from the conductance measurement. Single-electron-tunnelling spectroscopy of ultra-small metallic grains has been used to probe superconducting pairing correlations in Al grains [603,604]. The measured d -values (ranged from 0.02 to 0.3 meV) were much larger than $k_B T$ for the lowest temperatures attained (around $T \simeq 30$ mK), but of the order of $\tilde{\Delta}$ (the bulk superconducting gap $\tilde{\Delta} = 0.18$ meV for Al). The number of conduction electrons for grains of this size was still rather large (between 10^4 and 10^5). By studying the evolution of the discrete spectrum of Al grains ($r > 5$ nm) in an applied magnetic field, RBT have observed that a grain with an even number of electrons had a distinct spectroscopic gap ($\Delta \gg d$), but a grain with an odd number of electrons did not [603–605]. As is known from nuclear physics [606], this is a clear evidence for the presence of superconducting pairing correlations in these grains.

The RBT experiments initiated numerous studies of electron correlations in metallic grains in order to understand the evolution of electron correlations with the decrease of the sample size. A thorough overview of early experiments is given by von Delft and Ralph [607]. Although tunnel-spectroscopic studies of metallic grains are similar in spirit to those of semiconductor QDs, there are a number of important differences. They are as follows [607]:

1. Since metals have much higher densities of states than semiconductors (because the latter have smaller electron densities and effective masses), the size of the metal samples should be much smaller (≤ 10 nm) to observe discrete levels.
2. Metallic grains have much larger charging energies than QDs. Therefore, one can minimize the electron number fluctuations.
3. In metallic grains, one can control the strength and type of electron interactions in a great variety of materials through the periodic table, including samples doped with impurities. This creates a remarkable opportunity for studying superconductivity and itinerant ferro-magnetism.
4. While in QDs it is possible to accomplish electrostatic control of the tunnel barriers to the leads, for metallic grains, the tunnel barriers are insulating oxide layers and, therefore, insensitive to the applied voltage. This is well suited for studying nonequilibrium effects in grains, contrary to those in QDs, where a large source-drain voltage lowers the tunnel barrier in a poorly controlled way.
5. Spin effects are easily probed in metallic grains by applying magnetic field. Contrary to QDs, where the orbital effects are strongly enhanced due to a small effective electron mass (see Secs. 4.1 and 4.2.1), spin effects (in particular, a Zeeman splitting) are dominant in metallic grains.
6. For the same reason, spin-orbital effects are more easily studied in metallic grains than in QDs.

6.2 Pairing effects and shell structure

6.2.1 Theoretical approaches

The phenomenon of superconductivity or superfluidity in nuclear and condensed-matter systems is typically described by assuming a pairing Hamiltonian in the BCS approximation [235]. As a simplest model for a metallic grain, which incorporates pairing interactions and a Zeeman coupling to a magnetic field, one can adopt the following BCS Hamiltonian

$$H_{BCS} = \sum_{j\sigma=\pm} (\varepsilon_j - \mu - \sigma h) c_{j\sigma}^+ c_{j\sigma} - \frac{G}{2} \sum_{ij} c_{i+}^+ c_{i-}^+ c_{j-} c_{j+} . \quad (6.1)$$

Here, $-\sigma h \equiv \mu_B g \sigma B/2$ is the Zeeman energy of an electron spin σ in a magnetic field B ($h > 0$). To analyze experimental data for Al grains at zero magnetic field $h = 0$, von Delft *et al.* [605] proposed to consider the reduced BCS model, assuming a completely uniform spectrum with level spacing d and $G = 2\lambda d$, where λ is regarded as a phenomenological parameter. Braun *et al.* [608] studied, in the same model, the case of nonzero magnetic field $h \neq 0$; see for a review [609].

One of the quantities, used for the analysis of superconducting properties of ultra-small grains, is the condensation energy

$$E_b^C = E_b^{GS} - \langle FS | H_{BCS} | FS \rangle , \quad (6.2)$$

where $b = 0$ for grains with even number of electrons and $b = 1$ for those with odd number. The condensation energy is the difference between the ground state energy of the pairing Hamiltonian (6.1) and the energy of the Fermi state (FS). The latter implies the Slater determinant obtained by simply filling all levels up to the Fermi surface. For a large number of electrons, the leading-order behaviour of E^C is given by $-\tilde{\Delta}^2/(2d)$ [610], which is a standard result for the condensation energy. Thus, E^C should be independent of the number of electrons in the system. However, a grain with the odd number has a single electron occupying the level nearest to the Fermi energy. The unpaired electron Pauli-blocks the scattering of other pairs into its own singly-occupied level, i.e. it restricts the phase space available to pair scattering and, therefore, weakens the pairing correlations. This is the so-called "blocking effect" considered by Soloviev [611], who discussed it extensively in the context of nuclear physics [606]. Due to the "blocking effect", the single electron contributes through its free energy. Furthermore, since there is one less active level at the Fermi energy, it is harder for the pairing interaction to overcome the gap and the total energy thus increases. This is the physical origin of the odd-even effect in superconducting grains, similar to nuclei. The BCS approach suggests that an abrupt crossover between the superconducting and the normal states should occur.

As it is well known, the BCS approximation violates particle number conservation [403, 404, 606]. While this feature of the BCS approximation has a negligible effect for macroscopic systems, it can lead to significant errors when dealing with small or ultra-small systems. Since the fluctuations of the particle number in BCS are of the order of \sqrt{N} , improvements of the BCS theory are required for systems with $N \sim 100$ particles. One can improve results by means of the number projection well known in nuclear physics [403]. Indeed, the sharp transition between the superconducting regime and the fluctuation-dominated regime that arises in BCS is smoothed out by the particle number projection

[612]. Nevertheless, the number projection did not remove completely some BCS features, in particular, for odd-electron grains. Fernandez and Egido [613] proposed a generalized BCS ansatz, which improved the BCS results and agreed with the exact solution for the pairing Hamiltonian (6.1).

The exact numerical solution of the pairing model for small number of particles has been developed in nuclear physics by Kerman *et al.* [614] and Pawlikowski and Rybarska [615]. The basic idea of this approach was elaborated by Richardson [616–622] and Richardson and Sherman [623], who developed in a series of papers an analytical approach to this problem. Nowadays it is called the Richardson model. This model was rediscovered and applied successfully to small metallic grains [624]; see for a review [607, 625]. The spontaneous breaking of the $U(1)$ symmetry occurring in this model for the degenerate situation is studied in [626].

The major ingredients of this model are as follows. As discussed above, the pairing interaction does not affect the singly-occupied levels. Due to the "blocking effect", it is sufficient to diagonalize the BCS Hamiltonian (6.1) (in which we set $\mu = 0$, $\hbar = 0$) in the single-particle subspace \mathcal{U} of empty and doubly occupied levels. In this case, the eigenenergies are given by

$$E_n = \sum_i^n E_i . \quad (6.3)$$

Here E_i are the parameters that characterize the eigenstate with the number of electrons $N = 2n + b$, where b is the number of singly occupied levels. Richardson's parameters E_i are found by solving the set of n coupled non-linear equations

$$\frac{1}{G} + 2 \sum_{i=1, \neq m}^n \frac{1}{E_i - E_m} = \sum_{k \in \mathcal{U}} \frac{1}{2\varepsilon_k - E_m}, \quad m = 1, \dots, n . \quad (6.4)$$

These equations are to be solved numerically; see details and comparison of exact solutions with different approximations in literature [607, 625].

6.2.2 Effects of magnetic field

The superconducting gap and low-energy excitation energies, in a rectangular grain, were computed numerically within the Richardson model by Gladilin *et al.* [627]. These authors have further developed an approximation to study the magnetic response of superconductor grains (when $N \sim 10^5$ per grain) as a function of both temperature and magnetic field [628]. An approach, based on the Monte Carlo method, was suggested in [629], which is able to simulate the reduced BCS model for any fixed number of particles without a sign problem. Simulations can be performed at any finite temperature and any level spacing d for large system sizes. All these calculations demonstrate that the magnetic field attenuates the pairing correlations in a grain. However, with increasing temperature pair correlations may reappear for high magnetic field strengths [630], while being quenched at $T = 0$. Nuclei, with angular momenta along a symmetry axis, behave in the similar way [631]. The pair correlations are destroyed in a stepwise manner by subsequent alignment of the angular momenta of individual nucleon orbitals along the symmetry axis. These steps are washed out with increasing temperature, and pair correlations appear at values of the rotational frequency, while they are quenched at $T = 0$. A reentrance of

pair correlations has been discussed, first, by Balian, Flocard, and Veneroni [632], who studied the ensembles of either even or odd numbers of particles.

6.2.3 Shell effects

Shell effects in superconducting grains, with radial symmetry, were studied in [633, 634]. Recent experiments on Al grains were interpreted by Kresin *et al.* [635] as evidence that shell effects can drive critical temperatures in these grains above 100 K. Kresin and Ovchinnikov [633] proposed that a phase transition can occur for some metal nanoclusters with $10^2 - 10^3$ valence electrons. The effect of shell structure in larger spherical nanoparticles, together with modifications in the effective interaction due to alteration of the electrons wave functions, as well as a nonuniform gap parameter, were considered in a recent study [636]. A large and strongly size dependent energy gap and critical temperature were predicted for these particles.

Using the semiclassical approach [486], one can study the pairing-gap fluctuations for arbitrary ballistic potentials. Such an analysis leads to a general picture of the typical fluctuation strength in terms of the properties of the corresponding classical systems, namely, regular or chaotic dynamics [637, 638]. In particular, Garsía-Garsía *et al.* [638] studied the dependence of low energy excitations of small superconducting grains on their size and shape, by combining the BCS mean field, semiclassical techniques, and leading corrections to the mean field. They found a smooth dependence of the BCS gap function on the excitation energy of chaotic grains. However, in the integrable case, for certain values of the electron number N , small changes in the number of electrons can substantially modify the superconducting gap.

An increase (decrease) of the spectral density around E_F would make the pairing more (less) favourable, thereby increasing (decreasing) the energy gap Δ . As a consequence, the gap becomes dependent on the size and the shape of the grain. For spherical grains, one may expect that the degeneracy of levels should decrease the pairing correlations [639]. Thus, for clusters, with parameters satisfying special, but realistic, conditions, one can expect a great strengthening of the pairing correlation and, correspondingly, a large increase in the critical temperature [633]. These conditions are: the proximity of the electronic state to a complete shell ("magic" number) and a relatively small gap between the highest occupied shell and the lowest free shell. Indeed, heat capacities measured for size-selected Al clusters exhibit a jump around 200 K [640] which may be interpreted as a transition from a highly degenerate electronic state near the Fermi level to a broken-symmetry superconducting state with a high T_c .

7 Summary

The study of finite quantum systems is now one of the hot topics in physics and applied sciences. This is caused by two interconnected reasons. First of all, such systems find numerous technological applications. This, in turn, requires to know well their properties that are employed in all these applications. Hence, it is necessary to have reliable theories accurately describing these systems.

In addition to the importance of technological applications, finite quantum systems are extremely interesting by themselves. Being on the boundary between macroscopic

bulk systems and microscopic particles, they, from one side, share the properties of large statistical systems and, from another side, possess their own specific properties that are absent in infinite systems. The appropriate name for such intermediate systems is *mesoscopic*. And their properties is a combination of those of large statistical systems and of small quantum objects.

The system finiteness imposes on them general features that are common for all such systems, though they can be of rather different physical nature. From the first glance, such physically different systems as trapped atoms, quantum dots, atomic nuclei, and metallic grains do not seem to have much in common. However, they do share a number of common features, all of them being finite quantum systems.

The system finiteness immediately results in the quantization of spectra, which, in turn, leads to the appearance of properties differing these systems from macroscopic matter. Thus, collective excitations in finite systems are essentially different in the short-wave and long-wave parts, depending on the relation between the wave length and the effective system size. Collective excitations, whose wavelength is much shorter than the system size, behave as excitations in bulk matter, while those excitations, whose wavelength is comparable or larger than the system size, become discrete and essentially dependent on the system shape. These properties are common for all finite systems, whether these are trapped atoms, quantum dots, atomic nuclei, or metallic grains.

The system spectra are intimately connected with characteristic symmetries. The latter changes under phase transitions. Effects of spontaneous symmetry breaking, related to phase transitions, are different in finite systems and in bulk matter. Strictly speaking, rigorous symmetry breaking can occur only in infinite systems. But in mesoscopic systems, with sufficiently large number of particles, phase transitions can be rather sharp, similar to those in bulk matter. Therefore, it is possible to characterize such transitions by asymptotic symmetry breaking. Respectively, one can consider such phase transitions as Bose-Einstein condensation occurring in finite traps, or superconducting pairing arising in trapped atomic clouds, atomic nuclei, and metallic grains.

A specific type of transitions, typical only for finite systems, is the geometric transition, including shape transitions and orientation transitions. The shape transition is due to the important role of shape for the stability of finite systems. Such transitions, happening because of instability developing in a system, with given particle interactions, under a given shape, are common for trapped atoms and atomic nuclei.

Rotating clouds of trapped atoms are analogous to rotating nuclei, as well as to quantum dots with magnetic fields. Generally, the mathematical description of different finite objects is done by so similar Hamiltonians and methods that very often the results of a theory, developed for one type of finite objects, can be straightforwardly extended to another type. Since the theory of atomic nuclei is much older than the theories of trapped atoms, quantum dots, and metallic grains, many results, obtained earlier in nuclear theory and related to collective excitations and shape transitions, were extended to the description of trapped atoms, quantum dots, and metallic grains. The peculiarity of superconducting pairing, studied for atomic nuclei, could also be investigated for trapped atoms and metallic grains.

Our aim has been to show, in the frame of one review, that finite quantum systems of very different physical nature share a lot of common features that invoke similar mathematical methods. We hope that comparing the content of different chapters of the review,

the reader can come to this conclusion. Of course, since the objects, considered here, anyway, physically are quite different, they possess a variety of particular features that could have different interpretations and applications. It is, certainly, impossible to discuss the whole variety of these features. We concentrated here mainly on the common properties of finite quantum systems, related to the effects of symmetry breaking. All additional information can be found in the cited literature.

Acknowledgments

The authors are grateful to late D.L. Mills for his interest and support of our work. We appreciate many useful discussions and fruitful collaboration with V.S. Bagnato, W.D. Heiss, N.S. Simonović, and E.P. Yukalova. We are grateful for collaboration to D. Almed, M. Dineykan, F. Döna, M.D. Girardeau, H. Kleinert, J. Kvasil, K.P. Marzlin, E.R. Marshalek, T. Puente, J.-M. Rost, L. Serra, and A. Tsvetkov. We also thank K.N. Pichugin and E.N. Nazmitdinova for their help in the preparation of the manuscript. The work of J.L.B. received some partial support from the CUNY Faculty Research Award Program/Professional Staff Congress (CUNY FRAP/PSC). Two of the authors (R.G.N. and V.I.Y.) acknowledge financial support from the Russian Foundation for Basic Research.

A Two-dimensional harmonic oscillator in a perpendicular magnetic field

The electronic spectrum, generated by the Hamiltonian (4.1) without interaction, is determined by the sum $\sum_i^N h_i$ of the single-particle harmonic oscillator Hamiltonians $h = h_0 + h_z$ (see Section 2). The properties of the Hamiltonian h_z are well known [87]. The eigenvalue problem for the Hamiltonian h_0 can be solved using the transformation

$$\begin{pmatrix} x \\ y \\ V_x \\ V_y \end{pmatrix} = \begin{pmatrix} X_+ & X_+^* & X_- & X_-^* \\ Y_+ & Y_+^* & Y_- & Y_-^* \\ V_x^+ & V_x^{+\star} & V_x^- & V_x^{-\star} \\ V_y^+ & V_y^{+\star} & V_y^- & V_y^{-\star} \end{pmatrix} \begin{pmatrix} a_+ \\ a_+^\dagger \\ a_- \\ a_-^\dagger \end{pmatrix}. \quad (\text{A.1})$$

Here, $a_i^\pm(a_i)$ is a creation(annihilation) operator of a new mode $i = \pm$, with the following commutation relations

$$[a_i, a_j^+] = \delta_{i,j}, \quad [a_i, a_j] = [a_i^+, a_j^+] = 0. \quad (\text{A.2})$$

One can solve the equation of motion

$$[a_i, h_0] = \Omega_i a_i \quad (i = \pm) \quad (\text{A.3})$$

and express the Hamiltonian h_0 through the new normal modes

$$h_0 = \hbar\Omega_+(a_+^\dagger a_+ + 1/2) + \hbar\Omega_-(a_-^\dagger a_- + 1/2), \quad (\text{A.4})$$

where

$$\begin{aligned}\Omega_{\pm}^2 &= \frac{1}{2}(\omega_x^2 + \omega_y^2 + 4\omega_L^2 \pm \Delta) \\ \Delta &= \sqrt{(\omega_x^2 - \omega_y^2)^2 + 8\omega_L^2(\omega_x^2 + \omega_y^2) + 16\omega_L^4}.\end{aligned}\tag{A.5}$$

The coefficients of the transformation (A.1) can be expressed in terms of $\omega_x, \omega_y, \omega_L$ as well:

$$\begin{aligned}Y_{\pm} &= iy_{\pm}, \quad X_{\pm} = x_{\pm}, \quad x_{\pm} = 2\omega_L \frac{\Omega_{\pm}}{\Omega_{\pm}^2 - \omega_1^2 + \omega_L^2} y_{\pm}, \\ V_x^{\pm} &= -i\omega_L \frac{\Omega_{\pm}^2 + \omega_1^2 - \omega_L^2}{\Omega_{\pm}^2 - \omega_1^2 + \omega_L^2} y_{\pm} = -i\Omega_{\pm} \frac{\Omega_{\pm}^2 - \omega_2^2 - \omega_L^2}{\Omega_{\pm}^2 - \omega_2^2 + \omega_L^2} x_{\pm}, \\ V_y^{\pm} &= \Omega_{\pm} \frac{\Omega_{\pm}^2 - \omega_1^2 - \omega_L^2}{\Omega_{\pm}^2 - \omega_1^2 + \omega_L^2} y_{\pm} = \omega_L \frac{\Omega_{\pm}^2 + \omega_2^2 - \omega_L^2}{\Omega_{\pm}^2 - \omega_2^2 + \omega_L^2} x_{\pm}, \\ y_{\pm}^2 &= \pm \frac{\hbar}{2m\Omega_{\pm}} \frac{\Omega_{\pm}^2 - \omega_1^2 + \omega_L^2}{\Omega_{+}^2 - \Omega_{-}^2}, \\ x_{\pm}^2 &= \pm \frac{\hbar}{2m\Omega_{\pm}} \frac{\Omega_{\pm}^2 - \omega_2^2 + \omega_L^2}{\Omega_{+}^2 - \Omega_{-}^2}.\end{aligned}\tag{A.6}$$

The eigenstates of the Hamiltonian h_0 are

$$|n_+ n_-\rangle = \frac{1}{\sqrt{n_+! n_-!}} (a_+^{\dagger})^{n_+} (a_-^{\dagger})^{n_-} |00\rangle.\tag{A.7}$$

The operator l_z is diagonal in this basis,

$$l_z = n_- - n_+.\tag{A.8}$$

In the case of circular symmetry, i.e., $\omega_x = \omega_y = \omega_0$, the eigenstate Eq. (A.7) reduces to the form of the Fock-Darwin state (see [272]). Quite often, it is useful to invoke the representation of the Fock-Darwin state in cylindrical coordinates (ρ, φ) , which has the form

$$\Phi_{n_r m}(\rho, \varphi) = \frac{1}{\sqrt{2\pi}} \exp^{im\varphi} R_{n_r m}(\rho).\tag{A.9}$$

This state is an eigenfunction of the operator l_z , with an eigenvalue m and with the radius-dependent function of the form

$$\begin{aligned}R_{n_r m}(\rho) &= \frac{\sqrt{2}}{l_0^B} \sqrt{\frac{n_r!}{(n_r + |m|)!}} \left(\frac{\rho}{l_0^B}\right)^{|m|} \times \\ &\exp\left[-\frac{\rho^2}{2l_0^{B^2}}\right] \mathcal{L}_{n_r}^{|m|}\left(\frac{\rho^2}{l_0^{B^2}}\right).\end{aligned}\tag{A.10}$$

Here $l_0^{B^2} = \hbar/(2m^*\Omega)$, $\Omega = \sqrt{\omega_0^2 + \omega_L^2}$, and \mathcal{L} denotes the Laguerre polynomials

$$\mathcal{L}_n^{|m|}(x) = \sum_{k=0}^n \frac{(-1)^k}{k!} \binom{n + |m|}{n - k} x^k.\tag{A.11}$$

The pair of quantum numbers (n, m) and (n_+, n_-) are related as

$$n = n_+ + n_-, \quad m = n_- - n_+, \quad (\text{A.12})$$

with $n = 2n_r + |m|$. The single-particle energy in the Fock-Darwin state is

$$\varepsilon(n, m) = \hbar\Omega(n + 1) - \hbar\omega_L m = \hbar\Omega(2n_r + |m| + 1) - \hbar\omega_L m. \quad (\text{A.13})$$

The quantum number n is associated with the shell number N_{sh} for an N -electron quantum dot in the $2D$ approach.

References

- [1] V.I. Arnold, Phys. Usp. 42 (1999) 1205.
- [2] E.P. Wigner, Group Theory, Academic Press, New York, 1959.
- [3] M. Hamermesh, Group Theory, Addison-Wesley, Reading, 1964.
- [4] E.P. Wigner, Symmetries and Reflections, Indiana University, Bloomington, 1970.
- [5] J.L. Birman, Theory of Crystal Space Groups and Infra-Red and Raman Lattice Processes of Insulating Crystals, Springer, Berlin, 1974.
- [6] J.D. Louck, Unitary Symmetry and Combinatorics, World Scientific, Singapore, 2008.
- [7] P. Weiss, J. Phys. Theor. Appl. 6 (1907) 667.
- [8] L.D. Landau, J. Exp. Theor. Phys. 7 (1937) 19.
- [9] L.D. Landau, Collected Papers, Gordon and Breach, New York, 1967.
- [10] K. Huang, Statistical Mechanics, Wiley, New York, 1963.
- [11] A. Isihara, Statistical Physics, Academic Press, New York, 1971.
- [12] L.D. Landau, E.M. Lifshitz, Statistical Physics, Butterworth-Heinemann, Oxford, 1980.
- [13] M. Fisher, The Nature of Critical Points, University of Colorado, Boulder, 1965.
- [14] H.E. Stanley, Introduction to Phase Transitions and Critical Phenomena, Clarendon, Oxford, 1971.
- [15] S.K. Ma, Modern Theory of Critical Phenomena, Benjamin, London, 1976.
- [16] V.I. Yukalov, A.S. Shumovsky, Lectures on Phase Transitions, World Scientific, Singapore, 1990.
- [17] M. Keyl, Phys. Rep. 369 (2002) 431.

- [18] A. Vedral, *Rev. Mod. Phys.* 74 (2002) 197.
- [19] A. Galindo, M.A. Martin-Delgado, *Rev. Mod. Phys.* 74 (2002) 347.
- [20] V.I. Yukalov, *Phys. Rev. Lett.* 90 (2003) 167905.
- [21] V.I. Yukalov, *Phys. Rev. A* 68 (2003) 022109.
- [22] P. Ehrenfest, *Collected Scientific Papers*, North-Holland, Amsterdam, 1959.
- [23] M.V. Jaric, J.L. Birman, *J. Math. Phys.* 18 (1977) 1456.
- [24] L. Michel, *Rev. Mod. Phys.* 52 (1980) 617.
- [25] J.L. Birman, *Physica A* 114 (1982) 564.
- [26] D. Belitz, T.R. Kirkpatrick, T. Vojta, *Rev. Mod. Phys.* 77 (2005) 579.
- [27] V.L. Ginzburg, L.D. Landau, *J. Exp. Theor. Phys.* 20 (1950) 1064.
- [28] V.L. Ginzburg, *Rev. Mod. Phys.* 76 (2004) 981.
- [29] K.G. Wilson, J. Kogut, *Phys. Rep.* 12 (1974) 75.
- [30] M. Fisher, *Rev. Mod. Phys.* 46 (1974) 597.
- [31] K.G. Wilson, *Rev. Mod. Phys.* 47 (1975) 773.
- [32] M.N. Barber, *Phys. Rep.* 29 (1977) 1.
- [33] B. Hu, *Phys. Rep.* 91 (1982) 233.
- [34] N.N. Bogolubov, *Lectures on Quantum Statistics*, Gordon and Breach, New York, 1970, Vol. 2.
- [35] G.G. Emch, *Algebraic Methods in Statistical Mechanics and Quantum Field Theory*, Wiley, New York, 1972.
- [36] O. Bratteli, D.W. Robinson, *Operator Algebras and Quantum Statistical Mechanics*, Springer, New York, 1979.
- [37] J.G. Kirkwood, *Quantum Statistics and Cooperative Phenomena*, Gordon and Breach, New York, 1965.
- [38] N.N. Bogolubov, *Lectures on Quantum Statistics*, Gordon and Breach, New York, 1967, Vol. 1.
- [39] V.I. Yukalov, *Physica A* 108 (1981) 402.
- [40] V.I. Yukalov, *Int. J. Mod. Phys. B* 5 (1991) 3235.
- [41] P. Brout, *Phase Transitions*, Benjamin, New York, 1965.
- [42] N.N. Bogolubov, A.S. Shumovsky, V.I. Yukalov, *Theor. Math. Phys.* 60 (1984) 921.

- [43] V.I. Yukalov, Phys. Rep. 208 (1991) 395.
- [44] K.J. Strandburg, Rev. Mod. Phys. 60 (1988) 161.
- [45] V.I. Yukalov, Phys. Rev. A 72 (2005) 033608.
- [46] V.I. Yukalov, Laser Phys. 19 (2009) 1.
- [47] R. Kubo, 1968, Thermodynamics, North-Holland, Amsterdam.
- [48] R. Blinc, B. Zeks, Soft Modes in Ferroelectrics and Antiferroelectrics, North Holland, Amsterdam, 1974.
- [49] R.M. White, T.H. Geballe, Long Range Order in Solids, Academic, New York, 1979.
- [50] A. Scott, ed., Encyclopedia of Nonlinear Science, Routledge, New York, 2005.
- [51] J.M. Kosterlitz, D.J. Thouless, J. Phys. C 6 (1973) 1181.
- [52] J.M. Kosterlitz, J. Phys. C 7 (1974) 1046.
- [53] W. Janke, T. Matsui, Phys. Rev. B 42 (1990) 10673.
- [54] V.I. Yukalov, Laser Phys. Lett. 1 (2004) 435.
- [55] V.I. Yukalov, Laser Phys. Lett. 2 (2005) 156.
- [56] V.I. Yukalov, Phys. Lett. A 340 (2005) 369.
- [57] V.I. Yukalov, Phys. Rev. E 72 (2005) 066119.
- [58] M. Kac, Probability and Related Topics in Physical Sciences, Interscience, London, 1957.
- [59] O. Penrose, Rep. Prog. Phys. 42 (1979) 1937.
- [60] J.L. Lebowitz, Physica A 194 (1993) 1.
- [61] V.I. Yukalov, Moscow Univ. Phys. Bull. 25 (1970) 49.
- [62] V.I. Yukalov, Moscow Univ. Phys. Bull. 26 (1971) 22.
- [63] V.I. Yukalov, Physica A 234 (1997) 725.
- [64] V.I. Yukalov, Phys. Rev. E 65 (2002) 056118.
- [65] V.I. Yukalov, Phys. Lett. A 308 (2003) 313.
- [66] J.M. Deutsch, Phys. Rev. A 43 (1991) 2046.
- [67] M. Srednicki, J. Phys. A 32 (1999) 1163.
- [68] P. Reimann, Phys. Rev. Lett. 101 (2008) 190403.

- [69] M. Rigol, V. Dunjko, M. Olshanii, *Nature* 452 (2008) 854.
- [70] N.N. Bogolubov, *Problems of Dynamical Theory in Statistical Physics*, North-Holand, Amsterdam, 1962.
- [71] J.W. Gibbs, *Collected Works*, Longmans, New York, 1931, Vol. 2.
- [72] R.C. Tolman, *Phys. Rev.* 57 (1940) 1160.
- [73] D. ter Haar, *Rev. Mod. Phys.* 27 (1955) 289.
- [74] E. Jaynes, *Phys. Rev.* 106 (1957) 171.
- [75] P. Reimann, *New J. Phys.* 12 (2010) 055027.
- [76] J. Dziarmaga, *Adv. Phys.* 59 (2010) 1063.
- [77] A. Polkovnikov, K. Sengupta, A. Silva, M. Vengalattore, *Rev. Mod. Phys.* 83 (2011) 863.
- [78] V.I. Yukalov, *Laser Phys. Lett.* 8 (2011) 485.
- [79] R. Arias, P. Chu, D.L. Mills, *Phys. Rev. B* 71, (2005) 224410.
- [80] R. Arias, D.L. Mills, *Phys. Rev. B* 72 (2005) 104418.
- [81] D.L. Mills, *J. Magn. Magn. Mater.* 306 (2006) 16.
- [82] A.T. Costa, R.B. Muniz, D.L. Mills, *Phys. Rev. B* 74 (2006) 214403.
- [83] R.E. Arias, D.L. Mills, *Phys. Rev. B* 75 (2007) 214404.
- [84] H.A. Jahn, E. Teller, *Proc. Roy. Soc. London A* 161 (1937) 220.
- [85] I.B. Bersuker, *The Jahn-Teller Effect*, Cambridge University, Cambridge, 2006.
- [86] P. Cejnar, J. Jolie, R.F. Casten, *Rev. Mod. Phys.* 82 (2010) 2155.
- [87] L.D. Landau, E.M. Lifshitz, *Quantum Mechanics*, Butterworth-Heinemann, Oxford, 2003.
- [88] M.I. Petrashen, E.D. Trifonov, *Application of Group Theory in Quantum Mechanics*, Dover, New York, 2009.
- [89] M.C. O'Brien, C.C. Chancey, *Am. J. Phys.* 61 (1993) 688.
- [90] Q.C. Qiu, Y.M. Liu, C.A. Bates, J.L. Dunn, *Z. Phys. Chem.* 200 (1997) 103.
- [91] P. Alberto, F. Nogueira, H. Rocha, L.N. Vicente, *SIAM J. Opt.* 14 (2004) 1216.
- [92] K. Ziegler, *Phys. Rev. B* 72 (2005) 075120.
- [93] A.F. Wells, *Structural Inorganic Chemistry*, Oxford Science, Oxford, 1984.

- [94] F.A. Cotton, G. Wilkinson, C.A. Murillo, M. Bochmann, *Advanced Inorganic Chemistry*, Wiley, New York, 1999.
- [95] A.F. Hollman, E. Wiberg, *Inorganic Chemistry*, Academic, San Diego, 2001;
- [96] J. Clayden, N. Greeves, S. Warren, *Organic Chemistry*, Oxford University, Oxford, 2012.
- [97] R. Englman, *Jahn-Teller Effect in Molecules and Crystals*, Wiley, London, 1972.
- [98] M.D. Kaplan, G.O. Zimmerman, *Vibronic Interactions: Jahn-Teller Effect in Crystals and Molecules*, Springer, Berlin, 2001.
- [99] V.I. Yukalov, E.P. Yukalova, *Phys. Rev. A* 78 (2008) 063610.
- [100] V.I. Yukalov, E.P. Yukalova, *Phys. Lett. A* 373 (2009) 1301.
- [101] A.D. Bruce, R.A. Cowley, *Structural Phase Transitions*, Taylor and Francis, London, 1981.
- [102] S.V. Tyablikov, *Methods in Quantum Theory of Magnetism*, Springer, Berlin, 1995.
- [103] C. Mathews, K.E. Van Holde, *Biochemistry*, Benjamin Cummings, London, 1990.
- [104] K. Blaum, *Phys. Rep.* 425 (2006) 1.
- [105] V.I. Balykin, V.G. Minogin, V.S. Letokhov, *Rep. Prog. Phys.* 63 (2000) 1429.
- [106] V. Letokhov, *Laser Control of Atoms and Molecules*, Oxford University, New York, 2007.
- [107] S.N. Bose, *Z. Phys.* 26 (1924) 178.
- [108] A. Einstein, *Sitzber. Preuss. Akad. Wiss.* (1924) 261.
- [109] F. London, *Superfluids: Microscopic Theory of Superfluid Helium*, Dover, New York, 1954, Vol. 2.
- [110] F.H. Wirth, R.B. Hallock, *Phys. Rev. B* 35 (1987) 89.
- [111] M.H. Anderson, J.R. Ensher, M.R. Matthews, C.E. Wieman, E.A. Cornell, *Science* 269 (1995) 198.
- [112] K.B. Davis, M.O. Mewes, M.R. Andrews, N.J. van Druten, D.S. Durfee, D.M. Kurn, W. Ketterle, *Phys. Rev. Lett.* 75 (1995) 3969.
- [113] C.C. Bradley, C.A. Sackett, J.J. Tollett, R.G. Hulet, *Phys. Rev. Lett.* 75 (1995) 1687.
- [114] L. Pitaevskii, S. Stringari, *Bose-Einstein Condensation*, Clarendon, Oxford, 2003.
- [115] C.J. Pethick, H. Smith, *Bose-Einstein Condensation in Dilute Gases*, Cambridge University, Cambridge, 2008.

- [116] F. Dalfovo, S. Giorgini, L.P. Pitaevskii, S. Stringari, *Rev. Mod. Phys.* 71 (1999) 463.
- [117] P.W. Courteille, V.S. Bagnato, V.I. Yukalov, *Laser Phys.* 11 (2001) 659.
- [118] J.O. Andersen, *Rev. Mod. Phys.* 76 (2004) 599.
- [119] K. Bongs, K. Sengstock, *Rep. Prog. Phys.* 67 (2004) 907.
- [120] V.I. Yukalov, M.D. Girardeau, *Laser Phys. Lett.* 2 (2005) 375.
- [121] A. Posazhennikova, *Rev. Mod. Phys.* 78 (2006) 1111.
- [122] O. Morsch, M. Oberthaler, *Rev. Mod. Phys.* 78 (2006) 179.
- [123] C. Moseley, O. Fialko, K. Ziegler, *Ann. Phys. (Berlin)* 17 (2008) 561.
- [124] N.P. Proukakis, B. Jackson, *J. Phys. B* 41 (2008) 203002.
- [125] V.I. Yukalov, *Phys. Part. Nucl.* 42 (2011) 460.
- [126] O. Penrose, L. Onsager, *Phys. Rev.* 104 (1956) 576.
- [127] A.J. Coleman, V.I. Yukalov, *Reduced Density Matrices*, Springer, Berlin, 2000.
- [128] V.I. Yukalov, *Laser Phys. Lett.* 4 (2007) 632.
- [129] F.A. Berezin, *Method of Second Quantization*, Academic Press, New York, 1966.
- [130] J. Ginibre, *Commun. Math. Phys.* 8 (1968) 26.
- [131] G. Roepstorff, *J. Stat. Phys.* 18 (1978) 191.
- [132] A. Süto, *Phys. Rev. A* 71 (2005) 023602.
- [133] E.H. Lieb, R. Seiringer, J.P. Solovej, J. Yngvason, *The Mathematics of the Bose Gas and Its Condensation*, Birkhauser, Basel, 2005.
- [134] J.W. Gibbs, *Collected Works*, Longmans, New York, 1928, Vol. 1.
- [135] A. Leggett, *Quantum Liquids*, Oxford University, New York, 2006.
- [136] N.N. Bogolubov, *J. Phys. (Moscow)* 11 (1947) 23.
- [137] H. Umezawa, H. Matsumoto, M. Tachiki, *Thermo Field Dynamics and Condensed States*, North-Holland, Amsterdam, 1982.
- [138] V.I. Yukalov, *Laser Phys.* 16 (2006) 511.
- [139] V.I. Yukalov, *Laser Phys. Lett.* 3 (2006) 406.
- [140] V.I. Yukalov, *Phys. Lett. A* 359 (2006) 712.
- [141] V.I. Yukalov, *Ann. Phys. (N.Y.)* 323 (2008) 461.

- [142] P.C. Hohenberg, P.C. Martin, *Ann. Phys. (N.Y.)* 34 (1965) 291.
- [143] N.M. Hugenholtz, D. Pines, *Phys. Rev.* 116 (1959) 489.
- [144] V.I. Yukalov, *Phys. Lett. A* 375 (2011) 2797.
- [145] V.I. Yukalov, H. Kleinert, *Phys. Rev. A* 73 (2006) 063612.
- [146] V.I. Yukalov, E.P. Yukalova, *Phys. Rev. A* 74 (2006) 063623.
- [147] V.I. Yukalov, E.P. Yukalova, *Phys. Rev. A* 76 (2007) 013602.
- [148] E.P. Gross, *Phys. Rev.* 106 (1957) 161.
- [149] E.P. Gross, *Ann. Phys. (N.Y.)* 4 (1958) 57.
- [150] E.P. Gross, *Nuovo Cimento* 20 (1961) 454.
- [151] L.P. Pitaevskii, *J. Exp. Theor. Phys.* 13 (1961) 451.
- [152] J.R. Klauder, B.S. Skagerstam, *Coherent States*, World Scientific, Singapore, 1985.
- [153] D. ter Haar, *Lectures on Selected Topics in Statistical Mechanics*, Pergamon, Oxford, 1977.
- [154] V.I. Yukalov, E.P. Yukalova, *Phys. Rev. A* 72 (2005) 063611.
- [155] A. Griesmaier, J. Werner, S. Hensler, J. Stuhler, T. Pfau, *Phys. Rev. Lett.* 94 (2005) 160401.
- [156] M.A. Baranov, *Phys. Rep.* 464 (2008) 71.
- [157] E. Timmermans, P. Tommasini, M. Hussein, A.K. Kerman, *Phys. Rep.* 315 (1999) 199.
- [158] R.A. Duine, H.T.C. Stoof, *Phys. Rep.* 396 (2004) 115.
- [159] T. Köhler, K. Góral, P.S. Julienne, *Rev. Mod. Phys.* 78 (2006) 1311.
- [160] V.A. Yurovsky, M. Olshanii, D.S. Weiss, *Adv. At. Mol. Opt. Phys.* 55 (2008) 61.
- [161] S. Giorgini, L.P. Pitaevskii, S. Stringari, *J. Low Temp. Phys.* 109 (1997) 309.
- [162] R. Ozeri, N. Katz, J. Steinhauer, N. Davidson, *Rev. Mod. Phys.* 77 (2005) 187.
- [163] J. Gavoret and P. Nozières, *Ann. Phys. (N.Y.)* 28 (1964) 349.
- [164] J. Goldstone, *Nuovo Cimento* 19 (1961) 154.
- [165] S. Stringari, *Phys. Rev. Lett.* 77 (1996) 2360.
- [166] M. Fliesser, A. Csordás, P. Szépfalusy, R. Graham, *Phys. Rev. A* 56 (1997) 2533.
- [167] S. Stringari, *Phys. Rev. A* 58 (1998) 2385.

- [168] A. Bohr, B.R. Mottelson, Nuclear Structure, Benjamin, New York, 1975, Vol. 2.
- [169] T. Suzuki, D.J. Rowe, Nucl. Phys. A 289 (1977) 461.
- [170] K. Heyde, P. von Neumann-Cosel, A. Richter, Rev. Mod. Phys. 82 (2010) 2365.
- [171] N.D. Mermin, H. Wagner, Phys. Rev. Lett. 17 (1966) 1133.
- [172] E.M. Lifshitz, L.P. Pitaevskii, Statistical Physics, Butterworth-Heinemann, Oxford, 1980.
- [173] L. Wasserman, Thermal Physics, Cambridge University, Cambridge, 2011.
- [174] W. Ketterle, N.J. van Druten, Phys. Rev. A 54 (1996) 656.
- [175] B. Klünder, A. Pelster, Eur. Phys. J. B 68 (2009) 457.
- [176] V.S. Bagnato, D. Kleppner, Phys. Rev. A 44 (1991) 7439.
- [177] W.J. Mullin, J. Low Temp. Phys. 106 (1997) 615.
- [178] J. Carrasquilla, M. Rigol, arXiv:1205.6484 (2012).
- [179] V.I. Yukalov, Laser Phys. Lett. 7 (2010) 831.
- [180] N. Shohno, Prog. Theor. Phys. 31 (1964) 553.
- [181] S.T. Beliaev, J. Exp. Theor. Phys. 7 (1958) 289.
- [182] V.N. Popov, Functional Integrals in Quantum Field Theory and Statistical Physics, Reidel, Dordrecht, 1983.
- [183] V.N. Popov, Functional Integrals and Collective Modes, Cambridge University, New York, 1987.
- [184] H.M. Wiseman, Phys. Rev. A 56 (1997) 2068.
- [185] B. Kneer, T. Wong, K. Vogel, W.P. Schleich, D.F. Walls, Phys. Rev. A 58 (1998) 4841.
- [186] V.I. Yukalov, Phys. Rev. A 56 (1997) 5004.
- [187] N.E. Rehler, J.H. Eberly, Phys. Rev. A 3 (1971) 1735.
- [188] A.S. Parkins, D.F. Walls, Phys. Rep. 303 (1998) 1.
- [189] Y.A. Nepomnyashchy, Theor. Math. Phys. 20 (1974) 904.
- [190] V.I. Yukalov, Acta Phys. Pol. A 57 (1980) 295.
- [191] V.I. Yukalov, E.P. Yukalova, Laser Phys. Lett. 1 (2004) 50.
- [192] H. Takeuchi, S. Ishino, M. Tsubota, Phys. Rev. Lett. 105 (2010) 205301.

- [193] L.D. Landau, E.M. Lifshitz, *Mechanics*, Pergamon, Oxford, 1960.
- [194] V. Fock, *Z. Phys.* 47 (1928) 446.
- [195] D.A. Butts, D.S. Rokhsar, *Nature* 397 (1999) 327.
- [196] A.A. Abrikosov, *J. Exp. Theor. Phys.* 32 (1957) 1442.
- [197] M.V. Berry, *Proc. Roy. Soc. A* 392 (1984) 45.
- [198] I. Bloch, J. Dalibard, W. Zwerger, *Rev. Mod. Phys.* 80 (2008) 885.
- [199] N.R. Cooper, *Adv. Phys.* 57 (2008) 539.
- [200] A.L. Fetter, *Rev. Mod. Phys.* 81 (2009) 647.
- [201] H. Saarikoski, S.M. Reimann, A. Harju, M. Manninen, *Rev. Mod. Phys.* 82 (2010) 2785.
- [202] V.I. Yukalov, E.P. Yukalova, and V.S. Bagnato, *Phys. Rev. A* 56 (1997) 4845.
- [203] V.I. Yukalov, E.P. Yukalova, V.S. Bagnato, *Phys. Rev. A* 66 (2002) 043602.
- [204] V.I. Yukalov, K.P. Marzlin, E.P. Yukalova, *Phys. Rev. A* 69 (2004) 023620.
- [205] L. Mandel, E. Wolf, *Optical Coherence and Quantum Optics*, Cambridge University, Cambridge, 1995.
- [206] G.C. Baldwin, J.C. Solem, V.I. Goldanskii, *Rev. Mod. Phys.* 53 (1981) 687.
- [207] P. Slichter, *Principles of Magnetic Resonance*, Springer, Berlin, 1980.
- [208] E.R. Ramos, E.A. Henn, J.A. Seman, M.A. Caracanhas, K.M. Magalhães, K. Helmerson, V.I. Yukalov, V.S. Bagnato, *Phys. Rev. A* 78 (2008) 063412.
- [209] V.I. Yukalov, V.S. Bagnato, *Laser Phys. Lett.* 6 (2009) 399.
- [210] S.K. Adhikari, *Phys. Lett. A* 308 (2003) 302.
- [211] S.K. Adhikari, *Phys. Rev. A* 69 (2004) 063613.
- [212] E.R. Ramos, L. Sanz, V.I. Yukalov, V.S. Bagnato, *Phys. Rev. A* 76 (2007) 033608.
- [213] J. Williams, R. Walser, J. Cooper, E.A. Cornell, M. Holland, *Phys. Rev. A* 61 (2000) 033612.
- [214] E.B. Sonin, *Rev. Mod. Phys.* 59 (1987) 87.
- [215] B.V. Svistunov, *Phys. Rev.* 52 (1995) 3647.
- [216] S.K. Nemirovskii, W. Fiszdon, *Rev. Mod. Phys.* 67 (1995) 37.
- [217] W.F. Vinen, J.J. Niemela, *J. Low Temp. Phys.* 128 (2002) 167.

- [218] W.F. Vinen, J. Low Temp. Phys. 145 (2006)7.
- [219] M. Tsubota, J. Phys. Soc. Jap. 77 (2008) 111006.
- [220] M. Tsubota, K. Kasamatsu, M. Kobayashi, arXiv:1004.5458 (2010).
- [221] M. Tsubota, M. Kobayashi, H. Takeuchi, arXiv:1208.0422 (2012).
- [222] E.A. Henn, J.A. Seman, G. Roati, K.M. Magalhães, V.S. Bagnato, Phys. Rev. Lett. 103 (2009) 045301.
- [223] R.F. Shiozaki, G.D. Telles, V.I. Yukalov, V.S. Bagnato, Laser Phys. Lett. 8 (2011) 393.
- [224] J.A. Seman, E.A. Henn, R.F. Shiozaki, G. Roati, F.J. Poveda-Cuevas, K.M. Magalhães, V.I. Yukalov, M. Tsubota, M. Kobayashi, K. Kasamatsu, V.S. Bagnato, Laser Phys. Lett. 8 (2011) 691.
- [225] B.B. Mandelbrot, The Fractal Geometry of Nature, Freeman, New York, 1983.
- [226] V.I. Yukalov, Int. J. Mod. Phys. B 17 (2003) 2333.
- [227] L.D. Landau, E.M. Lifshitz, Fluid Mechanics, Butterworth-Heinemann, Oxford, 1987.
- [228] D. ter Haar, V.N. Tsytovich, Phys. Rep. 73 (1981) 175.
- [229] V.E. Zakharov, S.L. Musher, A.M. Rubenchik, Phys. Rep. 129 (1985) 285.
- [230] S. Giorgini, L.P. Pitaevskii, S. Stringari, Rev. Mod. Phys. 80 (2008) 1215.
- [231] W. Ketterle, M.W. Zwierlein, Riv. Nuovo Cimento 31 (2008) 247.
- [232] F. Chevy, C. Mora, Rep. Prog. Phys. 73 (2010) 112401.
- [233] C. Chin, R. Grimm, P. Julienne, E. Tiesinga, Rev. Mod. Phys. 82 (2010) 1225.
- [234] J. Stenger, S. Inouye, M.R. Andrews, H.J. Miesner, D.M. Stamper-Kurn, W. Ketterle, Phys. Rev. Lett. 82 (1999) 2422.
- [235] J. Bardeen, L.N. Cooper, J.R. Schrieffer, Phys. Rev. 108 (1957) 1175.
- [236] E. Timmermans, K. Furuya, P.W. Milloni, A.K. Kerman, Phys. Lett. A 285 (2001) 228.
- [237] M. Holland, S.J. Kokkelmans, M.L. Chiofalo, R. Walser, Phys. Rev. Lett. 87 (2001) 120406.
- [238] G.V. Skorniakov, K.A. Ter-Martirosian, J. Exp. Theor. Phys. 4 (1957) 648.
- [239] D.S. Petrov, Phys. Rev. A 67 (2003) 010703.
- [240] D.S. Petrov, C. Salomon, G.V. Shlyapnikov, Phys. Rev. Lett. 93 (2004) 090404.

- [241] A. Perali, P. Pieri, L. Pisani, G.C. Strinati, *Phys. Rev. Lett.* 92 (2004) 220404.
- [242] D. Belitz, T.R. Kirkpatrick, *Rev. Mod. Phys.* 66 (1994) 261.
- [243] T.D. Stanescu, C. Zhang, V. Galitski, *Phys. Rev. Lett.* 99 (2007) 110403.
- [244] T.D. Stanescu, B. Anderson, V. Galitski, *Phys. Rev. A* 78 (2008) 023616.
- [245] L. Keldysh, A.N. Kozlov, *JETP Lett.* 27 (1968) 521.
- [246] W. Kohn, D. Sherrington, *Rev. Mod. Phys.* 42 (1970) 1.
- [247] L.V. Butov, *Solid State Commun.* 127 (2003) 89.
- [248] J.P. Eisenstein, A.H. MacDonald, *Nature* 432 (2004) 691.
- [249] H. Deng, G. Weihs, C. Santory, J. Bloch, Y. Yamamoto, *Science* 298 (2002) 199.
- [250] J. Keeling, F.M. Marchetti, M.H. Szymanska, P.B. Littlewood, *Semicond. Sci. Technol.* 22 (2007) 1.
- [251] M.H. Szymanska, J. Keeling, P.B. Littlewood, *Phys. Rev. B* 75 (2007) 195331.
- [252] J. Klaers, J. Schmitt, F. Vewinger, M. Weitz, *Nature* 468 (2010) 545.
- [253] T. Matsubara, H. Matsuda, *Prog. Theor. Phys.* 16 (1956) 569.
- [254] E.G. Batyev, L.S. Braginskii, *J. Exp. Theor. Phys.* 60 (1984) 781.
- [255] D.L. Mills, *Phys. Rev. Lett.* 98 (2007) 039701.
- [256] T. Holstein, H. Primakoff, *Phys. Rev.* 58 (1940) 1098.
- [257] A. Rückriegel, A. Kreisel, P. Kopietz, *Phys. Rev. B* 85 (2012) 054422.
- [258] S.O. Demokritov, V.E. Demidov, O. Dzyapko, G.A. Melkov, A.A. Serga, B. Hillebrands, A.N. Slavin, *Nature* 443 (2006) 430.
- [259] V.E. Demidov, O. Dzyapko, S.O. Demokritov, G.A. Melkov, A.N. Slavin, *Phys. Rev. Lett.* 100 (2008) 047205.
- [260] G.E. Volovik, *J. Low Temp. Phys.* 153 (2008) 266.
- [261] Y.M. Bunkov, G.E. Volovik, *J. Phys. Condens. Matter* 22 (2010) 164210.
- [262] V.I. Yukalov, *Phys. Rev. Lett.* 75 (1995) 3000.
- [263] V.I. Yukalov, *Phys. Rev. B* 53 (1996) 9232.
- [264] V.I. Yukalov, E.P. Yukalova, *Phys. Part. Nucl.* 35 (2004) 348.
- [265] V.I. Yukalov, *Phys. Rev. B* 71 (2005) 184432.
- [266] V.I. Yukalov, E.P. Yukalova, *Laser Phys. Lett.* 8 (2011) 804.

- [267] S. Sachdev, R.N. Bhatt, Phys. Rev. B 41 (1990) 9323.
- [268] N.N. Bogolubov, Lectures on Quantum Statistics, Ryadyanska Shkola, Kiev, 1949.
- [269] J. Schwinger, On Angular Momentum, US Atomic Energy Commission, Washington, 1952.
- [270] M.A. Kastner, Phys. Today 46 (1993) 24.
- [271] R.C. Ashoori, Nature (London) 379 (1996) 413.
- [272] L. Jacak, P. Hawrylak, A. Wojs, Quantum Dots, Springer, Berlin, 1998.
- [273] L.P. Kouwenhoven, D.G. Austing, S. Tarucha, Rep. Prog. Phys. 64 (2001) 701.
- [274] T. Ihn, Semiconductor Nanostructures. Quantum States and Electronic Transport, Oxford University, New York, 2010.
- [275] T. Chakraborty, Quantum Dots: A Survey of the Properties of Artificial Atoms, North-Holland, Amsterdam, 1999.
- [276] P.A. Maksym, H. Imamura, G.P. Mallon, H. Aoki, J. Phys. Condens. Matter 12 (2000) R299.
- [277] S.M. Reimann, M. Manninen, Rev. Mod. Phys. 74 (2002) 1283.
- [278] C. Yannouleas, U. Landman, Rep. Prog. Phys. 70 (2007) 2067.
- [279] J.M. Elzerman, R. Hanson, L.H.W. van Beveren, S. Tarucha, L.M.K. Vandersypen, L.P. Kouwenhoven, in: W.D. Heiss (Ed.), Lecture Notes in Physics 667, Springer, Berlin, 2005, p. 25.
- [280] R. Hanson, L.P. Kouwenhoven, J.R. Petta, S. Tarucha, L.M.K. Vandersypen, Rev. Mod. Phys. 79 (2007) 1217.
- [281] M.J. Biercuk, D.J. Reilly, Nat. Nanotech. 6 (2011) 9.
- [282] L.P. Kouwenhoven, C.M. Marcus, P.L. McEuen, S. Tarucha, R.M. Westervelt, N.S. Wingreen, in: L.L. Sohn, L.P. Kouwenhoven, and G. Schön (Eds.), Mesoscopic Electron Transport, Proceedings of the NATO Advanced Study Institute on Mesoscopic Electron Transport, Series E345, Kluwer, Dordrecht/Boston, 1997, p.105.
- [283] Ch. Sikorski, U. Merkt, Phys. Rev. Lett. 62 (1989) 2164.
- [284] C.G. Darwin, Proc. Cambridge Philos. Soc. 27 (1930) 86.
- [285] W. Kohn, Phys. Rev. 123 (1961) 1242.
- [286] L. Brey, N.F. Johnson, B.I. Halperin, Phys. Rev. B 40 (1989) 10647.
- [287] Q.P. Lie, K. Karrai, S.K. Yip, S. Das Sarma, H.D. Drew, Phys. Rev. B 43 (1991) 5151.

- [288] T. Demel, D. Heitmann, P. Grambow, K. Ploog, Phys. Rev. Lett. 64 (1990) 788.
- [289] B. Meurer, D. Heitmann, K. Ploog, Phys. Rev. B 48 (1993) 11488.
- [290] V. Gudmundsson, R.R. Gerhardts, Phys. Rev. B 43 (1991) 12098.
- [291] D. Pfannkuche, R.R. Gerhardts, Phys. Rev. B 44 (1991) 13132.
- [292] M. Dineykhan, S.A. Zhaugasheva, R.G. Nazmitdinov, Zh. Eksp. Teor. Fiz. 119 (2001) 1210 [JETP 92 (2001) 1049].
- [293] S. Tarucha, D.G. Austing, T. Honda, R.J. van der Hage, L.P. Kouwenhoven, Phys. Rev. Lett. 77 (1996) 3613.
- [294] Y. Nishi, P.A. Maksym, D.G. Austing, T. Hatano, L.P. Kouwenhoven, H. Aoki, S. Tarucha, Phys. Rev. B 74 (2006) 033306.
- [295] Y. Nishi, Y. Tokura, J. Gupta, G. Austing, S. Tarucha, Phys. Rev. B 75 (2007) 121301(R).
- [296] M. Macucci, K. Hess, G.J. Iafrate, Phys. Rev. B 48 (1993) 17354.
- [297] M. Macucci, K. Hess, G.J. Iafrate, J. Appl. Phys. 77 (1995) 3267.
- [298] W.D. Heiss, R.G. Nazmitdinov, Phys. Lett. A 222 (1996) 309.
- [299] A. Wojs, P. Hawrylak, S. Fafard, L. Jacak, Phys. Rev. B 54 (1996) 5604.
- [300] M. Dineykhan, R.G. Nazmitdinov, Phys. Rev. B 55 (1997) 13707.
- [301] M. Fujito, A. Natori, H. Yasunaga, Phys. Rev. B. 53 (1996) 9952.
- [302] Y.H. Zeng, B. Goodman, R.A. Serota, Phys. Rev. B 47 (1993) 15660.
- [303] A. Wojs, P. Hawrylak, Phys. Rev. B 53 (1996) 10841.
- [304] W.A. de Heer, Rev. Mod. Phys. 65 (1993) 611.
- [305] M. Brack, Rev. Mod. Phys. 65 (1993) 677.
- [306] U. Nähera, S. Bjørnholm, S. Frauendorf, F. Garcias, C. Guete, Phys. Rep. 285 (1997) 245.
- [307] W.D. Heiss, R.G. Nazmitdinov, Phys. Rev. B 55 (1997) 16310.
- [308] R.P. Feynman, Phys. Rev. 56 (1939) 340.
- [309] I.V. Zozulenko, A.S. Sachrajda, C. Could, K.-F. Berggren, P. Zawadzki, Y. Feng, Z. Wasilewski, Phys. Rev. Lett. 83 (1999) 1838.
- [310] D. Hirose, N. Wingreen, Phys. Rev. B 59 (1999) 4604.
- [311] W.D. Heiss, R.G. Nazmitdinov, Pis'ma Zh. Eksp. Teor. Fiz. 68 (1998) 870 [JETP Lett. 68 (1998) 915].

- [312] R.C. Ashoori, H.L. Stormer, J.S. Weiner, L.N. Pfeiffer, K.W. Baldwin, K.W. West, Phys. Rev. Lett. 71 (1993) 613.
- [313] B. Su, V.J. Goldman, J.E. Cunningham, Phys. Rev. B. 46 (1992) 7644.
- [314] T. Schmidt, M. Tewordt, R.H. Blick, R.J. Haug, D. Pfannkuche, K. von Klitzing, A. Förster, H. Lüth, Phys. Rev. B 51 (1995) 5570.
- [315] Yu.Ts. Oganessian, J. Phys. G 34 (2007) R165.
- [316] L. Stavsetra, K.E. Gregorich, J. Dvorak, P.A. Ellison, I. Dragojević, M.A. Garcia, H. Nitsche, Phys. Rev. Lett. 103 (2009) 132502.
- [317] S.G. Nilsson, I. Ragnarsson, Shapes and Shells in Nuclear Structure, Cambridge University, Cambridge, 1995.
- [318] M.B. Tavernier, E. Anisimovas, F.M. Peeters, B. Szafran, J. Adamowski, S. Bednarek, Phys. Rev. B 68 (2003) 205305.
- [319] F.M. Peeters, V.A. Schweigert, Phys. Rev. B 53 (1996) 1468.
- [320] W.D. Heiss, R.G. Nazmitdinov, Physica D 118 (1998) 134.
- [321] G. Hackenbroich, W.D. Heiss, H.A. Weidenmuller, Phys. Rev. Lett. 79 (1997) 127.
- [322] I. Hamamoto, B.R. Mottelson, Phys. Rev. C 79 (2009) 034317.
- [323] W.D. Heiss, R.G. Nazmitdinov, Phys. Rev. Lett. 73 (1994) 1235.
- [324] B.L. Altshuler, Y. Gefen, Y. Imry, Phys. Rev. Lett. 66 (1991) 88.
- [325] B.L. Altshuler, Y. Gefen, Y. Imry, G. Montambaux, Phys. Rev. B 47 (1993) 10335.
- [326] F. von Oppen, Phys. Rev. B 50 (1994) 17151.
- [327] K. Richter, D. Ulmo, R. Jalabert, Phys. Rep. 276 (1996) 1.
- [328] M.O. Terra, M.L. Tiago, M.A.M. de Aguiar, Phys. Rev. E 58 (1998) 5146.
- [329] D. Yoshioka, H. Fukuyama, J. Phys. Soc. Jap. 61 (1992) 2368.
- [330] P.A. Maksym, T. Chakraborty, Phys. Rev. B 45 (1992) 1947.
- [331] M. Wagner, U. Merkt, A.V. Chaplik, Phys. Rev. B 45 (1992) 1951.
- [332] D. Pfannkuche, V. Gudmundsson, P. Maksym, Phys. Rev. B 47 (1993) 2244.
- [333] S. Kais, D.R. Herschbach, R.D. Levine, J. Chem. Phys. 91 (1989) 7791.
- [334] M. Taut, Phys. Rev. A 48 (1993) 3561.
- [335] A. Turbinder, Phys. Rev. A 50 (1994) 5335.
- [336] J.-L. Zhu, J.-Z. Yu, Z.-Q. Li, Y. Kawazoe, J. Phys. Condens. Matter 8 (1996) 7857.

- [337] P.S. Drouvelis, P. Schmelcher, F.K. Diakonov, Phys. Rev. B 69 (2004) 035333.
- [338] P. Kościk, A. Okopińska, J. Phys. A 40 (2007) 1045.
- [339] M. Taut, J. Phys. A 27 (1994) 1045.
- [340] Yu.E. Lozovik, V.D. Mur, N.B. Narozhnyi, Zh. Eksp. Teor. Fiz. 123 (2003) 1059 [JETP 96 (2003) 932].
- [341] B.S. Kandemir, J. Math. Phys. 46 (2005) 032110.
- [342] M. Dineykhon, R.G. Nazmitdinov, J. Phys. Condens. Matter 11 (1999) L83.
- [343] F. Grossmann, T. Kramer, J. Phys. A 44 (2011) 445309.
- [344] W. Zhu, S.B. Trickey, Phys. Rev. A 72 (2005) 022501.
- [345] N.S. Simonović, R.G. Nazmitdinov, Phys. Rev. B 67 (2003) 041305(R).
- [346] W. Zhu, S.B. Trickey, J. Chem. Phys. 125 (2006) 094317.
- [347] K. Bohlin, Bull. Astron. 28 (1911) 144.
- [348] T. Levi-Civita, Oper. Math. 2 (1906) 411.
- [349] P. Kustaanheimo, E. Stiefel, J. Reine. Angew. Math. 218 (1965) 204.
- [350] A. Hurwitz, Mathematische Werke, Vol. 2, Birkhäuser, Basel, 1933, p.641.
- [351] C.J. Zeng, K.-L. Su, M. Li, Phys. Rev. A G50 (1994) 4373.
- [352] J.M. Jauch, E.L. Hill, Phys. Rev. 57 (1940) 641.
- [353] Yu.N. Demkov, Sov. Phys. JETP 17 (1963) 1349.
- [354] F. Duimio, G. Zambotti, Nuovo Cimento 43 (1966) 1203.
- [355] R.A. Brandt, O.W. Greenberg, J. Math. Phys. 10 (1969) 1168.
- [356] I. Vendramin, Nuovo Cimento 54 (1968) 190.
- [357] G. Maiella, G. Vilasi, Lett. Nuovo Cimento 1 (1969) 57.
- [358] A. Cisneros, H.V. McIntosh, J. Math. Phys. 11 (1970) 870.
- [359] W. Nazarewicz, J. Dobaczewski, Phys. Rev. Lett. 68 (1992) 154.
- [360] J.P. Elliott, Proc. Roy. Soc. London A 245 (1958) 128.
- [361] M. Bander, C. Itzykson, Rev. Mod. Phys. 38 (1996) 330.
- [362] R. Blümel, C. Kappler, W. Quint, H. Walther, Phys. Rev. A 40 (1989) 808.
- [363] Y. Alhassid, E.A. Hinds, D. Meschede, Phys. Rev. Lett. 59 (1987) 1545.

- [364] R.G. Nazmitdinov, N.S. Simonović, J.-M. Rost, Phys. Rev. B 65 (2002) 155307.
- [365] I.V. Komarov, L.I. Ponomarev, S.Yu. Slavyanov, Spheroidal and Coulomb Spheroidal Functions, Nauka, Moscow, 1976.
- [366] M. Rontani, F. Rossi, F. Manghi, E. Molinari, Phys. Rev. B 59 (1999) 10165.
- [367] N.A. Bruce, P.A. Maksym, Phys. Rev. B 61 (2000) 4718.
- [368] L.P. Kouwenhoven, T.H. Oosterkamp, M.W.S. Danoesastro, M. Eto, D.G. Austig, T. Honda, S. Tarucha, Science 278 (1997) 1788.
- [369] J.J. Palacios, L. Martin-Moreno, G. Chiappe, E. Louis, C. Tejedor, Phys. Rev. B 50 (1994) 5760.
- [370] A.H. MacDonald, S.-R. Eric Yang, M.D. Johnson, Aus. J. Phys. 46 (1993) 345.
- [371] P.A. Maksym, T. Chakraborty, Phys. Rev. Lett. 65 (1990) 108.
- [372] P. Hawrylak, Phys. Rev. Lett. 71 (1993) 3347.
- [373] C. Ellenberger, T. Ihn, C. Yannouleas, U. Landman, K. Ensslin, D. Driscoll, A.C. Gossard, Phys. Rev. Lett. 96 (2006) 126806.
- [374] D.V. Melnikov, J.-P. Leburton, Phys. Rev. B 73 (2006) 085320.
- [375] R.G. Nazmitdinov, N.S. Simonović, Phys. Rev. B 76 (2007) 193306.
- [376] E.P. Wigner, Phys. Rev. B 46 (1934) 1002.
- [377] P.A. Maksym, Physica B 184 (1993) 385.
- [378] H.-M. Müller, S.E. Koonin, Phys. Rev. B 54 (1996) 14532.
- [379] C. Yannouleas, U. Landman, Phys. Rev. Lett. 85 (2000) 1726.
- [380] B. Szafran, S. Bednarek, J. Adamowski, J. Phys. Condens. Matter 15 (2003) 4189.
- [381] C. Creffield, W. Häusler, J.H. Jefferson, S. Sakar, Phys. Rev. B 59 (1999) 10719.
- [382] A. Puente, Ll. Serra, R.G. Nazmitdinov, Phys. Rev. B 69 (2004) 125315.
- [383] C. Yannouleas, U. Landman, Phys. Rev. B 69 (2004) 113306.
- [384] N.S. Simonović, R.G. Nazmitdinov, Phys. Rev. A 78 (2008) 032115.
- [385] A.J. Lichtenberg, M.A. Liberman, Regular and Stochastic Motion, Springer, New York, 1983,.
- [386] I.S. Gradshteyn, I.M. Ryzhik, Table of Integrals, Series, and Products, Academic Press, New York, 1994, pp.898,1096.
- [387] D.M. Zumbühl, C.M. Marcus, M.P. Hanson, A.C. Gossard, Phys. Rev. Lett. 93 (2004) 256801.

- [388] M. Eto, Jpn. J. Appl. Phys. 36 (1997) 3924.
- [389] S.A. Mikhailov, Phys. Rev. B 65 (2002) 115312.
- [390] S.A. Mikhailov, Phys. Rev. B 66 (2002) 153313.
- [391] B. Szafran, F.M. Peeters, S. Bednarek, J. Adamowski, Phys. Rev. B 69 (2004) 125344.
- [392] M. Rontani, C. Cavazzoni, D. Bellucci, G. Goldon, J. Chem. Phys 124 (2006) 124102.
- [393] R. Egger, W. Häusler, C.H. Mak, H. Grabert, Phys. Rev. Lett. 82 (1999) 3320.
- [394] A.V. Filinov, M. Bonitz, Y.E. Lozovik, Phys. Rev. Lett. 86 (2001) 3851.
- [395] F. Pederiva, C.J. Umrigar, E. Lipparini, Phys. Rev. B 62 (2000) 8120.
- [396] F. Pederiva, C.J. Umrigar, E. Lipparini, Phys. Rev. B 68 (2003) 089901.
- [397] A. Ghosal, A.D. Güçlü, C.J. Umrigar, D. Ulmo, H.U. Baranger, Phys. Rev. B. 76 (2007) 085341.
- [398] L. Zeng, W. Geist, W.Y. Ruan, C.J. Umrigar, M.Y. Chou, Phys. Rev. B 79 (2009) 235334.
- [399] E. Lipparini, Modern Many-Particle Physics: Atomic Gases, Quantum Dots and Quantum Fluids, World Scientific, Singapore, 2008.
- [400] R.J. Bartlett, M. Musial, Rev. Mod. Phys. 79 (2007) 291.
- [401] T.M. Henderson, K. Runge, R.J. Bartlett, Chem. Phys. Lett. 337 (2001) 138.
- [402] D.J. Rowe, Nuclear Collective Motion, Methuen, London, 1970.
- [403] P. Ring, P. Schuck, The Nuclear Many-Body Problem, Springer, New York, 1980.
- [404] J.P. Blaizot, G. Ripka, Quantum Theory of Finite Systems, MIT, Cambridge, 1986.
- [405] Yu.E. Lozovik, , Usp. Fiz. Nauk 153 (1987) 356 [Sov. Phys. Usp. 30 (1987) 912].
- [406] Yu.E. Lozovik, V.A. Mandelshtam, Phys. Lett. A 145 (1990) 269.
- [407] F. Bolton, U. Rössler, Superlatt. Microstruct. 13 (1992) 139.
- [408] V.M. Bedanov, F. Peeters, Phys. Rev. B 49 (1994) 2667.
- [409] S. Åberg, H. Flocard, W. Nazarewicz, Annu. Rev. Nucl. Part. Sci. 40 (1990) 439.
- [410] S. Frauendorf, Rev. Mod. Phys. 73 (2001) 463.
- [411] W. Satula, R.A. Wyss, Rep. Prog. Phys. 68 (2005) 131.
- [412] T. Vorrath, R. Blümel, Eur. Phys. J. B 32 (2003) 227.

- [413] R.S. Berry, Contemp. Phys. 30 (1989) 1.
- [414] L. Serra, R.G. Nazmitdinov, A. Puente, Phys. Rev. B 68 (2003) 035341.
- [415] B. Reusch, H. Grabert, Phys. Rev. B 68 (2003) 045309.
- [416] B.H. Bransden, C. J. Joachain, Physics of Atoms and Molecules, Longman Scientific & Technical, New York, 1994.
- [417] A. Matulis, F.M. Peeters, Solid State Commun. 117 (2001) 655.
- [418] V. Schweigert, F.M. Peeters, Phys. Rev. B 51 (1995) 7700.
- [419] S. Sachdev, Quantum Phase Transitions (2nd Edition), Cambridge University Press, Cambridge, 2011.
- [420] K. von Klitzing, G. Dorda, M. Pepper, Phys. Rev. Let. **45** (1980) 494.
- [421] D. C. Tsui, H. L. Stormer, and A. C. Gossard, Phys. Rev. Let., **48** (1982) 1559.
- [422] L. Amico, R. Fazio, A. Osterloh, and V. Vedral, Rev. Mod. Phys. **80** (2008) 517.
- [423] M. Tichy, F. Mintert, A. Buchleitner, J. Phys. B: At. Mol. Opt. Phys. **44** (2011) 192001.
- [424] J. Naudts, T. Verhulst, Phys. Rev. A **75** (2007) 062104.
- [425] J. P. Coe, A. Sudbery, I. D' Amico, Phys. Rev. B **77** (2008) 205122.
- [426] J. Pipek, I. Nagy, Phys. Rev. A **79** (2009) 052501.
- [427] R. J. Yañez, A. R. Plastino, J.S. Dehesa, Eur. Phys. J. D **56** (2010) 141.
- [428] P. Kościk, A. Okopińska, Phys. Lett. A **374** (2010) 3841.
- [429] R.G. Nazmitdinov, N.S. Simonović, A. R. Plastino, A.V. Chizhov, J. Phys. B: At. Mol. Opt. Phys. **45** (2012) 205503.
- [430] P.A. Maksym, Y. Nishi, D.G. Austing, T. Hatano, L.P. Kouwenhoven, H. Aoki, S. Tarucha, Phys. Rev. B 79 (2009) 115314.
- [431] A. Puente, M. Pons, R.G. Nazmitdinov, J. Phys. Conf. Ser. 248 (2010) 012017.
- [432] J.J. Thomson, Phil. Mag. 7 (1904) 237.
- [433] W.Y. Ruan, Y.Y. Liu, C.G. Bao, Z.Q. Zhang, Phys. Rev. B 51 (1995) 7942.
- [434] B. Partoens, F.M. Peeters, J. Phys. Condens. Matter 9 (1997) 5383.
- [435] D.J. Thouless, Nucl. Phys. 21 (1960) 225.
- [436] D.J. Thouless, Nucl. Phys. 22 (1961) 78.
- [437] E.R. Marshalek, J. Weneser, Ann. Phys. (N.Y.) 53 (1969) 569.

- [438] F. Döna u, D. Al mehed, R.G. Nazmitdinov, Phys. Rev. Lett. 83 (1999) 280.
- [439] K. Kaneko, M. Hasegawa, Phys. Rev. C 72 (2005) 061306.
- [440] D.J. Thouless, J. G. Valatin, Nucl. Phys. 31 (1962) 211.
- [441] D.J. Rowe, Phys. Rev. 175 (1968) 1283.
- [442] K. L. G. Heyde, Basic Ideas and Concepts in Nuclear Physics: An Introductory Approach, Taylor & Francis, Bristol, 2004.
- [443] E. Caurier, G. Martinez-Pinedo, F. Nowacki, A. Poves, A.P. Zuker, Rev. Mod. Phys. 77 (2005) 427.
- [444] L. Gaudefroy, J.M. Daugas, M. Hass, *et al.*, Phys. Rev. Lett. 102 (2009) 092501.
- [445] L.A. Riley, P. Adrich, T.R. Baugher *et al.*, Phys. Rev. C 79 (2009) 051303(R).
- [446] N. Michel, W. Nazarewicz, M. Ploszajczak, T. Vertse, J. Phys. G. 36 (2009) 013101.
- [447] O. Sorlin, M.-G. Porquet, Prog. Part. Nucl. Phys. 61 (2008) 602.
- [448] D. Al mehed, F. Döna u, R.G. Nazmitdinov, J. Phys. G 29 (2003) 2193.
- [449] E.R. Marshalek, J. Phys. G. 30 (2004) 1861.
- [450] A. Bohr, B.R. Mottelson, D. Pines, Phys. Rev. 110 (1958) 936.
- [451] N.N. Bogolubov, Dokl. Akad. Nauk SSSR 119 (1958) 52.
- [452] A.V. Afanasjev, D.B. Fossan, G.J. Lane, I. Ragnarsson, Phys. Rep. 322 (1999) 1.
- [453] A. Johnson, H. Ryde, J. Sztarkier, , Phys. Lett. B 34 (1971) 605.
- [454] <http://www.nndc.bnl.gov/nudat2/>, 2006.
- [455] J. Kvasil, R.G. Nazmitdinov, Pis'ma Zh. Eksp. Teor. Fiz. 83 (2006) 227 [JETP Lett. 83 (2006) 187].
- [456] F.S. Stephens, Rev. Mod. Phys. 47 (1975) 43.
- [457] B.R. Mottelson, J.G. Valatin, Phys. Rev. Lett. 5 (1960) 511.
- [458] B.T. Geilikman, in: D.A. Branley, E.W. Vogt (Eds.) Proceedings of International Conference on Nuclear Structure, University of Toronto, Toronto, 1960, p. 874.
- [459] P.J. Twin, B.M. Nyakó, A.H. Nelson, J. Simpson, M.A. Bentley, H.W. Cranmer-Gordon, P.D. Forsyth, D. Howe, A.R. Mokhtar, J.D. Morrison, J.F. Sharpey-Schafer, G. Sletten, Phys. Rev. Lett. 57 (1986) 811.
- [460] R.V.F. Janssens, T.L. Khoo, Annu. Rev. Nucl. Part. Sci. 41 (1991) 321.
- [461] C. Baktash, B. Haas, W. Nazarewicz, Annu. Rev. Nucl. Part. Sci. 45 (1995) 485.

- [462] K.T. Hecht, A. Adler, Nucl. Phys. A 137 (1969) 129.
- [463] R.D. Ratna Raju, J.P. Draayer, K.T. Hecht, Nucl. Phys. A 202 (1973) 433.
- [464] A.L. Blokhin, C. Bahri, J.P. Draayer, Phys. Rev. Lett. 74 (1995) 4149.
- [465] J. Dudek, Prog. Part. Nucl. Phys. 28 (1992) 131.
- [466] T. Bengtsson, M.E. Faber, G. Leander, P. Möller, M. Ploszajczak, I. Ragnarsson, S. Åberg, Phys. Scr. 24 (1981) 200.
- [467] E.S. Paul, P.J. Twin, A.O. Evans, *et al.*, Phys. Rev. Lett. 98 (2007) 012501.
- [468] J. Ollier, J. Simpson, X. Wang, *et al.*, Rhys. Rev. C 80 (2009) 064322.
- [469] R.M. Clark, A.O. Macchiavelli, Annu. Rev. Nucl. Part. Sci. 50 (2000) 1.
- [470] I. Ahmad, P.A. Butler, Annu. Rev. Nucl. Part. Sci. 43 (1993) 71.
- [471] P. Butler, W. Nazarewicz, Rev. Mod. Phys. 68 (1996) 349.
- [472] X. Wang, R.V.F. Janssens, M.P. Carpenter, *et al.*, Phys. Rev. Lett. 102 (2009) 122501.
- [473] S.S. Ntshangase, R.A. Bark, D.G. Aschman, *et al.*, Phys. Rev. C 82 (2010) 041305(R).
- [474] J. Blocki, J.-J. Shi, W.J. Swiatecki, Nucl. Phys. A 554 (1993) 387.
- [475] R. Arvieu, F. Brut, J. Carbonell, J. Touchard, Phys. Rev. A 35 (1987) 2389.
- [476] M.C. Gutzwiller, Chaos in Classical and Quantum Mechanics, Springer, New York, 1990.
- [477] K. Arita, Phys. Lett. B 336 (1994) 279.
- [478] K. Arita, K. Matsuyanagi, Prog. Theor. Phys. 91 (1994) 723.
- [479] W.D. Heiss, R.G. Nazmitdinov, S. Radu, Phys. Rev. Lett. 72 (1994) 2351.
- [480] W.D. Heiss, R.G. Nazmitdinov, S. Radu, Phys. Rev. C 52 (1995) 3032.
- [481] W.D. Heiss, R.A. Lynch, R.G. Nazmitdinov, Phys. Rev. C 60 (1999) 034303.
- [482] H.A. Weidenmüller, G. E. Mitchell, Rev. Mod. Phys. 81 (2009) 539.
- [483] R. Balian, C. Bloch, Ann. Phys. (N.Y.) 69 (1972) 76.
- [484] V.M. Strutinsky, A.G. Magner, S.R. Ofengenden, T. Dossing, Z. Phys. A 283 (1977) 269.
- [485] H. Frisk, Nucl. Phys. A 511 (1990) 309.
- [486] M. Brack, R.K. Bhaduri, Semiclassical Physics, Addison-Wesley, New York, 1997.

- [487] B.D. Serot, J.D. Walecka, *Adv. Nucl. Phys.* 16 (1986) 1.
- [488] P.-G. Reinhard, *Rep. Prog. Phys.* 52 (1989) 439.
- [489] P. Ring, *Prog. Part. Nucl. Phys.* 37 (1996) 193.
- [490] J. Meng, H. Toki, S.G. Zhou, S.Q. Zhang, W.H. Long, L.S. Geng, *Prog. Part. Nucl. Phys.* 57 (2006) 470.
- [491] Z.P. Li, T. Niksic, D. Vretenar, J. Meng, G.A. Lalazissis, P. Ring, *Phys. Rev. C* 79 (2009) 054301.
- [492] A.V. Afanasjev, H. Abusara, *Phys. Rev. C* 82 (2010) 034329.
- [493] C. Eckart, *Phys. Rev.* 46 (1934) 383.
- [494] C. Eckart, *Phys. Rev.* 47 (1935) 552.
- [495] A.V. Meremianin, J.S. Briggs, *Phys. Rep.* 384 (2003) 121.
- [496] A.V. Meremianin, *J. Chem. Phys.* 120 (2004) 7861.
- [497] A. Bohr, K. Dan. Vidensk. Selsk. Mat. Fys. Medd. 26 (1952) 14.
- [498] A. Arima, F. Iachello, *Ann. Phys. (N.Y.)* 99 (1976) 253.
- [499] A. Arima, F. Iachello, *Ann. Phys. (N.Y.)* 111 (1978) 201.
- [500] A. Arima, F. Iachello, *Ann. Phys. (N.Y.)* 123 (1979) 468.
- [501] D. Janssen, R.V. Jolos, F. Dönaau, *Nucl. Phys. A* 224 (1974) 93.
- [502] F. Iachello, A. Arima, *The Interacting Boson Model*, Cambridge University Press, Cambridge, 1987.
- [503] A. Arima, T. Otsuka, F. Iachello, I. Talmi, *Phys. Lett. B* 66 (1977) 205.
- [504] D. Warner, *Nature (London)* 420 (2002) 614.
- [505] J.N. Ginocchio, M. W. Kirson, *Phys. Rev. Lett.* 44 (1980) 1744.
- [506] A.E.L. Dieperink, O. Scholten, F. Iachello, *Phys. Rev. Lett.* 44 (1980) 1747.
- [507] P. Navrátil, S. Quaglioni, I. Stetcu, B.R. Barrett, *J. Phys. G* 36 (2009) 083101.
- [508] A.L. Goodman, *Adv. Nucl. Phys.* 11 (1979) 263.
- [509] M. Bender, P.-H. Heenen, P.-G. Reinhard, *Rev. Mod. Phys.* 75 (2003) 121.
- [510] B.A. Brown, B.H. Wildenthal, *Annu. Rev. Nucl. Part. Sci.* 38 (1988) 29.
- [511] M.A. Bentley, S.M. Lenzi, *Prog. Part. Nucl. Phys.* 59 (2007) 497.

- [512] L. Coraggio, A. Covello, A. Gargano, N. Itaco, T.T.S. Kuo, *Prog. Part. Nucl. Phys.* 62 (2009) 135.
- [513] A.V. Afanasjev, T.L. Khoo, S. Frauendorf, G.A. Lalazissis, I. Ahmad, *Phys. Rev. C* 67 (2003) 024309.
- [514] M. Bender, J. Dobaczewski, J. Engel, W. Nazarewicz, *Phys. Rev. C* 65 (2002) 054322.
- [515] J. Terasaki, J. Engel, M. Bender, J. Dobaczewski, W. Nazarewicz, M. Stoitsov, *Phys. Rev. C* 71 (2005) 034310.
- [516] P. Vesely, J. Kvasil, V.O. Nesterenko, W. Kleinig, P.-G. Reinhard, V.Yu. Ponomarev, *Phys. Rev. C* 80 (2009) 031302(R).
- [517] C.L. Bai, H.O. Zhang, X.Z. Zhang, F.R. Xu, H. Sagawa, G. Coló, *Phys. Rev. C* 79 (2009) 041301.
- [518] J. Erler, P. Klüpfel, P.-G. Reinhard, *J. Phys. G* 37 (2010) 064001.
- [519] B.J. Giraud, *J. Phys. G* 37 (2010) 064002.
- [520] V.O. Nesterenko, J. Kvasil, P. Vesely, W. Kleinig, P.-G. Reinhard, V.Yu. Ponomarev, *J. Phys. G* 37 (2010) 064034.
- [521] J.E. Drut, R.J. Furnstahl, L. Platter, *Prog. Part. Nucl. Phys.* 64 (2010) 120.
- [522] D.R. Inglis, *Phys. Rev.* 96 (1954) 1059;
- [523] D.R. Inglis, *Phys. Rev.* 97 (1954) 701.
- [524] K.W. Schmid, *Prog. Part. Nucl. Phys.* 52 (2004) 565.
- [525] J. Kvasil, R.G. Nazmitdinov, *Phys. Part. Nucl.* 17 (1986) 265 [*Fiz. Elem. Chast. At. Yadra* 17 (1986) 613].
- [526] T. Nakatsukasa, K. Matsuyanagi, S. Mizutori, Y.R. Shimizu, *Phys. Rev. C* 53 (1996) 2213.
- [527] M. Brack, J. Damgaard, A.S. Jensen, H.C. Pauli, V.M. Strutinsky, C.Y. Wong, *Rev. Mod. Phys.* 44 (1972) 320.
- [528] R. Bengtsson, S.E. Larsson, G. Leander, P. Möller, S.G. Nilsson, S.Åberg, Z. Szymański, *Phys. Lett. B* 57 (1975) 301.
- [529] K. Neergard, V.V. Pashkevich, *Phys. Lett. B* 59 (1975) 218.
- [530] T. Troudet, R. Arvieu, *Ann. Phys. (N.Y.)* 134 (1981) 1.
- [531] E.R. Marshalek, R.G. Nazmitdinov, *Phys. Lett. B* 300 (1993) 199.
- [532] R.G. Nazmitdinov, D. Almehed, F. Döna, *Phys. Rev. C* 65 (2002) 041307(R).

- [533] W.D. Heiss, R.G. Nazmitdinov, Phys. Rev. C 65 (2002) 054304.
- [534] Z. Szymanski, Fast Nuclear Rotation, Clarendon, Oxford, 1983.
- [535] H. Hübel, Prog. Part. Nucl. Phys. 54 (2005) 1.
- [536] Y.R. Shimizu, J.D. Garrett, R.A. Broglia, M. Gallardo, E. Viguzzi, Rev. Mod. Phys. 61 (1989) 131.
- [537] R.R. Chasman, Phys. Lett. B 96 (1980) 7.
- [538] S. Frauendorf, V.V. Pashkevich, Phys. Lett. B 141 (1984) 23.
- [539] W. Nazarewicz, P. Olanders, I. Ragnarsson, J. Dudek, G. Leander, Phys. Rev. Lett. 52 (1984) 1272.
- [540] W. Nazarewicz, P. Olanders, I. Ragnarsson, J. Dudek, G. Leander, Phys. Rev. Lett. 53 (1984) 2060.
- [541] J. Dobaczewski, J. Dudek, S.G. Rohozinski, T.R. Werner, Phys. Rev. C 62 (2000) 014310.
- [542] J. Dobaczewski, J. Dudek, S.G. Rohozinski, T.R. Werner, Phys. Rev. C 62 (2000) 014311.
- [543] A.V. Ignatyuk, I.N. Mikhailov, L.H. Molina, R.G. Nazmitdinov, K. Pomorsky, Nucl. Phys. A 346 (1980) 191.
- [544] Y. Alhassid, J. Zingman, S. Levit, Nucl. Phys. A 469 (1987) 205.
- [545] Y. Alhassid, J.M. Manoyan, S. Levit, Phys. Rev. Lett. 63 (1989) 31 .
- [546] M.N. Harakeh, A. van der Woude, Giant Resonances: Fundamental High-Frequency Modes of Nuclear Excitation, Clarendon, Oxford, 2001.
- [547] S.N. Fedotkin, I.N. Mikhailov, R.G. Nazmitdinov, Phys. Lett. B 121 (1983) 15.
- [548] M.E. Faber, J.L. Egido, P. Ring, Phys. Lett. B 127 (1983) 5.
- [549] K.A. Snover, Annu. Rev. Nucl. Part. Sci. 36 (1986) 545.
- [550] J.J. Gaardhøje, Annu. Rev. Nucl. Part. Sci. 42 (1992) 483.
- [551] D. Kusnezov, Y. Alhassid, K.A. Snover, W.E. Ormand, Nucl. Phys. A 687 (2001) 212c.
- [552] F. Iachello, Phys. Rev. Lett. 91 (2003) 132502.
- [553] F. Iachello, N.V. Zamfir, Phys. Rev. Lett. 92 (2004) 212501.
- [554] J. Kvasil, R.G. Nazmitdinov, Phys. Rev. C 73 (2006) 014312.
- [555] G. Do Dang, A. Klein, N.R. Walet, Phys. Rep. 335 (2000) 93.

- [556] K. Matsuyanagi, M. Matsuo, T. Nakatsukasa, N. Hinohara, K. Sato, J. Phys. G 37 (2010) 064018.
- [557] J.A. Krumhansl R.J. Gooding, Phys. Rev. B 39 (1989) 3047.
- [558] P. Möller, S.G. Nilsson, Phys. Lett. B 31 (1970) 283.
- [559] F. Garote, J.L. Egido, L.M. Robledo, Phys. Rev. Lett. 80 (1998) 4398.
- [560] R.R. Chasman, Phys. Lett. B 266 (1991) 243.
- [561] M. Yamagami, K. Matsuyanagi, Nucl. Phys. A 672 (2000) 123.
- [562] T. Tanaka, R.G. Nazmitdinov, K. Iwasawa, Phys. Rev. C 63 (2001) 034309.
- [563] A. Tsvetkov, J. Kvasil, R.G. Nazmitdinov, J. Phys. G 28 (2002) 2187.
- [564] R.G. Nazmitdinov, J. Kvasil, A. Tsvetkov, Phys. Lett. B 657 (2007) 159.
- [565] S. Frauendorf, Phys. Rev. C 77 (2008) 021304(R).
- [566] Ch. Briancon, I.N. Mikhailov, in: R.A. Meyer, V. Paar (Eds.), Proceedings of the International Conference on Nuclear Structure, Reactions and Symmetries, Dubrovnik, Yugoslavia, World Scientific, Singapore, 1986, Vol.I, p.131.
- [567] X. Li, J. Dudek, Phys. Rev. C 49 (1994) R1250.
- [568] D. Curien, J. Dudek, K. Mazurek, J. Phys. Conf. Ser. 205 (2010) 012034.
- [569] J. Dudek, D. Curien, N. Dubray, J. Dobaczewski, V. Pangon, P. Olbratowski, N. Schunck, Phys. Rev. Lett. 97 (2006) 072501.
- [570] R.A. Bark, J.F. Sharpey-Schafer, S.M. Maliage, *et al.*, Phys. Rev. Lett. 104 (2010) 022501.
- [571] A.V. Afanasjev, J. König, P. Ring, L.M. Robledo, J.L. Egido, Phys. Rev. C 62 (2000) 054306.
- [572] J.L. Egido, H.J. Mang, P. Ring, Nucl. Phys. A 341 (1980) 229.
- [573] J.G. Valatin, Proc. Roy. Soc. London A 238 (1956) 132.
- [574] G. Ripka, J.P. Blaizot, N. Kassis, in: International Extended Seminar, Trieste, 1973, IAEA, Vienna, 1975, Vol. 1, p. 445.
- [575] V.G. Zelevinsky, Yad. Fiz. 22 (1975) 1085 [Sov. J. Nucl. Phys. 22 (1975) 565].
- [576] H. Sakamoto, T. Kishimoto, Nucl. Phys. A 501 (1989) 205.
- [577] S. Åberg, Phys. Lett. B 157 (1985) 9.
- [578] E.R. Marshalek, Nucl. Phys. A 275 (1977) 416.

- [579] P.-G. Reinhard, V.O. Nesterenko, E. Suraud, S. El Gammal, W. Kleinig, Phys. Rev. A 66 (2002) 013206.
- [580] I. Bialynicki-Birula, T. Sowinski, Phys. Rev. A 71 (2005) 043610.
- [581] K.W. Madison, F. Chevy, W. Wohlleben, J. Dalibard, Phys. Rev. Lett. 84 (2000) 806.
- [582] F. Chevy, K.W. Madison, J. Dalibard, Phys. Rev. Lett. 85 (2000) 2223.
- [583] E.R. Marshalek, Phys. Rev. C 54 (1996) 159.
- [584] I.N. Mikhailov, D. Janssen, Phys. Lett. B 72 (1978) 303.
- [585] D. Janssen, I.N. Mikhailov, R.G. Nazmitdinov, B. Nerlo-Pomorska, K. Pomorski, R.Kh. Safarov, Phys. Lett. B 79 (1978) 347.
- [586] Y.R. Shimizu, M. Matsuzaki, Nucl. Phys. A 588 (1995) 559.
- [587] D. Janssen, I. N. Mikhailov, Nucl. Phys. A 318 (1979) 390.
- [588] E.R. Marshalek, Nucl. Phys. A 331 (1979) 429.
- [589] S.W. Ødegård, G.B. Hagemann, D.R. Jensen, *et al.*, Phys. Rev. Lett. 86 (2001) 5866.
- [590] D.R. Jensen, G.B. Hagemann, I. Hamamoto, *et al.*, Nucl. Phys. A 703 (2003) 3.
- [591] H. Amro, W.C. Ma, G.B. Hagemann, *et al.*, Phys. Lett. B 553 (2003) 197.
- [592] G. Schönwasser, H. Hübel, G.B. Hagemann, *et al.*, Phys. Lett. B 552 (2003) 9.
- [593] A. Görge, R.M. Clark, M. Cromaz, P. Fallon, G.B. Hagemann, H. Hübel, L.Y. Lee, A.O. Macchiavelli, G. Sletten, D. Ward, R. Bengtsoon, Phys. Rev. C 69 (2004) 031301.
- [594] D.R. Jensen, G.B. Hagemann, I. Hamamoto, *et al.*, Eur. Phys. J. A 19 (2004) 173.
- [595] R.G. Nazmitdinov, J. Kvasil, Zh. Eksp. Teor. Fiz. 132 (2007) 1100 [JETP 105 (2007) 962].
- [596] T. Shoji, Y.R. Shimizu, Prog. Theor. Phys. 121 (2009) 319.
- [597] P.W. Anderson, J. Phys. Chem. Solids 11 (1959) 28.
- [598] R. Parmenter, Phys. Rev. 166 (1968) 392.
- [599] J.M. Blatt, C.J. Thompson, Phys. Rev. Lett. 10 (1963) 332.
- [600] B. Mühlischlegel, D.J. Scalapino, R. Denton, Phys. Rev. B 6 (1972) 1767.
- [601] R. Denton, M. Mühlischlegel, D.J. Scalapino, Phys. Rev. B 7 (1973) 3589.

- [602] D.C. Ralph, C.T. Black, M. Tinkham, Phys. Rev. Lett. 74 (1995) 3241.
- [603] C.T. Black, D.C. Ralph, M. Tinkham, Phys. Rev. Lett. 76 (1996) 688.
- [604] D.C. Ralph, C.T. Black, M. Tinkham, Phys. Rev. Lett. 78 (1997) 4087.
- [605] J. von Delft, A.D. Zaikin, D.S. Golubev, W. Tichy, Phys. Rev. Lett. 77 (1996) 3189.
- [606] V.G. Soloviev, Theory of Complex Nuclei, Pergamon, London, 1976.
- [607] J. von Delft, D.C. Ralph, Phys. Rep. 345 (2001) 61.
- [608] F. Braun, J. von Delft, D.C. Ralph, M. Tinkham, Phys. Rev. Lett. 79 (1997) 921.
- [609] J. von Delft, Ann. Phys. (Leipzig) 10 (2001) 219.
- [610] J. Dukelsky, G. Sierra, Phys. Rev. B 61 (2000) 12302.
- [611] V.G. Soloviev, Mat. Fys. Skrif. Kong. Dan. Vid. Selsk. 1 (1961) 1.
- [612] F. Braun, J. von Delft, Phys. Rev. Lett. 81 (1998) 4712.
- [613] M.A. Fernandez, J.L. Egido, Phys. Rev. B 68 (2003) 184505.
- [614] A.K. Kerman, R.D. Lawson, M.H. MacFarlane, Phys. Rev. 124 (1961) 162.
- [615] A. Pawlikowski, V. Rybarska, Zh. Eksp. Teor. Fiz. 43 (1962) 543 [Sov. Phys. JETP 16 (1963) 388].
- [616] R.W. Richardson, Phys. Lett. B 3 (1963) 277.
- [617] R.W. Richardson, Phys. Lett. B 5 (1963) 82.
- [618] R.W. Richardson, J. Math. Phys. 6 (1965) 1034.
- [619] R.W. Richardson, Phys. Rev. 141 (1966) 949.
- [620] R.W. Richardson, Phys. Rev. 144 (1966) 874.
- [621] R.W. Richardson, Phys. Rev. 159 (1967) 792.
- [622] R.W. Richardson, J. Math. Phys. 9 (1968) 1327.
- [623] R.W. Richardson and N. Sherman, Nucl. Phys. B 52 (1964) 221.
- [624] G. Sierra, J. Dukelsky, G.G. Dussel, J. von Delft, F. Braun, Phys. Rev. B 61 (2000) 11890.
- [625] J. Dukelsky, S. Pittel, G. Sierra, Rev. Mod. Phys. 76 (2004) 643.
- [626] M.B. Barbaro, R. Cenni, S. Chiacchiera, A. Molinari, F. Palumbo, Ann. Phys. (N.Y.) 322 (2007) 2665.
- [627] V.N. Gladilin, V.M. Fomin, J.T. Devreese, Solid State Commun. 121 (2002) 519.

- [628] V.N. Gladilin, V.M. Fomin, J.T. Devreese, Phys. Rev. B 70 (2004) 144506.
- [629] K. Van Houcke, S.M.A. Rombouts, L. Pollet, Phys. Rev. B 73 (2006) 132509.
- [630] S. Frauendorf, N.K. Kuzmenko, V.M. Mikhajlov, J.A. Sheikh, Phys. Rev. B 68 (2003) 024518.
- [631] D.J. Dean, K. Langanke, H. Nam, W. Nazarewicz, Phys. Rev. Lett. 105 (2010) 212504.
- [632] R. Balian, H. Flocard, M. Veneroni, Phys. Rep. 317 (1999) 251;
- [633] V.Z. Kresin, Y.N. Ovchinnikov, Phys. Rev. B 74 (2006) 024514.
- [634] V.N. Gladilin, J. Tempere, I.F. Silvera, J.T. Devreese, Phys. Rev. B 74 (2006) 104512.
- [635] V.Z. Kresin, Y.N. Ovchinikov, S.A. Wolf, Phys. Rep. 431 (2006) 231.
- [636] D. Croitoru, A. A. Shanenko, C. C. Kaun, F. M. Peeters, Phys. Rev. B 83 (2011) 214509 .
- [637] H. Olofsson, S. Åberg, P. Leboeuf, Phys. Rev. Lett. 100 (2008) 037005.
- [638] A.M. Garsía-Garsía, J.D. Urbina, E.A. Yuzbashyan, K. Richter, B.L. Altshuler, Phys. Rev. B 83 (2011) 014510.
- [639] H. Heiselberg, Phys. Rev. A 68 (2003) 053616.
- [640] B. Cao, C.M. Neal, A.K. Starace, Y.N. Ovchinikov, V.Z. Kresin, M.F. Jarrold, J. Supercond. Nov. Magn. 21 (2008) 163.